GEOLOGICAL SURVEY OF CANADA
COMMISSION GÉOLOGIQUE DU CANADA

PAPER 79-1C
ÉTUDE

CURRENT RESEARCH
PART C

RECHERCHES EN COURS
PARTIE C

Energy, Mines and Resources Canada
Énergie, Mines et Ressources Canada

1979

Notice to Librarians and Indexers

The Geological Survey's thrice-yearly *Current Research* series contains many reports comparable in scope and subject matter to those appearing in scientific journals and other serials. All contributions to the Scientific and Technical Report section of *Current Research* include an abstract and bibliographic citation. It is hoped that these will assist you in cataloguing and indexing these reports and that this will result in a still wider dissemination of the results of the Geological Survey's research activities.

Avis aux bibliothécaires et préparateurs d'index

La série Recherches en cours *de la Commission géologique paraît trois fois par année; elle contient plusieurs rapports dont la portée et la nature sont comparable à ceux qui paraissent dans les revues scientifiques et autres périodiques. Tous les articles publiés dans la section des rapports scientifiques et techniques de la publication* Recherches en cours *sont accompagnés d'un résumé et d'une bibliographie, ce qui vous permettra, nous l'espérons, de cataloguer et d'indexer ces rapports, d'où une meilleure diffusion des résultats de recherche de la Commission géologique.*

Technical editing and compilation
Rédaction et compilation techniques
R.G. Blackadar
P.J. Griffin
H. Dumych
E.R.W. Neale

Production editing and layout
Préparation et mise en page
Leona R. Mahoney
Lorna A. Firth
Michael J. Kiel

Typed and checked by
Dactylographie et vérification
Debby Busby
Judy Coté
Sharon Parnham
Susan Gagnon
Cathy Bell
Jane Desautels

GEOLOGICAL SURVEY
PAPER 79-1C

COMMISSION GÉOLOGIQUE
ÉTUDE 79-1C

CURRENT RESEARCH
PART C

RECHERCHES EN COURS
PARTIE C

1979

ERRATUM

Current Research/Recherches en cours,
Paper/étude 79-1B
Page 416

Theoretical aspects of alpha coefficients used in X-ray fluorescence analysis; G.R. Lachance,
The two equations were incorrectly printed. The correct forms follow.

1. $$W_i = R_i (1 + W_j\alpha_{ij}' \ldots + W_j W_k \alpha_{ijk})$$

is a function of

$\alpha_{ij} + W_m(\alpha_{imj} + W_m^2 \alpha_{immj})$ where

i = analyte element
j = matrix element, absorption or enhancement
W = weight fraction
R = relative intensity to pure i
m = matrix elements j, k, . . .
α_{ijk} = a "crossed effect" coefficient

2. $$\alpha_{ik} = (\alpha_{ij} + 1)\left(\frac{Z_k}{Z_j}\right)^{n-1}$$

where Z = atomic number
n = exponent ≃ 2.6

3. $u = C\lambda^{\alpha}$ should read $u = C\lambda^{a}$

SCIENTIFIC AND TECHNICAL REPORTS

RAPPORTS SCIENTIFIQUES ET TECHNIQUES

SCIENTIFIC AND TECHNICAL NOTES
NOTES SCIENTIFIQUES ET TECHNIQUES

DISCUSSIONS AND COMMUNICATIONS
DISCUSSIONS ET COMMUNICATIONS

Note To Contributors

Submissions to the *Discussion* section of *Current Research* are welcome from both the staff of the Geological Survey and from the public. Discussions are limited to 6 double-spaced typewritten pages (about 1500 words) and are subject to review by the Chief Scientific Editor. Discussions are restricted to the scientific content of Geological Survey reports. General discussions concerning branch or government policy will not be accepted. Illustrations will be accepted only if, in the opinion of the editor, they are considered essential. In any case no redrafting will be undertaken and reproducible copy must accompany the original submissions. Discussion is limited to recent reports (not more than 2 years old) and may be in either English or French. Every effort is made to include both *Discussion* and *Reply* in the same issue. *Current Research* is published in January, June and November. Submissions for these issues should be received not later than November 1, April 1, and September 1 respectively. Submissions should be sent to the Chief Scientific Editor, Geological Survey of Canada, 601 Booth Street, Ottawa, Canada, K1A 0E8.

Avis aux auteurs d'articles

Nous encourageons tant le personnel de la Commission géologique que le grand public à nous faire parvenir des articles destinés à la section discussion *de la publication* Recherches en cours. *Le texte doit comprendre au plus six pages dactylographiées à double interligne (environ 1500 mots), texte qui peut faire l'objet d'un réexamen par le rédacteur en chef scientifique. Les discussions doivent se limiter au contenu scientifique des rapports de la Commission géologique. Les discussions générales sur la Direction ou les politiques gouvernementales ne seront pas acceptées. Les illustrations ne seront acceptées que dans la mesure où , selon l'opinion du rédacteur, elles seront considérées comme essentielles. Aucune retouche ne sera faite aux textes et dans tous les cas, une copie qui puisse être reproduite doit accompagner les textes originaux. Les discussions en français ou en anglais doivent se limiter aux rapports récents (au plus de 2 ans). On s'efforcera de faire coincider les articles destinés aux rubriques* discussions et réponses *dans le même numéro. La publication* Recherches en cours *paraît en janvier, en juin et en novembre. Les articles pour ces numéros doivent être reçus au plus tard le 1er novembre, le 1er avril et le 1er septembre respectivement. Les articles doivent être renvoyés au rédacteur en chef scientifique: Commission géologique du Canada, 601, rue Booth, Ottawa, Canada, K1A 0E8.*

Separates

A limited number of separates of the papers that appear in this volume are available by direct request to the individual authors. The addresses of the Geological Survey of Canada offices follow:

601 Booth Street,
OTTAWA, Ontario
K1A 0E8

Institute of Sedimentary and Petroleum Geology,
3303-33rd Street N.W.,
CALGARY, Alberta
T2L 2A7

British Columbia Office,
100 West Pender Street,
VANCOUVER, B.C.
V6B 1R8

Atlantic Geoscience Centre,
Bedford Institute of Oceanography,
P.O. Box 1006,
DARTMOUTH, N.S.
B2Y 4A2

When no location accompanies an author's name in the title of a paper, the Ottawa address should be used.

Tirés à part

On peut obtenir un nombre limité de "tirés à part" des articles qui paraissent dans cette publication en s'adressant directement à chaque auteur. Les adresses des différents bureaux de la Commission géologique du Canada sont les suivantes:

601, rue Booth
OTTAWA, Ontario
K1A 0E8

Institut de géologie sédimentaire et pétrolière
3303 N. – O., 33rd, ST. N.W.,
CALGARY, Alberta
T2L 2A7

Bureau de la Colombie-Britannique
100 West Pender Street
VANCOUVER, Colombie-Britannique
V6B 1R8

Centre géoscientifique de l'Atlantique
Institut océanographique de Bedford
B.P. 1006
DARTMOUTH, Nouvelle-Écosse
B2Y 4A2

Lorsque l'adresse de l'auteur ne figure pas sous le titre d'un document, on doit alors utiliser l'adresse d'Ottawa.

1. LACUSTRINE GEOCHEMISTRY AROUND THE NORTH SHORE OF LAKE SUPERIOR: IMPLICATIONS FOR EVALUATION OF THE EFFECTS OF ACID PRECIPITATION

Projects 760044 and 690095

W.B. Coker and W.W. Shilts[1]
Resource Geophysics and Geochemistry Division

Coker, W.B. and Shilts, W.W., Lacustrine geochemistry around the north shore of Lake Superior: Implications for evaluation of the effects of acid precipitation; in Current Research, Part C, Geological Survey of Canada, Paper 79-1C, p. 1-15, 1979.

Abstract

Geochemical data from the north shore of Lake Superior illustrate how natural variations in the chemistry of the environment, caused by differing bedrock lithologies, mineralization, and/or glacial sediment compositions, can be used to predict or evaluate anthropogenic changes in geochemical patterns, particularly as they relate to acid precipitation. Patterns of pH variations in lake waters show lakes of the northeastern part of the study area to be buffered by a sheet of calcareous till and glaciolacustrine sediment transported southward and southwestward from the carbonate bedrock of the Hudson Bay Lowland. In the remaining parts of the area, pH is more closely related to underlying bedrock types. Trace metal levels in Lake waters and sediments vary significantly with changing bedrock types; patterns of variations can be used to predict areas most susceptible to metal mobilization as a result of terrain acidification.

Introduction

Lake water and sediment geochemical data have primarily been utilized for mineral resource evaluation, aiding bedrock mapping, and delineating natural regional geochemical trends. In regional lake surveys a subsurface sediment sample is purposely collected in order to avoid modern contamination due to man's activities. Collecting a subsurface sample allows a sample medium to be obtained that is correlative with natural chemical variations in bedrock lithology, glacial sediment composition and/or mineralization (i.e. before mining development). The above notwithstanding, some significant environmental observations can be drawn from regional lake water and sediment geochemical data. Regions with significant natural chemical variations, which are now, or could be of potential environmental concern can be outlined. Accordingly these areas can be subjected to detailed sampling of surface sediments and/or sediment coring to differentiate between modern chemical variations and original natural levels.

Regional geochemical surveys around the north shore of Lake Superior were carried out during the summers of 1977 and 1978 as part of the Federal-Provincial Uranium Reconnaissance Program (U.R.P.) (Darnley et al., 1975) and National Geochemical Reconnaissance (N.G.R.). Portions of these data are presented to illustrate their bearing on present and potential effects of acid precipitation.

The geochemical surveys covered map sheets 52A, 52H (south half), 42D and 42E (south half) in 1977 and map sheets 42C, 42F, (south half), 41K (north half) and 41N in 1978 (Geological Survey of Canada, 1978a,b and 1979a,b). These surveys consisted of the collection of lake waters and sediments at an average density of one sample site per 13 km^2. Lake water samples were analyzed for U, F, and pH. Lake sediment samples were analyzed for Zn, Cu, Pb, Ni, Co, Ag, Mn, As, Mo, Fe, U, L.O.I. (loss-on-ignition), and Hg (1977 samples only).

Distribution patterns of arsenic and mercury in lake sediments and fluorine and pH in lake waters are presented as examples of elements whose natural concentrations vary with changing bedrock, mineralization, and/or drift chemistry. Among others, these elements could be of environmental concern as a result of present or potential acid precipitation.

Methods

Sample Collection

A total of 4293 samples of profundal centre-lake sediment and an equal number of surface lake water samples were collected under contract by Marshall Macklin Monoghan Ltd., Toronto from June 3rd to 22nd, 1977 and from June 13th to July 11th, 1978.

Sediment samples were obtained using a Geological Survey sampler from a winch-equipped turbo-helicopter. Surficial (top 5-10 cm) sediment was automatically excluded through sampler design. The majority of the sediment samples collected were brown, green-brown (olive), or black organic-rich gelatinous sediments. Surface lake water was collected in 250 mL polyethylene bottles. For a more complete description of sampling equipment, sample collection techniques and sampling logistics the reader is referred to Coker et al. (in press).

Sample Preparation and Analysis

Lake sediment samples were prepared to pass an 80-mesh (180 µm) sieve by the staff of Golder Associates, Ottawa. Control reference and blind duplicate samples were inserted into each analytical block of twenty sediment and water samples to evaluate analytical accuracy and precision. For a more complete description of the analytical control system see Hornbrook and Garrett (1976) and Coker et al. (in press).

[1] Terrain Sciences Division

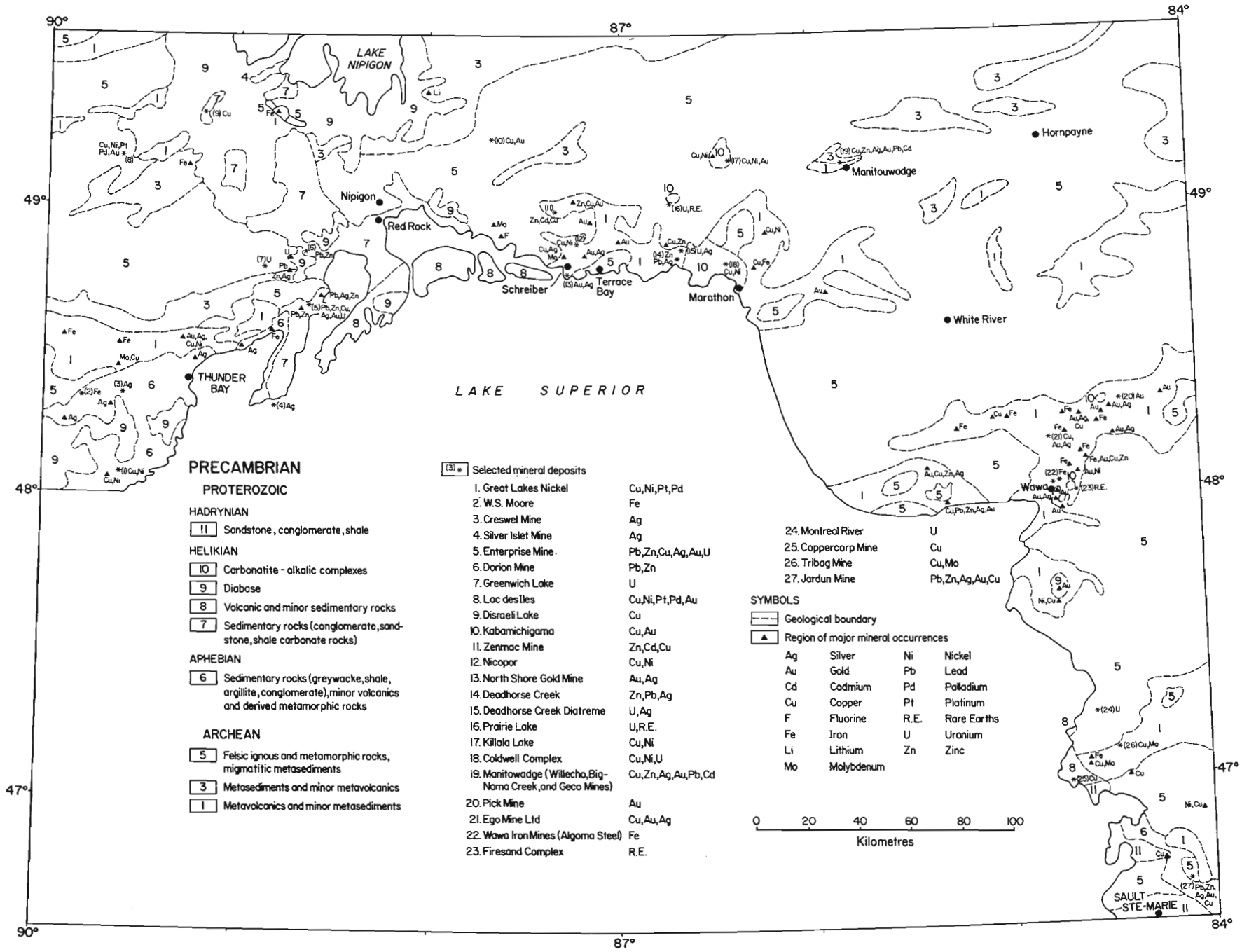

Figure 1.1. *Generalized regional geology and mineral occurrences, north shore, Lake Superior, Ontario (after Ayres et al., 1971a, b; Springer, 1977a, b, c, 1978a, b, c, d, e).*

Table 1.1

U.R.P.-N.G.R. Lake Sediments and Waters: Summary Statistics

		Range minimum	Range maximum	Arithmetic $\bar{x}$	Standard Deviation	Coefficient of Variation (%)	Geometric $\bar{x}$	$\log_{10}$ Standard Deviation
LAKE SEDIMENTS	Zn (ppm)	10	7000	106	120	113	94	0.207
	Cu (ppm)	2	1700	43	54	126	32	0.308
	Pb (ppm)	1*	5300	7	82	1171	4	0.317
	Ni (ppm)	1*	295	17	13	76	14	0.256
	Co (ppm)	1*	84	8	7	88	6	0.295
	Ag (ppm)	0.1*	17.0	0.1	0.3	300	0.1	0.110
	Mn (ppm)	10	47000	301	1124	373	167	0.407
	As (ppm)	0.5*	150.0	0.9	2.7	300	0.6	0.263
	Mo (ppm)	1*	31	2	2	100	2	0.255
	Fe (%)	0.05	17.00	1.20	1.16	97	0.92	0.309
	Hg (ppb)**	20	710	133	58	44	122	0.193
	U (ppm)	0.1*	129.0	5.0	7.8	156	2.9	0.411
	L.O.I. (%)	0.5*	96.8	43.4	17.2	40	38.3	0.261
LAKE WATERS	U (ppb)	0.005*	4.000	0.100	0.190	190	0.030	0.686
	F (ppb)	10*	760	45	24	53	42	0.152
	pH	3.1	8.3	6.9	0.6	9	-	-

Number of samples = 4293 **(except Hg where number of samples = 1816)
* Values equal to one-half the lower detection limit.
Coefficient of Variation (%) = (Standard Deviation/Arithmetic $\bar{x}$) x 100

Analyses of sediment samples for Zn, Cu, Pb, Ni, Co, Ag, Mn, Fe, Mo, Hg, As and L.O.I. (loss-on-ignition) were carried out by Chemex Labs. Ltd., Vancouver and for U by Atomic Energy of Canada Ltd., Ottawa.

The contents of Zn, Cu, Pb, Ni, Co, Ag, Mo, Mn, and Fe in the minus 80-mesh sediments were determined by atomic absorption spectroscopy.

The aresenic contents of the sediments collected in 1977 were determined colorimetrically using silver diethyldithiocarbamate. Colorimetric measurements were made at 520 nm. Atomic absorption, using a hydride evolution method as described by Aslin (1976), was utilized to determine the arsenic contents of the sediments collected in 1978. The extraction used in the hydride evolution method is more efficient than that used for the determination of arsenic by colorimetry thereby giving results that are a closer approximation of total arsenic. Data from a control reference sample analyzed by colorimetry in 1977 and by the hydride generation method in 1978 are summarized below:

	West (1977)	East (1978)
Arithmetic Mean(x)	4.2	9.4
Standard Deviation (s)	1.8	2.2
Number of Samples (n)	24	36

Mercury contents of the lake sediment samples were determined by the Hatch and Ott procedure, with some modifications, as described by Jonasson et al. (1973).

Loss-on-ignition (L.O.I.) was determined by ashing the sediment during a three hour time-temperature controlled rise to 500°C. The organic carbon content of a lake sediment sample is proportional to the percent weight loss-on-ignition (Coker and Nichol, 1975).

The delayed neutron activation method of analysis, by which the lake sediment samples were analyzed for total U, is described by Boulanger et al. (1975).

The determinations of U, F and pH in surface lake water samples were carried out by Barringer Magenta Ltd., Toronto.

Immediately upon receipt of the water samples in Toronto, fluoride and pH were determined by specific-ion electrode and glass-calomel combination electrode respectively. Fluoride and pH determinations were carried out from August 1st to 31st, 1977 and from August 7th to 25th, 1978.

Uranium was determined in the water samples by fission track analysis.

For a more complete description of preparation and analytical methods the reader is referred to Open Files 506, 507, 554, and 555 (Geological Survey of Canada, 1978a, b and 1979a, b).

Data Compilation and Map Production

For the purposes of this regional interpretation, the geochemical data from the lake sediments and waters collected around the north shore of Lake Superior (Geological Survey of Canada, 1978a, b, 1979a,b) were combined into one data set. A statistical summary of the geochemical data for the reconnaissance lake sediments and waters is presented in Table 1.1. The tendency of the data to be positively skewed and lognormally distributed, with the exception of pH (a logarithmic function), is indicated by the coefficients of variation (Table 1.1). Therefore, in the selection of appropriate data intervals for the production of moving average maps, a combination of percentile values, geometric mean and geometric standard deviation levels were employed (see Fig. 1.3-1.6).

The Applicon colour plotting system was used to produce 1:2 000 000 scale moving average maps of the geochemical data. For details on the Applicon colour plotting system the reader is referred to Coker et al. (in prep.).

General Geology

It is important to understand the distribution of the various lithologies (both bedrock and glacial), as the regional elemental distribution within the secondary environment may be a function of the mineralogy of specific lithologic units and associated metal deposit types. For this reason the regional bedrock geology, metallogeny, bedrock geochemistry and glacial geology will be reviewed. More detailed descriptions are included in Coker et al. (in prep.).

Regional Bedrock Geology

Bedrock within the survey area consists of lithologies of both the Superior and Southern provinces of the Canadian Shield. Immediately northeast of the survey area the Hudson Bay Lowland includes Paleozoic and Cretaceous sedimentary strata.

Archean bedrock of the Superior Province, within the Survey area, is composed of large, east-trending, metavolcanic and metasedimentary (Units 1 and 3, Fig. 1.1) supracrustal remnants (i.e. Shebandowan - Wawa and Quetico sub-provinces), intruded and partly surrounded by composite granodioritic batholiths and tonalitic gneiss domains (Unit 5, Fig. 1.1) (Goodwin, 1972).

The Southern Province consists largely of Proterozoic bedrock, unconformably deposited on deformed Archean basement, and later slightly deformed and metamorphosed (Card et al., 1972). The Proterozoic supracrustal rocks in the area consist of the Animikie Group and Keweenawan Supergroup.

Aphebian rocks of the Animikie Group consist of Gunflint and Rove formations (Moorhouse, 1960) exposed southwest of Thunder Bay and discontinuously along the shore of Lake Superior, eastward from Thunder Bay to Rossport (Unit 6, Fig. 1.1). The Gunflint Formation consists of a basal conglomerate, overlain by two cycles of chert, tuffaceous shale, and carbonate-taconite capped by a discontinuous limestone member (Kustra, et al., 1977). The Rove Formation conformably overlies the Gunflint Formation and consists largely of three lithologic units (Guel, 1970): black pyritic shale and argillite, argillite interbedded with greywacke and shale, and quartzitic greywacke with argillitic interbeds.

Helikian strata (Sibley Group, Osler Group) of the Keweenawan Supergroup, cover the Archean basement rocks through much of the Nipigon-Red Rock area (Fig. 1.1). The Sibley Group (Unit 7, Fig. 1.1) consists of three formations: Pass Lake, a basal quartz arenite locally conglomeratic; Rossport, comprising lower and upper red dolomitic members separated by an intermediate chert-carbonate and stromatolitic member; Kama Hill, purple moderately fissle shale and siltstone (Franklin, 1978). The Osler Group (Unit 8, Fig. 1.1) consists primarily of subaerially deposited tholeiitic basalt with very minor rhyolite and minor intercalated fluvial clastic rocks (Franklin, 1978).

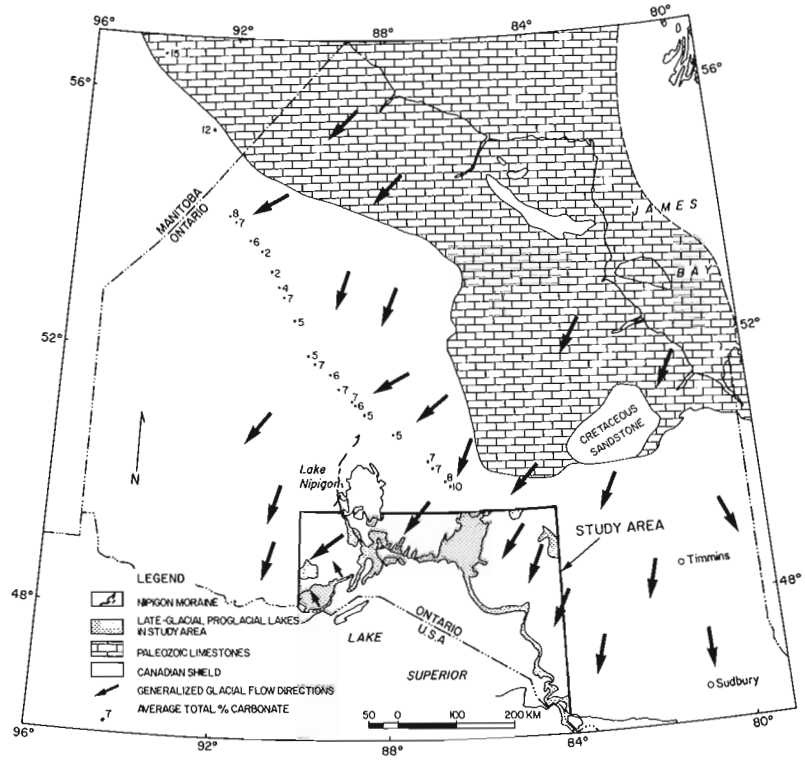

Figure 1.2. *Generalized glacial dispersal directions and selected glacial features for the Lake Superior study area and adjacent regions. Total carbonate contents determined on 44 μm-63 μm fractions of till from >3 m depth.*

Additional occurrences of Keweenawan bedrock occur along the east shore of Lake Superior. These occurrences (Unit 8, Fig.1.1) consist predominantly of basaltic flows, interlayered with polymictic conglomerate and rare volcaniclastic horizons, and intruded by small acid bodies, thin basic dykes and a few small quartz gabbro bodies (Annells, 1973).

A large variety of Helikian intrusions are present within the survey area around Lake Superior, including Logan tholeiitic diabase sills (Blackadar, 1956; Unit 9, Fig. 1.1) and alkaline intrusive complexes including the Port Coldwell (Mitchell and Platt, 1977) and Killala Lake alkali syenitic bodies and the Prairie Lake and Firesand River carbonatite complexes (Sage, 1975, 1977).

The Hadrynian Jacobsville Formation, exposed near Sault Ste. Marie (Fig. 1.1, Unit 11), is a clastic redbed sequence which underlies much of Lake Superior (Card et al., 1972; Dell, 1975). It is locally overlain by Paleozoic sedimentary strata.

The Paleozoic strata of the Hudson Bay Lowland are composed dominantly of carbonate. The Mesozoic strata are composed of lignite-bearing sandstones and associated kaolinitic beds.

Regional Metallogeny

Because the chemistry and mineralogy of metal occurrences and deposits can give some indication of expected element associations in lake environments a generalized deposit classification, summarized from Coker et al. (in prep.), is presented. Deposit types may be

conveniently grouped into four major classes. Selected deposits and occurrences representing each class are shown on Figure 1.1(*).

I. Stratiform deposits.
   (a) Archean volcanogenic massive sulphide deposits (*19).
   (b) Archean (*22) and Aphebian (*2) iron formations.
   (c) Archean gold deposits (*20, 21).

II. Intrusion hosted deposits
   (a) Ni-Cu-Pt deposits in both Archean (*8) and Helikian (*1) intrusions.
   (b) Helikian alkalic and carbonatite deposits (*16, 17, 18, 23).
   (c) Archean massive sulphide (*11).

III Veins
   (a) Veins related to Helikian intrusions
      (1) Ag-Pb-Zn-Cu veins (*4)
      (2) Pb-Zn-Ag (*14)
      (3) Pitchblende (*24)
   (b) Genetically similar veins related to the unconformity between the Sibley Group and Archean (locally Aphebian) rocks.
      (1) Pb-Zn-Ba-amethyst (*5, 6)
      (2) Pitchblende and uraniferous apatite (*7)
   (c) Copper veins and disseminations related to various Helikian strata (*9, 10, 25).
   (d) Archean gold-bearing veins (*13).

IV Breccia pipes (*15, 26).

Regional Bedrock Geochemistry

Relevant chemical characteristics (Hg, F, As, CaO, MgO, CO_2 and SiO_2) of the various bedrock lithologies within the east half of the survey area are summarized in Table 1.2.

Bedrock samples were crushed, ground, and ball milled to pass a 100-mesh (150 μm) sieve. The resultant material was analyzed for: mercury, by the Hatch and Ott procedure (Jonàsson et al., 1973); arsenic, by atomic absorption-hydride generation (Aslin, 1976); fluorine, after fusion, leaching and mixing with TISAB, by selective ion electrode; CaO, MgO and SiO_2 by X-ray spectrometry; and CO_2 by wet chemistry.

The survey area is primarily underlain by silicate bedrock, as indicated by SiO_2 contents (Table 1.2). Exceptions are the two carbonate-rich (as depicted by relatively elevated $CaO+MgO+CO_2$ contents, Table 1.2) lithologies: the Prairie Lake carbonatite (Fig. 1.1, *16) and the Rossport Formation of the Sibley Group (Fig. 1.1, Unit 7).

Further examination of the data summarized in Table 1.2 reveals other bedrock lithologies with distinctive chemical characteristics. The Rove Formation of the Animikie Group (Fig. 1.1, Unit 6) is characterized by highly elevated mercury contents. Elevated average fluorine contents occur in the Coldwell syenitic complex (Fig. 1.1, *18), the Rove and Gunflint formations of the Animikie Group (Fig. 1.1, Unit 6), and the Kama Hill and Rossport (dolomitic members) formations of the Sibley Group (Fig. 1.1, Unit 7). Significant levels of arsenic are found in the Rove and Gunflint formations of the Animikie Group (Fig. 1.1, Unit 6), Archean pegmatites (Fig. 1.1, Unit 5) and metasedimentary rocks (Fig. 1.1, Unit 3), and the Kama Hill Formation of the Sibley Group (Fig. 1.1, Unit 7).

Carbonate facies iron formations that occur in the vicinity of Wawa (Fig. 1.1, *22) have appreciable arsenic contents averaging 210 ppm, based on 97 samples (Goodwin, 1964).

Regional Glacial Geology

Regional Ice Flow History. The study area lies directly down ice from the major Paleozoic carbonate basin of Hudson Bay (Fig. 1.2). Through several glaciations the general ice flow pattern in this region was southerly and southwesterly from a glacial centre in Labrador-Quebec (Prest, 1970, p. 712, 713; Shilts et al., in press; Skinner, 1973). During retreat of the ice sheet from the region, lobes were formed by ice flow channeled along major depressions or by surging of unstable ice fronts into glacial lakes. These last ice movements were in some cases at considerable angles to general flow patterns during the maximum development of the Quebec-Labrador sector of the ice sheet, but they probably had little effect on the composition of the drift.

Glacial Lakes. During the recession of the ice sheet, proglacial lakes were formed in Lake Superior and adjoining basins. Zoltai (1965) reported that varved sediments deposited in these lakes can be found in depressions along the north shore of Lake Superior to altitudes of at least 250 m above sea level. They attain thicknesses of more than 11 m but average about 3 m. Boissonneau (1966) reported areas of varved clay at altitudes of 300-330 m in the northeastern part of the study area. Ryder (1964) related patterns of alkalinity and total dissolved solids in lake waters of western Ontario to areas of former submergence in glacial lakes or marine waters. According to Boissonneau and Zoltai, however, the occurrence of fine grained water-laid sediments in areas covered by these glacial lakes is spotty and the formerly submerged areas are mainly underlain by till or bedrock.

Drift Composition. Although many types of glacial drift and postglacial sediments occur in the region, most of the study area is covered by grey, sandy till with abundant stones derived from local bedrock. Beneath Lake Superior itself, the till is red and more fine grained, reflecting derivation from hematite - cemented, Hadrynian Jacobsville sandstone that underlies much of the basin (Dell, 1975). According to Dell, late glacial northward flow from the north flank of a Lake Superior glacial lobe carried red, hematite-rich till onto land west of the Sibley Peninsula. It is not known how far north this dispersal extends.

East of Lake Nipigon, the till contains, according to Zoltai (1965, p. 251) "A great number of fossiliferous limestone fragments...", presumably derived from the Paleozoic bedrock of the Hudson Bay Lowland. West of the Nipigon moraine (Fig. 1.2), Zoltai (1965) reported that no carbonate erratics were known to occur. Boissonneau (1966) stated that the northeastern part of the study area, north of Wawa, is covered by sandy till that contains abundant carbonate erratics. Boissonneau (1966, p. 560) aptly summarized the influence of glacially transported carbonate bedrock; "Since ice masses moving from James Bay have transported great quantities of carbonate rocks into the (Boissonneau's) study area, the Paleozoic rocks to the north have had an important influence upon the petrography of the drift materials".

Zoltai (1965, p. 251) measured "... up to 15% calcium in the fine matrix.." in sandy tills. He also noted that tills derived from the Proterozoic "red shale bedrock" north of Lake Superior (presumeably the Rossport Formation of the Sibley Group) contained up to 40% "carbonates." Boissonneau (1966) found that sandy tills occurring in the northeastern part of the present study area contained 15-20% "carbonates."

Ryder (1964) did not mention the effects of the chemical composition of drift on regional lake water alkalinity patterns. He implied that the patterns were related solely to factors associated with marine or lacustrine submergence, but gave no indication of what physical or chemical properties of sediments in the submerged areas

Table 1.2

The Hg, F, As, CaO, MgO, CO_2 and SiO_2 contents of various lithologies, north shore, Lake Superior (52A, 52H(S 1/2), 42D and 42E(S 1/2))

Lithologic Unit (Fig. 1.1)	Age and General Description	Specific Group, Formation or Lithology	N*	Hg (ppb)	F (ppm)	As (ppm)	CaO (%)	MgO (%)	CO_2 (%)	SiO_2 (%)
	PRECAMBRIAN									
	PROTEROZOIC									
	Hadrynian									
11	Sandstone, conglomerate, shale		0							
	Helikian									
10	Carbonatite-alkalic complexes	Praire Lake Carbonatite	2		55 -	0.3 -	53.9 53.3-54.4	0.4 0.2-0.6	42.3 41.8-42.8	1.2 0.8-1.7
		Coldwell Syentic Complex	10		1740 190-3700	2.5 0.3-6.6	4.1 1.2-11.4	2.0 0.1-8.0	0.4 0.0-2.7	55.7 44.8-63.9
9	Diabase		4		180 105-270	0.7(3) 0.3-1.2	9.4 7.9-10.1	9.2 5.6-13.5	0.3 0.0-1.3	49.3 47.8-50.7
8	Volcanic and minor sedimentary rocks	Osler Group	0							
7	Sedimentary rocks(Conglomerate, sandstone,shale,carbonate rocks)	Sibley Group Kama Hill Formation	3	20(1) -	606(4) 390-1155	5.5(2) 2.5-8.5	1.6 1.1-2.1	5.3 2.6-6.9	0.8 0.0-2.4	62.4 57.3-69.2
		Rossport Formation Upper and lower dolomitic member	21	15(4) 5-28	499(25) 61-1825	1.6(14) 0.2-4.6	10.6 0.5-19.8	8.9 0.3-17.7	14.6 0.3-32.1	52.2 23.0-94.2
		Medial chert member	3	5(1) -	138(4) 36-205	0.3(3) 0.2-0.3	18.0 13.0-25.1	7.4 3.6-10.8	19.7 14.9-24.4	51.6 40.2-64.0
		Pass Lake Formation Sandstone member	5		150 81-205	0.6(4) 0.3-1.2	2.1 0.1-8.1	1.2 0.2-2.6	2.0 0.0-7.6	86.1 78.6-94.8
		Conglomeratic member	2	28(1) -	142(3) 77-190	0.8(2) 0.7-0.9	2.1 2.0-2.2	1.3 0.3-2.3	3.2 1.7-4.7	88.0 84.4-91.5
	Aphebian									
6	Sedimentary rocks (Greywacke, shale,argillite,conglomerate), minor volcanics and derived metamorphic rocks.	Animikie Group Rove Formation	3	235(13) 54-568	683(16) 200-1425	16.8(14) 1.8-54.4	0.5 0.3-0.6	3.0 2.6-3.3	0.1 0.1-0.2	65.5 63.9-68.1
		Gunflint Formation	10		1120 41-3700	20.0(1) -	4.0 0.1-9.2	1.8 0.1-4.8	5.6 0.0-27.3	64.6 29.1-94.5
	ARCHEAN									
5	Felsic igneous and metamorphic rocks, migmatitic metasediments	Granite	18		153 55-450	0.5(17) 0.3-1.2	0.4 0.1-1.5	0.6 0.1-1.5	0.0 0.0-0.3	73.2 70.3-75.8
		Quartz monzonite	16		280 85-1065	1.4(11) 0.3-8.5	0.9 0.1-2.7	0.8 0.3-2.2	0.1 0.0-1.0	70.8 59.9-75.5
		Granodiorite	5		153 90-205	0.6(3) -	0.5 0.2-0.6	0.5 0.3-0.8	0.0 0.0-0.1	72.8 70.3-74.2
		Trondhjemite	1		130 -	0.6 -	0.5 -	0.3 -	0.0 -	74.8 -
		Tonalite	1		115 -	0.6 -	1.5 -	0.6 -	0.0 -	69.7 -
		Pegmatite	13		116 68-205	9.3(11) 0.3-96.9	0.5 0.2-1.1	0.4 0.1-1.0	0.0 0.0-0.1	74.9 70.6-82.9
		Granite gneiss	7		154 45-270	0.7(6) 0.3-1.2	1.0 0.3-1.7	1.0 0.2-2.8	0.1 0.0-0.6	71.0 63.2-74.2
		Migmatitic metasediments	2		250 230-270	0.6 0.3-0.8	3.2 3.1-3.2	2.2 1.6-2.8	0.3 0.0-0.6	63.3 61.4-65.2
3	Metasediments and metavolcanics	Metasedimentary rocks	7		259 60-450	5.6(6) 0.6-24.6	2.0 1.1-2.4	3.0 2.3-3.8	0.0 0.0-0.1	64.3 61.3-68.2
1	Metavolcanics and metasediments	Metavolcanic rocks	2		185 125-245		3.2 1.5-4.8	2.6 1.2-4.0	1.7 0.1-3.2	65.8 64.3-67.2

606 - Arithmetic mean
390-1155 - Range (minimum - maximum)

N* = Number of Samples
* If the number of samples for any individual parameter differs from the total it is indicated in brackets beside the arithmetic mean (i.e. 606 (4)).

Table 1.3

A comparison of the pH and fluorine content of lake waters, and of the mercury and arsenic contents of lake sediments from northwestern Manitoba, north shore of Lake Superior and southeastern Ontario

	Lake Water		Lake Sediments		
Area (N.T.S.)	pH	F (ppb)	Hg (ppb)	As (ppm)	Reference
Northwestern Manitoba (64 J, K, N, O)	6.8(0.5) - 4.2-8.2 (1111)	177(266) 108(0.403) 20-2440 (852)	43(22) 37(0.244) 5-190 (3661)	1.2(6.8) 0.8(0.290) 0.5-400.0 (3661)	pH and F (Coker, 1976) Hg and As (Hornbrook et al, 1976a,b,c,d)
North Shore of Lake Superior (52 A, H; 42 C, D, E, F; and 41 K, N)	6.9(0.6) - 3.1-8.3 (4293)	45(24) 42(0.152) 10-760 (4293)	133(58) 122(0.193) 20-710 (1816)	0.9(2.7) 0.6(0.263) 0.5-150.0 (4293)	Geological Survey of Canada (1978a,b, and 1979a,b)
Southeastern Ontario (31 C, F)	6.6(0.7) - 3.9-8.1 (352)	77(54) 65(0.244) 21-359 (298)	94(54) 76(0.314) 10-580 (1250)	1.5(4.0) 0.9(0.350) 0.5-80.0 (1250)	pH and F (Coker and Closs, 1979) Hg and As (Geological Survey of of Canada, 1977a, b)

177(266) - Arithmetic mean (Standard Deviation)
108(0.403) - Geometric mean ($\log_{10}$ Standard Deviation)
20-2440 - Range (minimum - maximum)
(852) - Number of samples

pH : Northwestern Manitoba and southeastern Ontario pH measured in situ using a Matek Mark V Water Quality Analyzer. North shore of Lake Superior pH measured using a glass-calomel combination electrode.
F : Selective ion electrode.
Hg : Hatch and Ott procedure (Jonasson et al, 1973).
As : Northwestern Manitoba, north shore of Lake Superior (west half of area only) and southeastern Ontario As measured by colorimetry. North shore of Lake Superior (east half) As determined by atomic absorption-hydride generation (Aslin, 1976).

could have influenced alkalinity or concentrations of dissolved solids. It seems to the present authors that the pockets or sheets of fine grained lacustrine sediments in former areas of submergence would be subject to more erosion than other types of drift and would cause heavier sediment loads in the modern drainage systems. As this fine grained detritus is calcareous, being originally derived from calcareous glacial debris, much of it may dissolve causing disproportionate effects on alkalinity and concentrations of dissolved solids.

Zoltai (1965) analyzed a number of samples of varved sediments for carbonate content, finding them to contain 16-20 per cent "carbonates" by weight within the study area. Since it is not known by what method the carbonate analyses of Boissonneau and Zoltai were accomplished nor on what specific textural fraction the analyses were performed, not much can be concluded about the buffering capacity of the lake sediments or tills, other than to say that the tills are exceptionally carbonate rich in comparison to "normal" sandy tills of the Canadian Shield.

The present authors have analyzed the carbonate content of the 63μm to 44μm fraction of unweathered till samples from boreholes drilled by the Polar Gas Consortium just north of the study area. Total carbonate was determined with a Leco carbon analyzer using a method described by Foscolos and Barefoot (1970). The results of these analyses (depicted on Fig. 1.2) give some idea of how carbonate content of this fraction varies with increasing distance down ice from the Paleozoic carbonate terrane. For comparison, analyses of the same fraction of till from three boreholes in the area of Paleozoic outcrop in northeastern Manitoba yielded total carbonate contents of 10 to 17 per cent with a mean of 15 per cent (11 samples).

Geochemical Distribution Patterns of Lake Water and Lake Sediment Samples

pH of Lake Waters

There is documentation of the incidence of acid precipitation and the subsequent acidification of freshwater lakes within Ontario, specifically in the vicinity of Sudbury (Gorham and Gordon 1960; Conroy et al., 1975; Beamish and Van Loon, 1977) and south-central Ontario (Dillon et al., 1978; Scheider et al., 1979 and Jeffries et al., 1979). However, there is to date no documentation of acidification of lakes within Ontario west of Sudbury.

The east shore of Lake Superior is at times subjected to surface winds (Bryson, 1966) that pass through the east-central U.S.A., the dominant source of sulphur dioxide and nitrogen oxide emissions in North America (Voldner and Shah, 1979). Likens (1976) illustrated that whereas the east shore of Lake Superior received precipitation with weighted annual average pH greater than 5.6 in 1955-56 (5.6 being the value for "clean" precipitation in equilibrium with atmospheric carbon dioxide), it received precipitation with weighted annual average pH varying between 4.5 and 5.0 in 1972-73. Shaw (1979) also has demonstrated that high aerosol sulphate concentrations in the Great Lakes area (as high as 5 to 15 $\mu g/m^3$ along the east shore of Lake Superior) are being

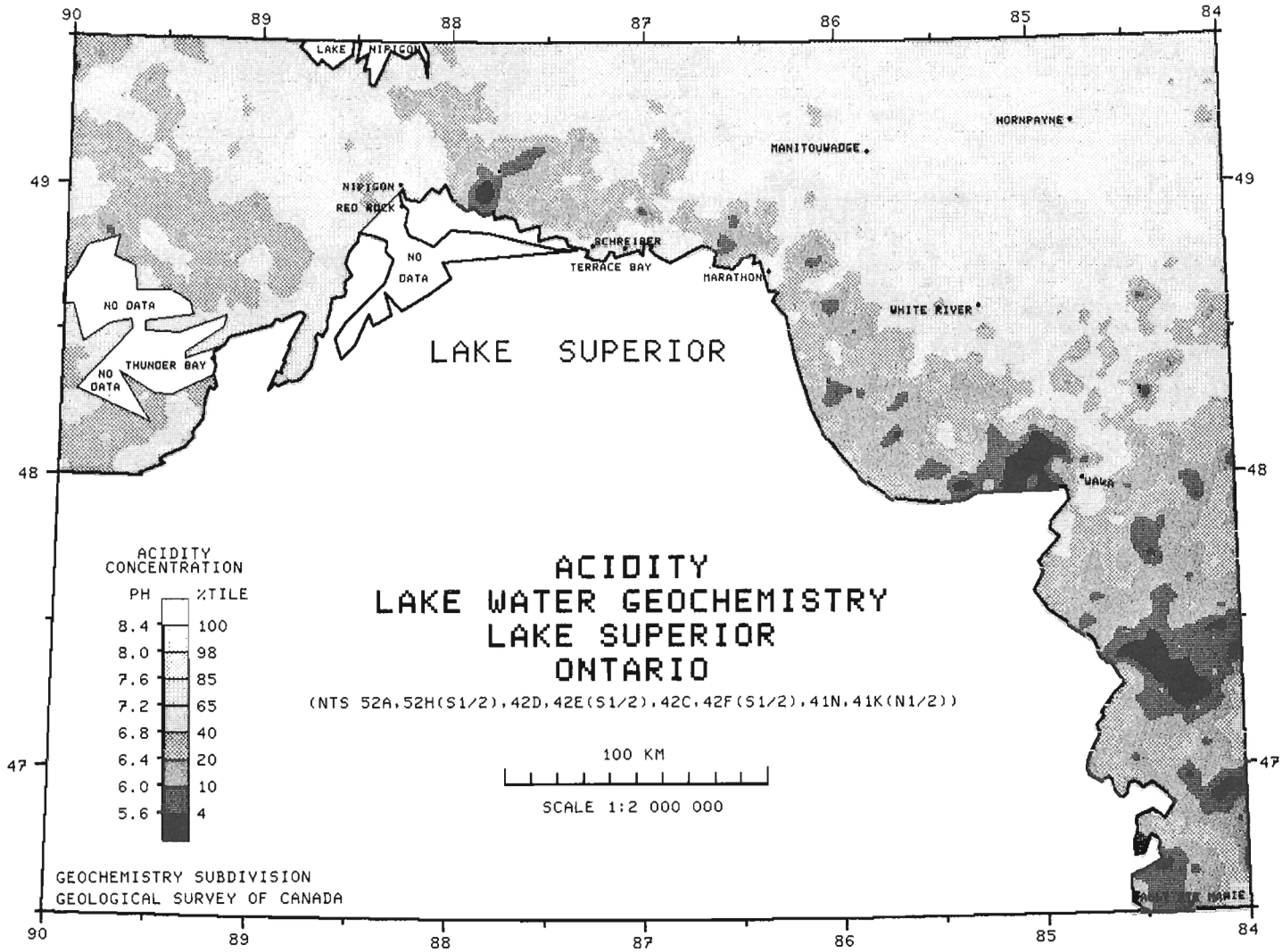

Figure 1.3. *Lake water acidity (pH), north shore, Lake Superior, Ontario.*

transported by wind and deposited by precipitation as far east as the Maritime provinces. It is evident, therefore, that the east shore of Lake Superior receives acid precipitation.

The determination of the pH of surface lake waters around the north shore of Lake Superior gives an estimate of the present degree of acidification of lakes within this region (Fig. 1.3). The pH of the surface lake waters within the survey area varies from 3.1 to 8.3, averaging 6.9 (Table 1.1). The variations in pH are the result of the combined effects of natural and anthropogenic factors.

North of Lake Superior, pH is governed by the same three factors that Kramer (1975) cited for lakes of the Sudbury area: (a) the rate of input of strong acid; (b) the location of the lake relative to the prevailing winds, which can modify (a); and (c) the geochemistry of the surficial sediments and bedrock, which determines the buffering capacity of the lake and the runoff waters entering it.

The Lake Superior survey area is primarily underlain by siliceous bedrock (Table 1.2, Fig. 1.1). In other areas of the Canadian Shield with similar siliceous bedrock, such as northwestern Manitoba and southeastern Ontario, surface lake waters average neutrality (pH=7.0) (Table 1.3). The main differences between the other areas and the north shore of Lake Superior are: (1) the localization of groups of acid lakes, primarily along the east shore of Lake Superior (2) the higher incidence of more severely depressed pH values, to a minimum of 3.1, in surface lake waters; and (3) the large region of alkaline lakes in the northeastern part of the area (Fig. 1.3, Table 1.3).

Within the survey area there is similar bedrock on the east shore of Lake Superior and immediately north and northwest of Thunder Bay (Fig. 1.1). However, surface lake waters from the east shore of Lake Superior are the most acid within the survey area, whereas those north and northwest of Thunder Bay are generally neutral to slightly acid (Fig. 1.3), the common range of surface water pH for lakes associated with siliceous bedrock. The pH of the highly acidified lakes on the east shore of Lake Superior has possibly been depressed as a result of acid precipitation (i.e. directly equatable to Kramer's (a) and (b) factors, as earlier described and as documented for the east shore of Lake Superior (Bryson, 1966; Likens, 1976; Voldner and Shah, 1979; and Shaw, 1979)).

Northeasterly trending reentrants of acid surface lake waters into the area of alkaline surface lake waters, east of Nipigon-Red Rock, at Schreiber-Terrace Bay and at Marathon may be related to pulp and paper manufacturing operations in these centres.

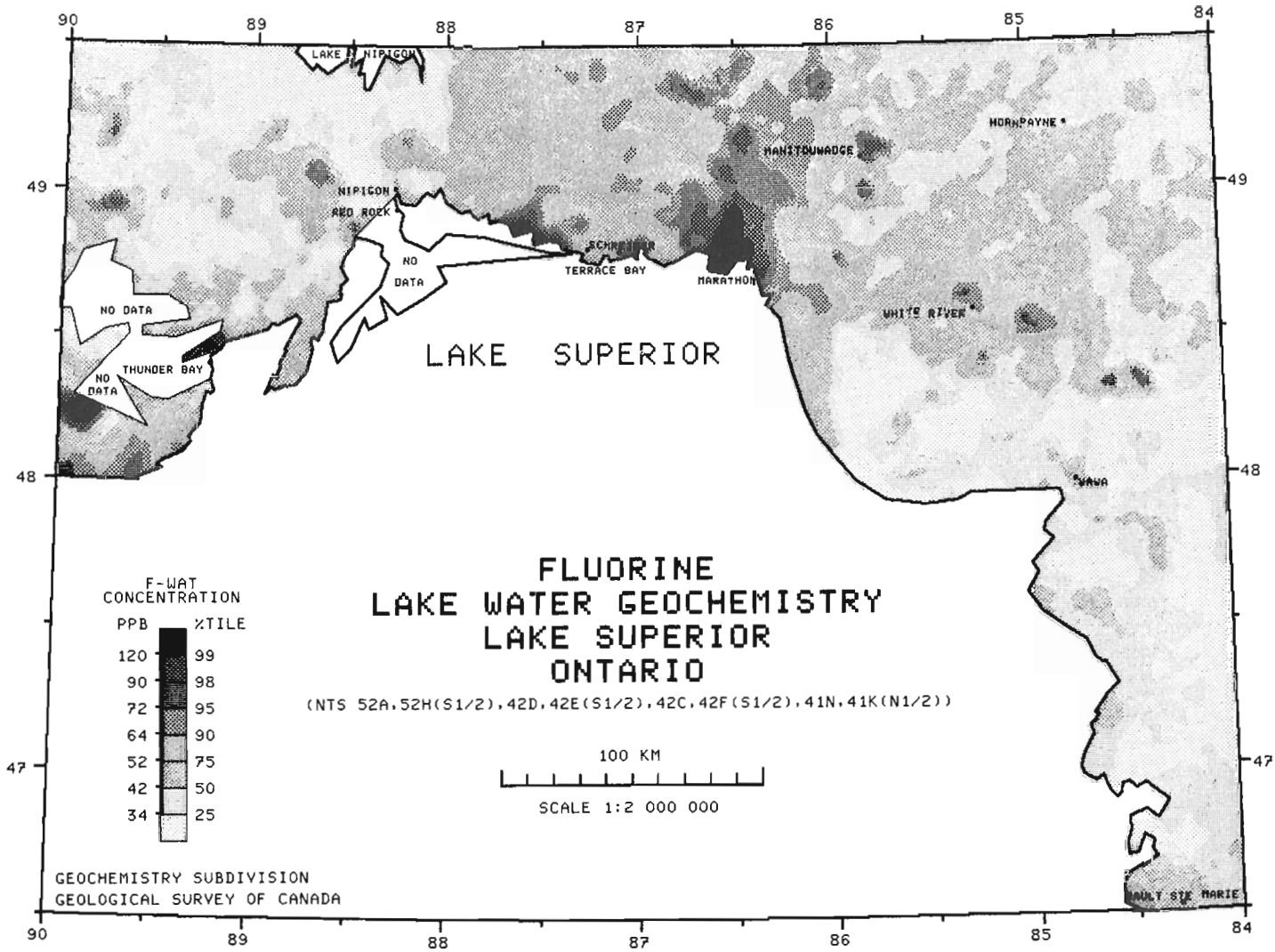

Figure 1.4. *The distribution of fluorine in lake waters, north shore, Lake Superior, Ontario.*

Kramer (1975) suggested (factor c) that calcareous surficial sediments and/or bedrock lithologies can assimilate hydrogen ions and continuously buffer local waters, thereby overriding all other factors affecting pH. This phenomenon is illustrated by the large area of relatively alkaline surface lake water extending from just east of Lake Nipigon to the northeast corner and centre of the eastern border of the survey area (Fig. 1.3). This area is underlain by calcareous "drift" (till and proglacial lake sediments). The carbonate component has been transported southerly and southwesterly, from the Paleozoic bedrock that forms the Hudson Bay basin and adjoining lowlands, several hundred kilometres out onto the Canadian Shield. The alkaline nature of the surface lake waters in this part of the area is indicative of the capacity of the calcareous drift to buffer them and suggests their enhanced tolerance to acid precipitation, compared with other Shield areas.

Carbonate-bearing bedrock (Table 1.2) within the survey area has a definite buffering effect on the waters of lakes located on it. A region of relatively neutral to alkaline surface lake waters northeast of Thunder Bay and both east and west of Nipigon - Red Rock (Fig. 1.3) is underlain by the Sibley Group (Fig. 1.1, Unit 7), in particular its carbonate members (Table 1.2). Along the east shore of Lake Superior most surface lake waters are acid with the exception of an area trending northeasterly from Wawa in which lakes are underlain by carbonate (as well as minor sulphide and oxide) facies iron formations (Fig. 1.1, *22). In both these areas the pH of the surface lake waters is a reflection of the buffering capacities of the associated bedrock lithologies.

Fluorine in Lake Waters

Variation in the fluorine content of surface lake waters around the north shore of Lake Superior is depicted in Figure 1.4. The north shore of Lake Superior is characterized by relatively low average fluorine concentrations in surface lake waters compared with northwestern Manitoba and southeastern Ontario (Table 1.3).

Within the survey area elevated fluorine contents in surface lake waters (Fig. 1.4) are directly correlative with high average fluorine contents in specific bedrock lithologies (Table 1.2). At Marathon high fluorine is related to the Coldwell alkali syenitic complex (Fig. 1.1, *18); southwest of Thunder Bay relatively elevated fluorine contents are associated with the Rove and Gunflint formations of the Animikie Group (Fig. 1.1, Unit 6); west of Schreiber high fluorine probably reflects the fluorite that occurs in veins in granite near Rossport (Fig. 1.1.); and, northeast and northwest of Nipigon - Red Rock elevated fluorine is associated with the Kama Hill and Rossport formations of the Sibley Group (Fig. 1.1, Unit 7).

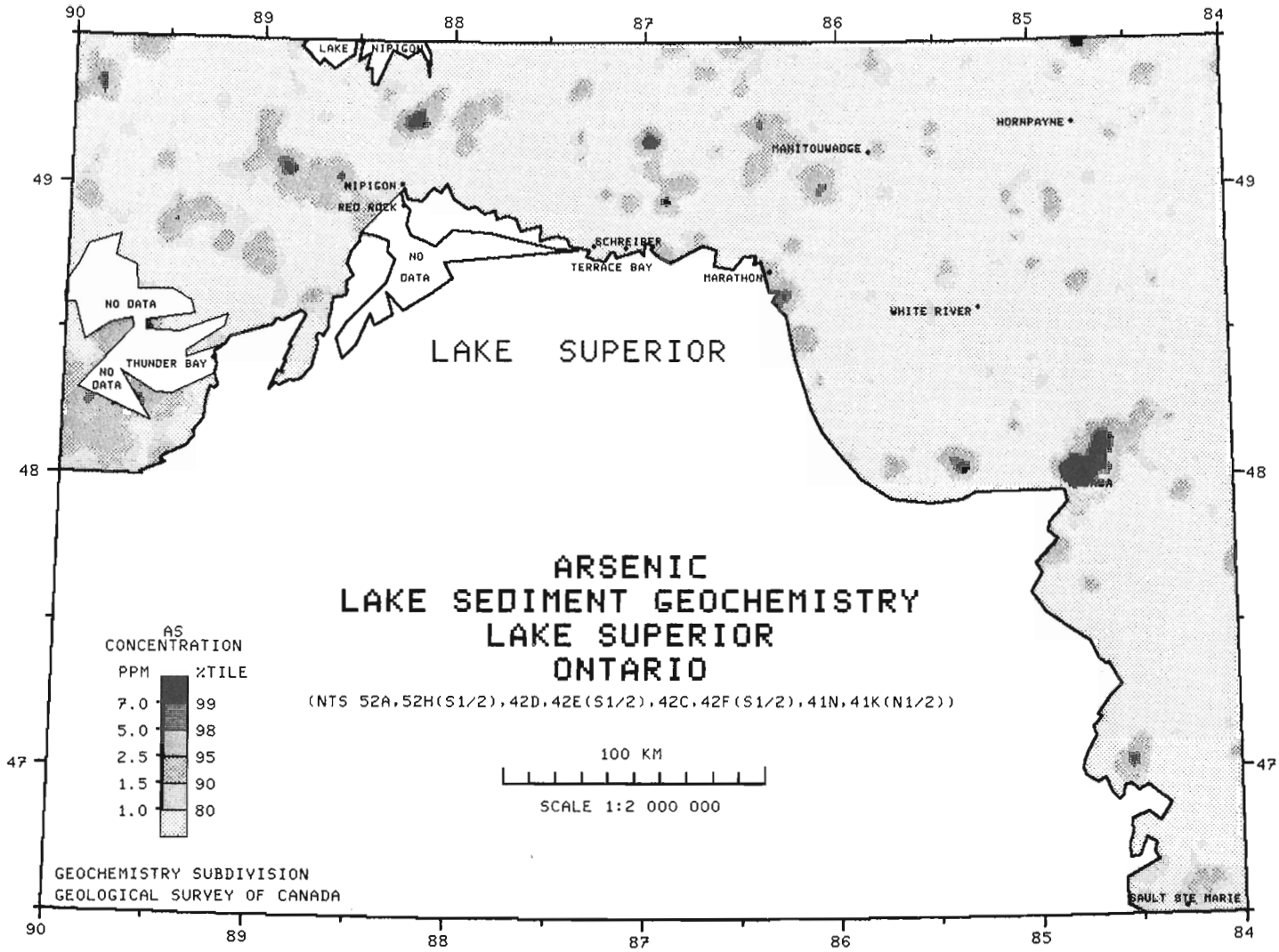

Figure 1.5. *The distribution of arsenic in lake sediments, north shore, Lake Superior, Ontario.*

There is a moderate positive correlation (Fig. 1.7) between fluorine and pH (ie. alkaline) in surface lake waters (Fig. 1.3, 1.4). This association possibly explains the relatively elevated fluorine contents of lakes over certain carbonate lithologies, such as the carbonate members of the Sibley Group around Nipigon-Red Rock (Fig. 1.1, Unit 7) and the carbonatite bodies north of Marathon (Fig. 1.1, Unit 10). Although variations in drift types and thicknesses may also exert some influence on fluorine patterns, such as the relatively enhanced fluorine levels in surface lake waters around White River, an area of granitic (pegmatitic) bedrock overlain by calcareous drift, there are no obvious relationships in the data.

Arsenic in Lake Sediments

As previously discussed, the analytical method for the determination of arsenic in lake sediments varied between the east (atomic adsorption-hydride generation) and west (colorimetry) halves of the survey area. Statistical computations carried out on the arsenic contents of the total, east half (east of 86°) and west half (west of 86°) lake sediment populations are summarized as follows:-

	Total	West (1977)	East (1978)
Range (minimum-maximum)	0.5-150.0	0.5-30.0	0.5-150.0
Arithmetic mean	0.9	1.0	0.8
Standard deviation	2.7	1.7	3.4
Coefficient of Variation	300	161	397
Geometric mean	0.6	0.7	0.6
$\log_{10}$ Standard deviation	0.263	0.296	0.228
Number of Samples	4293	1833	2460

As 80 per cent (Fig. 1.5) of the arsenic data lies at or below the detection limit for both analytical methods (1.0 ppm), the extraction method used is only of significance for comparing values of samples containing more than 1.0 ppm. Therefore, even though the arsenic contents of lake sediments from the east half of the survey area show more variation (i.e. larger range, standard deviation and coefficient of variation) than those from the west half, all lake sediments with arsenic levels above 1.0 ppm should be regarded as significant, with the realization that the arsenic levels (>1.0 ppm) in the west are only partial levels, relative to those in the east.

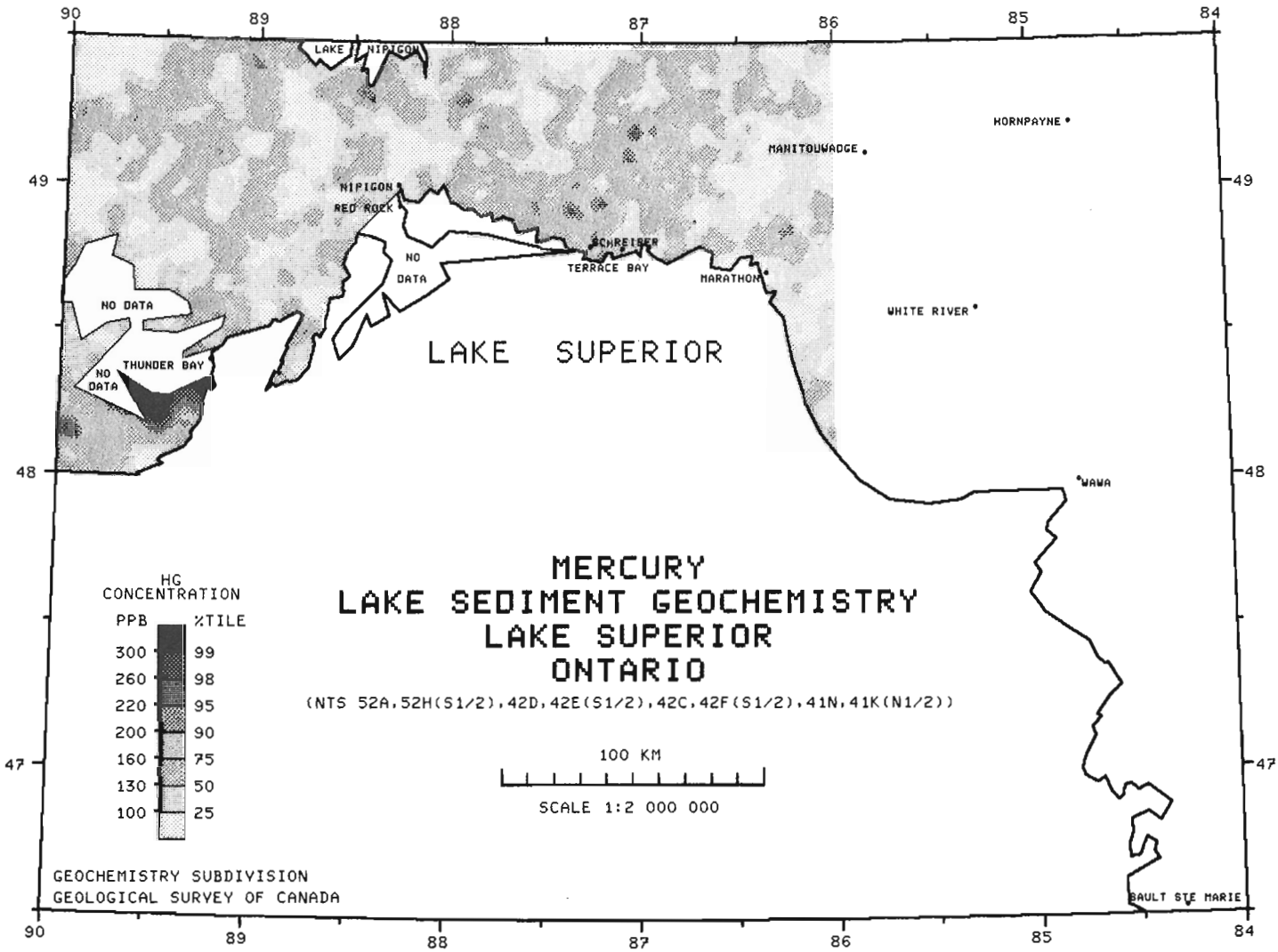

Figure 1.6. *The distribution of mercury in lake sediments, north shore, Lake Superior, Ontario.*

The arsenic contents of lake sediments around the north shore of Lake Superior (Fig. 1.5), are relatively lower, on average, than in northwestern Manitoba or southeastern Ontario (Table 1.3).

Elevated contents of arsenic in lake sediments (Fig. 1.5) appear to be related to bedrock lithologies (Table 1.2) and/or to sulphide mineralization known to be associated with elevated arsenic concentrations, such as: the iron formations at Wawa (Fig. 1.1, *22); the Rove and Gunflint formations of the Animikie Group (Fig. 1.1, Unit 6), west and southwest of Thunder Bay; the Kama Hill Formation of the Sibley Group (Fig. 1.1, Unit 7), west of Nipigon - Red Rock; and various sulphide and gold occurrences, as well as specific arsenic-bearing Archean pegmatites (Fig. 1.1, Unit 5) and metasedimentary rocks, (Fig. 1.1, Unit 3) throughout the survey area.

There is a definite correlation among the arsenic, iron and manganese contents of lake sediments (Fig. 1.7). The hydrous oxides of iron and manganese are known to be scavengers of many trace elements (i.e. Co, Ni, Zn, As) within the lacustrine environment of this region (Coker et al., in press). Some of the elevated arsenic contents in lake sediments are undoubtedly related to this scavenging phenomenon, but for scavenging to occur, a source of arsenic, iron and/or manganese must be coincident with suitable limnological conditions.

Mercury in Lake Sediments

The distribution of mercury in lake sediments within the west half of the survey area is illustrated in Figure 1.6. Mercury in lake sediments around the north shore of Lake Superior is appreciably higher than in northwestern Manitoba or southeastern Ontario (Table 1.3). This is primarily the result of the influence of elevated levels of mercury in the Rove Formation of the Animikie Group (Fig. 1.1, Unit 6; Table 1.2), as reflected by elevated levels of mercury in lake sediments southwest of Thunder Bay (Fig. 1.6). Elevated mercury in lake sediments also appears to be related to some of the sulphide and gold occurrences, as well as to some of the Helikian intrusions (Fig. 1.1, Units 9 and 10), within the survey area.

Mercury is correlated with loss-on-ignition (L.O.I.) and with Cu, Ni, Zn and Co in lake sediments within the survey area (Fig. 1.7). The association of Hg (and Zn) with loss-on-ignition (L.O.I.) illustrates the affinity of these elements for organic matter within the lacustrine environment. The association of Hg with Cu, Ni, Zn and Co is a reflection of the association of these elements within certain bedrock lithologies such as Rove Formation of the Animikie Group and some of the Helikian intrusions within the survey area (see Coker et al., in prep.)

A

		water			sediment												
		pH	F	U	L.O.I.	U	*Hg	Fe	Mo	As	Mn	Ag	Co	Ni	Pb	Cu	Zn
sediment	Zn	-.19	-.06	-.17	.38	.12	.42	.32	.16	.08	.23	.18	.50	.46	.21	.45	
	Cu	-.00	-.10	-.14	.21	.07	.41	.30	.27	.16	.21	.21	.47	.63	-.05		
	Pb	-.24	.04	.09	-.08	.15	.17	.08	-.12	.07	.07	.12	.15	.06			
	Ni	-.04	.00	-.18	.04	-.01	.33	.41	.09	.18	.27	.16	.66				
	Co	-.11	-.03	-.08	-.14	.10	.28	.68	.04	.21	.61	.13					
	Ag	-.05	.02	-.01	-.00	.03	.21	.13	.10	.13	.10						
	Mn	.19	.06	-.01	-.40	.01	.05	.81	.08	.32							
	As	.15	.06	.01	-.17	-.01	-.05	.34	.11								
	Mo	.10	.15	-.02	.20	.11	.05	.07									
	Fe	.15	.02	-.02	-.33	.03	.09										
	*Hg	-.23	-.05	-.15	.35	.08											
	U	-.08	.23	.61	.04												
	L.O.I.	-.15	-.08	-.15													
water	U	.15	.28														
	F	.28															
	pH																

n= 4293 (*Hg = 1816)

(- indicates a negative correlation)

B

·····>0.3 <0.5
----->0.5 <0.7
——>0.7

(a bar over the parameter indicates a negative correlation)

Figure 1.7. *Correlation matrix (A) and schematic representation (B) of the significant chemical associations in the lake waters and lake sediments from the north shore of Lake Superior, Ontario.*

Discussion and Conclusions

The examples of variation of pH, F, As and Hg in modern lakes around the north shore of Lake Superior illustrate the strong and predictable influence of geology on patterns of chemical variation. Data on these four chemical parameters are presented here as an example of the type of geological information that can be brought to bear on evaluation of the nature and extent of anthropogenic modifications of natural chemical systems. For instance, knowing the areas north of Lake Superior where F, Hg and As are naturally enhanced in lakes (and most probably in associated soils) allows some predictions to be made about areas where these toxic substances may become dangerous in an "acidified" landscape. Arsenic and mercury in lake sediments and adjacent soils are likely bound in stable forms under present natural environmental conditions, i.e. they are in relative equilibrium with their natural environment. Significant decreases in soil and/or water pH may upset this natural equilibrium and could possibly release these and other metals into streams, rivers, lakes, groundwaters, etc. in potentially noxious forms, for eventual uptake by vegetation and terrestial or aquatic organisms (Beamish and Van Loon, 1977; Scheider et al., 1979).

Figures 1.3 through 1.6 illustrate that many of the details of the geochemical variation of lake sediments and lake waters are related to the chemical characteristics of bedrock in or adjacent to the lake's drainage basin. For example, elevated mercury contents of lake sediments southwest of Thunder Bay are clearly related to abnormal levels of mercury in the Rove Formation; high arsenic near

Wawa reflects the elevated arsenic contents of the iron formations mined there; locally alkaline pH in lakes northeast and northwest of Nipigon-Red Rock is related to calcareous strata of the Sibley Group.

Superimposed on these local variations, correlative with bedrock, are the buffering effects (and unknown trace element chemical variations) caused by glacial dispersal of carbonate erratics southward and southwestward from the Hudson Bay Lowland. This glacial event has spread a sheet of calcareous drift over much of the study area. Although it is not known at what rate this carbonate detritus was diluted during glacial transport by non-calcareous, locally derived debris, it can be assumed that the drift of the northeastern part of the study area has the highest carbonate contents and, therefore, should have the greatest potential for buffering lakes lying on it. Perturbations in the general pattern of carbonate dispersal could be caused by 1) late glacial lobations, which may have redistributed drift along flow directions related to topography or glacial surging, 2) lack of significant drift cover either where waves of proglacial lakes have removed drift, or where drift is thin or patchy over Precambrian highlands, 3) derivation of carbonate-rich debris from local Precambrian bedrock sources, such as the Sibley Group, 4) cover by thick, non-calcareous post or late-glacial fluvial or wind-blown sediments, such as outwash or loess which are known to reach significant thicknesses in some parts of the study area, or 5) derivation of carbonate-rich debris from lacustrine clayey silts, which are relatively susceptible to fluvial erosion and can produce relatively high concentrations of (calcareous) dissolved solids because of their fine grain size and potential for high sediment loading of drainage systems.

From the above discussions two major conclusions may be drawn:-

(1) Variations of pH of lake waters can be predicted to some extent on the basis of a knowledge of glacial and bedrock geology. Variations of pH related to the natural geological environment can be significant over a region.

(2) Knowledge of natural patterns of elevated metal concentrations in lake sediments and soils can be used to "pinpoint" locations where pH reduction as a result of anthropogenic acid precipitation can release potentially noxious components into drainage systems, and into the surficial environment in general.

Acknowledgments

A request by R.G. Skinner (Coordinator, Office of Environmental Affairs, Department of Energy, Mines and Resources) for relevant G.S.C. data pertaining to acid precipitation was instrumental in initiating this article. Computer plotted pH and element distribution maps were prepared with the assistance of D.J. Ellwood. Many helpful discussions were had with J.M. Franklin on the regional geology and metallogeny of the Lake Superior area. This paper was critically read by R.N.W. DiLabio and B.W. Smee.

References

Annells, R.N.
1973: Proterozoic flood basalts of eastern Lake Superior: The Keweenawan volcanic rocks of the Mamainse Point area, Ontario; Geological Survey of Canada, Paper 72-10, p. 51.

Aslin, G.E.M.
1976: The determination of arsenic and antimony in geological materials by flameless atomic absorption spectrometry; Journal of Geochemical Exploration, v. 6, no. 3, p. 321-330.

Ayres, L.D., Lumbers, S.B., Milne, V.G., and Robeson, D.W.
1971a: Ontario Geological Map, East Central Sheet; Ontario Department of Mines, Map 2198.

1971b: Ontario Geological Map, West Central Sheet; Ontario Department of Mines, Map 2199.

Beamish, R.J. and Van Loon, J.C.
1977: Precipitation loading of acid and heavy metals to a small acid lake near Sudbury, Ontario; Journal of the Fisheries Research Board of Canada, v. 34, no. 5, p. 649-658.

Blackadar, R.G.
1956: Differentiation and assimilation in the Logan Sills, Lake Superior District, Ontario; American Journal of Science, v. 254, p. 623-645.

Boissonneau, A.N.
1966: Glacial history of northeastern Ontario, I. The Cochrane - Hearst area; Canadian Journal of Earth Sciences, v. 3, p. 559-578.

Boulanger, A., Evans, D.J.R., and Raby, B.F.
1975: Uranium analysis of neutron activation delayed neutron counting; Proceedings 17th Annual Symposium of the Canadian Mineral Analysts, Thunder Bay, Ontario, Sept. 22-23, 1975.

Bryson, R.A.
1966: Air masses, streamlines, and the Boreal Forest; Geographical Bulletin, v. 8, no. 3, p. 228-269.

Card, K.D., Church, W.R., Franklin, J.M., Frarey, J.J., Robertson, J.A., West, G.F., and Young, C.M.
1972: The Southern Province; in Variations in Tectonic Styles in Canada; R.A. Price and R.J.W. Douglas, ed.; Geological Association of Canada, Special Paper 11, p. 335-380.

Coker, W.B.
1976: Geochemical follow-up studies, northwestern Manitoba; in Report of Activities, Part C, Geological Survey of Canada, Paper 76-1C, p. 263-267.

Coker, W.B. and Closs, L.G.
1979: Detailed geochemical studies, southeastern Ontario; in Current Research, Part A, Geological Survey of Canada, Paper 79-1A, p. 247-252.

Coker, W.B. and Nichol, I.
1975: The relation of lake sediment geochemistry to mineralization in the northwest Ontario region of the Canadian Shield; Economic Geology, v. 71, no. 5, p. 955-963.

Coker, W.B., Hornbrook, E.H.W., and Cameron, E.M.
Lake sediment geochemistry applied to mineral exploration; in Geophysics and Geochemistry in the search for Metallic Ores; Peter J. Hood, ed; Geological Survey of Canada, Economic Geology, Report 31. (in press)

Coker, W.B., Franklin, J.M., Shilts, W.W. and Ellwood, D.J.
Interpretation of the compiled regional geochemical lake sediment and lake water data, north shore, Lake Superior, Ontario; Geological Survey of Canada (in prep)

Conroy, N., Hawley, K., Keller, W. and Lafrance, C.
1975: Influence of the atmosphere on lakes in the Sudbury area; Proceedings of the First Special Symposium on atmospheric contributions to the chemistry of lake waters, International Association of Great Lakes Research, p. 146-165.

Darnley, A.G., Cameron, E.M., and Richardson, K.A.
1975: The Federal-Provincial uranium reconnaissance programs; in Uranium Exploration 1975; Geological Survey of Canada, Paper 75-26, p. 49-68.

Dell, C.I.
1975: Relationships of till to bedrock in the Lake Superior region; Geological Society of America, Geology, p. 563-564.

Dillon, P.J. Jeffries, D.S., Snyder, W., Reid, R., Yan, N.D., Evans, D., Moss, J., and Scheider, W.A.
1978: Acidic precipitation in south-central Ontario: recent observations; Journal of the Fisheries Research Board of Canada, v. 35, no. 6, p.809-815.

Franklin, J.M.
1978: Uranium mineralization in the Nipigon area, Thunder Bay District, Ontario; in Current Research, Part A, Geological Survey of Canada, Paper 78-1A, p. 275-282.

Foscolos, A.E. and Barefoot, R.R.
1970: A rapid determination of total organic and total inorganic carbon in shales and carbonates: A rapid determination of total sulphur in rocks and minerals; Geological Survey of Canada, Paper 70-11, 14 p.

Geological Survey of Canada
1977a: Regional lake sediment geochemical reconnaissance data, eastern Ontario, NTS 31C (N 1/2); Geological Survey of Canada, Open File 405.

1977b: Regional lake sediment geochemical reconnaissance data, eastern Ontario, NTS 31F; Geological Survey of Canada, Open File 406.

1978a: Regional lake sediment and water geochemical reconnaissance data, Ontario 1977, NTS 42D, 42E (S 1/2); Geological Survey of Canada, Open File 506.

1978b: Regional lake sediment and water geochemical reconnaissance data, Ontario 1977, NTS 52A, 52H (S 1/2); Geological Survey of Canada, Open File 507.

1979a: Regional lake sediment and water geochemical reconnaissance data, Ontario 1978, NTS 41K (N 1/2), 41N; Geological Survey of Canada, Open File 554.

1979b: Regional lake sediment and water geochemical reconnaissance data, Ontario 1978, NTS 42C, 42F (S 1/2); Geological Survey of Canada, Open File 555.

Goodwin, A.M.
1964: Genetic aspects of Michipicoten iron Formations; Canadian Institute of Mining and Metallurgy, Transactions, v. 64, p. 24-28.

1972: The Superior Province; in Variations in Tectonic Styles in Canada; R.A. Price and R.J.W. Douglas, ed.; Geological Association of Canada, Special Paper 11, p. 527-623.

Gorham, E. and Gordon, A.G.
1960: The influence of smelter fumes upon the chemical composition of lake waters near Sudbury, Ontario and upon surrounding vegetation; Canadian Journal of Botany, v. 38, p. 477-487.

Guel, J.J.C.
1970: Geology of Devon and Pardee Townships and the Stuart Location; Ontario Division of Mines, Geological Report 87, 52 p.

Hornbrook, E.H.W. and Garrett, R.G.
1976: Regional geochemical lake sediment survey east-central Saskatchewan; Geological Survey of Canada, Paper 75-41, 20 p.

Hornbrook, E.H.W., Garrett, R.G., and Lynch, J.J.
1976a: Regional lake sediment geochemical reconnaissance data, north-central Manitoba, NTS 64J; Geological Survey of Canada, Open File 320.

1976b: Regional lake sediment geochemical reconnaissance data, northwestern Manitoba, NTS 64K; Geological Survey of Canada, Open File 321.

1976c: Regional lake sediment geochemical reconnaissance data, northwestern Manitoba, NTS 64N; Geological Survey of Canada, Open File 322.

1976d: Regional lake sediment geochemical reconnaissance data, north-central Manitoba, NTS 64O; Geological Survey of Canada, Open File 323.

Jeffries, D.S., Cox, C.M., and Dillon, P.J.
1979: Depression of pH in lakes and streams in central Ontario during snowmelt; Journal of the Fisheries Research Board of Canada, v. 36, no. 6, p. 640-646.

Jonasson, I.R., Lynch, J.J., and Trip, L.J.
1973: Field and laboratory methods used by the Geological Survey of Canada in geochemical surveys: No. 12, Mercury in ores, rocks, soils, sediments and water; Geological Survey of Canada, Paper 73-21.

Kramer, J.R.
1975: Geochemical and lithological factors in acid precipitation; Proceedings of the First International Symposium on acid precipitation and the forest ecosystem: United States Forest Service General Technical Report, NE 23:611-618.

Kustra, C.R., McIlwaine, W.H., Fenwick, F.G. and Scott, J.
1977: Proterozoic rocks of the Thunder Bay area, northwestern Ontario; Guidebook, Institute on Lake Superior Geology, 23rd Annual Meeting, Lakehead University, Thunder Bay, Ontario.

Likens, G.E.
1976: Acid precipitation; Chemical Engineering News, v. 54, p. 29-44.

Mitchell, R.H. and Platt, R.G.
1977: The Port Coldwell Complex; Guidebook, Institute on Lake Superior Geology, 23rd Annual Meeting, Lakehead University, Thunder Bay, Ontario.

Moorhouse, W.W.
1960: Gunflint Iron Range in the vicinity of Port Authur; Ontario Department of Mines, Annual Report, v. 69, pt. 7, p. 1-40.

Prest, V.K.
1970: Quaternary Geology of Canada; in Geology and Economic Minerals of Canada, R.J.W. Douglas, ed.; Geological Survey of Canada, Economic Geology Report 1, p. 676-764.

Ryder, R.A.
1964: Chemical characteristics of Ontario lakes as related to glacial history; Transactions of American Fisheries Society, v. 93. p. 260-268.

Sage, R.P.
1975: Carbonatite-Alkalic Complexes; in Summary of Field Work, 1975; V.G. Milne, D.F. Hewitt, K.D. Card and J.A. Robertson, ed.; Ontario Division of Mines, Miscellaneous Report 63, p. 58-66.

Sage, R.P. (cont'd)
1977: Carbonatite-Alkalic Complexes; in Summary of Field Work, 1977; V.G. Milne, O.L. White, R.B. Barlow, and J.A. Robertson, ed.; Ontario Geological Survey, Miscellaneous Report 75, p. 69-79.

Scheider, W.A., Jeffries, D.S., and Dillon, P.J.
1979: Effects of acidic precipitation on Precambrian freshwater in southern Ontario; Journal of Great Lakes Research, v. 5, no. 1, p. 45-51.

Shaw, R.W.
1979: Acid precipitation in Atlantic Canada; Environmental Science and Technology, v. 13, no. 4, p. 406-411.

Shilts, W.W., Cunningham, C.M., and Kaszycki, C.A.
The Keewatin ice sheet-reevaluation of the traditional concept of the Laurentide Ice Sheet; Geological Society of America, Geology. (in press)

Skinner, R.G.
1973: Quaternary stratigraphy of the Moose River Basin, Ontario; Geological Survey of Canada, Bulletin 225, 77 p.

Springer, Janet
1977a: Ontario Mineral Potential, Blind River Sheet and Part of Sault Ste. Marie Sheet, Districts of Algoma, Sudbury, and Manitoulin; Ontario Geological Survey, Preliminary Map P.1513, Mineral Deposits Series.

1977b: Ontario Mineral Potential, Michipicoten Sheet, Districts of Algoma and Thunder Bay; Ontario Geological Survey, Preliminary Map P. 1516, Mineral Deposits Series.

Springer, Janet (cont'd)
1977c: Ontario Mineral Potential, White River Sheet, Districts of Algoma and Thunder Bay; Ontario Geological Survey, Preliminary Map P. 1519, Mineral Deposits Series.

1978a: Ontario Mineral Potential, Schreiber Sheet, District of Thunder Bay; Ontario Geological Survey, Preliminary Map P. 1520, Mineral Deposits Series.

1978b: Ontario Mineral Potential, Thunder Bay Sheet, District of Thunder Bay; Ontario Geological Survey, Preliminary Map P. 1521, Mineral Deposits Series.

1978c: Ontario Mineral Potential, Hornepayne Sheet, Districts of Algoma, Thunder Bay, and Cochrane; Ontario Geological Survey, Preliminary Map P. 1526, Mineral Deposits Series.

1978d: Ontario Mineral Potential, Longlac Sheet, Districts of Thunder Bay and Cochrane; Ontario Geological Survey, Preliminary Map P. 1527, Mineral Deposits Series.

1978e: Ontario Mineral Potential, Nipigon Sheet, District of Thunder Bay; Ontario Geological Survey, Preliminary Map P. 1528, Mineral Deposits Series.

Voldner, E.C. and Shah, Y.
1979: Preliminary North American emissions inventory for sulphur and nitrogen oxides and total suspended particulates - A summary; Environment Canada, Atmospheric Emissions Survey Report NRTAP-79-4, p. 40.

Zoltai, S.C.
1965: Glacial features of the Quetico-Nipigon area, Ontario; Canadian Journal of Earth Sciences, v. 2, p. 247-269.

ERRATUM

In the discussion of Quaternary geology and on Figure 1.2, figures represented as "total carbonate" in the 63 μm-44 μm fractions of till from Polar Gas boreholes actually represent % CO_2 equivalent in the sample. To convert these figures to weight % calcium carbonate ($CaCO_3$) equivalent, each number should be multiplied by 2.27.

WISCONSIN GLACIAL RETREAT, SOUTHERN LABRADOR

Project 690043

R.J. Fulton and D.A. Hodgson
Terrain Sciences Division

Fulton, R.J. and Hodgson, D.A., Wisconsin glacial retreat, southern Labrador, in Current Research, Part C, Geological Survey of Canada, Paper 79-1C, p. 17-21, 1979.

Abstract

Ice flow during retreat of the last ice sheet from southern Labrador was generally easterly but was affected greatly by two major topographic features. The Mealy Mountains parted the general flow as well as generating local ice caps. Lake Melville basin was a calving bay beheading the easterly ice stream that lay to the south of the basin.

Radiocarbon dates indicate that the coast was deglaciated before 8640 years ago, that the Goose Bay area was ice free before 7460 years ago, and that inland Labrador was deglaciated prior to 6460 years ago. A moraine system lying south of Goose Bay herein named the Little Drunken Moraine tentatively is correlated with the Manitou-Matamek moraine system on the north shore of the St. Lawrence. The Late Wisconsin ice limit may lie in the southwest corner of the area, at the Paradise Moraine.

Introduction

This report is based on a reconnaissance Quaternary geology study of southeast Labrador. Data were gathered largely by airphoto interpretation and checked during 3 1/2 months field work in 1969 and 1970. About 165 000 km^2 of terrain was mapped, and little detailed information was collected. The prime objective of the work was to produce surficial materials maps for subsequent biophysical surveys.

Aspects of the late Quaternary glacial history that are presented are: the general pattern of ice flow during deglaciation, timing of deglaciation, possible correlations between moraines in the study area and areas to the south and west, and the possible extent of Late Wisconsin ice.

The area discussed lies between 52° and 55°N and between the Labrador Sea and 64°W (Fig. 2.1). It is underlain by Precambrian Shield which in this area mainly consists of gneiss but also includes granitic intrusions, several major bodies of anorthosite, and small areas of unmetamorphosed sedimentary rocks. Landforms include bare rocky coasts, rock-controlled hills and mountains, drumlinoid plains, bog-covered flats, and extensive proglacial valley fills.

Ice Flow During Deglaciation

The area has been subdivided into a number of regions in which flow patterns are similar (Fig. 2.2). The boundaries are drawn at discontinuities in flow pattern or at major morainal features that are thought to mark a significant break in the flow history. The main ice-directional flow features – drumlinoid ridges and crag-and-tail feature – were mapped almost entirely from airphotos.

South Coastal Region (1)

Evidence for glacial flow in this area is sparse, but a few ice-directional features suggest regional ice movement towards the southeast. The southerly component in the flow suggests movement from an ice centre in the Mealy Mountains or from an inland centre thick enough to overtop the Mealy Mountains. There appears to be a discontinuity between flow in this area and flow in areas immediately to the west and north.

The South Coastal flow pattern appears to be the oldest in the study area and, as explained later, probably is not related to the Late Wisconsin maximum.

Mealy Mountains Region (6)

This area is predominantly bare rock with widely scattered crag-and-tail features. It is likely that the eastern part of the massif was not completely ice covered during the Late Wisconsin. Areas higher than about 750 m are rubble covered, lack a fresh glaciated appearance, and are surrounded by cirques. However, the lower western end of the Mealy Mountains apparently was occupied by a local ice cap that flowed to the south and to the north. An isolated region of parallel southeasterly flow, preserved to the east in the Sandwich Bay area, indicates that the Melay Mountains flow regime was more extensive than the area outlined in Figure 2.2 prior to development of the overall pattern presently preserved in the Sandwich Bay area.

The western Mealy Mountains region may have been an early accumulation centre with flow persisting through the Late Wisconsin. Confinement of local ice between mountains to the east and the ice sheet flowing from the inland centre lying to the west may have been the reason for the north and south flow from this area.

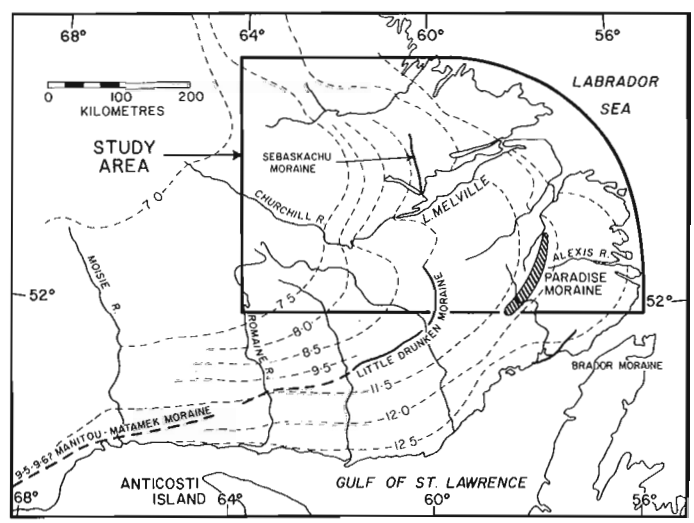

Figure 2.1. *Study area location map and regional correlations. Numbers (e.g., 9.5) refer to estimated age in thousands of years. Dashed lines show the shape and estimated age of ice front positions according to Prest (1969).*

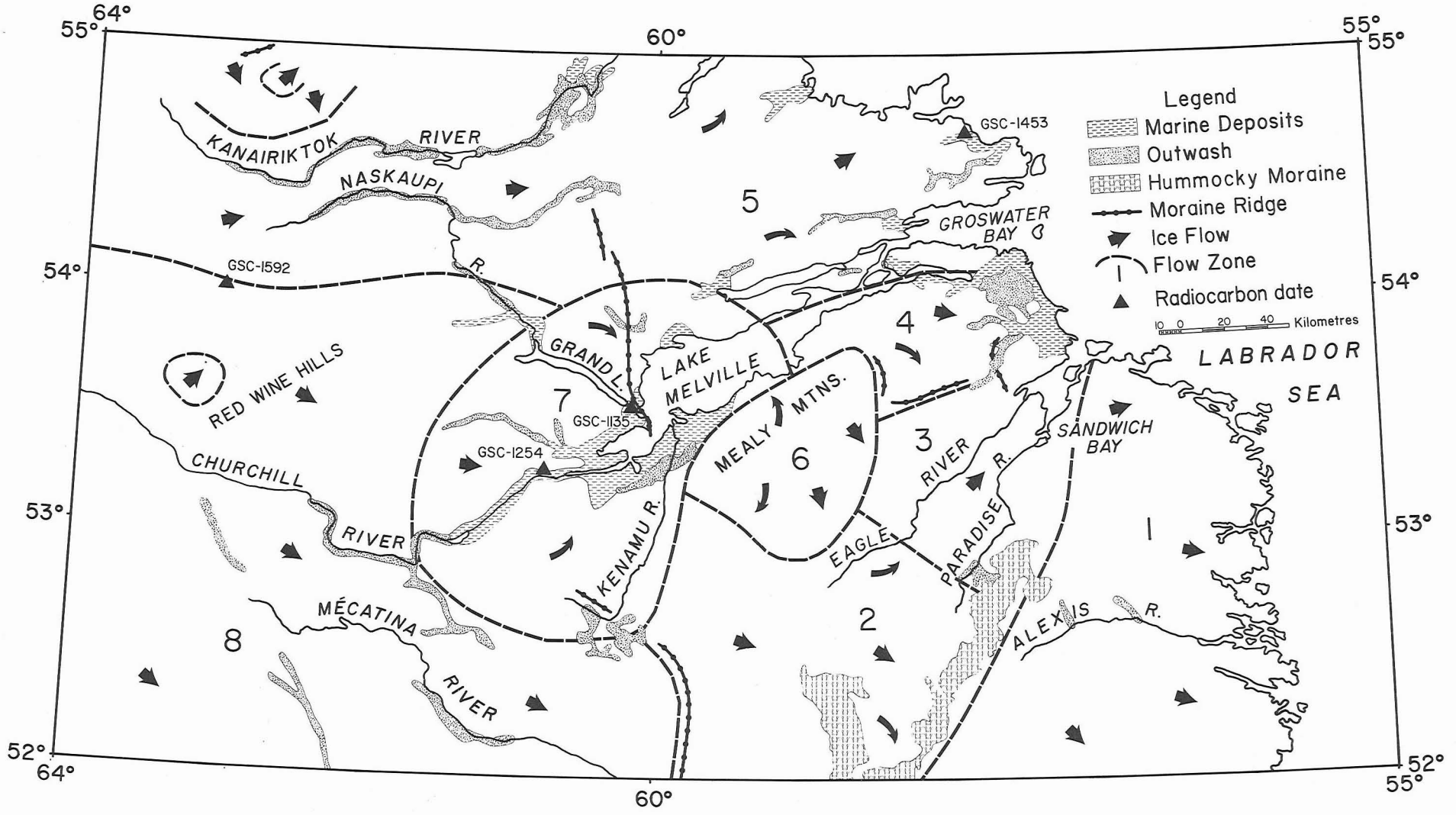

1. *South Coastal*
2. *Upper Eagle River*
3. *Sandwich Bay*
4. *North River*
5. *Kanairiktok River-Groswater Bay*
6. *Mealy Mountains*
7. *Lake Melville*
8. *Little Mécatina*

Figure 2.2. *Summary of main glacial features and subdivision of the study area into ice flow regions.*

Sandwich Bay Region (3)

Evidence of ice flow is abundant in this region though glacial deposits are thin. In general, flow was northeast towards Sandwich Bay from the confluent flow of the upper Eagle River region. This is interpreted as a regional flow swinging north to fill the area east of the Mealy Mountains.

The Sandwich Bay flow postdates flow from the Mealy Mountains, and because it is contiguous with, but downstream from, the upper Eagle River region, it must predate deglaciation of the latter area. The Sandwich Bay flow was possibly a very late glacial phenomenon caused by drawdown into Sandwich Bay rather than a movement from a regional ice centre.

North River Region (4)

This area has abundant glacial flow, outwash, and ice marginal features. Flow direction swings from east-northeast at the northern edge of the region to southeast in the south where the regional pattern appears to have been modified by the presence of the Mealy Mountains. Mountains adjacent to Sandwich Bay and the Labrador Sea do not appear to have been overtopped by ice during the Late Wisconsin; summits lack fresh glacial features, while fresh ice marginal features surround them. Extensive outwash aprons and ice marginal features indicate either a major stillstand or readvance; possibly they mark the margin of the maximum Late Wisconsin ice advance.

Flow southeast around the flanks of the Mealy Mountains culminated in a morainal ridge truncating Sandwich Bay flow features; consequently North River flow occurred later. Construction of the large outwash terrace in the northeast during deglaciation required the continued presence of ice to the north, in Groswater Bay.

Upper Eagle River Region (2)

Abundant glacial deposits and well developed glacial features indicate ice movement towards the east or southeast, apparently fed from a major inland Labrador ice centre. The eastern limit is a belt of well developed hummocky till in Paradise River basin, here referred to as the Paradise Moraine (Fig. 2.1). The western margin is a belt of well developed moraine ridges a few kilometres wide, extending south from the Little Drunken River (a tributary of the Kenamu River).

The flow pattern postdates the glacial maximum Mealy Mountains flow and predates the Lake Melville and Little Mécatina flow patterns. It is obviously truncated by the flow features formed by drawdown into Lake Melville basin; flow probably was beheaded by the opening of that basin.

Lake Melville Region (7)

The Lake Melville region includes the lake basin, low areas to the south and west, and some slightly higher areas to the west and north. Extensive marine and glaciofluvial deposits are present at the west end of Lake Melville and in valleys farther west. The easterly flow pattern over higher land north of the basin (region 5) shows only minor evidence of being affected by drawdown into the basin. To the south and west of Lake Melville, however, drawdown caused a major swing in flow through 90° from the regional southeast flow to a north-northeast flow.

Little Drunken Moraine (Fig. 2.1) is contemporaneous with this drawdown flow pattern because the northeast trending segment of the moraine was built by ice flowing northeast towards Lake Melville. Consequently, this moraine is in part contemporaneous with later stages of flow into the Lake Melville basin and may have developed as the ice sheet stabilized following the sudden drawdown of ice. The Lake Melville flow pattern is later than that of the downstream North River flow.

It seems odd that flow north of Lake Melville was affected so little by the opening of the basin. The reason may be that at this time ice to the north had thinned sufficiently for the relatively high ridges paralleling the north shore of the basin to prevent flow into it.

Little Mécatina Region (8)

Flow in this region was towards the southeast, apparently controlled by an inland Labrador ice centre. The regional pattern largely postdates the opening of Lake Melville and is contemporaneous with flow in adjacent parts of the Kanairiktok River-Groswater Bay region.

Kanairiktok River - Groswater Bay Region (5)

This region stretches across the northern part of the study area north of the Lake Melville basin. Flow was generally east or east-northeast and swung northward as the coast was approached. Several closely spaced minor till ridges are present, but there is no firm evidence of shifts in glacial movement, major stillstands, or readvances. This is considered to be an area of regional flow controlled by an inland Labrador ice centre.

Flow through the Kanairiktok River-Groswater Bay region must have been strong when the large ice contact terrace was forming at the border with the North River flow region. The ice must have thinned considerably and flow must have weakened by the time drawdown began into Lake Melville basin from the south. The Sebaskachu Moraine system (at the west end of Lake Melville, Fig. 2.1) is a narrow and yet relatively continuous feature (100 km) and may correspond to a significant glacial event. Possibly it correlates with the Little Drunken Moraine.

Local Flow Patterns

Scattered areas contain evidence of flows that contrast with the main patterns described. One of these anomalous flow patterns lies west of the Red Wine Hills; two others are in the northwest corner of the area (Fig. 2.2). There is little evidence of the relationship of these flows to regional flow patterns; however, they appear to be remnants of earlier movements rather than late flow phenomena. One local pattern that can be explained as a late feature is a drawdown flow pattern at the west side of Lake Michikamau, just west of the area shown in Figure 2.2.

Absolute Chronology

A relative chronology for ice flow events is given above; unfortunately it is not possible to fix this in time. The establishment of an absolute chronology was attempted by dating the lowest organic sediments in bog deposits. At 20 m a.s.l. at a Sandwich Bay a date of 6720 ± 140 years (Lowdon and Blake, 1975) was obtained; in the same area, at an elevation of about 70 m the bog material dated 5950 ± 150 years (Lowdon and Blake, 1975); and from an area 400 km inland, well above the marine limit, a date of 6460 ± 200 years (Lowdon and Blake, 1973) was obtained. This, together with shell dates mentioned below, indicates that the oldest organic material preserved in bogs accumulated well after deglaciation.

Marine shells are sparsely present in coastal deposits. Unfortunately the only samples found were in deposits that could not be related directly to sea level at the time of

deposition or to specific deglaciation events. It appears that the acidic nature of surficial materials, combined with high precipitation, has created a strong leaching environment that has removed most shell material from permeable near-surface deposits. A shell date of 8640 ± 230 years(GSC-1453) was obtained at the mouth of Michael River, north of Groswater Bay (Fig. 2.2). The shells were 2 m a.s.l., but stratigraphic relationships (Hodgson and Fulton, 1972) suggest that sea level at the time of shell deposition was at least 75 m. Marine limit in the area appears to be no more than 95 m. A shell date of 7490 ± 150 years (GSC-1254, Lowdon and Blake, 1975) was obtained for material about 4 m a.s.l. at Muskrat Falls about 40 km up Churchill River from Goose Bay (Fig. 2.2). The silt containing the shells was deposited when sea level was at least 85 m above present. Marine limit in this area appears to be about 135 m a.s.l. Shells collected from shoreline deposits at an elevation of 33 m at North West River (west end of Lake Melville) were dated at 5330 ± 170 years (GSC-1135, Fitzhugh, 1972). The only date of significance from interior Labrador was from the base of a 3 m peat section 40 km east of Lake Michikamau. This material gave a date of 6460 ± 200 years (GSC-1592, Lowdon and Blake, 1973).

The available dates supply minimum ages only. They show that the coast immediately north of Groswater Bay was ice free by 8640 years ago, that ice had retreated from Goose Bay by 7490 years ago, and that the ice had disappeared from the Lake Michikamau area (150 km east of the Labrador ice centre) by 6460 years ago.

Correlation with Adjacent Areas

It has proved difficult to correlate deglaciation of this area with that of adjacent regions. Some prominent moraines were traced to the south and west by means of airphoto interpretation; some success was achieved tracing Little Drunken Moraine, as a continuation of this feature was traced on airphotos southwestward for about 200 km almost to the area where Dubois (1977) had delineated the Manitou-Matamek Moraine, also by airphoto interpretation (Fig. 2.1). Unfortunately evidence of the moraine could not be found in rugged terrain in the vicinity of the Lower Romaine River. It would appear however that the Little Drunken Moraine is at least approximately correlative with the Manitou-Matamek Moraine.

Dubois (1977) placed an age of 9500 to 9600 years on the Manitou-Matamek Moraine – an estimate based on a 10 230 ± 180 year maximum date for the moraine system, and a 9350 ± 200 year minimum date for formation of the Lac Daigle moraine (Dubois, 1977), at the west end of the system.

The Paradise Moraine was traced due south to within 50 km of the Gulf of St. Lawrence. At present, however, it cannot be related to any other morainic features nor to datable marine features. The Brador Moraine (Fig. 2.1) lies southeast of the Paradise Moraine and south of region 1 (D.R. Grant, unpublished manuscript).

Late Wisconsin Ice Limit

Coleman (1921) proposed that southeastern Labrador was not ice covered during the last glaciation. All recent regional reconstructions of the Quaternary ice cover of the area (except for Ives, 1978) have assumed that the whole of southern Labrador was covered by ice during the last glaciation. In general, however, there has been little hard evidence put forward to support either point of view.

Observations made during this study pointed to a marked difference in landforms between southeastern Labrador and the rest of the study area. All aspects of relief in the southeast are rock controlled, and glacial depositional features are conspicuously absent. The only materials at the surface in upland areas in region 1 are boulders and grus. In the course of airphoto interpretation only one or two scattered features thought to be due to ice streamlining were found in the entire area. Eskers are scarce, and only a few channels thought to have been cut by meltwater flow were found. The coastal area north of Lake Melville contains abundant eskers and glaciofluvial systems that end as ice contact deltas near marine limit. In contrast, to the south, valleys are not filled with glaciofluvial sediments, and alluvial terraces thought to be related to former high sea levels are found well back from the coast. Several valleys with extensive terraces are connected to a low divide area near the Paradise Moraine by underfit channels that possibly were carved by meltwater. Elevations of these terraces, where they might have graded to maximum sea level, are about 95 m.

It has thus been established that the southern corner differs from the rest of the study area in type of surficial deposits and landforms. The question is whether this difference is due to the length of time since the area was deglaciated or to a change in glacial conditions and processes. The southeast likely was near the margin of the ice sheet and consequently erosion and deposition were not as rigorous as in areas up ice. Also, the length of time that glacial processes would have acted in the area would have been less than in central Labrador and hence fewer recognizable glacial landforms might develop. There is also a possibility that non-erosive cold-based ice covered this area; however if the model of Laurentide Ice developed by Sugden (1978) is followed, southeast Labrador lay in an area covered by erosive, warm, melting ice.

Pollen stratigraphy of offshore cores from the Labrador Shelf off Groswater Bay (Vilks and Mudie, 1978) shows a well developed and thick sedge-shrub tundra pollen zone, dated 12 900 to 21 000 years, to be present. Vilks and Mudie consider that these tundra pollen could have been deposited only if an extensive ice free area existed in the region at this time. Because of isostatic depression due to the inland ice load, little of the shelf could have been land during the last glacial maximum. Consequently they feel that the area supporting the sedge-shrub tundra vegetation at this time was in the present onshore area.

H.E. Wright (pers. comm., 1979) of the University of Minnesota recently began a coring program in southern Labrador. He obtained one date from a lake bottom core 90 km inland from the coast of region 1 that corroborates the data of Vilks and Mudie.

In summary, the scanty evidence favours an ice free area in southern Labrador during the last glaciation. The logical place to draw the maximum Late Wisconsin ice margin is at the Paradise Moraine. From this moraine the ice front might have extended along the eastern side of Sandwich Bay. Continuing to the north it would be logical to include the extensive outwash area south of Groswater Bay as an ice marginal deposit. Immediately north of Groswater Bay no evidence has been found to suggest that the Late Wisconsin margin was on land.

Conclusions

During retreat of the last ice sheet from southern Labrador, major topographic features greatly influenced an easterly ice flow pattern that was controlled by an inland ice centre. In the southern part of the study area, where topography is relatively uniform, flow was generally in an east-southeast direction. Likewise, in the northern part, regional flow characteristics dominated, and movement was easterly and northerly. The Mealy Mountains obstructed this

flow and ice swept around them; in addition, they generated their own ice cap which flowed north and south. Drawdown into Lake Melville basin diverted movement south of it from the regional east-southeast direction to north and northeast.

Radiocarbon dates available indicate that the coast north of Groswater Bay was deglaciated prior to 8640 years ago; that the Goose Bay area was ice free before 7490 years ago; and that ice had disappeared from inland Labrador prior to 6460 years ago.

It is possible that the Little Drunken Moraine, which extends south from the west end of Lake Melville, can be correlated with the Manitou-Matamek Moraine on the north shore of the St. Lawrence.

Scanty evidence indicates that about 20 000 km^2 of southeast Labrador was not ice covered at the maximum of the last glaciation.

References

Coleman, A.P.
1921: Northeastern part of Labrador and New Quebec; Geological Survey of Canada, Memoir 124.

Dubois, J-M.
1977: La déglaciation de la côte nord du Saint-Laurent: analyse sommaire; Géographie physique et Quaternaire, v. XXXI, no. 3-4, p. 229-246.

Fitzhugh, W.W.
1972: Environmental archeology and cultural systems in Hamilton Inlet, Labrador; Smithsonian Contribution to Anthropology, no. 16, 299 p.

Hodgson, D.A. and Fulton R.J.
1972: Site description, age and significance of a shell sample from the mouth of the Michael River, 30 km south of Cape Harrison, Labrador; in Report of Activities, Part B; Geological Survey of Canada, Paper 72-1B, p. 102-105.

Ives, J.D.
1978: The maximum extent of the Laurentide ice sheet along the east coast of North America during the last glaciation; Arctic, v. 31, p. 24-53.

Lowdon, J.A. and Blake, W., Jr.
1973: Geological Survey of Canada radiocarbon dates XIII; Geological Survey of Canada, Paper 73-7, 61 p.

1975: Geological Survey of Canada radiocarbon dates XV; Geological Survey of Canada, Paper 75-7, 32 p.

Prest, V.K.
1969: Retreat of Wisconsin and Recent ice in North America; Geological Survey of Canada, Map 1257A, scale 1:5 000 000.

Sugden, D.E.
1978: Glacial erosion by the Laurentide Ice Sheet; Glaciology, v. 20, no. 83, p. 367-391.

Vilks, G. and Mudie, P.J.
1978: Early Wisconsinan deglaciation on Labrador Shelf; Geological Association of Canada, Abstracts with programs, v. 3, p. 509.

3.

THERMAL SENSITIVITY AND THE DEVELOPMENT OF TUNDRA PONDS AND THERMOKARST LAKES IN THE MANITOBA PORTION OF THE HUDSON BAY LOWLAND

Project 750072

L.A. Dredge and F.M. Nixon
Terrain Sciences Division

Dredge, L.A. and Nixon, F.M., Thermal sensitivity and the development of tundra ponds and thermokarst lakes in the Manitoba portion of the Hudson Bay Lowland; in Current Research, Part C, Geological Survey of Canada, Paper 79-1C, p. 23-26, 1979.

Abstract

The development of tundra ponds begins with the thawing of exposed ice wedges, followed by saturation of formerly dry peat and the development of low centre polygons. Wetting and refreezing the peat gives it an increased thermal conductivity. Subsequent thawing produces shallow, flat-bottomed ponds within the peat, which eventually coalesce and deepen until mineral substrate is reached. Once this occurs large, shallow lakes develop and continue to expand by both wave and thermal erosion of marginal peat banks. Lakes and ponds drain where ice dykes are breached or when stream channels migrate. The delicate balance between the development of thermokarst features and their demise indicates that peatlands in the Hudson Bay Lowland are highly sensitive to slight changes in moisture and temperature regime.

Introduction

This report traces the probable development of tundra ponds and thermokarst lakes in polygonal peatlands, using visual field observations on ponding characteristics as they existed during the summer of 1978, combined with calculations of predicted seasonal changes in thawing which would occur with changes in thermal and moisture properties of the peat. The results indicate that there is a delicate balance between the development and degradation of permafrost in this terrain type.

Nature of the Peatland

The peatlands under study constitute open, flat terrain within the Hudson Bay Lowland between sea level and about 120 m a.s.l. (Fig. 3.1). The frozen peat is fairly dry, having less than 22 per cent water content by volume apart from ice wedges, and is 150 to 200 cm thick. The mineral substrate is a silt-clay till or fine grained marine sediment.

The surface of the peat is characterized by high centre polygons defined by systems of ice wedge troughs (Fig. 3.2), many of which are filled with water. Low centre polygons are also present as secondary features in the landscape. The terrain is dotted by numerous, very shallow, flat-bottomed ponds measuring several metres to several tens of metres across. These ponds lie totally within the peat and are usually less than 1 m deep (cf. Fig. 3.3). Large, generally elongate lakes more than 1 km long are also common features (Fig. 3.4). These water bodies are irregular in shape but their outlines consist of a series of arcs with fairly tight radii of curvature (cf. Fig. 3.5). Lakes of this sort have silty sediments around the edges and beaches at their leeward ends. Like the smaller ponds, they are fairly shallow, probably less than 3 m deep, and flat bottomed. Lake floors are covered by a dark layer of disseminated peat fibres.

Thermal Conductivity and Depth of Thawing

The thermal conductivity of a material is the facility (ease or difficulty) by which heat is able to travel through that material. In the case of a wet, porous material, the thermal conductivity depends on whether the material is in a frozen or thawed state. With peat, it is also highly dependent on the volumetric moisture content. Table 3.1 shows the range of thermal conductivities and the magnitude of changes in conductivity as peat changes from one state to another. The moisture contents listed are typical of those found in the peats in the study area.

Thermal conductivity values can be used to calculate depth of thaw (below), and hence thermokarst subsidence. Table 3.1 also lists the depth of thaw that could be expected to occur over a typical season, based on Churchill airport temperatures, for given values of thermal conductivity. These thaw depths are determined using the Stefan equation (Dredge, 1979; modified from Tuma and Abdel-Hady, 1973):

$$x = \sqrt{\frac{2 \cdot 86400 \cdot TI \cdot K}{L}}$$

where x is annual thaw depth (cm)

TI is thawing index (°C degree-days) = 1155 for Churchill

L is the latent heat of fusion (millical cm^{-3}) = $80 \cdot W \cdot 10^{3} \cdot 10^{-2}$

K is thermal conductivity of the soil (millical $cm^{-1}s^{-1}°C^{-1}$)

W is water content in per cent (g $cm^{-3} \cdot 100$)

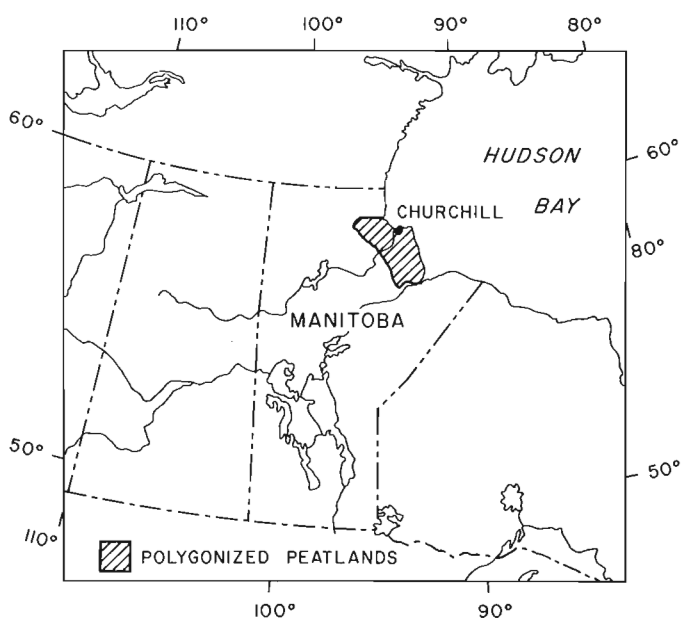

Figure 3.1. *Location of polygonal peatlands within the study area.*

Figure 3.2. *Open, flat peatland with ice wedge polygons. The troughs are approximately 50 cm deep.*

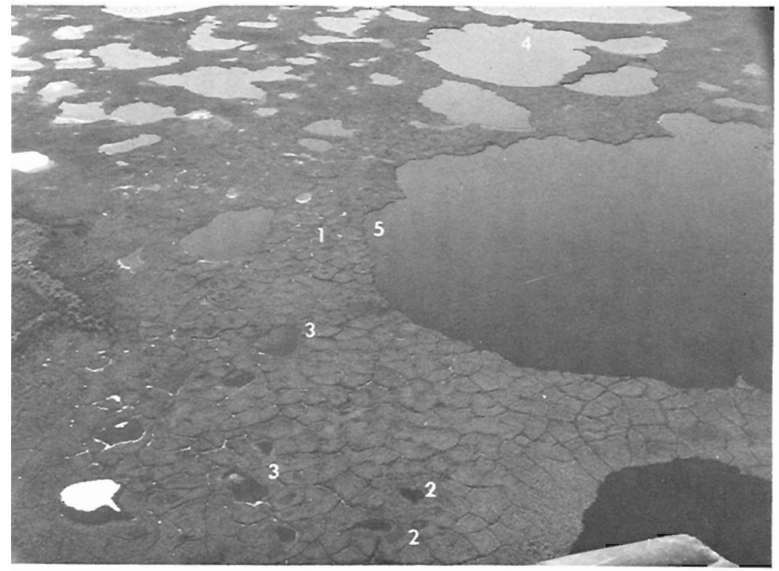

Figure 3.4. *Aerial view of polygonal peatlands portraying various stages in the development of thermokarst ponds. Numbers are keyed to developmental stages described in the text: (1) water-filled ice wedge troughs, (2) pools and saturated polygons, (3) ponds, (4) expanded ponds, and (5) lakes.*

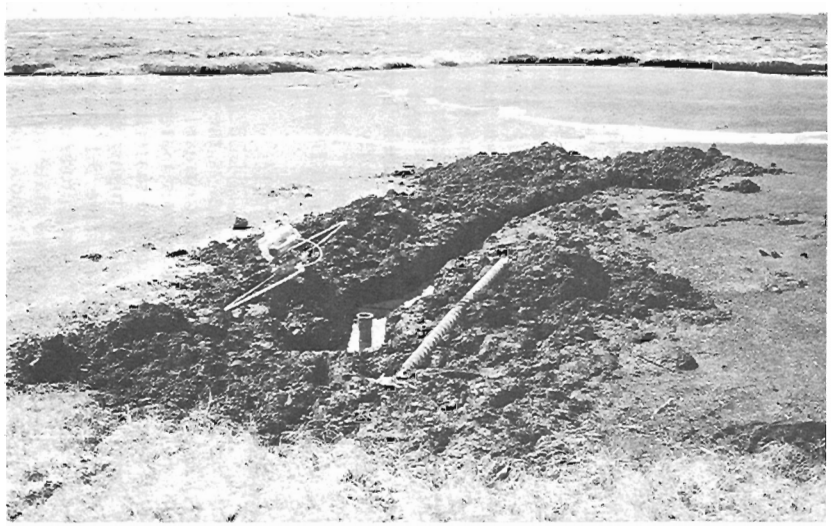

Figure 3.3. *Shallow pond about 60 cm deep (stage 3)which has drained naturally. Foreground shows power head and flight augers used for coring the peat.*

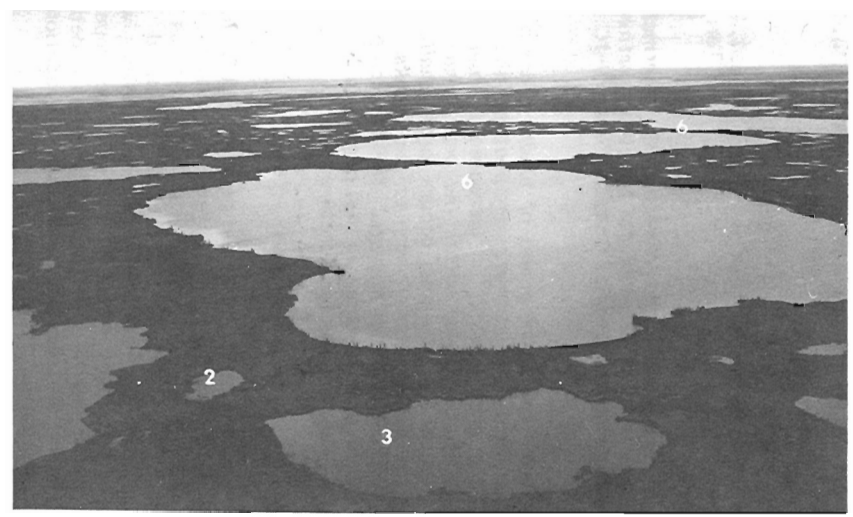

Figure 3.5. *Large lakes in polygonal peatlands (stage 6). The arcuate outlines indicate that the lakes have formed by the coalescence of ponds. These three large lakes, separated by narrow isthmuses of peat, are about to coalesce.*

Hypothesis for the Development of Thermokarst Ponds and Lakes

The following stages constitute one model for explaining the development of large thermokarst lakes in polygonal peat terrain based on average conditions. The model is based on visual field observations, measured summer thaw and lake depths, and predicted thawing based on changing thermal characteristics. The stages explain sequentially what was observed spatially in the field. At any given site, which may be wetter than average or have a shallower peat cover, one or more steps may not have occurred.

This sequence differs from others that have appeared in the literature in that it considers landforms and processes in peat, whereas others deal primarily with loams or marine sediments (cf. Black, 1969; Czudek and Demek, 1970; Hussey and Michelson, 1966; Johnston and Brown, 1964; Sellman et al., 1975). Peaty material has different primary physical characteristics (e.g. density, permeability) and a greater range of moisture contents. Consequently, peat has more variable thermal transmission properties in its various frozen/unfrozen and wet/dry states. As a result peatland thermokarst features differ in form, magnitude, and developmental sequence from those found in inorganic terrain. For example, the baydjarakh and dujoda stages (Czudek and Demek, 1970) are absent in peatland, thermokarst valleys are not produced, and lakes have maximum depths of about 4 m.

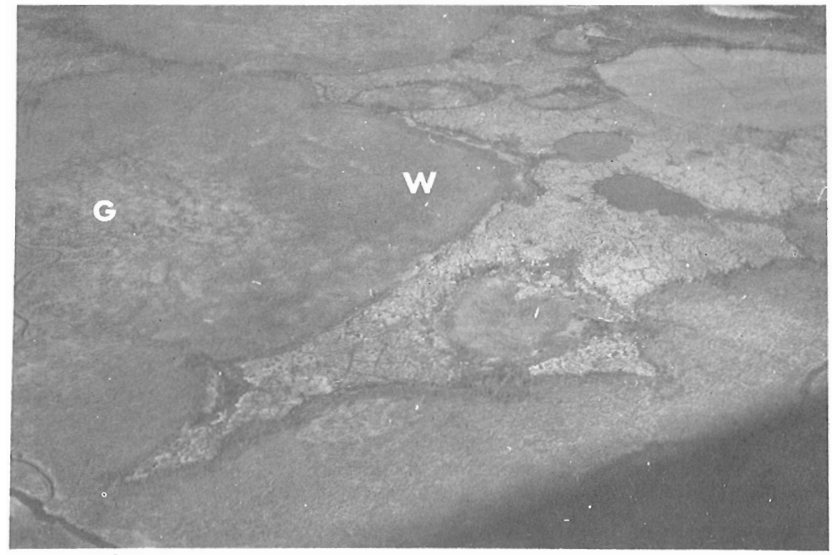

Figure 3.6. *Drained lakes and ponds vegetated by grass (G) and willow scrub (W).*

0. Equilibrium condition. In the initial case peat in this terrain is generally dry (22% moisture by volume) and therefore has a low conductivity (K ≃ 0.23, Table 3.1). Seasonal thawing extends only to about 50 cm and does not penetrate through the peat, which is 150 to 200 cm thick in most places.

1. Thawing of ice wedges. Thermokarst development commences with the thawing of ice wedges that have become exposed due to a variety of factors, including rupturing of the overlying peat during growth of the wedge. Melting proceeds along the wedges; ice wedge troughs, and particularly where troughs intersect, develop into water filled depressions (Fig. 3.4).

2. Saturation of peat within polygons. Water from depressed ice wedge troughs seeps into the adjacent relatively dry active layer of the peat and freezes in winter. The following season these zones, now having higher moisture contents and hence higher thermal conductivities (K ≃ 2.3 to 4.8), experience an increased depth of thaw (up to 115 cm). Ice melts in the polygons, some subsidence occurs (20 to 40 cm observed), and small pools of water form over these polygons with lowered centres. (Fig. 3.4).

3. Development of ponds. Once the depth of water in the pools exceeds approximately 25 cm, the pool acts as a radiation trap in summer and the thawing process accelerates. Thawing and subsidence proceed radially from the pool, but lateral thawing exceeds vertical thawing, for two reasons. Firstly, the active layer beneath the pond gradually reaches an equilibrium thickness, and no further downward thaw occurs until the characteristics of the heat source or transmitting medium change. Secondly, the thermal conductivity is greater, and the rate of heat flow is therefore faster, in a refrozen saturated active layer than in the underlying peat having lower ice content. The result in both cases is the expansion of pools to form the shallow flat-bottomed ponds (Fig. 3.4) which are so widespread in the area. These ponds are between 50 and 70 cm deep (Fig. 3.3).

Table 3.1

Thermal conductivity values and thaw depths calculated from the Stefan equation

Material	Water content (% of volume)	Thermal conductivity (millical $cm^{-1}s^{-1}\,°C^{-1}$)	Reference	Predicted thaw depth at Churchill (cm)
Frozen peat	22	0.23	Dredge, 1979	50
	50	2.3	MacFarlane, 1969	107
	90	4.8	MacFarlane, 1969	115
Ice	100	5.0		
Unfrozen peat	50	0.7	MacFarlane, 1969	50
	90	1.3	MacFarlane, 1969	60
Water	100	1.36		
Frozen or unfrozen silt-clay	10-30	4-8	Sanger, 1963	270-250

4. Expansion of ponds. As the pond grows, both lateral and vertical thawing are augmented, increased subsidence by melting of ground ice occurs, and ponds coalesce. As the ponds deepen, thawing extends into the mineral substrate at about 200 cm[1].

5. Development of lakes. Further lateral expansion of large ponds occurs by the mechanical processes of ice ramming during spring break-up and wave battering and undercutting of peat banks in summer, combined with the thermal erosion of ice wedges and ground ice adjacent to the lakes. In some cases lakes have expanded preferentially along a southerly or south easterly axis, in response to the prevailing winds from the north and northwest. Not all lakes develop in this manner, however, since the direction of preferential thawing is also related to random occurrences of massive ground ice and to elongated topographic highs (related to beach ridges) in the underlying mineral substrate. Both thaw depths and lake depths are greater where mineral soil is near the surface than in adjacent areas of deeper peat because the thermal conductivity of the mineral soil is greater (K = 4 to 8).

6. Coalescence of lakes. Expansion of lakes occurs by the coalescence of adjacent ponds. Large lakes tend to lose any pre-existing elongation during this stage. The lakes are irregular in shape, and the shorelines form a series of arcs which demark the outlines of former ponds (Fig. 3.5).

Cessation of Lake Growth

The expansion of lakes is halted in several ways:

1. A general vertical geothermal equilibrium is reached between seasonal freezing and depth of thawing.
2. As peat banks around lakes and ponds collapse, a layer a peat fibres is dispersed across the lake bottom. The wet, unfrozen peat gradually forms an insulating layer which reduces the rate of heat penetration and thawing.
3. Subsidence is limited by the volumetric excess ice originally available. Once this excess is depleted, thermokarst subsidence halts.
4. Ponds drain when spring flooding, natural melt, or migration of water courses cause ice wedges connecting lakes to melt to a level below the surface of the higher lake. Drainage also occurs when the frozen confining bottoms or sides of ponds thaw due to local thickening of the active layer. Many scars of lakes are visible on airphotos of this area (Fig. 3.6). If the water table drops slightly, paludification commonly occurs; if lakes drain completely, grass and scrub willow commonly colonize the wet centres and drier margins of the lakebeds, respectively.

Thermokarst Ponds and Thermal Sensitivity

Visual evidence for the active development and demise of tundra ponds and thermokarst lakes in the area suggests that the processes are presently in a steady state. This equilibrium is sensitive, however, for two reasons. Many tundra pools are just at the point where, if a marginal increase in thawing occurs, progressive thermokarst development into the mineral substrate will begin. Due to the higher conductivity of the mineral soil (Table 3.1), rapid increased thawing and subsidence can occur in icy sediments. Secondly, the thermal conductivity of peat is highly sensitive to changes in moisture content. Doubling the water content will increase the thermal conductivity of frozen peat by an order of magnitude. Presently, the polygonal peat terrain is atypically dry relative to moisture contents in peat in other regions (cf. all references) and hence has a very low thermal conductivity. However, any natural or man induced process which impedes soil drainage may cause deep thawing, both in the peat and through the peat into the mineral substrate, with the possible accelerated expansion of thermokarst ponds and lakes over a broad area.

References

Black, R.F.
1969: Thaw depressions and thaw lakes, a review; Biuletyn Peryglacjalny, v. 20, p. 131-150.

Czudek, T. and Demek, J.
1970: Thermokarst in Siberia and its influence on the development of lowland relief; Quaternary Research, v. 1, p. 103-120.

Dredge, L.A.
1979: Thaw depths and permafrost in polygonized peat terrain, Hudson Bay Lowland, Manitoba; in Current Research, Part C, Geological Survey of Canada, Paper 79-1C, Report 4.

Hussey, K.M. and Michelson, R.W.
1966: Tundra relief features near Point Barrow, Alaska; Arctic, v. 19 p. 162-184.

Johnston, G.H. and Brown, R.J.E.
1964: Some observations on permafrost distribution at a lake in the Mackenzie Delta, N.W.T., Canada; Arctic, v. 17, p. 162-175.

MacFarlane, I.C.
1969: Engineering characteristics of peat; Chapter 4 in Muskeg Engineering Handbook, University of Toronto Press, p. 78-126.

Sanger, F.J.
1963: Degree-days and heat conduction in soils; Proceedings 1st International Conference on Permafrost (Lafayette), p. 253-262.

Sellman, P.V., Brown, J., Lewellen, R., McKim, H., and Merry, C.
1975: Classification and geomorphic implications of thaw lakes on the arctic coastal plain, Alaska; Cold Regions Research and Engineering Laboratory (CRREL) Research Report 344, 21 p.

Tuma, J.J. and Abdel-Hady, M.
1973: Engineering Soil Mechanics; Prentice Hall, Englewood Cliffs, N.J., 335 p.

[1] All ponds of this size (less than 250 cm deep) freeze to the bottom in winter, but a talik can develop in the peat and sediments below the water bodies. The presence of a talik accelerates the expansion process, and the basin can deepen to a maximum which can occur by thawing alone.

4. THAW DEPTHS AND PERMAFROST IN POLYGONAL PEAT TERRAIN, HUDSON BAY LOWLAND, MANITOBA

Project 750072

L.A. Dredge
Terrain Sciences Division

Dredge, L.A., Thaw depths and permafrost in polygonal peat terrain, Hudson Bay Lowland, Manitoba; in Current Research, Part C, Geological Survey of Canada, Paper 79-1C, p. 27-30, 1979.

Abstract

The thermal conductivity of thick, relatively dry polygonal peat is 0.23 millicalories $cm^{-1}s^{-1}{}^{\circ}C^{-1}$. The maximum depth of seasonal thawing in this type of peat is about 50 cm. Thawing does not extend through polygonal peat (which is 150 to 200 cm thick) into the subsoil. Subsoil temperatures are sufficiently below freezing to maintain the soil in a continuously frozen state, despite the presence of capillary moisture. Wetter peats have a higher thermal conductivity, ground temperatures are warmer, and thawing may penetrate through to the mineral substrate. Thaw depths in peat can be predicted from air temperature data, and an equation which expresses the relationship between these two parameters has been derived. The distribution of permafrost in the Hudson Bay Lowland depends on the thermal regime of the peat; the actual boundary between discontinuous and continuous permafrost lies to the south of that boundary defined on the basis of mean annual air temperature alone.*

Introduction

Mapping of the surficial geology in National Topographic System map areas 54 E, F, K, and L was undertaken during summer 1978. This paper presents observations on permafrost conditions and data on thaw depths determined during the course of the work.

The Hudson Bay Lowland between Churchill, Manitoba, and the Nelson River is an almost flat plain composed of marine silts or silty till. The lack of relief and low permeability of the soil inhibit drainage; this, combined with a cool, humid summer climatic regime, provides conditions suitable for the growth and accumulation of organic material over a broad area. The presence of widespread peatland and its character have affected active layer depths and influenced both the nature and distribution of permafrost in this area.

Nature of the Peat

One of the most widespread and distinctive peatland types in the region is relatively dry, polygonal bog (Fig. 4.1) which began to form about 6500 years ago as the postglacial Tyrrell Sea withdrew from the lowlands. It extends from about 30 m to 100 m ASL; on the north and south it grades into wet sedge meadow/fen and into open wet fen and thence into forested bog to the west. Polygonal peat forms a virtually featureless open plain, with regional slopes of less than 1 m km^{-1}. The main features within this plain include the polygonal system of depressed ice wedge troughs measuring roughly 10 m on a side; shallow, roughly circular ponds within the peat; and flat-bottomed, deeper thermokarst lakes which have extended through the peat and into the mineral substrate (Fig. 4.2).

The peat deposits are commonly about 2 m thick over the entire area. They consist of moderately fibrous, horizontally matted yellow or brown moss layers, interspersed with darker, more decomposed fen peat. The base commonly consists of a woody zone which is separated from the mineral substrate by a layer of ice 2 to 10 cm thick. Ice is also present in small amounts as thin strata and random crystals in the rest of the peat profile and in at least the upper part of the mineral substrate.

Physical properties of the peat, determined from frozen core samples, show that it is remarkably uniform, both areally and vertically through the profile. The peat is uncompressed, and bulk and dry densities average 0.24 and 0.039 g cm^{-3}, respectively. These values are less than those determined for peat in other studies (see Table 4.1). Moisture contents average about 600% of the dry weight and account

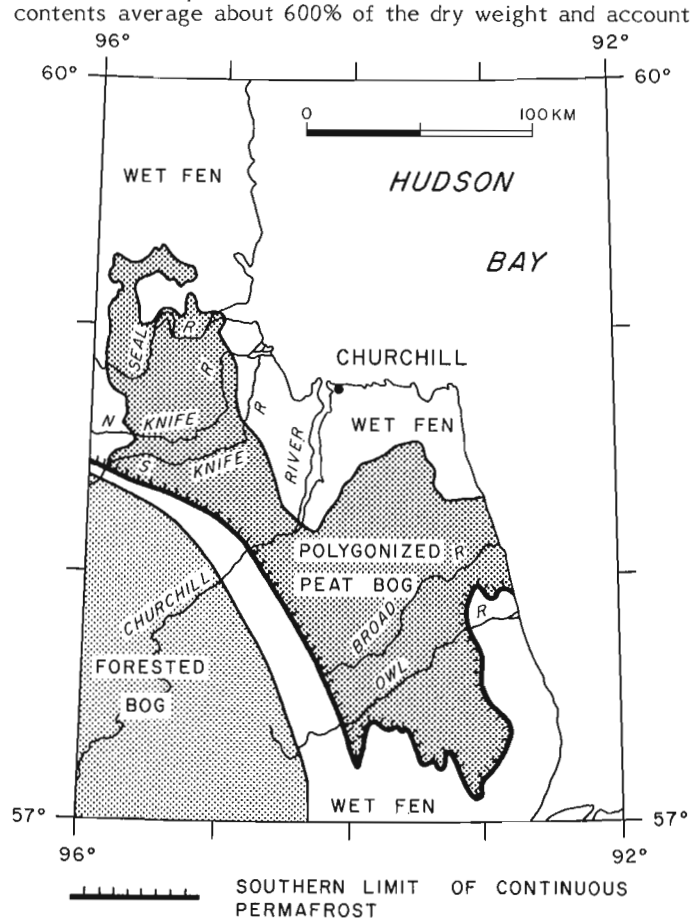

Figure 4.1. *Peat types in the study area.*

*1 cal $cm^{-1}s^{-1}{}^{\circ}C^{-1}$ = 418.68 $Wm^{-1}{}^{\circ}C^{-1}$; 1W = 1J s^{-1}

Figure 4.2. *Polygonal peatland. The main features of this peat type are ice wedge polygons, shallow ponds, and thermokarst lakes.*

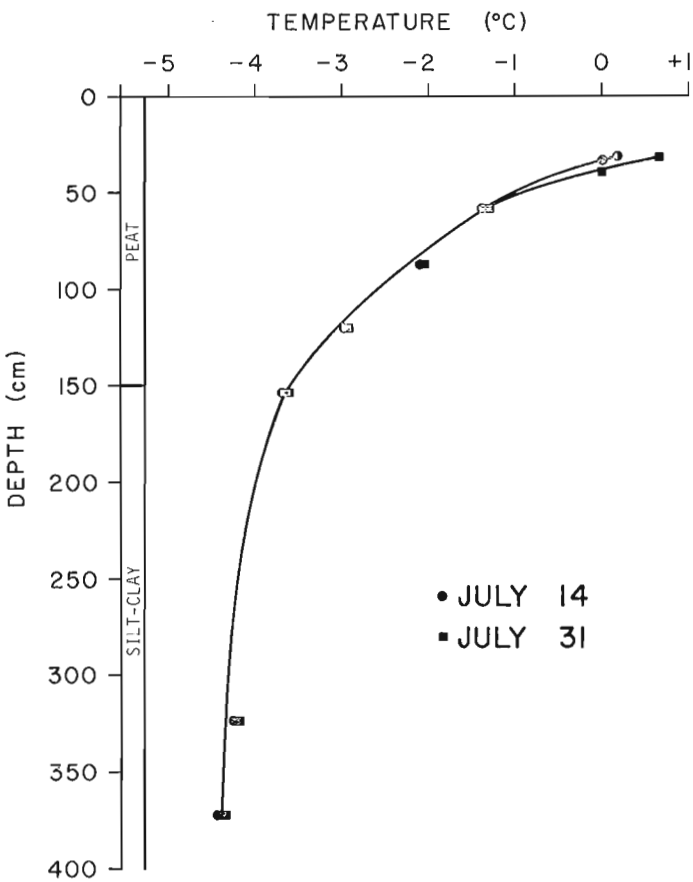

Figure 4.3. *Temperature profile, midsummer 1978.*

for less than 25% of volume of material. These figures are also low relative to 'typical' peat described in the literature, where water comprises 50% to 90% of the volume (75% to 1500% of the dry weight). These moisture differences greatly affect the thermal properties of the peat. The thermal conductivity (K) calculated from density and moisture data and measured soil temperatures is 0.23 millical cm^{-1} s^{-1} $°C^{-1}$ (0.056 BTU ft^{-1} h^{-1} $°F^{-1}$).

Midsummer Temperature Profiles

Sets of seven-bead thermistor strings were installed in two boreholes in the peat and underlying mineral substrate. These were read at intervals between July 14 and July 31. During this period the Churchill area experienced 157 thawing degree–days (Celsius), about 18% of the annual total.

1. By July 31 more than 50% of the cumulative degree–days had passed.
2. The thawing index for 1978 is 861 (°C). In normal years the thawing index is 1155(°C); the freezing index is 3698(°C); and mean annual air temperature is -7.3 °C.

The beads were not optimally placed for measuring variations in the depth of thaw because the expected magnitude of temperature change was much greater than that actually observed. Thaw depths, therefore, were measured with a stainless steel frost probe at the thermistor sites over the course of the summer. Despite problems with the placement of the beads, a number of conclusions can be drawn from the data (Fig. 4.3).

1. Active layer depths are very shallow. Total depth of thaw by the end of July was 31 cm. This is significantly less than measured depths in mineral soil on the same day, where no frozen ground was present to at least 120 cm. (At some sites no permafrost was encountered.)
2. Through the peat the average temperature gradient is 0.03 °C cm^{-1}. (Brown and Williams (1972) quote averages of about 0.06 °C cm^{-1} for wetter peats.) Below a depth of about 150 to 200 cm, the gradient falls off rapidly and temperatures remain uniform at about -4.5°C. Thus, effective heat penetration is limited to the upper 150 cm.
3. Over the period of measurement, when the area experienced its highest rate of thaw and an 18% increment in thawing degree–days, there was little change in active layer depth and no change in the temperature profile below 60 cm. This further attests to the low thermal conductivity of the peat.
4. The temperature values, and lack of change over time, indicate that the 0° isotherm does not penetrate through the peat into the mineral subsoil and that the temperatures are sufficiently low to prevent thawing of capillary moisture in the fine grained substrate. In all boreholes, the subsoil beneath polygonal peatland was frozen. This was not the case for wetter, nonpolygonal peat types with higher thermal conductivity, where thawing either extended through to the substrate, or else the temperature was high enough for capillary water to be present in an unfrozen state in the mineral soil.

Measured Progression of Regional Thawing, 1978

Thaw depths were measured over the region during the summer of 1978 by ringing to permafrost with a stainless steel frost probe. Measurements were read on the probe to 5 cm. Figure 4.4 shows the measured thaw depths and how they changed with time.

1. The graph shows a general increase from about 10 cm on June 15 to about 35 cm on August 15.
2. Peat depths (150 to 200 cm) greatly exceeded thaw depths at all sites in polygonal peatlands.

Table 4.1

Physical properties of peat

Moisture W (%wt)	Moisture W (% vol)	Density bulk (g/cm^3)	Density dry (g/cm^3)	Reference
619	22	0.24	0.039	this study
750-1500	50-90	0.4-1.2	0.08-0.32	MacFarlane, 1969
		0.4-1.2	0.02-0.34	Walmsley, 1977

Material	Moisture W (% volume)	Thermal Conductivity K (millical cm^{-1}s^{-1}°C^{-1})	Reference
Frozen peat	22	0.23	this study
Frozen peat	50	2.3	MacFarlane, 1969
Frozen peat	90	4.8	MacFarlane, 1969
Unfrozen peat	50	0.7	MacFarlane, 1969
Unfrozen peat	90	1.3	MacFarlane, 1969
Frozen or unfrozen silt-clay	10-30	4-8	Sanger, 1963

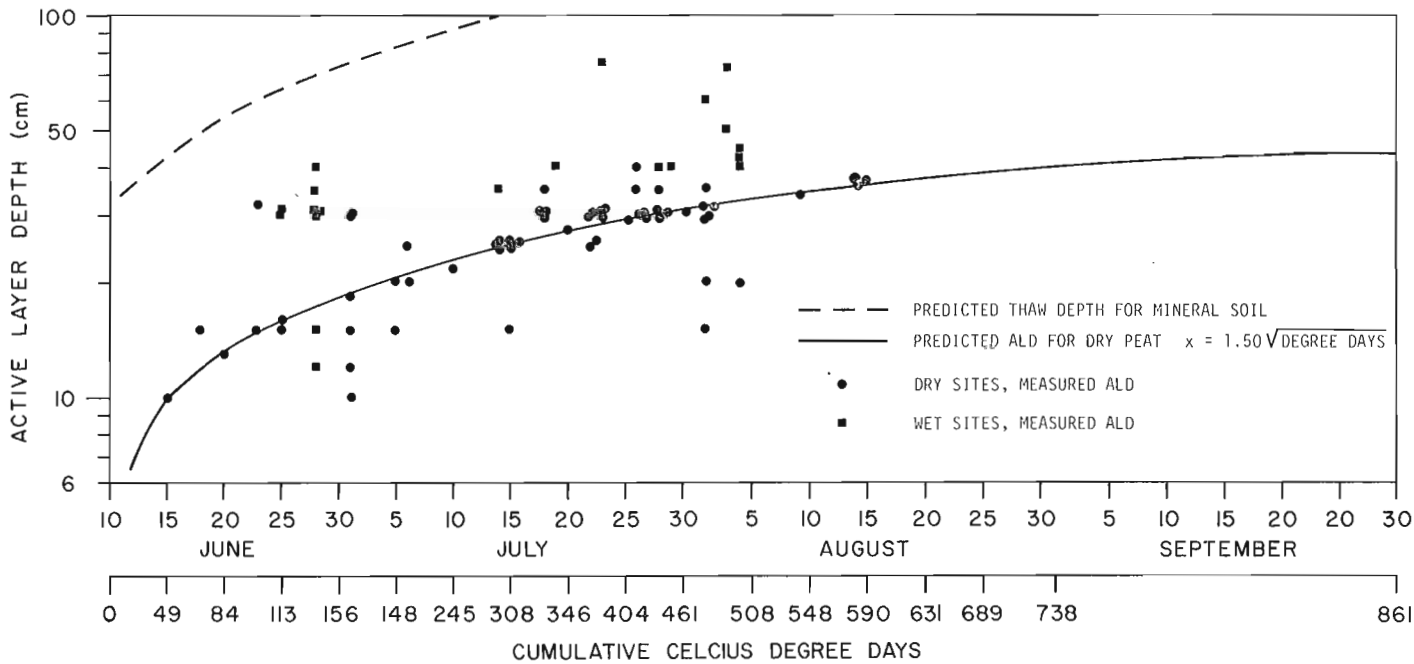

Figure 4.4. *Progression of thawing in peat, summer 1978. And predicted increase in active layer depth (ALD).*

3. Although there is a systematic clustering, a fairly high degree of scatter is apparent. This scatter probably reflects differing moisture contents at various sites. The conclusion that the thermal properties of peat are highly dependent on moisture content is borne out by field observations; those sites noted in the field as being particularly wet, for example, had significantly greater thaw depths.

Theoretical Progression of Thawing, Using Air Temperature Data

The hypothetical depth of thawing or freezing can be predicted using standard meteorological data by calculating the number of degree-days available for thawing (or freezing) and substituting this value into the Stefan (or modified Berggren) equation (modified from Tuma and Abdel-Hady, 1973):

$$x = \sqrt{\frac{2 \cdot 86400 \cdot K \cdot TI}{L}}$$

where x = depth of thaw (cm)
K = thermal conductivity of the soil (millical s^{-1} cm^{-1} °C^{-1})
TI = thawing index in degree-days (°C)
L = latent heat of fusion (millical cm^{-3})

The Berggren equation differs from the Stefan model in that it has an additional multiplier contant. In this case, because of the thermal properties of the peat, the multiplier approaches unity. Therefore, the results from the two equations are almost identical.

The Stefan equation is based on a model of uniform heat flow and has been found to be accurate in predicting thawing or freezing in mineral soils. For this study, temperature data from Churchill airport are sufficiently representative for degree-day calculations, because the entire area is an open plain and is exposed to the effects of Hudson Bay. Latent heat values were calculated from density and moisture data derived from the analysis of cores. The thermal conductivity used in the equation was empirically derived by substituting known measured thaw depths into the Stefan equation. Standard values for conductivity published in the literature (cf. Table 1) could not be used in the calculation because they apply to peats with much higher volumetric water contents.

Using the Stefan model, with conductivity of 0.23 millical cm^{-1} s^{-1} $°C^{-1}$, progressive seasonal thaw values were calculated and plotted (Fig. 4.4). The graph shows relatively good agreement between the clusters of measured data and predicted thawing in dry peats. This correspondence permits calculated values to be extrapolated beyond the last measured value to the end of the thawing season (end of September) where an expected maximum thaw depth would be 43 cm in 1978 and 49 cm in average years.

These values indicate that total annual thawing is also less than the thickness of peat and that the subsoil must remain frozen throughout the year over the broad area covered by polygonal peat. In contrast to this, up to 2 m of thawing is expected to occur in wetter peats and 1.75 to 2.5 m of seasonal thawing in mineral soils in the same general area.

Significance of the Thermal Regime to the Regional Boundary Between Continuous and Discontinuous Permafrost

Three significant conclusions about the upper thermal regime can be summarized from examination of the vertical temperature profiles and progressive seasonal thawing calculations:

1. Thawing does not extend through polygonal peat into the subsoil.
2. In polygonal peatland, subsoil temperatures are sufficiently below freezing to maintain the underlying clayey mineral soil in a frozen state despite capillary moisture.
3. For wetter peats, which have a higher thermal conductivity, or for thinner peat accumulations, temperatures are warmer and thawing may penetrate to the mineral substrate.

Climate is a basic factor in the formation and preservation of permafrost, and continent-wide studies have shown a broad relationship between mean annual air temperature, ground temperature, and permafrost occurrence. Based on Soviet studies it has been found that the limit between continuous and discontinuous permafrost corresponds in a general way to the location of the -8.5°C mean annual air temperature isotherm, which in turn corresponds to a mean annual ground temperature of -5°C (Brown and Péwe, 1973, p. 75). This relationship is known to be valid for much of Canada as well. On the basis of this correlation between air temperatures and permafrost, the expected limit of continuous permafrost in this area should pass through Churchill.

Field observations and the preceding numerical calculations indicate that in the Hudson Bay Lowlands air temperatures and permafrost distribution do not correlate well. This is due to the low thermal conductivity of regionally significant peat accumulations; thus permafrost is much more widespread than expected on the basis of air temperatures alone. Figure 4.1 shows the predicted boundary between continuous and discontinuous permafrost, determined on the basis of observations on the types of peat, measured thaw depths, and data from shallow boreholes. Continuous permafrost is assumed to underlie dry, polygonal peatlands; regionally discontinuous permafrost, or taliks, underlie wetter fen lands to the west, and thinner wet peatlands near the coast. In these areas, although the peat in places is frozen completely, temperatures are sufficiently high that capillary water in the underlying, clayey substrate is present in an unfrozen state.

Conclusions

1. Thermal conductivity values for polygonal peat are very low ($K \simeq 0.23$ millical cm^{-1} s^{-1} $°C^{-1}$). Dry organic deposits are an effective frost barrier.
2. Maximum thaw depths in dry peat are about 50 cm.
3. Over broad areas of the Hudson Bay Lowland, peat deposits are thicker than the depth of seasonal thawing. The mineral substrate remains frozen throughout the year, and continuous permafrost conditions prevail.
4. Thawing in peatland is highly dependent on the moisture content of peat. If the moisture content is volumetrically doubled, the thermal conductivity may increase by an order of magnitude.
5. Thaw depths in peat can be predicted from air temperature data. For polygonal peatlands in this region, the Stefan equation

$$x = \sqrt{\frac{2 \cdot 86400 \cdot 0.23 \cdot TI}{17600}} = 1.50\ TI$$

describes the depth of thawing, where x is thaw depth (cm) and TI is the thawing index (degree-days Celsius.)

References

Brown, R.J.E. and Péwé, T.L.
1973: Distribution of permafrost in North America and its relationship to the environment: A review, 1963-1973; North American Contribution to the 2nd International Conference on Permafrost. (Yakutsk, Siberia), p. 71-100.

Brown, R.J.E. and Williams, G.P.
1972: The freezing of peatland; National Research Council, Division of Building Research, Technical Paper No. 381, 24 p.

MacFarlane, I.C.
1969: Engineering characteristics of peat; in Muskeg Engineering Handbook, University of Toronto Press, P. 78-126.

Sanger, F.J.
1963: Degree days and heat conduction in soils; Proceedings of the 1st International Conference on Permafrost (LaFayette), P. 253-262.

Tuma, J.J. and Abdel-Hady, M.
1973: Engineering Soil Mechanics; Prentice Hall, Englewood Cliffs, N.J., 335 p.

Walmsley, M.E.
1977: Physical and chemical properties of peat; in Muskeg and the Northern Environment in Canada, ed. N.W. Rathforth and C.O. Brawner, University of Toronto Press, p. 82-129.

5. URANIUM CONTENT OF ROCKS, COAL AND ASSOCIATED MINERALS FROM THE SYDNEY COALFIELD, CAPE BRETON ISLAND, NOVA SCOTIA

EMR Research Agreement 2239-4-83/77

Erwin L. Zodrow[1] and Marcos Zentilli[2]
Regional and Economic Geology Division

Zodrow, Erwin L. and Zentilli, Marcos; Uranium content of rocks, coal and associated minerals from the Sydney Coalfield, Cape Breton Island, Nova Scotia; in Current Research, Part C, Geological Survey of Canada, Paper 79-1C, p. 31-36, 1979.

Abstract

Samples of coal, associated minerals and sedimentary rocks of Pennsylvanian age from the Sydney Coalfield were analyzed for U. The U content of coal samples ranges from 0.03 to 4.2 ppm (avg. 0.46 ppm U) , but over 50 per cent of them contain less than 0.2 ppm U. The highest concentrations are found in shaly coal (9.22 ppm U) or shale within coal seams, and both overshales and undershales are enriched (3.9 ppm U). The average U contents for shale (3.4 ppm U) and sandstone (2.9 ppm U) in the Sydney Coalfield are not different from those of similar rocks elsewhere. No significant enrichment has been found in sulphates of sulphides associated with coal. Ash from Sydney coal probably averages less than 4 ppm U.

Introduction

Although coal is commonly considered to be one of the least radioactive rocks (Russell, 1945), ore-grade concentrations of uranium (U) in coal have been reported from many parts of the world (Benson and Gill, 1956). Because U is concentrated in the ash when coal is burned as a fuel, consideration has been given to its economic recovery from ash (Vine, 1956), and concern is often manifested on the possible effects of releasing these products of combustion to the environment (e.g. Roffman et al., 1977).

This paper presents data on the content of U of coal and associated pyrite, hydrated sulphates, and sedimentary rocks from the Upper Carboniferous sequence of Sydney Coalfield, situated on the northeastern part of the Island of Cape Breton, Nova Scotia, Canada (Fig. 5.1) The geology has been described by Brown (1845, Dawson (1878), and more recently summarized by Rose et al. (1970). Detailed studies on its fossil flora and secondary mineralogy (Zodrow and McCandlish, 1978a, b) provided the momentum for the present study. Trace elements in Nova Scotia coals were studied by Hawley (1955a, b) and Hawley and Rimsaite (1954), but to our knowledge, no U analyses have been published for Nova Scotia coals.

The studied rock sequence represents the exposed part of a gently folded basin that trends northeast and plunges 3 to 20° into the Atlantic Ocean. The Pennsylvanian strata comprise Westphalian C and D floral zones (Zodrow and McCandlish, 1978a) and are probably 2000 m thick. They are composed chiefly of micaceous, coarse grained to conglomeratic sandstones ("millstone grit") of fluvial origin, with intercalations of red and grey (carbonaceous) shales, the latter forming the hangingwall (overshale) and footwall (undershale; underclay) of the larger coal seams. These undershales and overshales are extremely variable in thickness and lateral extent (from zero to several metres). The coal seams themselves vary from a few millimetres to over 2.3 m. Several of the 13 seams (Table 5.1) were mined in the past and two of them are presently mined by the Cape Breton Development Corporation (DEVCO) at the Lingan, No. 26 and Prince mines, producing bituminous coal.

The samples used in this study were collected by E.L.Z. or selected from the collections of the College of Cape Breton, Sydney, Nova Scotia and the Nova Scotia Museum, Halifax, Nova Scotia.

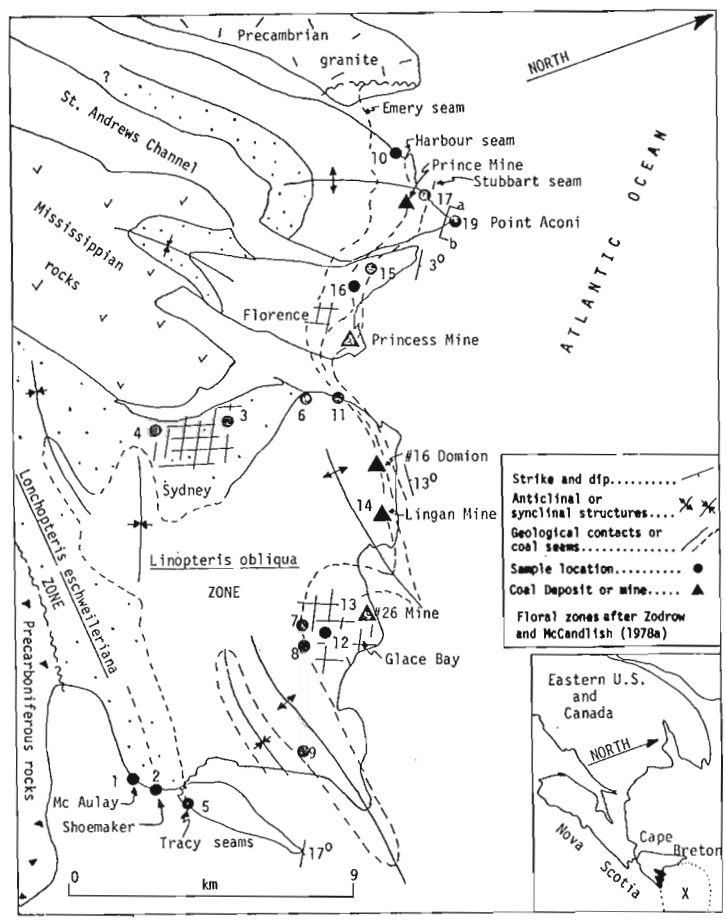

Figure 5.1. *Location of uranium samples in Sydney Coalfield, Cape Breton Island, Nova Scotia. Sydney basin is identified by "X".*

Analytical Procedures

Most samples were analyzed by an Induced Fission Track Technique (IFT) as routinely used at Dalhousie University (Zentilli et al., 1977; Mitchell and Aumento, 1977). Precision and accuracy of the method have been discussed by Fisher (1970) and Dostal et al. (1975). Because for the IFT analyses one does not weigh the sample but measures the

[1] Department of Geology, College of Cape Breton, Sydney, N.S. B1P 6J1
[2] Department of Geology, Dalhousie University, Halifax, N.S. B3H 3J2

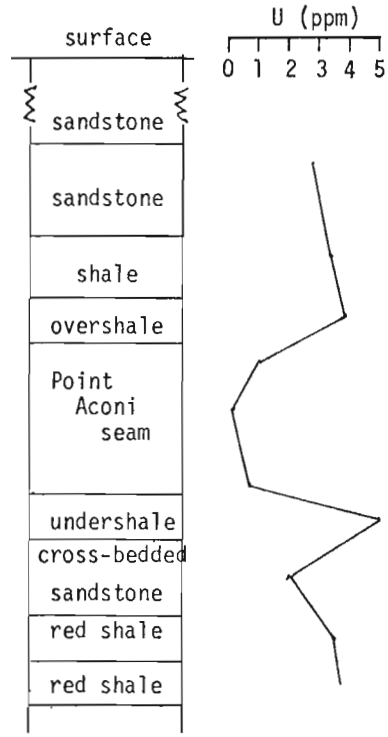

Figure 5.2. *Composite and schematic profile a-b from Point Aconi (Fig. 5.1) and uranium content (Table 5.2). Measured thickness of the coal seam is 110 cm.*

amount of U per unit area (volume) of a sample pellet, we have found (Zentilli and Taylor, in prep.) that for samples whose specific gravity is significantly different from that of the standard used, a correction for density must be introduced. Only then can the IFT results be compared with results obtained by other methods that give results in ppm (e.g. g/ton by weight). This correction, generally equivalent to the ratio, S.G. sample/S.G. standard, has been introduced for our coal analyses. The precision of the IFT method using a standard glass of 0.32 ppm U is generally better than ± 20 per cent. The IFT method can measure concentrations as low as 0.001 ppm U, making it especially appropriate for coal analyses.

A number of the samples for this study was analyzed by a Delayed Neutron Activation (DNA) method with a precision of ± 20 per cent at the 0.5 ppm U level, increasing to ± 5 per cent at the 10.0 ppm U level. The limit of analytical detection for routine DNA analysis is about 0.1 ppm U.

Uranium Content

Tables 5.2 to 5.4 show the results of the analyses of over 100 samples, including rocks, coal and associated hydrated sulphate minerals. U contents of pyrite-rich fractions from coal and acid mine waters are also mentioned.

Average values for the sandstone in the area are close to 3 ppm U (Table 5.2), with the lowest values found in the "millstone grit" (brown, coarse grained to conglomeratic sandstone, 1.5 ppm U) whereas fine grained sandstone contains nearly twice the amount of U. These values are consistently higher than published data for "North American average ortho-quartzite" (0.45 ppm U; Rogers and Adams, 1969), or even for "average arkose" (1.5 ppm U; Rogers and Adams, 1969) or greywacke. It is similar, however, to the average value for "Atlantic Coast beach sands" (3.21 ppm U, Mahdavi, 1964).

Our shale samples are, as expected, slightly higher in U content than the sandstones, with an average of 3.4 ppm U, in agreement with the "average North American grey and green shale" (3.2 ppm U; Rogers and Adams, 1969). No significant difference was found in the U content of shales rich in coalified fossil plan remains (about 3 to 15% by volume) and those devoid of megaplant remains. However, shales immediately (within 10-15 cm) about and below coal seams are enriched, with 3.9 ppm U (overshale) and 3.8 ppm U (undershale; underclay) respectively. The highest values in the Sydney Coalfield were detected in samples described as "shaly coal" (Table 5.3), highly carbonaceous shale within coal seams.

These values are generally lower than the "average black shale" (8 ppm U) and much lower in U content than most "marine black shales" (Rogers and Adams, 1969).

Coal samples (Table 5.3) are on the average low in U content (about 0.5 ppm U); 67 per cent of the coal samples have less than 0.25 ppm U. Most of the uranium appears to be associated with the clayey impurities producing local concentrations over 4 ppm U. These average values are comparable with the results obtained from one sample of coal from Pennsylvania and two from Germany, but the latter individual values can hardly be considered representative.

Across a seam, the U content appears to be at a minimum at the centre and to increase towards the hanging and footwalls (Fig. 5.2, Table 5.2). See also Table 5.3, the Mc Aulay seam. It is not certain whether this reflects variations in the clay contents of the coal or if it is the general pattern for all the seams. The observation by Hawley (1955a) that many trace elements (Mn, As, Pb, Ge, Co, and Ni) are enriched in the top and bottom parts of most seams in the Sydney Coalfield, suggests this may also be the general case for U.

Table 5.1

Coal Measures of Sydney Coalfield, Cape Breton Island, Nova Scotia, in their relative stratigraphic position (youngest to oldest)

Age[1]	Seam	Stratigraphic Thickness[2]	Present Producer
WESTPHALIAN D	Point Aconi	110 cm	
	Lloyd Cove	185 cm	
	Stubbart	225 cm	Prince Mine
	Harbour	180 cm	Lingan & no. 26 Mines
	Bouthillier	90 cm	
	Backpit	150 cm	
	Phalen	210 cm	
	Emery	180 cm	
	Gardiner	120 cm	
WESTPHALIAN C	Tracy	180 cm	
	Shoemaker	15 cm	
	Mc Aulay	45 cm	
	Round Island	50 cm	
Mississippian			

[1] Zodrow and McCandlish (1978a).
[2] Maximum is quoted: refer to Hacquebard (1979) for variations in thickness.

Table 5.2

Uranium content of sedimentary rocks from Sydney Caolfield. Refer to Figure 5.1 for location of samples which are arranged in ascending stratigraphic order.

Location	Seam	Description of Rocks	U (ppm) mean	range	Standard Deviation	Number of Samples
1	Mc Aulay	Overshale, carbonaceous*	4.3	4.2-4.4		2
2	Shoemaker	sandstone, fine grained,	3.3	3.1-3.5		2
3		sandstone, conglomeratic, quartz-rich	1.7			1
4		sandstone, conglomeratic, quartz-rich	2.4			1
5	Tracy	shale*	3.3			1
6		sandstone, conglomeratic, quartz-rich	1.7	1.5-1.9		2
7	Emery	shale*	3.5	3.3-3.6		2
8	Emery	shale*	3.3	3.1-3.5		2
9		shale*	3.5			1
10		shale*	3.1			1
11		sandstone, conglomeratic, quartz-rich	1.9			1
12	Phalen	sandstone, fine grained, micaceous, grey	3.6			1
13	Phalen no. 26 Mine	sandstone, micaceous*	3.7	3.7		2
13	no. 26 Mine	overshale, within 15cm of the seam	3.1	2.4 4.0	±0.76	4
14	Harbour Lingan Mine	overshale, within 15cm of the seam, slicken sided	5.5			1
14	Harbour Lingan Mine	sandstone, fine grained, dark, micaceous*	3.1	2.5-3.9	±0.71	3
15		sandstone, grey, cross-bedded	5.7			1
16		shale*	3.5	3.3-3.6		2
17		sandstone, micaceous, grey	3.6			1
	Prince Mine Stubbart	overshale, dark, within 15 cm of the seam*	4.2	3.7-4.6	±0.37	4
	" "	undershale, grey, within 15 cm of the seam	3.1			1
18**	Upper Bonar	undershale, grey	3.3			1
19	Point Aconi	shale*	3.6	3.2-4.0	±0.43	4
	Point Aconi	Composite Profile from Fig. 5.1: a-b. See Fig. 5.2				
		sandstone, medium grained	2.7			1
		shale*	3.4			1
		overshale*	3.7			1
		top of seam	1.1	(Repeated in)		1
		centre of seam	0.2	( )		1
		bottom of seam	0.7	(Table 5.3)		1
		undershale	5.0			1
		sandstone, crossbedded	2.2			1
		red shale	3.5			1
		red shale	3.7			1
		AVERAGE OF SHALES	3.4	3.1-4.0	±0.27	16
		AVERAGE OF SANDSTONE	2.9	1.5-5.7	±1.05	17
		AVERAGE OF OVERSHALES	3.9	3.1-5.5	±0.86	12
		AVERAGE OF UNDERSHALES	3.8	3.1-5.0	±1.04	3
				TOTAL SAMPLE SIZE (excluding coal)		48

*Contains fossil plant remains.
**Between Locations 17 & 19.

Note: all uranium analyses by the DNA method.

Table 5.3

Uranium content of coals from Sydney Coalfield arranged in stratigraphic sequence from oldest to youngest. Refer to Figure 5.1 for location of samples.

Location	Seam	Description or Remarks	·U (ppm) mean	range	Standard deviation	Number of Samples
1	Mc Aulay†	top of seam, outcrop	0.21			1
1	Mc Aulay	15cm below top of seam, outcrop	0.06			1
2	Shoemaker††	shaly coal	4.82	1.11-9.22	4.1	3
5	Tracy	from mine dump	2.15	0.08-4.22	2.9	2
8	Emery*	100 m of outcrop	0.43	0.03-3.18	0.7	23
12	Phalen	80 to 100cm below top of seam, outcrop	0.17	0.09-0.23	0.06	4
No. 16 Dominion	Phalen	former producer	0.04	0.03-0.05	0.01	4
1-B Mine (13)	Phalen	former producer	0.11	0.06-0.17	0.07	2
Lingan Mine	Harbour	present producer	0.82	0.05-1.65	0.80	3
Princess Mine	Harbour	former producer	0.24	0.14-0.35	0.15	2
Prince Mine	Stubbart	present producer	0.49	0.06-2.51	0.74	10
16	Upper Bonar	shaly coal	3.50+			1
Point Aconi	Point** Aconi	refer to Fig. 5.2	0.67+	1.1-0.2-0.7		3
		AVERAGE FOR ABOVE COALS (excepting shaly coal)	0.46	0.03-4.2	0.80	55
		AVERAGE FOR SHALY COALS	4.49	1.11-9.22	3.40	4
Wilkes Barre, Pennsylvania			0.45			1
Oberhausen, Germany			0.17			1
Siebengebirge, Germany			0.03			1

Measured stratigraphic thickness at sample site:
† 35-40 cm *150 to 180 cm
†† 11 cm **110 cm
See Table 5.1 for information on the other seams.

+Determined by DNA.

The Sydney Coalfield coals appear to be poorer in U than those from other Pennsylvanian coalfields in the Appalachian region of the United States (avg. 1.4 ppm U, Swanson et al., 1976). With the limited number of samples, it is difficult to detect a consistent trend of U content and the relative age of the coal seams. There appears to be a positive correlation of uranium content and amount of clay impurities and a relationship between uranium content and stratigraphic position of a sample within a coal seam.

Nine pyrite-rich samples (FeS_2between 90 to 97%, the remainder being coal) from various coal seams around Sydney, were concentrated using heavy liquids and analyzed by DNA. Of eight samples, seven contain less than 0.2 and one 0.5 ppm U; hence no trend is discernible at this resolution of results. Although it is probable that a part of the uranium is present in the pyrite as solid solution, higher values would probably be indicative of enrichment in the iron oxide coating (King, 1953) of the pyrite (Zentilli, unpublished data).

Acid waters collected from drainage ditches of coal stored in the open air contained between 0.1 and 0.2 ppm U as determined by DNA (the samples are from no. 26 and Prince mines, respectively). These samples also provided a favourable environment for prolific growth of the bacterium of the type **Thiobacillus** species especially at 4° C.

Coal associated hydrated sulphates (Table 5.4) such as melanterite ($FeSO_4.7H_2O$) contain almost identical amounts of uranium at the Lingan and no. 26 mines, and are richer in uranium than sideronatrite ($Na_2Fe(SO_4)_6(OH).3H_2O$) and epsomite ($MgSO_4.7H_2O$). Chemical results of these minerals are given by Zodrow and McCandlish (1979). Halite from no. 26 mine contains less than 0.2 ppm U. Of all the analyzed hydrated sulphates, iron tamarugite has the highest concentration of U, 5.3 ppm, whereas tamarugite ($NaAl(SO_4)_2.6H_2O$) has 2.5 ppm.[3] It appears that coal-associated minerals from no. 26 mine are richer in uranium than those from the Prince mine.

Preliminary experiments were conducted to evaluate the enrichment of uranium achieved with progressive ashing of some of the coal samples listed in Table 5.3. The results, however, were erratic, leading to severalfold enrichment in some experiments, no enrichment or even to U loss in others. It is possible that during combustion of the coal some of the

[3] Pickeringite ($MgAL_2(SO_4)_4 \cdot 22H_2O$), sample location no. 8, Fig. 5.1, contains on the average 17 ppm U (added note in proof).

uranium is lost with the volatile fraction, i.e., ashing should be done at low temperatures and under carefully controlled conditions (e.g. Lloyd and Francis, 1975). Some ashes remained black and sticky even after a long period of heating, and one such ash from the Mc Aualy seam violently exploded when being hydraulically pressed into a pellet for IFT analysis shattering the massive steel cylinder: ashing experiments were discontinued.

Discussion

The above results are an indication that the uranium content in most sedimentary rocks from the Sydney Coalfield is low, and not significantly different from that of other Upper Paleozoic rocks on the Island of Cape Breton. The higher uranium contents are found within shales in the proximity of coal. Kirkham (1978) has published uranium analyses of sedimentary rocks near the Horton-Windsor unconformity of Early Carboniferous age, which are locally mineralized with Cu, Pb and Zn. The sandstone averages about 2.5 ppm U and other associated lithologies, such as conglomerate and limestone, contain 4 to 5 ppm U on the average. Against these values, the Sydney Coalfield sandstone (2.9 ppm U), shale (3.4 ppm U), and undershale and overshale (about 4 ppm U) do not appear very different. The low concentrations of uranium in coal are lower than those reported for most Paleozoic coals in the North Central and Eastern U.S. (Vine, 1956, Swanson et al., 1976). The average coal in the U.S. contains 1.8 ppm U (Swanson et al., 1976) but their Neutron Activation analyses did not detect values lower than 0.2 ppm U. Considering that 67 per cent of the Sydney coal samples have less than 0.2 ppm U, if all these analyses are arbitrarily given a value of 0.2 ppm U and if shaly coal samples are included, the average U content of Sydney coal would be 0.9 ppm. As in the Sydney coalfield, shales and underclays from the U.S. Paleozoic coalfields are richer in uranium than the coal (Snider, 1954). Local enrichments of up to 80 ppm U in Illinois coal, and up to 190 ppm U in Pennsylvania (Patterson, 1955) are considered anomalies due to secondary processes that have affected the coal (Vine, 1956). High-rank, low-ash coals of the type most desired for fuels appear to be rarely uraniferous, and significant, widespread concentrations of U are better represented in low rank and impure coal, including lignite and subbituminous coal. In most cases, these higher concentrations are not considered to be syngenetic (Benson and Gill, 1956; DeVoto, 1978). The rather consistent low values in the Sydney coal suggest that conditions of water circulation in the very extensive Pennsylvanian peat bogs (with an early removal of U from the waters near the basin's margins?) and the lack of glassy volcanic debris in the sequence contributed to make this coal uranium-poor. During coalification, it is possible that a certain proportion of the uranium was lost. Breger et alu (1955, and Breger and Deul (1956) indicated that 98 per cent of the uranium in lignite from Wyoming is present in the form of organo-uranium complexes. At about 100°C organic degradation of the humic acid present in coal takes place and kerogen, which is inert to uranium, is formed (DeVoto, 1978). Furthermore, Moore (1954) demonstrated experimentally that although peat, lignite and subbituminous coal extract 98 per cent or more the uranium from an aqueous solution, bituminous coal retains only 17 per cent. This would diminish the possibility of secondary uranium enrichment in the Sydney bituminous coals, but suggests that anomalous uranium concentrations could be found locally in lower rank coals in the proximity of unconformities or permeable portions of sedimentary sequences elsewhere in Nova Scotia.

Table 5.4

Uranium content in ppm of coal-associated Minerals from Sydney Coalfield

Mineral	Lingan Mine	no. 26 Mine (Phalen seam)	Prince Mine
Melanterite[2]	0.27	0.28	$<0.2^{+}$
Aluminocopiapite[1]		0.4^{+}	$<0.2^{+}$
Fibroferrite[2]		0.3^{+}	$<0.2^{+}$
Sideronatrite[2]		0.09	
Epsomite[2]		0.003	
Tamarugite		2.5	
Iron-bearing Tamarugite		5.3	
Halite		$<0.2^{+}$	

[1] From no. 26:

$(Na_{0.058}Ca_{0.006}Mg_{0.085}Mn_{0.013}Fe^{2+}_{0.175}Al_{0.663})$

$(Fe^{3+}_{0.983}AL_{0.017})_4(OH)_2(SO_4)_6 \cdot 18.4H_2O$.

[2] For discussion of interrelated paragenesis and chemical composition refer Zodrow and McCandlish (1978).

[+] Determined by the DNA method.

The relatively high values above and below coal seams and the very low concentration of uranium in their middle sections should be detectable with gamma borehole logging techniques. Hawley (1955a) attempted stratigraphic correlation based on trace elements of the seams, and suggested there is an enrichment in certain trace elements (e.g. As) as the seams get younger. Probably uranium content could be used in a similar manner, but a larger number of samples and a more detailed study would be required to evaluate this possibility. However, on a preliminary basis it appears that roughly coincidental with the Westphalian C-D boundary (Table 5.1), on the average, uranium values show some tendency to increase (shaly coal is not considered).

Complete ashing of coal from the Sydney Coalfield leads to an average 8.6-fold enrichment of most of its trace elements (Hawley, 1955a). For the average concentration of 0.46 ppm U determined in this study for coal (excepting shaly coal) combustion should lead to an average about 4 ppm U in the ash, provided no uranium is lost with the volatile fraction. We have not determined the Th content of the coal, but considering that the average Th/U ratio for 799 samples of coal from 28 states in the U.S. is 2.6 (Swanson et al., 1976), the ashes from Sydney coal may contain less than 1.5 ppm thorium.

Acknowledgments

This investigation has been supported by the National Research Council of Canada through grants to both authors, by the Geological Survey of Canada, through a Research Agreement with Zentilli, and by the College of Cape Breton, Grant CCB-10058 to Zodrow. Special thanks are extended to Mr. Keith A. Taylor of Dalhousie University, for all the IFT uranium determinations and to officials notably Mr. G. MacLean, of Devco for repeated and ongoing arrangements to visit the coal mines (especially no. 26 mine).

References

Benson, N.M. and Gill, J.R.
1956: Uranium-bearing lignite and its relation to volcanic tuffs in eastern Montana and North and South Dakota; U.S. Geological Survey Professional Paper 300, p. 413-418.

Breger, I.A. and Deul, M.
1956: The organic geochemistry of uranium; in Contributions to the Geology of Uranium and Thorium; U.S. Geological Survey Professional Paper 300, p. 505-510.

Breger, I.A., Deul, M., and Meyrowitz, R.
1955: Geochemistry and mineralogy of a uraniferous subbituminous coal; Economic Geology, v. 50. p. 610-624.

Brown, R.
1845: On the geology of Cape Breton; Quarterly Journal of Geological Society, London, v. 1, p. 23-26; p. 207-213.

Dawson, J.W.
1878: Acadian Geology; 3rd. ed. (Macmillan and Co.), London, 694 p.

DeVoto, R.H.
1978: Uranium geology and exploration; Lecture notes and references; Colorado School of Mines, Golden, Colorado, 396 p.

Dostal, J., Capedri, S., and Aumento, F.
1975: Uranium as an indicator of the origin of the Thethyan ophiolites; Earth and Planetary Science Letters, v. 26, p. 345-352.

Fisher, D.E.
1970: Homogenized fission track determination of uranium in whole rock geologic samples; Analytical Chemistry, v. 42, No. 3, p. 414-416.

Gabelman, J.W.
1977: Migration of uranium and thorium-exploration significance; Studies in Geology No. 3, American Association of Petroleum Geologists, Tulsa, Oklahoma, 168 p.

Hacquebard, P.A.
1979: A geological appraisal of the coal resources of Nova Scotia; Canadian Institute of Mining and Metallurgy, Bulletin 72, No. 802, p. 76-87.

Hawley, J.E.
1955a: Spectrographic study of some Nova Scotia Coals; Canadian Institute of Mining and Metallurgy, Transactions, v. 58, p. 412-426.

Hawley, J.E.
1955b: Germanium content of some Nova Scotia coals; Economic Geology, v. 50, p. 517-532.

Hawley, J.E. and Rimsaite, L.
1954: Spectrographic studies of Nova Scotia coal; (Abs.) Spectrochimica Acta, v. 6, p. 444-445.

King, L.H.
1953: Occurrence, distribution and weathering of pyrites in coals from the Sydney coalfield, N.S.; (Abs.) Economic Geology, v. 48, p. 623.

Kirkham, R.V.
1978: Base metal and uranium distribution along the Windsor-Horton contact, Central Cape Breton Island, Nova Scotia; in Current Research, Part B, Geological Survey Canada, Paper 78-1B, p. 121-135.

Lloyd, W.G. and Francis, H.E.
1975: Fate of minor and trace elements in alternate gasification schemes: II symposium on Coal Utilization, NCA/BCR Coal Conference, Louisville, Kentucky, p. 329-340.

Mahdavi, A.
1964: Thorium, uranium and potassium contents of Atlantic and Gulf Coast beach sands; in J.A.S. Adams, and W.M. Lowder (ed.), The Natural Radiation Environment, Chicago University Press, Chicago: 86 p.

Mitchell, W.S. and Aumento, F.
1977: Uranium in oceanic rocks: DSDP Leg 37; Canadian Journal of Earth Sciences, v. 14, p. 974-808.

Moore, G.W.
1954: Extraction of uranium from aqueous solution by coal and some other materials; Economic Geology, v. 49, no. 6, p. 652-658.

Patterson, E.D.
1955: Radioactivity of part of the bituminous coal region of Pennsylvania: U.S. Geological Survey TEI-479, issued by U.S. Atomic Energy Commission Technical Information Service, Oak Ridge, Tenn. (In: Vine, 1956).

Roffman, H.K., Kary, R.E., and Hudgins, T.
1977: Ecological distribution of trace elements emitted by coal-burning power generating units employing scrubbers and electrostatic precipitators: IV Symposium on Coal Utilization, NCA/BCR Coal Conference Louisville, Kentucky, p. 192-215.

Rogers, J.J.W. and Adams, J.A.S.
1969: Uranium; in K.H. Wedepohl, ed., Handbook of Geochemistry; New York, Springer-Verlag, v. 2, pt. 1, chapt. 92, 50 p.

Rose, E.R., Sanford, B.V., and Hacquebard, P.A.
1970: Economic minerals of Southeastern Canada; in R.J.W. Douglas, Editor, Geology and Economic Minerals of Canada; Geological Survey of Canada, Economic Geology Report No. 1, p. 305-306.

Russell, W.L.
1945: Relation of radioactivity, organic content, and sedimentation; American Association of Petroleum Geologist Bulletin 29, no. 10, p. 1470-1494.

Snider, J.L.
1954: Reconnaissance for uranium in the Indian coalfield: U.S. Geological Survey TEM-784, 26 p. issued by U.S. Atomic Energy Commission Technical Information Service, Oak Ridge, Tenn.

Swanson, V.E., Medlin, J.H., Hatch, J.R., Coleman, S.L., Wood, G.H., Jr., Woodruff, S.D., and Hildebrand, R.T.
1976: Collection, chemical analysis, and evaluation of coal samples in 1975; U.S. Geological Survey Open File Report 76-468, 503 p.

Vine, J.D.
1956: Uranium-bearing coal in the United States; in Contributions to the Geology of Uranium and Thorium, U.S. Geological Survey, Professional Paper 300, p. 405-411.

Zentilli, M., Mitchell, W.S., Taylor, K.A., and Taylor, P.F.
1977: Studies of distribution of uranium in selected ore environments using nuclear track techniques; Report of Activities, Part B; Geological Survey Canada, Paper 77-1b, p. 141-143.

Zodrow, E.L. and McCandlish, K.
1978a: Distribution of **Linopteris obliqua** in the Sydney Coalfield of Cape Breton, Nova Scotia; Paleontographica, v. 168, Ser. B. p. 1-16.

1978b: Hydrated sulfates in the Sydney Coalfield, Cape Breton, Nova Scotia; Canadian Mineralogist.; v. 16, p. 17-22.

Zodrow, E.L., Wiltshire, Jim, and McCandlish, K.
1979: Hydrated sulfates in the Sydney Coalfield, Cape Breton, Nova Scotia. II Pyrite and its alteration products; Canadian Mineralogist, v. 17, p. 63-70.

6.

THE EFFECTS OF BOREHOLE DIAMETER, BOREHOLE FLUID, AND CASING THICKNESS ON GAMMA RAY LOGS IN LARGE DIAMETER BOREHOLES

Project 740085

J.G. Conaway, K.V. Allen, Y.B. Blanchard,
Q. Bristow, W.G. Hyatt, and P.G. Killeen
Resource Geophysics and Geochemistry Division

Conaway, J.G., Allen, K.V., Blanchard, Y.B., Bristow, Q., Hyatt, W.G., and Killeen, P.G., The effects of borehole diameter, borehole fluid, and casing thickness on gamma ray logs in large diameter boreholes; in Current Research, Part C, Geological Survey of Canada, Paper 79-1C, p. 37-40, 1979.

Abstract

The response of a gamma ray logging system to a thin zone of radioactive material depends on a number of instrumental, borehole, and formation parameters. This paper considers the effects of borehole diameter, borehole fluid, and casing thickness on the shape of the system response function and the area beneath it in total-count gamma ray logging.

Introduction

The noise-free response of a gamma ray logging system to a thin zone of radioactive material perpendicular to the borehole is called the system response function. The shape and amplitudes of the gamma ray log from a borehole are determined by the ore distribution and the system response function; thus, successful quantitative interpretation of the log depends on a knowledge of the form of the system response function. The shape and area of this function depend on many instrumental, formation, and borehole parameters. In this paper we consider the effects of three borehole parameters: borehole diameter (over the range from 9-33 cm), borehole fluid (air or water), and casing thickness (from 1.6-12.7 mm steel casing). The results presented here are based on tests in the borehole calibration models located at the U.S. Department of Energy radiometric calibration facilities at Grand Junction Colorado (Mathews et al., 1978).

Theoretical Background

The theoretical basis for quantitative interpretation of gamma ray logs is given by the equation

$$\bar{G}T = KA \qquad (1)$$

(Scott et al., 1961). Here, A is the area beneath a given anomaly on the gamma ray log, T is the thickness of the radioactive zone causing the anomaly, $\bar{G}$ is the average radioelement concentration or grade over that thickness, and K is the constant of proportionality. Equation (1) assumes that the system is linear (i.e. follows the principle of superposition). The constant K is generally determined in model calibration boreholes under standard conditions of casing thickness, borehole diameter, and borehole fluid. If these conditions are different in the field than in the model, the sensitivity of the system to a given radioelement may change, requiring a compensating change in K (usually applied in the form of separate correction factors, e.g. Dodd and Eschliman, 1972).

The validity of equation (1) is independent of the shape of the system response function. However, if the gamma ray log is to be deconvolved to produce a record of radioelement concentration as a function of depth (e.g. Scott, 1963; Conaway and Killeen, 1978) then the shape of the system response function must be known at least approximately so that an appropriate deconvolution operator can be derived.

A digital inverse filter for deconvolution of gamma ray logs has been given by Conaway and Killeen (1978) based on earlier work by Suppe and Khaikovich (1960), Davydov (1970), and Czubek (1971) wherein the noise-free response $\phi(z)$ of a point detector to a thin zone of radioactive material at depth z = 0 was approximated by

$$\phi(z) = \frac{\alpha}{2} e^{-\alpha|z|} \qquad (2)$$

where α is a constant for a given set of instrument, borehole, and formation parameters. The inverse filter coefficients are given by

$$\left(-\frac{1}{(\alpha \Delta z)^2},\ 1 + \frac{2}{(\alpha \Delta z)^2},\ -\frac{1}{(\alpha \Delta z)^2} \right) \qquad (3)$$

where Δz is the sampling interval along the borehole.

A simple method for determining α which is valid in either model or field boreholes has been discussed by Conaway (in press). All that is required is a digital log across an interface between a barren zone and an ore zone, where the barren zone is essentially homogeneous over a distance of perhaps 1.5-2 m away from the interface (Fig. 6.1a). It is not necessary that the ore zone be homogeneous or infinitely thick. The constant (except for statistical noise) 'background' radiation intensity in the barren zone is subtracted from each discrete value, and the resulting data are plotted as the natural logarithm of the count rates ('background' corrected) as a function of depth (Fig. 6.1b). The desired value of α is the slope on this plot of the linear anomaly flank outside of the ore zone. This technique is more difficult to apply to data from an analog logging system because of the distortion introduced by the analog ratemeter (Conaway, in press). This semi-log slope technique for determining α is useful for studying the behavior of the system response function as a function of borehole diameter, borehole fluid, and casing thickness, and will be used in subsequent sections of this paper.

Steel Casing

Figure 6.2a shows a plot of gamma ray intensity as a function of depth measured in a model borehole containing a 1.5 m thick 'ore' zone between two barren zones, for no casing and for six thicknesses of steel casing (1.6, 3.2, 4.8, 6.4, 9.5, and 12.7 mm). The borehole is water filled and 11.4 cm in diameter. All of the curves have been normalized so that their areas are equal, for comparison; this has no effect on the computed value of α. The digital sampling interval Δz = 3 cm, logging velocity v = 0.3 m/min, and the detector is 25 x 75 mm NaI(Tl) with the lower energy threshold of the instrument set at 100 keV.

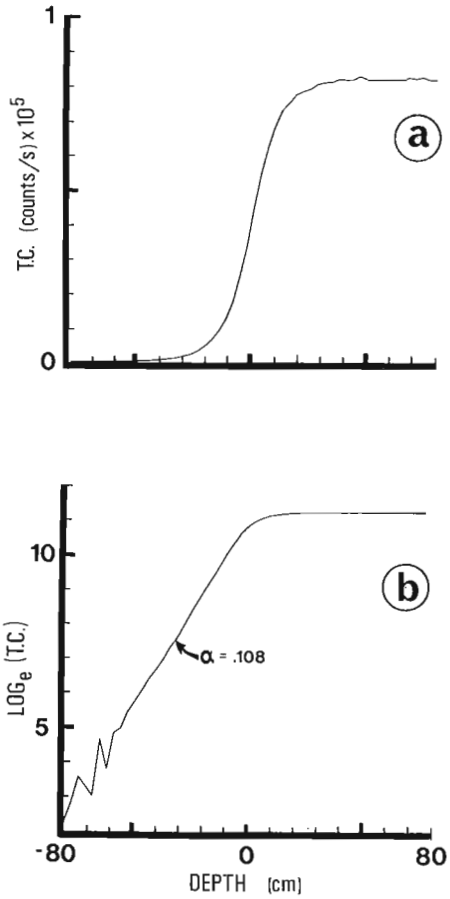

(a) Measured total count (T.C.) gamma ray response across a barren zone/ore zone interface.

(b) Natural logarithm of data in Figure 6.1(a) (background subtracted) plotted against depth. Units of α are cm^{-1}.

Figure 6.1.

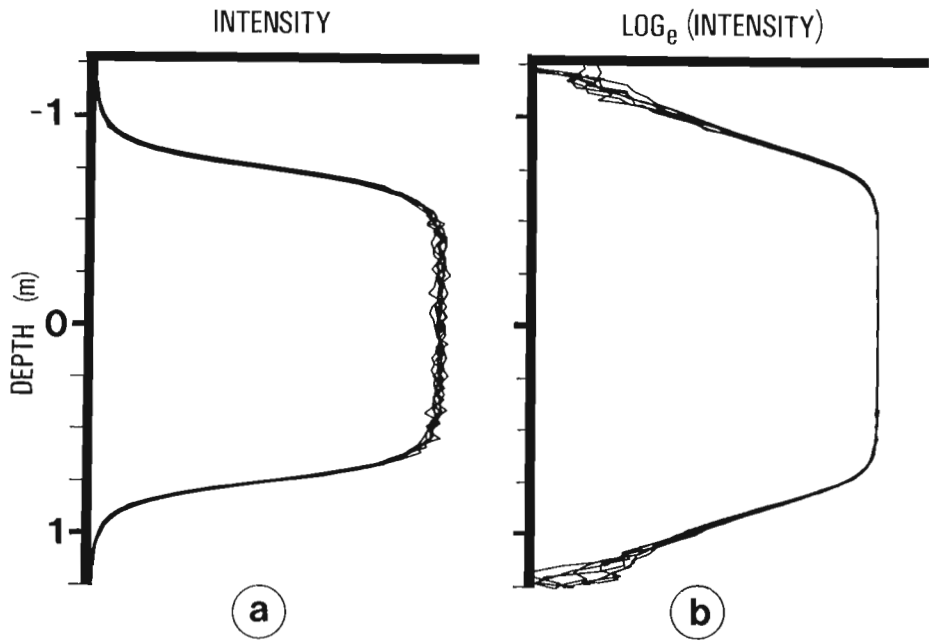

(a) Seven logs through a model ore zone with different thicknesses of steel casing, as described in text. All areas have been normalized to a constant value.

(b) Semi-log plot of the data shown in Figure 6.2.a, background subtracted.

Figure 6.2.

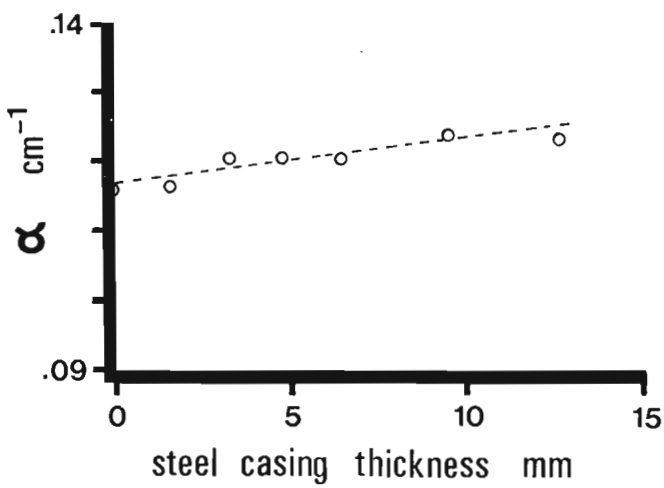

Figure 6.3. *Plot of α as a function of steel casing thickness based on data shown in Figure 6.2b. The straight line through the experimental points is not meant to imply that the data follow a linear pattern; statistical scatter is too large to determine this reliably.*

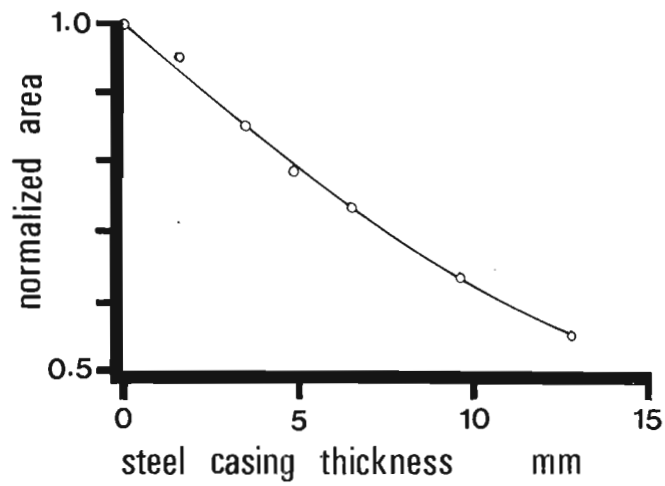

Figure 6.4. *Plot of anomaly area as a function of steel casing thickness, normalized to a value of 1 for no casing.*

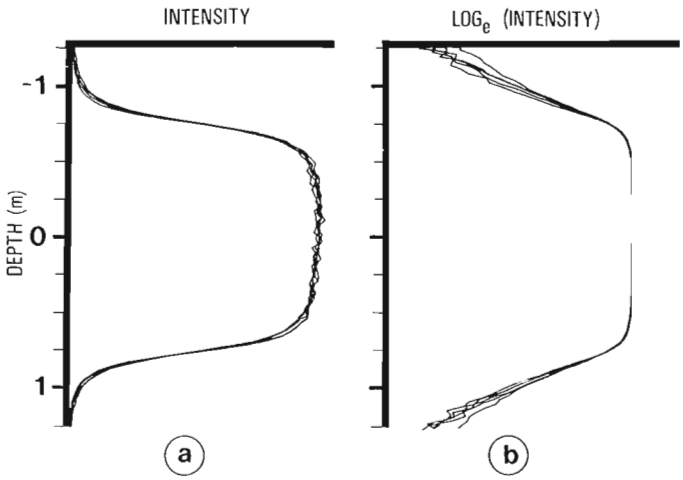

(a) Five logs through a model ore zone in uncased water-filled boreholes of different diameters, as described in text. All areas have been normalized to a constant value.

(b) Semi-log plot of the data shown in Figure 6.5a, background subtracted.

Figure 6.5.

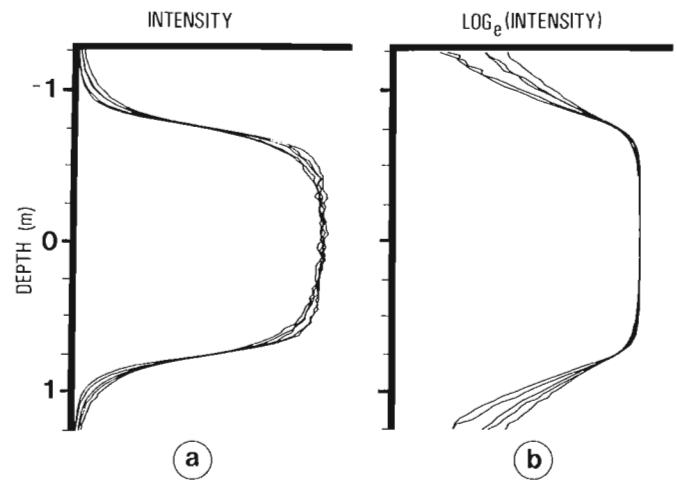

(a) Five logs through a model ore zone in uncased air-filled boreholes of different diameters, as described in text. All areas have been normalized to a constant value.

(b) Semi-log plot of the data shown in Figure 6.6a, background subtracted.

Figure 6.6.

It is clear from Figure 6.2a that the casing has little effect on the shape of the log. Subtracting the background and plotting the natural logarithm as described above gives Figure 6.2b. In spite of considerable statistical noise outside of the ore zone in this figure, some divergence of the curves can be seen as distance from the ore zone increases. Figure 6.3 shows a plot of α as a function of casing thickness based on a least-squares fit on the linear portion of the anomaly flanks in Figure 6.2b, over the range from 6-36 cm outside of the ore zone, on both sides.

Figure 6.4 shows the effect of casing on the total area of the anomaly, normalized to 1 for no casing. The inverse of this curve would give multiplicative casing correction factors which can be applied to gamma ray curves with different casing thickness. It should be emphasized that Figures 6.3 and 6.4 are dependent upon instrumental characteristics, and correction factors should be individually determined for each probe and logging system.

Borehole Diameter and Fluid

The effect of borehole diameter on α has been discussed by Suppe and Khaikovich (1960) and Davydov (1970) based on experimental results, and by Czubek (1971) based on an analytical expression for the point detector system response function. The data given in the present paper were obtained in five water-filled model boreholes of different diameters (8.9, 11.4, 17.8, 22.9 and 33 cm) through the same 1.5 m thick ore zone (Figure 6.5a). In all cases the borehole probe was kept in contact with the borehole wall throughout the log. The logs shown in Figure 6.5a have been normalized to give uniform area, as explained previously. These same logs ('background' corrected) are plotted on semi-log co-ordinates in Figure 6.5b. Examination of Figure 6.5b shows that the anomaly flanks are not completely linear. The corresponding normalized logs for the same boreholes air-filled are given in Figures 6.6a and 6.6b. The differences caused by the various borehole diameters are more pronounced in the case of air-filled boreholes. In large diameter boreholes, the ore zone will be detected from a greater distance if the borehole is air-filled rather than water-filled due to increased radiation passing through the borehole fluid in the case of air. This explains why there is a greater difference between the results in air and in water for large diameter boreholes than for small diameters.

The values of α determined using the semi-log slope technique, based on the data shown in Figures 6.5 and 6.6 are plotted in Figure 6.7. Figure 6.8 shows the total area under the anomaly curves for the five borehole diameters, both air and water filled, normalized to the 8.9 cm diameter case. In the case of an air-filled borehole one expects very little change in area, whereas for the water-filled case the curve asymptotically approaches a constant area corresponding to the case of infinite diameter (i.e. logging along a flat wall). If the probe were centred, of course, the curve for the water-filled case would asymptotically approach zero.

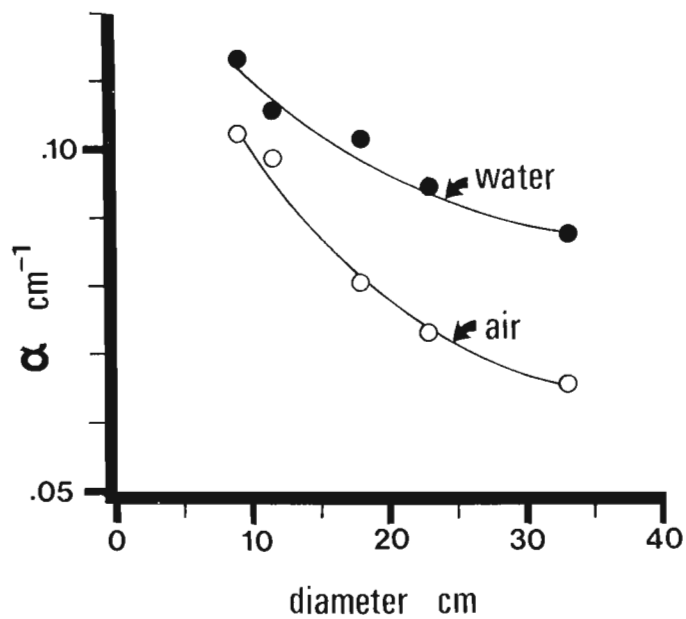

Figure 6.7. *Values of α as a function of borehole diameter, as explained in text.*

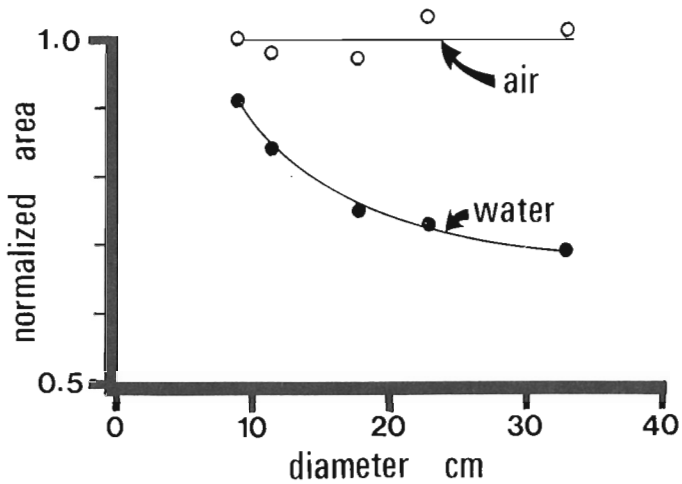

Figure 6.8. Area under the anomaly curves from boreholes of various diameters through a model ore zone, normalized to 100 per cent for air-filled case.

Discussion and Conclusions

In this paper we have illustrated the variations in the shape of the system response function (in particular the variations of the constant α in equation (2)) with changes in borehole diameter, borehole fluid, and steel casing thickness, for total count logging. In addition, variations in the system sensitivity (i.e. area beneath the response function) with these same borehole parameters have been described.

Results such as these, obtained with a particular set of equipment, should not be used to derive correction factors for other equipment. These factors should be determined individually for each logging system. The results presented here, however, serve to illustrate the effects which can be expected under these conditions.

In the case of gamma ray spectral logging equipment, correction factors should be determined individually for each spectral window, for best results. Differences between the behavior of the different windows under various conditions may be small, but this should be verified experimentally rather than assumed.

Acknowledgments

The authors thank J.M. Carson and K.A. Richardson for helpful comments and suggestions, and the U.S. Department of Energy and Bendix Field Engineering Corp. personnel for expediting the logging of the model boreholes at Grand Junction Colorado.

References

Conaway, J.G.
Direct determination of the gamma ray logging system response function in field boreholes. (in press)

Conaway, J.G. and Killeen, P.G.
1978: Quantitative uranium determinations from gamma ray logs by application of digital time series analysis; Geophysics, v. 43, p. 1204-1221.

Czubek, J.A.
1971: Differential interpretation of gamma ray logs: I. Case of the static gamma-ray curve; Report No. 760/I, Nuclear Energy Information Centre, Polish Government Commissioner for Use of Nuclear Energy, Warsaw, Poland.

Davydov, Y.B.
1970: Odnomernaya obratnaya zadacha gamma-karotazha skvazhin (one dimensional inversion problem of borehole gamma logging); Izv. Vyssh. Uchebn. Zaved., Geol. I. Razvedka, No. 2, p. 105-109 (in Russian).

Dodd, P.H. and Eschliman, D.H.
1972: Borehole logging techniques for uranium exploration and evaluation; in Uranium Prospecting Handbook, S.H.U. Bowie, M. Davis, and D. Ostle, eds., Inst. Min. Metall., London.

Mathews, M.A., Koizumi, C.J., and Evans, H.E.
1978: DOE - Grand Junction logging model data synopsis; Bendix Field Eng'g Corp. publication GJBX-76(78), Grand Junction, Colorado.

Scott, J.H.
1963: Computer analysis of gamma-ray logs; Geophysics, v. 28, p. 457-465.

Scott, J.H., Dodd, P.H., Droullard, R.F., and Mudra, P.J.
1961: Quantitative interpretation of gamma-ray logs; Geophysics, v. 26, p. 182-191.

Suppe, S.A. and Khaikovich, I.M.
1960: Resheniye pryamoi zadachi gamma-karotazha v sluchaye slozhnogo raspredeleniya radioaktivnogo elementa v aktivykh plastakh (Solution of the linear problem of gamma logging in the case of a complex distribution of the radioactive element in the active strata); Voprosy Rudnoi Geofiziki, Issue I (in Russian).

7.

BASIC COMPUTER PROGRAMS FOR THE POSITIONING, RECORDING AND DISPLAY OF SPATIALLY DISTRIBUTED DATA

Project 760005

Jean-Marie Sempels[1] and Patrick McLaren[2]
Atlantic Geoscience Centre, Dartmouth

Sempels, Jean-Marie and McLaren, Patrick; Basic computer programs for the positioning, recording and display of spatially distributed data; in Current Research Part C, Geological Survey of Canada, Paper 79-1C, p. 41-50, 1979.

Abstract

Three computer programs implemented in BASIC are used with a mini-computer, a graphic cathode ray tube (CRT), and a digital plotter to (i) record a variety of range and bearing information in order to calculate and display the position on the CRT, (ii) record data collected at the position, and (iii) display on separate maps produced on the digital plotter all positions and/or the data recorded at the positions. The first program is an interactive program for the positioning, CRT rapid display and data recording on magnetic tape. The other two programs are interactive with the first and are used to produce maps on the digital plotter of the positions or specific data respectively.

Introduction

The programs listed in this paper require a mini-computer, a graphic cathode ray tube (CRT), and a digital plotter and are particularly suited for positioning, recording and display of spatially distributed data. The system was designed for, but is not restricted to, rapid analysis of coastal and marine data enabling an in-field assessment of inter-relationships among numerous variables through the production of maps (McLaren and Sempels, 1978).

The objectives of the system are:

1. To record site information such as name, chosen reference points, length and bearing of baseline, latitude and longitude as well as qualitative description unique to the site. This information is referred to as Level I parameters.
2. To record the position of individual sample locations (fixes) relative to chosen reference points defined by Level I parameters. Information used either directly or indirectly to calculate position are referred to as Level II parameters.
3. To calculate a fix position according to several possible combinations of range and/or bearing data or, when necessary by dead reckoning.
4. To display rapidly on a graphic CRT the position of the fix as well as reference points and all previous fixes at which data have been recorded (Fig. 7.1). This is particularly useful in verifying the exactness of the positioning information and in some cases, as during geophysical work, in advising on modifications of the ship's course.
5. To record the kind of data obtained at a fix, either by an immediate quantitative result such as a water depth, or by a numeric qualifier designed to provide maximum on-site information; for example, 234 may represent a grab sample composed of less than 20 per cent gravel (2) and moderately sorted sand (3) which is predominantly fine (4). Furthermore the system is not restricted in either the type of data or the number of kinds of data that may be collected at a fix.
6. To produce, with the aid of a digital plotter, separate maps of the fixes and the numerical values of the data recorded at each fix (Fig. 7.2).

Acknowledgments

The authors wish to thank S.H. Whitlow of Environment Canada for providing computer time to develop these programs. Further refinements were completed on board **M.V. Gulf Star** during field operations in Lancaster Sound. The assistance provided by Captain M. Whelan is gratefully acknowledged.

Program Listings

Introduction

All components of the software are implemented in BASIC. Although the programs contain some machine dependent statements for a Tektronix 4051, they are easily adaptable to other types of mini-computers. To facilitate possible subsequent user modifications, the programming is in a clear, organized manner. Structured programming (very limited with the BASIC version used) and programming for time efficiency were not particularly sought as neither are limiting factors in the operations of this software.

[1] Petro-Canada Inc., Calgary, Alberta
[2] Atlantic Geoscience Centre, Dartmouth

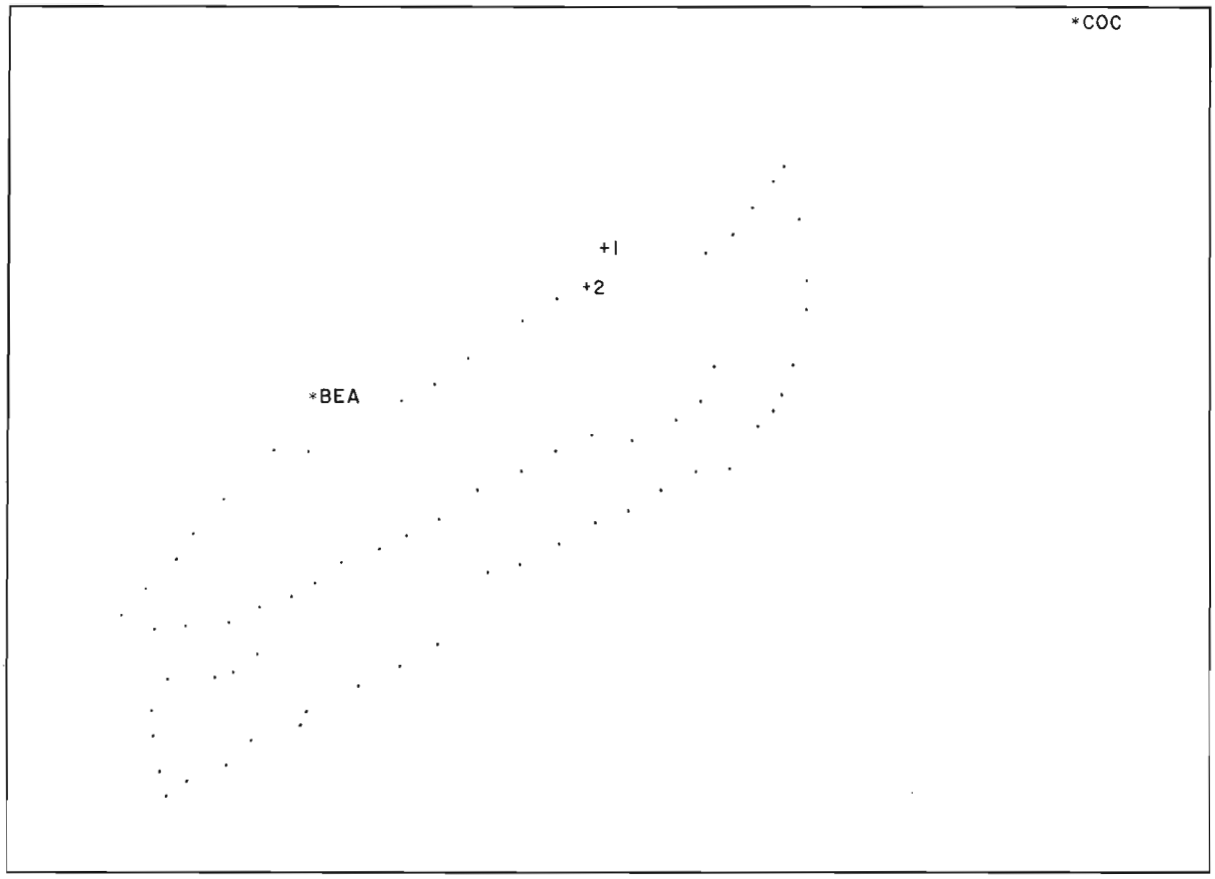

Figure 7.1 *Example of fix positions displayed on the graphic CRT relative to reference points BEA and COC. The last and second last fixes are identified by "+1" and "+2" respectively enabling ready identification of the present position.*

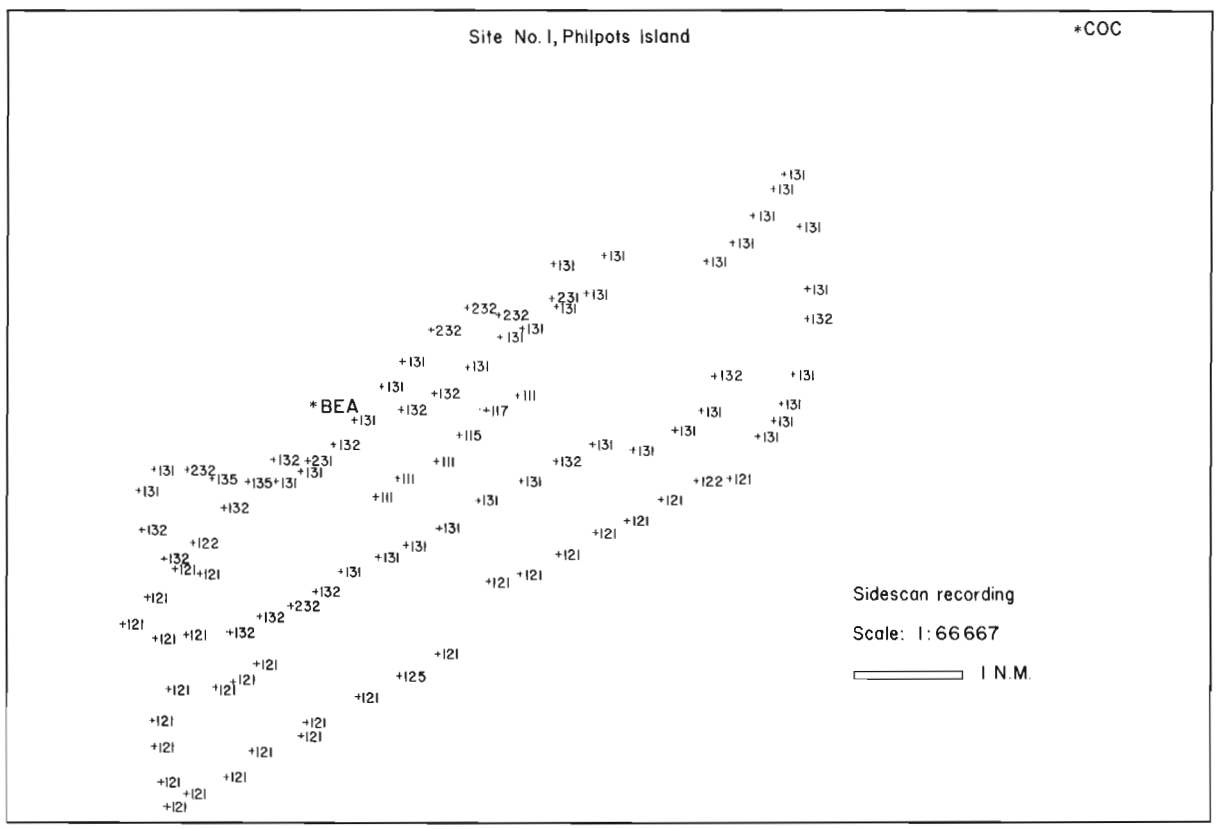

Figure 7.2. *Example of map produced by the digital plotter displaying the position and qualifiers for side scan sonar data. For example the qualifiers 232 indicate an immediate assessment of the record by the geophysicist that two patterns are present (2), the bottom is predominantly sandy (3) and there is moderate relief (2).*

The software is made up of two principal components. The first is an interactive program for the positioning, CRT rapid display and data recording on magnetic tape. The second comprises two separate interactive programs to produce maps on a digital plotter. The two components require 18 504 and 13 896 bytes of memory respectively to be stored in an external ASCII format.

Positioning, CRT Rapid Display and Data Recording Program

The program starts by creating a new data file with the input of Level I information as the file heading or by reading an existing file if it is used more than once at the same site (Fig. 7.3). When two reference points are used the westernmost point is always defined as reference point 1. The baseline distance ('Base distance', statement 790) is the distance between the two reference points expressed in the same units as the ranges that will be used in determining the fix position. Because conversion of distance units is never performed in the program, it is essential to be consistent with units. The baseline bearing ('Base bearing', statement 770) is the angle between the lines from reference point 1 to reference point 2 and from reference point 1 to true north. It follows that this angle must be such that 0 < Base bearing < 180°.

The program is then normally used to calculate the position and record the data for subsequent fixes (Level II and III data). The calculation of fix position follows a defined hierarchy depending on the availability of Level II data. This hierarchy is, (i) both ranges, (ii) range and bearing to reference point 1, (iii) range and bearing to reference point 2, (iv) both bearings and, failing all these (v) dead reckoning. Once calculated, the position can be displayed on the graphic CRT as well as all previous fix positions and the reference point(s) (Fig. 7.1). If acceptable, the latest fix information can be stored on tape, otherwise it may be deleted. The listing is as follows with appropriate annotations.

A user definable entry point (user definable key no 1 on a Tektronix 4051). Used to force control into plotting all data on the CRT. Can be used to obtain a plot of all positions after the program has been terminated voluntarily or accidentally.

```
1 REM *****     POSITIONING AND DATA RECORDING PROGRAM.      *****
3 GO TO 100
4 GO TO 2130
100 PAGE
110 PRINT "INSERT CORRECT TAPE AND ENTER APPROPRIATE FILE NUMBER   ";
120 INPUT Q2
130 FIND Q2
140 SET DEGREES
150 DIM A$(72),B$(3),C$(3),E$(4),F$(4),G$(2),T4(300),T5(300),H$(2)
160 DIM I$(3),J$(3),K$(3),L$(3),M$(3),N$(3),O$(3)
170 T6=0
180 T7=0
190 T8=0
200 T9=0
210 T2=0
220 R2=0
230 PRINT "J_IS THIS A NEW SITE? (YES=1, NO=0).   ";
240 INPUT Z1
250 IF Z1=1 THEN 560
260 INPUT @33:A$
270 PRINT "J_ FIX NUMBERS READ: J_"
280 ON EOF (0) THEN 500
290 INPUT @33:Z4
300 GO TO Z4 OF 310,360,480
310 INPUT @33:Q1,Z5,Z6,Z7,Z8,Z9,Y1,Y2,Z2,Z3
320 INPUT @33:B$,C$
330 V3=Z2
340 V4=Z3
350 GO TO 430
360 INPUT @33:D1,X2,V3,V4
370 INPUT @33:E$,I$,J$,K$,L$,M$,N$,O$
380 PRINT D1;
390 IF V3=9999 AND V4=9999 THEN 290
400 T2=T2+1
410 T4(T2)=V3
420 T5(T2)=V4
430 T6=T6 MIN V3
440 T7=T7 MAX V3
450 T8=T8 MIN V4
460 T9=T9 MAX V4
470 GO TO 290
480 INPUT @33:V2
490 GO TO 290
500 PRINT "J_"
510 PRINT "J_FILE READ, READY TO OVERWRITE END OF FILE.  LAST FIX=";D1
520 PRINT "-------------------------------------------------"
530 PRI "J_NOTE: PGM WILL FAIL IF NEXT FIX IS A DEAD RECKONNING CASE.G_G_"
540 PRINT "-------------------------------------------------------J_"
550 GO TO 590
560 PRINT "J_ENTER THE NAME OF THIS SITE IN 72 OR LESS CHARACTERS.J_"
570 INPUT A$
580 PRINT @33:A$
590 PRINT "J_TYPE OF INPUT? (HEADER=1, FIX=2, SUB-HEADER=3, END=4).   ";
600 INPUT Z4
610 PRINT "J_"
620 GO TO Z4 OF 630,990,2580,2630
630 PRINT "J_SITE NUMBER. ..... ";
640 INPUT Q1
650 PRINT "NAME (3 CHAR.) OF REF  PT. 1..... ";
660 INPUT B$
670 PRINT "LATITUDE OF REF. PT. 1 (6 DIGITS)..... ";
680 INPUT Z5
690 PRINT "LONGITUDE OF REF. PT. 1 (7 DIGITS).... ..... ";
700 INPUT Z6
710 PRINT "NAME (3 CHAR.) OF REF. PT. 2 (IF NONE, USE ***)..... ";
720 INPUT C$
730 PRINT "LATITUDE OF REF. PT. 2 (6 DIGITS, IF ABSENT 999999)... ";
740 INPUT Z7
750 PRINT "LONGITUDE OF REF. PT. 2 (7 DIGITS, IF ABSENT 9999999). ";
760 INPUT Z8
770 PRINT "BASE BEARING (IF 0 USE 360, IF ABSENT USE 9999) ..... ";
780 INPUT Z9
790 PRINT "BASE DISTANCE (IF ABSENT ENTER 9999).... ..... ";
800 INPUT Y1
810 PRINT "DATE (6 DIGITS)..... ..... ..... ";
820 INPUT Y2
830 IF C$<>"***" THEN 870
840 Z2=0
850 Z3=0
860 GO TO 890
870 Z2=Y1*COS(90-Z9)
```

Initialization of some of the program's variables and vectors.

Reading data stored on tape during a previous working session. This is necessary if the positions defined during a subsequent day are to be displayed along with all previous fixes.

Input of Level I data. This information is used in defining the selected reference point(s) and serves as header (statements 890-920) in the overall data file. The position of reference point 2, when used, is calculated with respect to reference point 1 (statements 870-880).

```
880 Z3=Y1*SIN(90-Z9)
890 PRINT @33:Z4
900 PRINT @33:Q1,Z5,Z6,Z7,Z8,Z9,Y1,Y2,Z2,Z3,
910 PRINT @33:B$
920 PRINT @33:C$
930 IF Z2=0 AND Z3=0 THEN 590
940 PRINT USING 950,Z2,Z3
950 IMAGE "_NOTE: COORDINATES OF REF.PT-2: X=",3D.2D,"  Y=",3D.2D,"G_G_"
960 V3=Z2
970 V4=Z3
980 GO TO 2530
990 PRINT "_FIX NUMBER..... . . .. ..... ..... ",
1000 INPUT D1
1010 PRINT "TIME (4 DIGITS) ..... . ..... ..... ..... ";
1020 INPUT E$
1030 PRINT "RADAR RANGE TO REF. PT. 1 (IF ABSENT, USE 0) ..... ";
1040 INPUT Y5
1050 PRINT "RADAR BEARING TO REF. PT. 1 (IF 0 USE 360, IF NONE 0). ";
1060 INPUT Y6
1070 PRINT "RADAR RANGE TO REF. PT. 2 (IF ABSENT USE 0)... ..... ";
1080 INPUT Y7
1090 PRINT "RADAR BEARING TO REF. PT  2 (IF 0 USE 360, IF NONE 0). ";
1100 INPUT Y8
1110 PRINT "SHIP0S SPEED..... ... ..  ..... ... ";
1120 INPUT Y9
1130 PRINT "SHIP0S HEADING (IF 0 USE 360)..... ... ..... ";
1140 INPUT X1
1150 PRINT "WATER DEPTH..... ..... ..... .. ";
1160 INPUT X2
1170 PRINT "ECHO SOUNDER QUALIFIER (3 CHAR.)..  ..  ..... .. .. ";
1180 INPUT I$
1190 PRINT "SIDE SCAN QUALIFIER (3 CHAR.)..... ";
1200 INPUT J$
1210 PRINT "SUB-BOTTOM PROFILER QUALIFIER (3 CHAR.)..... ";
1220 INPUT K$
1230 PRINT "GEOLOGICAL GRAB QUALIFIER (2 CHAR.)..... ..... ";
1240 INPUT L$
1250 PRINT "BIOLOGICAL GRAB QUALIFIER (3 CHAR.).. .. ..... ";
1260 INPUT M$
1270 PRINT "BENTHIC TRAWL QUALIFIER (3 CHAR.). ..... ";
1280 INPUT N$
1290 PRINT "SURFACE SUSPENDED SEDIMENT QUALIFIER (1 CHAR.)..... ";
1300 INPUT O$
1310 IF Y5<>0 AND Y7<>0 THEN 1530
1320 IF Y5<>0 AND Y6<>0 THEN 1620
1330 IF Y7<>0 AND Y8<>0 THEN 1680
1340 IF Y6<>0 AND Y8<>0 THEN 1740
1350 IF F$<>"    " AND E$<>"    " AND X1<>0 AND Y9<>0 THEN 1930
1360 PRINT "G_G_J_*****  FAILURE TO DETERMINE POSITION OF FIX  *****G_G_"
1370 PRINT "J_IS THE INFO TO BE STORED ON TAPE? (YES=1, NO=0)
1380 INPUT V5
1390 IF V5=0 THEN 590
1400 V3=9999
1410 V4=9999
1420 PRINT @23:Z4
1430 PRINT @33:D1,X2,V3,V4
1440 PRINT @33:E$
1450 PRINT @33:I$
1460 PRINT @33:J$
1470 PRINT @33:K$
1480 PRINT @33:L$
1490 PRINT @33:M$
1500 PRINT @33:N$
1510 PRINT @33:O$
1520 GO TO 590
1530 PRINT "J_IS FIX ABOVE (1) OR BELOW (2) BASE LINE?  ";
1540 INPUT R1
1550 GO TO R1 OF 1560,1590
1560 V3=Y5*COS(90-Z9+ACS((Y5^2+Y1^2-Y7^2)/(2*Y5*Y1)))
1570 V4=Y5*SIN(90-Z9+ACS((Y5^2+Y1^2-Y7^2)/(2*Y5*Y1)))
1580 GO TO 2000
1590 V3=Y5*COS(90-Z9-ACS((Y5^2+Y1^2-Y7^2)/(2*Y5*Y1)))
1600 V4=Y5*SIN(90-Z9-ACS((Y5^2+Y1^2-Y7^2)/(2*Y5*Y1)))
1610 GO TO 2000
1620 Y6=Y6+X1
1630 IF Y6<360 THEN 1650
1640 Y6=Y6-360
1650 V3=Y5*COS(90-(Y6-180))
1660 V4=Y5*SIN(90-(Y6-180))
1670 GO TO 2000
1680 Y8=Y8+X1
1690 IF Y8<360 THEN 1710
1700 Y8=Y8-360
1710 V3=Y7*COS(90-(Y8-180))+Z2
1720 V4=Y7*SIN(90-(Y8-180))+Z3
1730 GO TO 2000
1740 Y6=Y6+X1
1750 IF Y6<360 THEN 1770
1760 Y6=Y6-360
1770 V6=ABS(90-Z9-(90-(Y6-180)))
1780 IF Y6<360 THEN 1800
1790 Y6=Y6-360
1800 IF Y6<180 THEN 1820
1810 Y6=360-Y6
1820 Y8=Y8+X1
1830 IF Y8<360 THEN 1850
1840 Y8=Y8-360
1850 V7=ABS(90-Z9-180-(90-(Y8-180)))
1860 IF V7<360 THEN 1880
1870 V7=V7-360
1880 IF V7<180 THEN 1900
1890 V7=360-V7
1900 V3=Y1*SIN(V7)/SIN(180-(V7+V6))*COS(90-(Y6-180))
1910 V4=Y1*SIN(V7)/SIN(180-(V7+V6))*SIN(90-(Y6-180))
1920 GO TO 2000
1930 G$=SEG(E$,3,2)
1940 H$=SEG(F$,3,2)
1950 V7=VAL(G$)+60-VAL(H$)
1960 IF V7<60 THEN 1980
1970 V7=V7-60
1980 V3=(Y9+Y8)/120*V7*COS(90-X1)+Y9
1990 V4=(Y9+Y8)/120*V7*SIN(90-X1)+T1
2000 PRINT USING 2010:V3,V4
2010 IMAGE "J_POSITION OF FIX   X=",2D.2D,"  Y=",3D.2D,"J_"
2020 IF T2=0 THEN 2050
2030 PRINT "J_MAP? (YES=1, NO=0; IF 0, DATA IS STORED ON TAPE).  ",
2040 INPUT R2
2050 T2=T2+1
2060 T4(T2)=V3
2070 T5(T2)=V4
2080 Y9=V3
2090 T1=V4
```

Input of Level II and III data. This contains the information necessary to compute the position of a fix (Level II data, statements 1010-1140) and the coded results of measurements performed at that fix (Level III data, statements 1150-1300).

Branching to the appropriate positioning method according to the presence or absence of positioning data.

Optional tape storage of data in the event that the position of the fix could not be computed.

Calculation of fix position when ranges to two reference points are present.

Calculation of fix position when a range and a bearing to reference point 1 are present.

Calculation of fix position when a range and bearing to reference point 2 are present.

Calculation of fix position when both bearings to reference point 1 and 2 are present.

Calculation of fix position by dead reckoning, using elapsed time, ship's course and speed.

Display of the X Y coordinates of the last fix with respect to reference point 1 and optional CRT display of map.

CRT display of the position of all fixes and reference point(s) used. The scaling is performed automatically such that most of the CRT display area is used without creating a distortion in the X Y proportions of the field area. Fixes are denoted by '.', the second last fix by '+2' and the last fix by '+1' (Fig. 1) providing quick evaluation of the ship's position. Displaying the ship's track (by changing statement no. 2250 to 'DRAW Z2, Z3'), or labelling each fix with its number proved too confusing and time-consuming.

Optional tape storage of Level II and III data. If the information is not stored on tape, it is deleted from all further operations.

Input of sub-header type of data. This information is used to denote new days within the overall data file.

```
2100 V8=V9
2110 P$=E$
2120 IF R2=0 THEN 2430
2130 PAGE
2140 WINDOW T6 MIN V2,T7 MAX V2,T8 MIN V4,T9 MAX V4
2150 VIEWPORT 20,110,5,95
2160 S2=ABS((T7 MAX V2)-(T6 MIN V2))/90
2170 S2=S2 MAX ABS((T9 MAX V4)-(T8 MIN V4))/90
2180 MOVE 0,0
2190 SCALE S2,S2
2200 PRINT "+";B$
2210 IF Z2=0 AND Z3=0 THEN 2240
2220 MOVE Z2,Z3
2230 PRINT "+";C$;
2240 FOR N=1 TO T2
2250 MOVE T4(N),T5(N)
2260 S3=T2-N
2270 IF S3>1 THEN 2300
2280 IF S3=1 THEN 2320
2290 IF S3=0 THEN 2340
2300 PRINT ".";
2310 GO TO 2350
2320 PRINT "+2";
2330 GO TO 2350
2340 PRINT "+1";
2350 NEXT N
2360 HOME
2370 PRINT "O.K. TO STORE LAST FIX INFO. ON TAPE? (YES=1, NO=0)  ";
2380 INPUT R3
2390 PAGE
2400 IF R3=1 THEN 2430
2410 T2=T2-1
2420 GO TO 590
2430 PRINT @22,D4
2440 PRINT @22,D1;X8;V3;W4
2450 PRINT @22,E$
2460 PRINT @22,I$
2470 PRINT @22,J$
2480 PRINT @22,K$
2490 PRINT @22,L$
2500 PRINT @32,M$
2510 PRINT @33,N$
2520 PRINT @33,O$
2530 T6=T6 MIN V2
2540 T7=T7 MAX V2
2550 T8=T8 MIN V4
2560 T9=T9 MAX V4
2570 GO TO 590
2580 PRINT "(DATE (6 DIGITS)
2590 INPUT A2
2600 PRINT @22,Z4
2610 PRINT @22,A2
2620 GO TO 490
2630 END
```

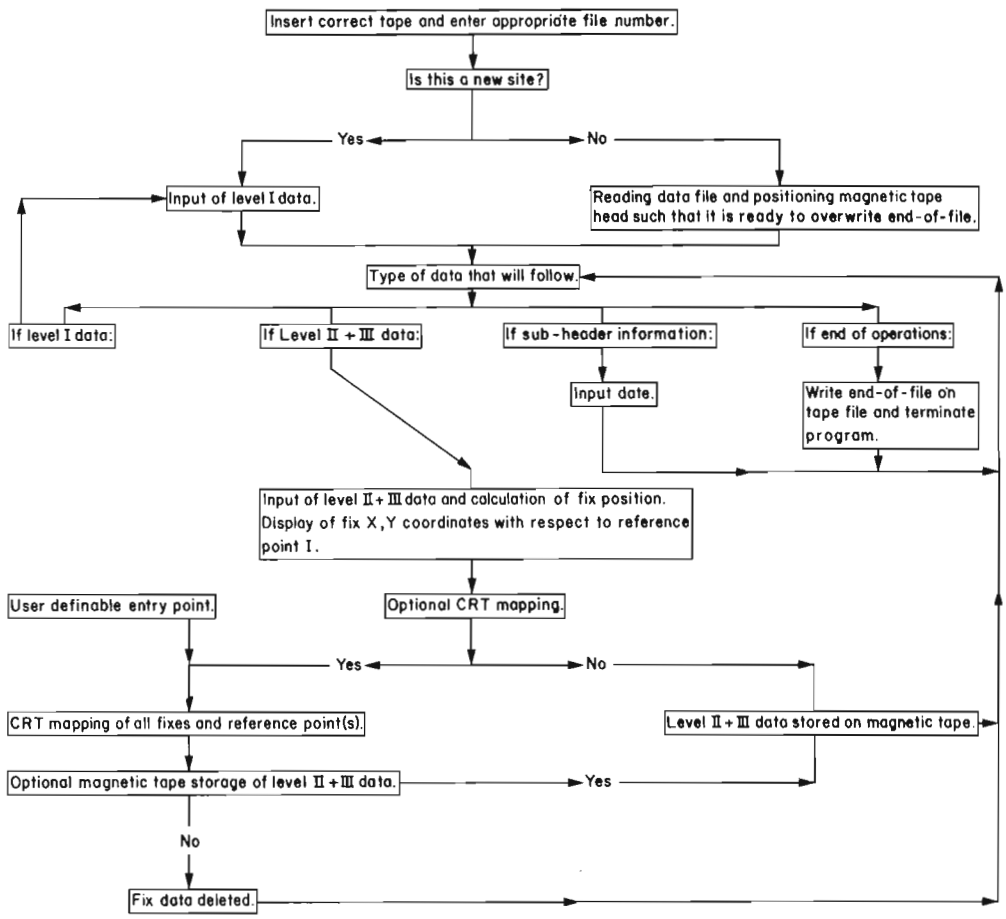

Figure 7.3. *Flow diagram of functions performed by the positioning, CRT rapid display and data recording program.*

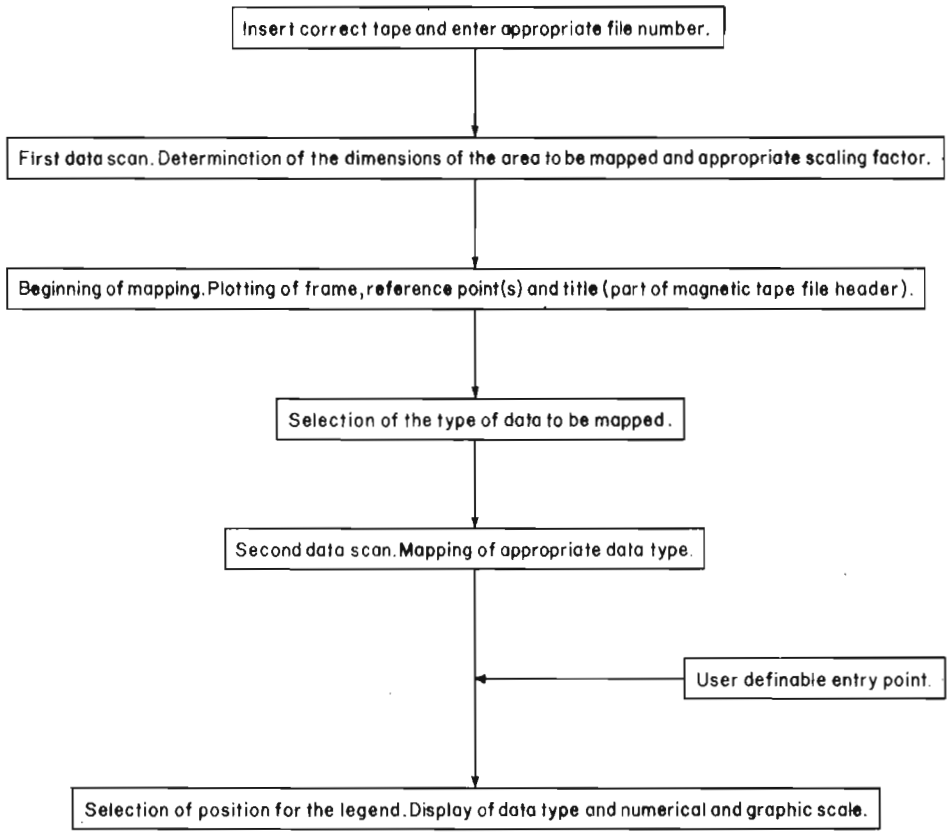

Figure 7.4. *Flow diagram of functions performed by the interactive mapping programs.*

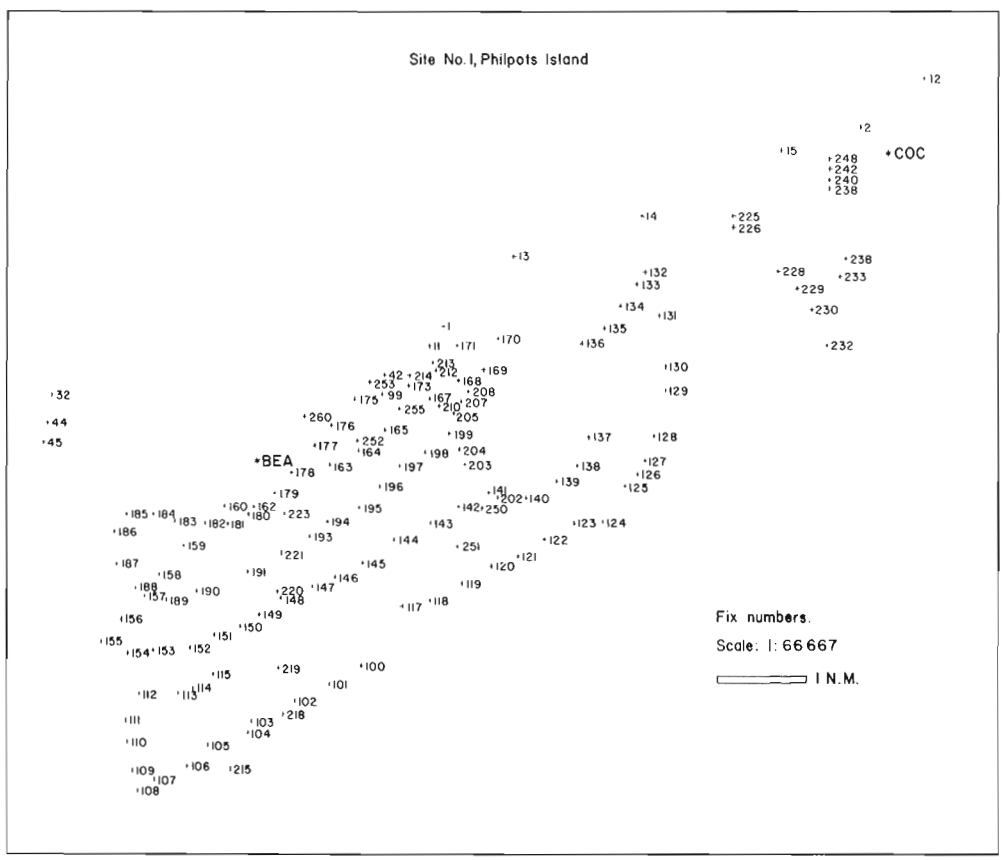

Figure 7.5. *Example of map produced by the digital plotter of all fix locations.*

Interactive Mapping Programs

Two programs are used to produce maps of the data which are stored on tape by the positioning and recording program. The programs are similar to each other and use an identical sequence of operations (Fig. 7.4). Both require two separate data scans to produce the maps. The first scan determines the maximum dimensions of the area to be plotted as well as a suitable scaling factor. The maximum dimensions are then compared with the corresponding dimensions of the area to be used on the digital plotter such that the maps will have identical overall dimensions with no distortion. The second scan reads and plots individual fix data. The use of two data scans avoids the necessity of storing all data in the computer's memory which could easily lead to storage requirements exceeding the machine's capacity.

In case of uncertainty as to whether or not the legend will interfere with the data plotted, it can be scribed a first time without pen or with the pen in the up position. After verification, the user definable entry point (user definable key no. 1 on a Tektronix 4051) can be used to plot the legend information with the pen down in the same or a more appropriate position. The legend consists of the type of data plotted and a numeric and graphic scale (Fig. 7.2).

The first interactive mapping program produces a map of the fixes and the coded results of the measurements performed at those fixes (Fig. 7.2). The type of data to be plotted is selected by the operator. The annotated listing is as follows:

User definable entry point. Used to force control into plotting the legend of the map. Can be used to repeat the legend if its position interferes with the data plotted.

Initialization of some of the program's variables and vectors.

Reading data stored on tape by the positioning and data recording program. Calculation of the overall dimensions of the area to be plotted and of a suitable scaling factor.

Beginning of the mapping phase. Drawing border, plotting locations and names of the reference point(s) used and scribing title.

```
1 REM *****  PLOTTER MAPPING OF POSITIONS AND QUALIFIERS   *****
3 GO TO 100
4 GO TO 1250
100 INIT
110 PRINT "INSERT APPROPRIATE TAPE AND ENTER FILE NUMBER."
120 INPUT @2
130 FIND @2
140 DIM A$(72),B$(2),C$(3),E$(4),F$(4),I$(2),J$(3),K$(3),L$(3)
150 DIM M$(3),N$(3),O$(3),P$(20)
160 T6=0
170 T7=0
180 T8=0
190 T9=0
200 INPUT @33:A$
210 PRINT "J_FIRST DATA SCAN IN PROCESS J_"
220 ON EOF (0) THEN 400
230 INPUT @33:Z4
240 GO TO Z4 OF 250,300,280
250 INPUT @33:Q1,Z5,Z6,Z7,Z8,Z9,Y1,Y2,Z2,Z3
260 INPUT @33:B$,C$
270 V3=Z2
280 V4=Z3
290 GO TO 320
300 INPUT @33:Q1,X2,V3,V4
310 INPUT @33 E$,I$,J$,K$,L$,M$,N$,O$
320 IF V3=9999 AND V4=9999 THEN 230
330 T6=T6 MIN V3
340 T7=T7 MAX V3
350 T8=T8 MIN V3
360 T9=T9 MAX V4
370 GO TO 330
380 INPUT @33:Y2
390 GO TO 230
400 PRINT "J_FILE READ, MAPPING CAN BEGIN J_"
410 PRINT T6,T7,T8,T9
420 VIEWPORT 0,150,0,100
430 WINDOW 0,150,0,100
440 MOVE @1:0.0
450 DRAW @1:0,100
460 DRAW @1:150,100
470 DRAW @1:150,0
480 DRAW @1:0,0
490 PRINT @1,17.1,1.4
500 MOVE @1:75-LEN(A$)/2,95
510 PRINT @1:A$
520 S2=ABS(T7-T6)/140
530 S2=S2 MAX ABS(T9-T8)/85
540 PRINT @1,17.0.6,1
550 WINDOW T6,T7,T8,T9
560 MOVE @1:0,0
570 VIEWPORT 5,145,5,90
580 SCALE S2,S2
590 PRINT @1,"H_H_H_H_H_";8#;" "
600 IF C$="***" THEN 630
610 MOVE @1,Z2,Z3
620 PRINT @1:"+ ";C$
630 PRINT "TYPE OF MAP?J_"
640 PRINT "FIX NUMBERS AND POSITIONS..... ..... ... 1"
650 PRINT "BATHYMETRY..... ..... ..... ..... ..... 2"
660 PRINT "ECHO SOUNDINGS. ..... ..... ..... ..... 3"
670 PRINT "SIDE SCAN. ..... ..... ..... ..... ..... 4"
680 PRINT "SUB BOTTOM. ..... ..... ..... ..... ..... 5"
690 PRINT "GEOLOGICAL GRABS..... ... ..... ..... 6"
700 PRINT "BIOLOGICAL GRABS. ..... ..... ..... 7"
710 PRINT "BENTHIC TRAWLS. ..... ..... ..... 8"
720 PRINT "SURFACE SUSPENDED SEDIMENTS..... ..... 9J_"
730 INPUT R1
740 PAGE
750 FIND @2
760 INPUT @33:A$
770 PRINT "J_SECOND DATA SCAN IN PROCESS J_"
780 ON EOF (0) THEN 1240
790 INPUT @33:Z4
800 GO TO Z4 OF 810,840,1220
810 INPUT @33:Q1,Z5,Z6,Z7,Z8,Z9,Y1,Y2,Z2,Z3
820 INPUT @33:B$,C$
830 GO TO 790
840 INPUT @33:Q1,X2,V3,V4
850 INPUT @33:E$,I$,J$,K$,L$,M$,N$,O$
860 IF V3=9999 AND V4=9999 THEN 790
870 GO TO R1 OF 880,910,940,980,1020,1060,1100,1140,1180
880 MOVE @1:V3,V4
890 PRINT @1:"+",Q1
900 GO TO 790
910 MOVE @1:V3,V4
920 PRINT @1:"+",INT(X2)
930 GO TO 790
```

Request for the type of map desired and second data scan with plotting of individual fix data.

```
940 IF I$="000" THEN 790
950 MOVE @1 V3,V4
960 PRINT @1:"+";I$
970 GO TO 790
980 IF J$="000" THEN 790
990 MOVE @1 V3,V4
1000 PRINT @1:"+";J$
1010 GO TO 790
1020 IF K$="000" THEN 790
1030 MOVE @1:V3,V4
1040 PRINT @1:"+";K$
1050 GO TO 790
1060 IF L$="000" THEN 790
1070 MOVE @1:V3,V4
1080 PRINT @1:"+";L$
1090 GO TO 790
1100 IF M$="000" THEN 790
1110 MOVE @1:V3,V4
1120 PRINT @1:"+";M$
1130 GO TO 790
1140 IF N$="000" THEN 790
1150 MOVE @1:V3,V4
1160 PRINT @1 "+";N$
1170 GO TO 790
1180 IF O$="0' OR O$='000' THEN 790
1190 MOVE @1:V3,V4
1200 PRINT @1 "+";O$
1210 GO TO 790
1220 INPUT @32 Y2
1230 GO TO 790
1240 PRINT "MAPPING COMPLETED "
```

Positioning and writing map legend.

```
1250 PRINT "J_INDICATE IN WHICH POSITION IS THE LEGEND TO BE PLACED. J_"
1260 PRINT "                              1"
1270 PRINT "                            8   2"
1280 PRINT "                          7       3"
1290 PRINT "                            6   4"
1300 PRINT "                              5              ";
1310 INPUT R2
1320 WINDOW 0,150,0,100
1330 VIEWPORT 0,150,0,100
1340 GO TO R2 OF 1350,1390,1430,1470,1510,1550,1590,1630
1350 MOVE @1:60,80
1360 R3=60
1370 R4=80
1380 GO TO 1660
1390 MOVE @1:115,80
1400 R3=115
1410 R4=80
1420 GO TO 1660
1430 MOVE @1:115,50
1440 R3=115
1450 R4=50
1460 GO TO 1660
1470 MOVE @1:115,15
1480 R3=115
1490 R4=15
1500 GO TO 1660
1510 MOVE @1:60,15
1520 R3=60
1530 R4=15
1540 GO TO 1660
1550 MOVE @1:5,15
1560 R3=5
1570 R4=15
1580 GO TO 1660
1590 MOVE @1:5,50
1600 R3=5
1610 R4=50
1620 GO TO 1660
1630 MOVE @1:5,80
1640 R3=5
1650 R4=80
1660 GO TO R1 OF 1670,1690,1710,1730,1750,1770,1790,1810,1830
1670 P$="FIX NUMBERS AND POSITIONS."
1680 GO TO 1840
1690 P$="BATHYMETRY."
1700 GO TO 1840
1710 P$="ECHO SOUNDINGS."
1720 GO TO 1840
1730 P$="SIDE SCAN."
1740 GO TO 1840
1750 P$="SUB-BOTTOM PROFILER."
1760 GO TO 1840
1770 P$="GEOLOGICAL GRABS."
1780 GO TO 1840
1790 P$="BIOLOGICAL GRABS."
1800 GO TO 1840
1810 P$="BENTHIC TRAWLS."
1820 GO TO 1840
1830 P$="SURFACE SUSPENDED SEDIMENTS."
1840 PRINT @1,17:1,1.4
1850 PRINT @1:P$
1860 MOVE @1:R3,R4-3
1870 R5=72960/(1/S2/10)
1880 PRINT @1: USING 1890:"SCALE  1:";R5
1890 IMAGE 9A,6D.2D
1900 MOVE @1:R3,R4-6
1910 R6=10/(R5/72960)
1920 DRAW @1:R3+R6,R4-6
1930 MOVE @1:R3,R4-7
1940 DRAW @1:R3+R6,R4-7
1950 DRAW @1:R3+R6,R4-6
1960 MOVE @1:R3,R4-6
1970 DRAW @1:R3,R4-7
1980 MOVE @1:R3+R6,R4-7
1990 PRINT @1:" 1 N. M."

2000 END
```

The second interactive mapping program which is only slightly different from the first, plots position and fix number of any data type rather than the coded measurements performed at those fixes (Fig. 7.5). The program is as follows:

```
1 REM *****     PLOTTER MAPPING OF POSITIONS AND FIX NUMBERS      *****
3 GO TO 100
4 GO TO 1250
100 INIT
110 PRINT "INSERT APPROPRIATE TAPE AND ENTER FILE NUMBER "
120 INPUT Q2
130 FIND Q2
140 DIM A$(72),B$(3),C$(3),E$(4),F$(4),I$(3),J$(3),K$(3),L$(3)
150 DIM M$(3),N$(3),O$(3),P$(30)
160 T6=0
170 T7=0
180 T8=0
190 T9=0
200 INPUT @33:A$
210 PRINT "J_FIRST DATA SCAN IN PROCESS.J_"
220 ON EOF (0) THEN 400
230 INPUT @33:Z4
240 GO TO Z4 OF 250,300,380
250 INPUT @33:Q1,Z5,Z6,Z7,Z8,Z9,Y1,Y2,Z2,Z3
260 INPUT @33:B$,C$
270 V3=Z2
280 V4=Z3
290 GO TO 320
300 INPUT @33:D1,X2,V3,V4
310 INPUT @33:E$,I$,J$,K$,L$,M$,N$,O$
320 IF V3=9999 AND V4=9999 THEN 230
330 T6=T6 MIN V3
340 T7=T7 MAX V3
350 T8=T8 MIN V4
360 T9=T9 MAX V4
370 GO TO 230
380 INPUT @33:Y2
390 GO TO 230
400 PRINT "J_FILE READ, MAPPING CAN BEGIN.J_"
410 PRINT T6,T7,T8,T9
420 VIEWPORT 0,150,0,100
430 WINDOW 0,150,0,100
440 MOVE @1:0,0
450 DRAW @1:0,100
460 DRAW @1:150,100
470 DRAW @1:150,0
480 DRAW @1:0,0
490 PRINT @1,17:1,1.4
500 MOVE @1:75-LEN(A$)/2,95
510 PRINT @1:A$
520 S2=ABS(T7-T6)/140
530 S2=S2 MAX ABS(T9-T8)/85
540 PRINT @1,17 0.6,1
550 WINDOW T6,T7,T8,T9
560 MOVE @1:0,0
570 VIEWPORT 5,145,5,90
580 SCALE S2,S2
590 PRINT @1:"H_H_H_H_H_";B#;" *"
600 IF C$="***" THEN 630
610 MOVE @1:Z2,Z3
620 PRINT @1:"* ";C$
630 PRINT "TYPE OF MAP?J_"
640 PRINT "FIX NUMBERS AND POSITIONS.... ... ... ..... ... 1"
650 PRINT "BATHYMETRY..... ..... ..... ... 2"
660 PRINT "ECHO SOUNDINGS..... ..... ..... ... 3"
670 PRINT "SIDE SCAN..... ..... ... 4"
680 PRINT "SUB BOTTOM..... ..... ... ..... ... 5"
690 PRINT "GEOLOGICAL GRABS ..... ..... 6"
700 PRINT "BIOLOGICAL GRABS..... ..... ... ... 7"
710 PRINT "BENTHIC TRAWLS..... ..... ... ..... 8"
720 PRINT "SURFACE SUSPENDED SEDIMENTS..... ... ..... ... 9J_"
730 INPUT R1
740 PAGE
750 FIND Q2
760 INPUT @33 A$
770 PRINT "J_SECOND DATA SCAN IN PROCESS.J_"
780 ON EOF (0) THEN 1240
790 INPUT @33:Z4
800 GO TO Z4 OF 810,840,1220
810 INPUT @33:Q1,Z5,Z6,Z7,Z8,Z9,Y1,Y2,Z2,Z3
820 INPUT @33:B$,C$
830 GO TO 790
840 INPUT @33:D1,X2,V3,V4
850 INPUT @33:E$,I$,J$,K$,L$,M$,N$,O$
860 IF V3=9999 AND V4=9999 THEN 790
870 GO TO R1 OF 880,910,940,980,1020,1060,1100,1140,1180
880 MOVE @1:V3,V4
890 PRINT @1:"+";D1
900 GO TO 790
910 MOVE @1:V3,V4
920 PRINT @1:"+";INT(X2+0.5)
930 GO TO 790
940 IF I$="000" THEN 790
950 MOVE @1:V2,V4
960 PRINT @1:"+",I$
970 GO TO 790
980 IF J$="000" THEN 790
990 MOVE @1:V3,V4
1000 PRINT @1:"+";J$
1010 GO TO 790
1020 IF K$="000" THEN 790
1030 MOVE @1:V2,V4
1040 PRINT @1:"+",K$
1050 GO TO 790
1060 IF L$="000" THEN 790
1070 MOVE @1:V3,V4
1080 PRINT @1:"+";L$
1090 GO TO 790
1100 IF M$="000" THEN 790
1110 MOVE @1:V3,V4
1120 PRINT @1:"+",D1
1130 GO TO 790
1140 IF N$="000" THEN 790
1150 MOVE @1:V2,V4
1160 PRINT @1:"+",D1
1170 GO TO 790
1180 IF O$="0" OR O$="000" THEN 790
1190 MOVE @1:V3,V4
1200 PRINT @1 "+",O$
1210 GO TO 790
1220 INPUT @33 Y2
1230 GO TO 790
1240 PRINT "MAPPING COMPLETED "
1250 PRINT "J_INDICATE IN WHICH POSITION IS THE LEGEND TO BE PLACED J_"
1260 PRINT "                                1"
1270 PRINT "                              2   2"
1280 PRINT "                            3       3"
1290 PRINT "                              4   4"
1300 PRINT "                                5"
1310 INPUT P2
1320 WINDOW 0,150,0,100
1330 VIEWPORT 0,150,0,100
1340 GO TO P2 OF 1390,1390,1410,1470,1510,1550,1590,1610
1350 MOVE @1 60,80
1360 R3=60
1370 R4=80
1380 GO TO 1660
1390 MOVE @1:115,80
1400 R3=115
1410 R4=80
1420 GO TO 1660
1430 MOVE @1:115,50
1440 R3=115
1450 R4=50
1460 GO TO 1660
1470 MOVE @1:115,15
1480 R3=115
1490 R4=15
1500 GO TO 1660
1510 MOVE @1:60,15
1520 R3=60
1530 R4=15
1540 GO TO 1660
1550 MOVE @1:5,15
1560 R3=5
1570 R4=15
1580 GO TO 1660
1590 MOVE @1:5,50
1600 R3=5
1610 R4=50
1620 GO TO 1660
1630 MOVE @1:5,80
1640 R3=5
1650 R4=80
1660 GO TO R1 OF 1670,1690,1710,1730,1750,1770,1790,1810,1830
1670 P$="FIX NUMBERS AND POSITIONS."
1680 GO TO 1840
1690 P$="BATHYMETRY."
1700 GO TO 1840
1710 P$="ECHO SOUNDINGS."
1720 GO TO 1840
1730 P$="SIDE SCAN "
1740 GO TO 1840
1750 P$="SUB-BOTTOM PROFILER "
1760 GO TO 1840
1770 P$="GEOLOGICAL GRABS."
1780 GO TO 1840
1790 P$="BIOLOGICAL GRABS."
1800 GO TO 1840
1810 P$="BENTHIC TRAWLS."
1820 GO TO 1840
1830 P$="SURFACE SUSPENDED SEDIMENTS."
1840 PRINT @1,17:1,1.4
1850 PRINT @1:P$
1860 MOVE @1:R3,R4-3
1870 R5=72960/(1/S2/10)
1880 PRINT @1: USING 1890:"SCALE  1: ",R5
1890 IMAGE 9A,ZD.2D
1900 MOVE @1:R3,R4-6
1910 R6=10/(R5/72960)
1920 DRAW @1:R3+R6,R4-6
1930 MOVE @1:R3,R4-7
1940 DRAW @1:R3+R6,R4-7
1950 DRAW @1:R3+R6,R4-6
1960 MOVE @1:R3,R4-6
1970 DRAW @1:R3,R4-7
1980 MOVE @1:R3+R6,R4-7
1990 PRINT @1:" 1 N. M."

2000 END
```

Discussion and Conclusions

During field operations a power failure during operation of the data positioning and recording program will cause the contents of the magnetic tape to become inaccessible. In this case retyping the original file is necessary. A back-up system such as batteries with an inverter, used in conjunction with the usual power source would avoid this problem.

In the present software, changing or editing a magnetic tape data record is impossible without retyping the whole record. This is a feature common to all tape drive recording systems. A secondary storage system (tape or disc) compatible with the main system would enable the data files to be edited as required.

When used in conjunction with a ship's radar, an added convenience in obtaining the position data would be to use a radar system that is linked with the ship's gyro-compass. This would enable true bearings to be obtained rather than relative bearings. Both the number of parameters required to compute the ship's position and possible sources of error for the computer operator would be less.

The approach described in this report for the positioning, recording and display of spatially distributed data was developed specifically for the study of marine and coastal environments. However, efforts have been made to keep the software simple, flexible and user oriented. By doing this, it is hoped that these programs may be of help to other studies requiring positioning and data handling, even if not specifically dealing with coastal environments.

Reference

McLaren, P. and Sempels, J.M.
1978: An approach to the recording, positioning and manipulation of coastal and marine data; in Current Research, Part B; Geological Survey of Canada, Paper 78-1B, p. 191-193.

8.

FUSED CLUSTERS OF PTILONCODUS SIMPLEX HARRIS; AN ORDOVICIAN PHOSPHATIC MICROFOSSIL

Project 500029

R.S. Tipnis
Institute of Sedimentary and Petroleum Geology, Calgary

Tipnis, R.S., Fused clusters of ***Ptiloncodus simplex*** *Harris; an Ordovician phosphatic microfossil; in Current Research, Part C, Geological Survey of Canada, Paper 79-1C, p. 51-54, 1979.*

Abstract

Fused clusters of ***Ptiloncodus simplex*** *Harris, a phosphatic microfossil common in the upper Lower and lower Middle Ordovician rocks of North America, are reported. Although the zoological affinities of this microfossil continue to be elusive, the geometry of individual elements within the clusters suggests affinities with the pedicellariae of echinoderms.*

Introduction

Ptiloncodus simplex Harris, a hook-shaped phosphatic microfossil has a fairly restricted age range [late Canadian to early Middle Ordovician, Sweet et al. (1971)] and has been found in widely separated parts of North America. At present no extra-North American occurrence is known. In Canada, this microfossil has been reported from the 'Lower Skoki' Formation of southern Alberta (Ethington and Clark, 1965), the upper part of the Broken Skull Formation, Mackenzie Mountains, Northwest Territories (Tipnis et al., 1979) and the Mystic Formation of southeastern Quebec (Barnes and Poplawski, 1973). Although Sweet et al. (1971) state that **P. simplex** is not known to occur in rocks older than those containing Fauna 1, near the level of the Canadian-Whiterockian (Middle Ordovician) boundary, the western and northwestern Canadian occurrences show that this is not true for all regions. For example, in the Mackenzie Mountains, the earliest occurrence of **P. simplex** has been dated, by means of conodonts, as late Canadian (equivalent to Fauna E of Ethington and Clark, 1971). The horizon containing **P. simplex** in the 'Lower Skoki' Formation of southern Alberta (Ethington and Clark, 1965) may also be late Canadian as pointed out to me by B.S. Norford. According to Norford, samples 48 and 50, which contain **P. simplex,** come from the Outram Formation immediately below the 'Skoki' Formation and contain shelly faunas belonging to zones H-J (See Barnes et al., 1976, Fig. 2). These zones are of late Canadian age and are more or less coeval with conodont Fauna E. Moreover, as communicated to me by Anita Harris (July, 1979), the upper stratigraphic range of this taxon also differs from that suggested by Sweet et al. (1971). According to Harris, **P. simplex** extends through the entire Whiterock and part of the Chazy [inclusive of Faunas 2 to 6 of Sweet et al. (1971)]. Despite the modified range, however, **P. simplex** may still be regarded as a stratigraphically useful microfossil.

The phosphatic composition of **P. simplex** allows it to be separated in the same manner as conodonts (acid digestion followed by heavy-liquid separation). Several similarities and a few significant differences exist between **Ptiloncodus** and conodonts (see the accompanying discussion of **Ptiloncodus**). Added to the similarity is the occurrence of **Ptiloncodus** as fused clusters (see Nowlan, 1979, and Tipnis and Chatterton, 1979, for additional data on fused clusters of conodonts). There is little doubt that the clusters reported here represent a true biological association. Quite probably they were formed by means of post-mortem fusion and diagenesis of adjacent ptiloncodan elements after the death of the animal.

Locality, Material and Age

Only one sample yielded all of the clusters described here. This sample was collected by W.T. Dean, in the company of R.J. Ross. Ross has kindly provided the following information on the sample locality. The collection is labelled as "USGS Coll. D1494a CO. Antelope Valley Limestone, in local sandstone unit near base of formation (**Orthidiella** zone). On hill overlooking Stargo Spring, northeast of Dobbins Summit and approximately 6,000 feet SSE from hill 9772, Monitor Range. T. 13 N., R. 49 E. Tonopah 2 degrees quadrangle, Nevada" (written communication August 7, 1978).

Most of the conodonts from this sample are moderately well preserved. Although a few of the larger ones are quite black, the smaller conodonts tend to be light brown in colour. The ptiloncodans which in size compare favourably with the smaller conodonts, also show a light brown to almost amber colour. The similarity in colour between conodonts and ptiloncodans may be explained by their identical chemical composition. The age of the sample, as determined by conodonts, is early middle Whiterockian. The following conodont taxa are present: **Histiodella sinuosa** Harris, **Oistodus multicorrugatus** Mound and **"Gothodus" marathonensis** Bradshaw. This conodont fauna would suggest an age equivalent to Fauna 2 or possibly Fauna 3 of Sweet et al. (1971).

SYSTEMATICS

Ptiloncodus Harris 1962

Discussion of Genus

Harris (1962) was the first to recognize the enigmatic hook-shaped microfossil **Ptiloncodus simplex** Harris, describing only the type species. Diagnostic characteristics of the genus (and the species) as recognized by Harris included "a simple, subcylindrical, hook-shaped pointed cusp bearing two subflattened, auricular expansions attached to opposite sides of base at right angles to plane of curvature of 'hook' (auricular 'wings' are broken off most specimens)" (Harris, 1962, p. 206). Harris regarded **Ptiloncodus** as a conodont, compared it with **Stereoconus** Branson and Mehl and believed that the two genera may be related by the fact that neither possessed a basal pit.

Sweet (1963) pointed out that **Stereoconus** did indeed contain a basal pit and disputed the placement of **Ptiloncodus** in the Conodontophorida. Sweet (op. cit.) also suggested a

holothurian affinity for this microfossil. This latter suggestion was disputed by both Mound (1965) and Ethington and Clark (1965). Ethington and Clark (op. cit.) emphasized the difference between the chemical composition of **Ptiloncodus** (calcium phosphate) and the sclerites (spicules?) of holothurians (calcium carbonate). Furthermore, these writers also noted that the specimens identified by them as **Ptiloncodus simplex** differed somewhat from those described by Harris (1962). Aside from being more complete, with both the 'hook' and 'wings' preserved, Ethington and Clark (1965) noted that the 'wings' in their specimens extended to a level near the start of the curvature of the 'hook' (in Harris's material, the 'wings' usually join the 'hook' well below this level). Ethington and Clark (1965) reported their specimens from the 'Lower Skoki' Formation of southern Alberta (late Canadian) which is older than the Joins Formation of Oklahoma from which the types were recovered (Harris, 1962). The latter is of early Middle Ordovician age [Sweet and Bergström, (1976)]. On the other hand, Mound's (1965) main criteria for including **Ptiloncodus** within Conodontophorida were: size, gross shape, lustre, opacity, chemical composition and fibrous crystal structure. Despite the impressive similarities between conodonts and **Ptiloncodus,** it is considered here that **Ptiloncodus** is not a conodont. The presence of a basal pit is regarded as an essential feature of conodonts. Hence, its absence in **Ptiloncodus** rules out its placement within the Conodontophorida. At present **Ptiloncodus** is regarded as an "enigmatic hook-shaped microfossil that is not a conodont" [Sweet et al. (1971), Barnes and Poplawski (1973) and Tipnis et al. (1979)].

Bordeau (1972) reported a new species of **Ptiloncodus, P. harrisi** from the Viola Limestone of Oklahoma. This species, according to Bordeau (1972) contained 'knob'-like protrusions at the proximal end of the 'shaft' instead of the auricular lobes (wings) characteristic of **P. simplex.** This distinction appears to be somewhat obscure and not obvious in the illustration of Bordeau's new species. Conodonts from the samples that yield **P. harrisi (Belodina compressa** Branson and Mehl, **Amorphognathus ordovicicus** Branson and Mehl), according to Bordeau, indicate a Late Ordovician age. [The age of the Viola Limestone in terms of conodont faunas may be late Middle (Fauna 9) to early Late (Faunas 10-11) Ordovician (Sweet and Bergström, 1976)]. At present it would be premature to assign any age significance to **P. harrisi** (i.e., as being confined to upper Middle and the lower Upper Ordovician strata) until further reports of this taxon from coeval strata from other regions are published. (Both Godfrey Nowlan, GSC, and Anita Harris, USGS, have communicated to me the fact that they have recovered ptiloncodans, possibly **Ptiloncodus harrisi,** from upper Middle to Upper Ordovician strata).

Discussion of the Present Occurrence of Ptiloncodus

Elements of **Ptiloncodus simplex** Harris occur in the sample as five clusters and one discrete individual. Cluster composition is as follows: one cluster with two elements; three clusters with three elements each and possibly one cluster with four elements. Although most of the clusters, excepting perhaps the three-element cluster shown in Plate 8.1., Figure 7, appear to be quite disorganized, close inspection suggests that some degree of symmetry and organization may exist. It is assumed that this symmetry resulted from the proximity of elements within the organism that contained them. The original mode of attachment, as is evident from most of the clusters, appears to have been between the 'winged' parts of the elements as these are most often found to be fused to one another (Fig. 8.2, 8.5, 8.6 in part, and 8.7). The hooks, on the other hand, often radiate away from this area of attachment (Fig. 8.2, 8.5, 8.6 in part, and 8.7). The surficial corrugation and damaged state of the 'wings' as compared to the 'hooks' (Fig. 8.4, Fig. 8.6) suggests that the 'wings' were structurally somewhat different from the 'hooks' (a loose structure?), and were involved in attachment to, or articulation with, other elements of the **Ptiloncodus** apparatus. The rough surfaces of the 'wings' could have acted as suitable sites for muscles or tendons through which the 'wings' maintained contact.

The discrete element of **Ptiloncodus simplex** (Fig. 8.1, 8.4) is found to be quite complete, with the 'hook' and the 'wings' preserved. In shape, the 'wings' are more auricular than knob-like and appear similar to 'wings' of the type specimens of **P. simplex** from the Joins Formation. Towards the ends where the 'wings' meet the cusp (oral margin), the curvature tends to be planar (flatter?) in comparison to the curved (hemispherical) nature of the margin seen in the Joins Formation specimens. The present specimen in this respect is similar to specimens described by Ethington and Clark (1965) from the 'Lower Skoki' although the two differ in age. It is still premature to speculate on the possibility of geographic and/or intra-specific variation.

The cluster consisting of two elements (Fig. 8.2) lacks most of the 'wing' portions. However, proximity of the bases of the 'shafts' of both the elements can be seen. 'Hooks' appear to be complete but lie in different planes.

Three clusters contain three elements each. In one of these (Fig. 8.3), only two 'shafts' are present, the occurrence of the third 'shaft' (and the element) being determined only by presence of its fused half 'wing' attached to the 'lower' element. The present arrangement of two elements, one above the other, could be due to slippage of one past the other. Of the remaining three-element clusters, one (Fig. 8.7) shows a fairly symmetrical arrangement with the 'hooks' radiating away from a central region that contains the bases of three elements, apparently joined together along the 'wings'. This morphology probably reflects most closely the tentative arrangement of a three-element apparatus in an 'open' position.* The other three-element cluster (Fig. 8.6) may represent a somewhat disturbed and/or disorganized stage of the three-element arrangement as depicted in the previous cluster (one of the elements appears to have 'toppled over' so that its 'hooks' points towards the bases of the other two elements and the 'wings' placed adjacent to the tips of the 'shafts').

Lastly, the cluster illustrated in Figure 8.5 may contain four elements. This cluster has three (? four) sets of 'wings' (partial to complete) fused towards one end while the 'hooks' radiate outwards.

The Affinities of Ptiloncodus

As noted earlier, Sweet (1963) considered these objects as holothurian sclerites (e.g. **Achistrum**). While the difference in chemical composition between the calcium phosphate of **Ptiloncodus** and the calcium carbonate of

* The term 'open' position is used in connection with the analogy drawn between ptiloncodans and pedicellariae discussed under the next heading. As noted therein, pedicellariae are jaw-like apparatuses usually consisting of clusters of three elements. The 'open' position in such an apparatus would be a position 'at rest' (nonfunctioning), when the three elements diverge from the centre. A 'closed' position would be that of the three elements converging in order to perform the function of grasping (scavenging? defence?). Tipnis and Chatterton (1979) have discussed a **"Prooneotodus"** cluster (Fig. 8.6-8.9) apparently frozen in an 'open' position. The likelihood of an apparatus (either of **"Prooneotodus"** or, in this case, **Ptiloncodus**) being preserved in an 'open' position vis-à-vis a closed one appears greater because of the expected rapid degradation of supporting muscular tissues after the death of the animal bearing these clusters.

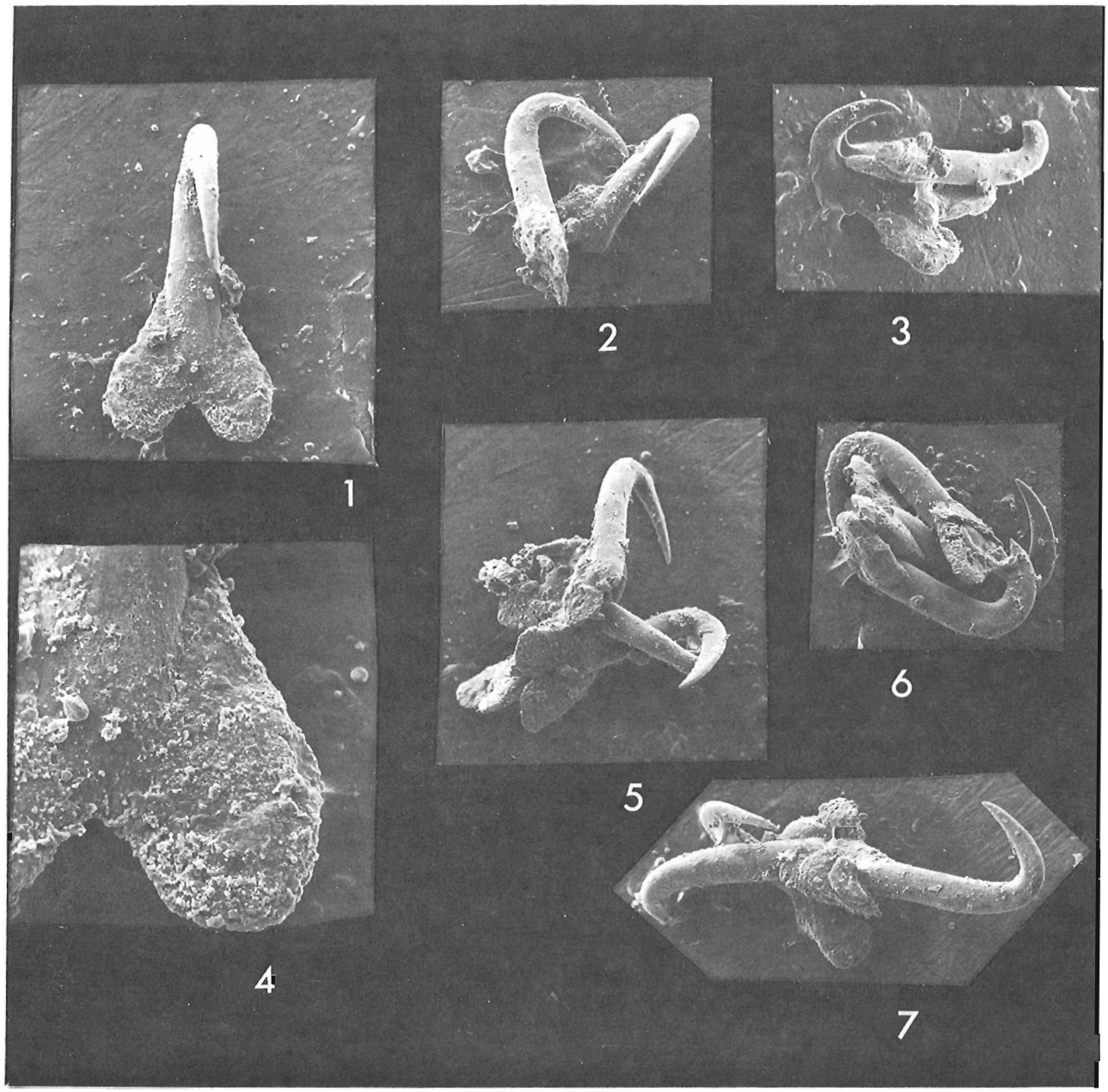

PLATE 8.1
Ptiloncodus simplex Harris

Figures 1 & 4: Single element. 1. "Posterior" view of a complete element showing the two lateral 'wings' and the median 'hook' x125 and 4. A magnified view showing the "zone" of attachment of the 'wing' to the 'hook' x1000. Figured specimen USNM 269501.

Figure 2: Two-element cluster, with parts of the 'wings' missing. Figured specimen USNM 269502, x125.

Figure 3: Three-element cluster. Note only broken 'wing' of third element present, attached to the lower element. Figured specimen USNM 269503, x125.

Figure 5: Four-element cluster? Note that 3 of the elements have the 'wings' more or less in close proximity. Figured specimen USNM 269504, x125.

Figure 6. Three-element cluster. Two of the elements are arranged parallel to each other with the 'wings' joined. The third element occurs as a parallel opposed element. Figured specimen USNM 269505, x125.

Figure 7: Three-element cluster. The three elements appear to be attached towards the 'bases' with the 'wings' mostly damaged. The 'hooks' are directed away from the area of attachment. Figured specimen USNM 269506, x125.

holothurians suggests they are not closely related, it is nonetheless interesting to speculate on a morphological basis if holothurian sclerites and ptiloncodans had a similar function. Though the similarity in morphology of **Ptiloncodus** to holothurian spicules, together with the occurrence of **Ptiloncodus** in multi-elemental clusters of rather disorganized appearance, might suggest that elements of **Ptiloncodus** could have been dermal spicules, it is worth noting that holothurian sclerites resembling **Ptiloncodus** (e.g. **Achistrum**) are usually associated with disc-like structures (no such structures were found), and that the presence of alar extensions ('wings') is not a common feature on holothurian sclerites. Admittedly this does not necessarily argue against ptiloncodans being dermal spicules. On the other hand, the similarity of **Ptiloncodus** to the modern pedicellariae, especially the tridentate type (Melville and Durham, 1966) of echinoderms is impressive. [Pedicellariae are "minute, grasping defensive and scavenging organs . . . . . attached to small tubercles on the test of echinoids" (Melville and Durham, op. cit., p. 581)]. The shape, size, and occurrence of attached elements in clusters of two's and three's of pedicellariae evokes comparison with the **Ptiloncodus** elements described here. For instance, Pokorny (1965) stated that the pedicellariae consist of a 'stem' and a 'head'. The latter is usually made up of three (and in some cases two or four) mobile jaws. These jaws may have a triangular outline, are convex internally and externally and have widened lateral alae on their lower part. The jaws are attached to one another by (adductor and diductor) muscles. Most features associated with the 'head' can be identified with the **Ptiloncodus** clusters described here.

Acknowledgments

I am grateful to T.T. Uyeno, for directing my attention to these clusters, providing general support and reading an earlier draft of this manuscript. B.D.E. Chatterton, Department of Geology, University of Alberta, and Ms. J. Kennedy, who also read the manuscript and offered useful comments. Comments by G.S. Nowlan, and B.S. Norford, are also acknowledged. I also thank Anita Harris, USGS, Washington and R.J. Ross, Jr., USGS, Denver, for their assistance. All illustrated specimens are to be deposited with the National Museum of Natural History, Smithsonian Institution, Washington, D.C. Dr. Fu-Shiang Chia, Department of Zoology, University of Alberta, discussed with me a possible affinity of **Ptiloncodus** with the pedicellariae of echinoderms - although the views expressed here are my own.

References

Barnes, C.R. and Poplawski, M.L.S.
1973: Lower and Middle Ordovician conodonts from the Mystic Formation Quebec, Canada; Journal of Paleontology, v. 47, p. 760-790.

Barnes, C.R., Jackson, D.E., and Norford, B.S.
1976: Correlation between Canadian Ordovician Zonations based on graptolites, conodonts and benthic microfossils from key successions; in Bassett, M.G., ed. The Ordovician System; Proceedings of a Palaeontological Association Symposium, Birmingham, September 1974, 666 p., Cardiff, p. 209-226.

Bordeau, K.V.
1972: **Ptiloncodus harrisi:** A new species of conodont from the Viola Limestone (Ordovician) of Oklahoma; Journal Tennessee Academy of Science, v. 47 (3), p. 118-120.

Ethington, R.L. and Clark, D.L.
1965: Lower Ordovician conodonts and other microfossils from the Columbia Ice Fields section, Alberta, Canada; Brigham Young University Geology Studies, 12, p. 185-206.

1971: Lower Ordovician conodonts in North America; Geological Society of America Memoir 127, p. 63-82.

Harris, R.W.
1962: New Conodonts from Joins (Ordovician) Formation of Oklahoma. Oklahoma Geology Notes, 22, p. 199-211.

Melville, R.V. and Durham, J.W.
1966: Skeletal morphology; in Treatise on Invertebrate Paleontology ed. R.C. Moore, Echinodermata 3, v. 1, University of Kansas Press.

Mound, M.C.
1965: Conodont fauna from the Joins Formation (Ordovician), Oklahoma; Tulane Studies in Geology 4, p. 1-46.

Nowlan, G.S.
1979: Fused clusters of the conodont genus **Belodina** Ethington from the Thumb Mountain Formation (Ordovician), Ellesmere Island, District of Franklin: in Current Research Part A, Geological Survey of Canada, Paper 79-1A, p. 213-218.

Pokorny, V.
1965: Principles of Zoological Micropaleontology, v. 2, International Series of Monographs on Earth Sciences, v. 20, 465 p., Pergamon Press (English Edition).

Sweet, W.C.
1963: Review of "New conodonts from Joins (Ordovician) Formation of Oklahoma" by R.W. Harris; Oklahoma Geology Notes, v. 22, no. 8, p. 199-211; in Journal of Paleontology 37(2), p. 505-506.

Sweet, W.C. and Bergström, S.M.
1976: Conodont biostratigraphy of the Middle and Upper Ordovician of the United States midcontinent; in Bassett, M.G., ed. The Ordovician System; Proceedings of a Palaeontological Association Symposium, Birmingham, September 1974, 666 p., Cardiff, p. 121-151.

Sweet, W.C., Ethington, R.L., and Barnes, C.R.
1971: North American Middle and Upper Ordovician conodont faunas. Geological Society of America Memoir 127, p. 163-193.

Tipnis, R.S., Chatterton, B.D.E., and Ludvigsen, R.
1979: Biostratigraphy of Ordovician conodonts from the Southern Mackenzie Mountains; in C.R. Stelck and B.D.E. Chatterton, ed., P.S. Warren Biostratigraphy Symposium, Geological Association of Canada, Special Paper 18, p. 39-91.

Tipnis, R.S. and Chatterton, B.D.E.
1979: An occurrence of the apparatus of **"Prooneotodus"** (Conodontophorida) from the Road River Formation, Northwest Territories; in Current Research Part B, Geological Survey of Canada, Paper 79-1B, p. 259-262.

9. A GAMMA RAY SPECTROMETRY SYSTEM FOR AIRBORNE GEOLOGICAL RESEARCH

Project 760048

Q. Bristow
Resource Geophysics Geochemistry Division

Bristow, Q., A gamma ray spectrometry system for airborne geological research; in Current Research, Part C, Geological Survey of Canada, Paper 79-1C, p. 55-61, 1979.

Abstract

A gamma ray spectrometer has been developed at the Geological Survey of Canada for airborne use in research studies related to uranium exploration and as an aid in geological mapping. The detector portion consists of an array of twelve sodium iodide scintillation detectors, with associated pre-amplifiers incorporating circuitry to eliminate overloading caused by high energy cosmic events and to reduce the effect of pulse-pileup at high count rates. A laboratory type analog-to-digital converter in conjunction with a Data General Corp. NOVA mini computer enables 256 or 1024 channel gamma ray spectra to be acquired at sampling intervals down to 0.25 seconds. The gamma energy peak due to naturally occurring ^{40}K, the radioisotope associated with potassium in the earth's crust, is used to monitor and correct for spectrum drift using a software stabilizing technique. The software developed for the NOVA also enables the operator to define a number of spectral windows by keyboard entry on a small hard copy data terminal, and to display the count rates in them corrected for dead-time on a CRT monitor. A six channel strip chart recorder provides on-line profiles of individual window count rates, or of simple algebraic functions involving more than one of these, as defined by keyboard entry. A nine-track magnetic tape unit records complete spectra and window count rate data, together with navigational and environmental data. The equipment is packaged as a single unit mounted on castor wheels for easy installation in the Short Skyvan aircraft used as the survey platform.

Introduction

The surface concentrations of the radio elements, potassium, uranium and thorium, can be quantified by measurements of the intensities of the gamma radiation emitted by their respective radioisotopes ^{40}K, ^{214}Bi and ^{208}Tl. Airborne gamma-ray spectrometry is commonly used to make such measurements (Darnley et al. 1968; Bristow and Donhoffer, 1968) which can then be related to surface concentrations by appropriate calibration procedures (Grasty and Darnley, 1971; Grasty, 1977). These data are then used to compile maps showing the surficial distributions of the three elements. The widest application of this technique to date has been in uranium exploration (Pemberton, 1969; Foote and Humphrey, 1976; Breiner et al. 1976; Grasty, 1975), however, it is also used as an aid in the geological mapping of bedrock, soil, and other overburden, (Darnley and Grasty, 1970; Darnley, 1970). More recently experiments have been conducted to determine snow cover thickness, based on the change in the shape of the natural gamma-ray spectrum brought about by scatter in the snow layer. (Loijens and Grasty, 1973; Grasty, 1979).

The radioisotope of potassium, ^{40}K, emits mono-energetic gamma radiation at 1.46 MeV. The radioisotopes ^{214}Bi and ^{208}Tl both emit radiation at a number of energies in the range zero to approximately 3.0 MeV. In the case of uranium, one of the radioactive daughter elements in the series is the gaseous element radon, which escapes into the atmosphere and can accumulate there in anomalous concentrations under certain weather conditions. The radioisotope ^{214}Bi is then formed in these clouds generating a background of gamma radiation for which airborne measurements must be corrected. Other sources of background radiation are contamination of the aircraft itself and interaction of high energy particles and gamma photons of cosmic origin with the spectrometer detectors.

Airborne gamma ray spectrometers for the applications outlined above usually consist of an array of sodium iodide scintillation detectors with signal conditioning and pulse height analysis electronics to provide count rate information in several spectral energy bands or windows. These data are recorded on magnetic tape along with navigational data and are profiled on a multi-channel strip chart recorder for in-flight monitoring by the operator.

A computer based airborne gamma ray spectrometer of advanced design has been developed at the Geological Survey of Canada for research oriented applications where a high degree of instrumental versatility is required. This equipment, which has now been in service for two field seasons, is the subject of this paper.

Common Instrumental Limitations and Problem Areas

The ability of a gamma ray spectrometer to resolve spectral peaks can be measured in terms of the resolution of the detector, or overall resolution of the detector array if several are used (Bristow, 1974, in press; Chase 1961). A standard procedure is to measure the full width at half the maximum height (FWHM) of the 661 keV photopeak of ^{137}Cs. The resolution expressed as a percentage is then given by:

peak width in keV X 100/661

There are a number of reasons why a spectrometer with a multidetector array can exhibit poor resolution. Individual detectors may have deteriorated due to a noisy photomultiplier tube (P.M.T.); or because of severe gain mismatch between PMTs where more than one is used on a single detector; or because the sodium iodide material is physically damaged or has become hydrated causing reduced optical transparency to scintillations. Gain mismatch between individual detectors can cause poor overall resolution; for example in the case of an array having more than eight detectors an accuracy of 0.5 per cent is desirable when matching the gains to avoid a significant loss in overall resolution.

The accuracy and stability of the spectral counting windows in the spectrometer are ultimately dependent on the stability of the overall gain of the PMT – preamplifier – main amplifier combination, and the stability of the threshold levels used for pulse height analysis. The two most common sources of inaccuracy are drift of PMT gains with temperature and count-rate dependent base-line shift. The latter causes all detector pulses to be effectively decreased in amplitude by the same amount, resulting in the entire spectrum being left-shifted on the energy scale. The effect is proportional to count-rate but is normally compensated for and effectively removed in well designed equipment.

Additional problems are caused by high energy events of cosmic origin which generate signals in the detector PMTs which are tens or hundreds of times the normal dynamic range. These overloads can result in paralysis or distortion of the signal for several milliseconds after each occurrence, thus contributing to a loss in overall resolution. This particular problem becomes more significant as the volume of the detector array increases. At high count rates (>25,000 c/s) the probability of pulses occurring within a few microseconds of each other increases, so that if there is any significant pulse "undershoot" requiring many microseconds to decay back to the base line level, then the amplitude of a pulse following may be modified by the residual undershoot of the previous one. This causes a statistical pulse height variation which adds to that already present from other noise sources and degrades the resolution.

Hardware Configuration of New Airborne Spectrometer

Detector Array and Signal Conditioning Electronics

The new system developed at the Geological Survey of Canada has a total detector volume of 50ℓ (3072 ins^3) made up of twelve 102 x 102 x 406 mm (4" x 4" x 16") square prismatic sodium iodide detectors manufactured by the Harshaw Chemical Company. Each one has a single 89 mm (3.5") diameter PMT mouted at one end. This was the primary reason for selecting this detector. Gain matching of individual detectors can be accomplished relatively easily, whereas the procedure for matching the gains of multiple PMTs on a single detector is tedious, time consuming and difficult to accomplish with the necessary precision. A secondary consideration was the more compact packaging afforded by the rectangular configuration of these detectors as opposed to the more conventional cylindrical types.

Figure 9.1 shows the method of packaging; two "slabs" are effectively formed by two sets of six detectors, each set being encased in 10 cm of polyethylene insulation and contained in a sheet metal box. These two boxes in turn are encased in 10 cm of hard foam insulation, which provides some structural support, the whole assembly being contained in an outer sheet metal box which is an integral part of the cabinet housing the spectrometer electronics.

Figure 9-1. Twelve square prismatic NaI detectors packaged with preamplifiers in thermally insulated containers.

The two inner boxes act as electrical shields and isothermal shells, and have strip heaters attached to them so that the detectors can be maintained at a predetermined constant temperature to minimize PMT gain drift. The inner insulation protects the detectors from both thermal and mechanical shock. A further potential benefit of the slab configuration is that gamma photons which are partially scattered from one detector, and which would be registered as of lower energy than was actually the case, have a higher probability of being absorbed by a neighbouring detector. The event is then registered by the system at more nearly the proper energy level, since the signals from all twelve detectors are summed before pulse height analysis.

Each detector has a charge sensitive preamplifier built on a 100 x 100 mm (4" x 4") printed circuit board which is mounted on the metal housing of the PMT. The low and high voltage supplies are daisy chained around each set of six preamplifiers using screw terminals on the circuit boards. This avoids the space and expense of individual connectors which would otherwise be required. A unique feature of the preamplifier design is the elimination of pulse undershoot by direct coupling of the PMT anode to the charge sensitive stage. This is accomplished without operating the PMT cathode at negative high voltage. A clipping circuit also operates at the PMT anode to drain off excess charge due to high energy cosmic events and thereby prevent any possibility of saturation of the charge sensitive stage. Differentiation with pole zero cancellation then provides pulses with a clean base line giving a detector resolution which is virtually unaffected by count rates of the order of 50 000 c/s. Shielded twisted pair cables carry these signals to a twelve input summing amplifier where front panel gain controls and switches allow detector gains to be matched. Active filter circuitry is used to produce the gaussian shaped pulses which are generally recommended for use with pulse height analysers. An active base line stabilising circuit removes any count-rate dependent base line shift without distorting individual pulses in the process.

Data Acquisition and Control System

The spectrometer was designed for research oriented applications and is based on a 16 bit minicomputer, the Data General Corp. NOVA 1220, in order to provide a high level of flexibility. Figure 9.2 is a block diagram which shows the main components of the system. Pulse height analysis is accomplished by a Wilkinson ramp type analogue-to-digital converter (ADC) the Nuclear Data Corp. Model ND 560. This unit is packaged in a two width nuclear instrument module (NIM) and is interfaced to the NOVA via direct memory access. A feature of the NOVA is an "increment memory" option in the direct memory access circuitry which increments the contents of the memory location whose address is called by the ADC. This allows selected blocks of memory to be used for acquiring spectra via the ADC with comparatively simple interface circuitry. The ADC has front panel controls for selection of conversion gain, number of channels, upper and lower level discriminator settings and other parameters.

The NOVA minicomputer consists of a chassis with horizontally mounted plug-in circuit boards. Each board is 38 cm square (15" x 15") and one is required for each peripheral device interfaced to the computer, whether this is by means of direct memory access (DMA) or by program interrupt. Each board has a strip approximately 10 cm wide for circuitry which can be added by the user to suit individual requirements.

The operator communicates with the spectrometer via a small hard copy data terminal, the Texas Instruments model 743KSR, and a CRT display which is based on a Tektronix model 604A monitor. Both are relatively inexpensive and light weight, a key consideration in an airborne system. The 604A monitor displays alphanumeric text and gamma ray spectra, all of this information being contained in the computer memory and fed out via DMA. All of the necessary circuitry to drive the display (character generator, raster scan, spot blanking etc.) is built onto the 10 cm strip provided on the NOVA interface board used for the display interface. The only connections to the monitor unit are for the X and Y deflection and Z modulation

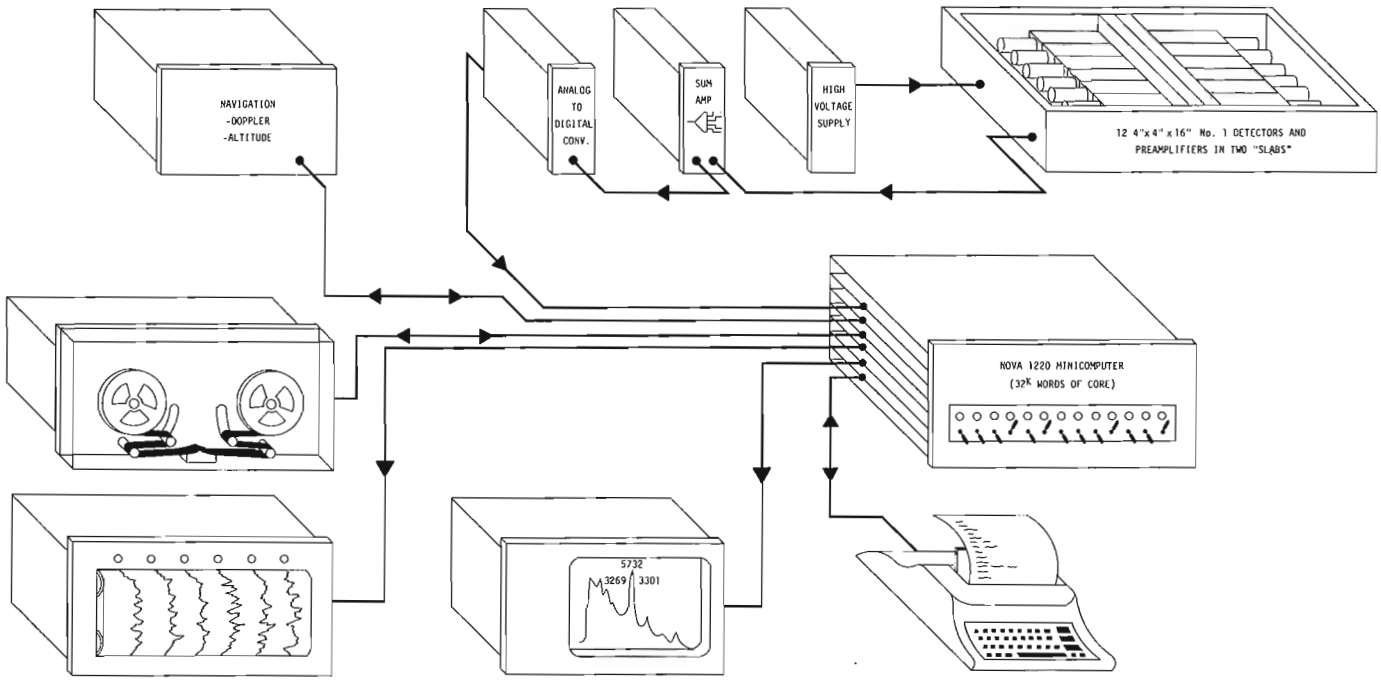

Figure 9-2. Block diagram showing main components of airborne gamma ray spectrometer.

signals. Different pages of information are displayed by the continuous scanning of different portions of memory where the text is stored as ASC11 characters in consecutive memory locations. When the software calls for display of spectra, the character generator is bypassed and the contents of successive memory locations are converted to vertical amplitude and plotted on the CRT via digital-to-analogue converters with a maximum range of 256 on the vertical scale and 1024 on the horizontal (energy) scale. A thumbwheel switch allows the contents of each memory location to be divided by 2, 4, 8, 16, 32, 64 and 128 before being displayed, thus enabling the operator to select the vertical scale for the spectrum. The display circuitry also allows the software to intensify points on the displayed spectrum to identify spectral counting windows, a valuable feature for in-flight monitoring of the spectrometer energy calibration. Since the display continuously scans portions of the computer memory by the DMA technique, it is "live" in the sense that whenever memory contents are changed the display is also updated without any additional software or CPU time being required. This would not have been possible had a commercially available CRT terminal been used.

The data are recorded by means of a nine-track magnetic tape drive which holds 1600 feet of tape on an 8.5 inch reel and has a write speed of 12.5 i.p.s. This corresponds to 10 000 characters/second at a bit density of 800 b.p.i. A read-after-write head enables alarms to be activated if the data are improperly recorded for any reason.

A six channel heated stylus type strip chart recorder is used to display on-line profiles of spectral window count rates. Six digital-to-analogue converters each with an 8 bit (256 full scale) resolution are built onto one of the NOVA interface boards, allowing for complete software control of the analogue outputs to the six channels.

A Bendix doppler and a Honeywell radar altimeter provide navigational data which are pre-processed in a microprocessor based unit developed for the purpose at the Geological Survey of Canada. These data are placed sequentially on a bus and fed to the NOVA via one of the standard interface boards.

Figure 9.3 shows photographs of the complete spectrometer installed in the Short Skyvan survey aircraft. The cabinet housing the NOVA and associated peripherals forms an integral unit with the detector array package. The whole assembly is mounted on castor wheels which allow easy transfer to and from the aircraft using a specially designed loading trolley. Mating rails on both ensure that the spectrometer (total weight approximately 540 kg) moves to a predetermined position in the aircraft where it is secured in a few minutes.

Software Operating System

The entire software operating system was written in assembly language rather than in FORTRAN or some other higher level language. This was done in order to minimize execution time involved in processing spectra on-line, and because the standard software modules available did not lend themselves readily to handling the locally developed and other specialized peripherals that are interfaced to the system. Other secondary benefits of this approach are the comparatively small core requirement, 16K words including 6K for data storage for this system, and the relative ease with which modifications can be made to suit the needs of the moment.

The system operates in a background/foreground mode when the spectrometer is acquiring data. Under these conditions the foreground portion, accessible via the terminal keyboard, allows parameters to be changed and display pages to be changed or copied on the terminal printer while the cycle of data acquisition and computation proceeds in the background. This cycle has absolute priority over the foreground; for example if a keyboard or printer interrupt occurs during the computation cycle it is recognized by the interrupt service routine but service is delayed until computation is complete for the current cycle. Maximum use is made of the CRT display for convenience and ease of operation. Data which can be displayed include spectra from six different blocks in core, and 14 pages of text and numerical data. Figure 9.4 shows examples of these page contents. Data entries are both printed and displayed as they are made and can be aborted by striking the ESC key. The printer is inactive for all other keyboard commands. Pages of displayed text can be reproduced as hard copy by the terminal on command for later reference.

There is no fixed protocol for entry of initial parameters such as sample time, date, line number, etc. This avoids the unnecessary repetition which is sometimes required in computer controlled systems in order to change one parameter. When the system is placed

in the "autocycle" mode, a complete spectrum and navigational data are acquired, repetitively, once per sample time as initially specified. The system has a choice of acquiring the spectral data as 256 or 1024 channel spectra and these are recorded along with other essential data on the nine-track magnetic tape once per sampling time. The computation for window counts, dead-time correction, etc., is carried out on the spectrum just acquired in one block of memory, while the text spectrum is accumulating via DMA in a second block. The shortest sampling time is approximately 0.25 secs, a limit which is set by the execution time required for the computation referred to above.

The software provides for off-line operations which include listing of spectra between specified channel limits; application of a staircase signal to the strip chart recorder channels; playback and processing of specific portions of taped data to recreate strip chart profiles with different spectral window functions, and an edit capability for keyboard entry of program changes in octal code.

Dead-time Correction

Whenever a detector pulse is being analyzed by the ADC any other pulses which may arrive during this period are ignored. The system is thus "dead" during the times that each accepted pulse is being analyzed, i.e. being digitized and sorted into the appropriate spectral memory location. With the Wilkinson ramp type of ADC this dead-time is a function of the pulse amplitude in each case and varies from a minimum of about 8 μs to a maximum of about 12 μs. The crystalled controlled NOVA timing clock is used as the master clock for generating data acquisition sampling times. Two counters on the ADC interface board are preloaded by keyboard entry with the required sampling time and run down to zero by the master clock. The pulse train to one of these counters is inhibited by a "busy" signal from the ADC whenever a pulse is being analyzed. The count still remaining in this counter when the other one reaches zero is thus a measure of the dead-time for that sampling interval and the information is used to correct the window count data before they are displayed or profiled on the strip chart recorder.

Detector Calibration and Spectrum Drift Compensation

Use is made of the live display capability which is inherent in the design, to provide a quick and accurate method of matching the twelve detector gains. A keyboard command produces a live spectrum display continuously accumulating from whichever detector or detectors are switched into the summing amplifier. Three narrow (45 keV wide) counting windows set up by software are shown as an intensified portion of the display and are centred on the required channel number for the ^{40}K peak and they are updated once every two seconds. The spectrum can be erased and the window counts reset at any time by striking the RUBOUT key. The gain of a single detector is adjusted using the display as a visual aid until the accumulating ^{40}K peak is symmetrically positioned in the intensified region. A finer adjustment is then made until the counts in the two side windows accumulate at an equal rate. Normally one or two "erase-adjust" cycles are all that is required to set the peak position to an accuracy of one tenth of a percent.

Hardware spectrum stabilisation techniques whether digital, analogue or a combination of both, all require the accumulation of sufficient counts in a spectral peak (generated either by a radioisotope or a light source implanted in the detector) to make a statistically valid estimate of the peak position. This information is usually generated as a difference signal from two counting windows straddling the peak and is used to alter the effective keV per channel (by changing the gain of an amplifier or the high voltage to the detector PMTs) to move the peak back to the proper position.

A software stabilisation technique is used in this system which involves the accumulation of the spectra acquired during successive sampling times (usually one second intervals) in a separate block of memory and calculating the position of the ^{40}K peak centroid to one tenth of a channel, after a predetermined number of counts have been accumulated in the peak channel. The program then uses this information to compute the keV per channel and the spectral counting window limits in terms of channel numbers. The search range used for finding the ^{40}K peak is preset automatically to bracket the proper location whenever the system is first put into the "autocycle" mode, on the assumption that the calibration procedure described above has been used. Thereafter however it moves to bracket the position where the peak was last found in order to minimize the possibility of locking-on to a wrong peak. The channel having the highest number of counts is used as the centre channel in determining the area limits for the centroid calculation and this area is restricted to the top triangular portion of the peak. The entire correction scheme assumes that the pulse height v energy transfer

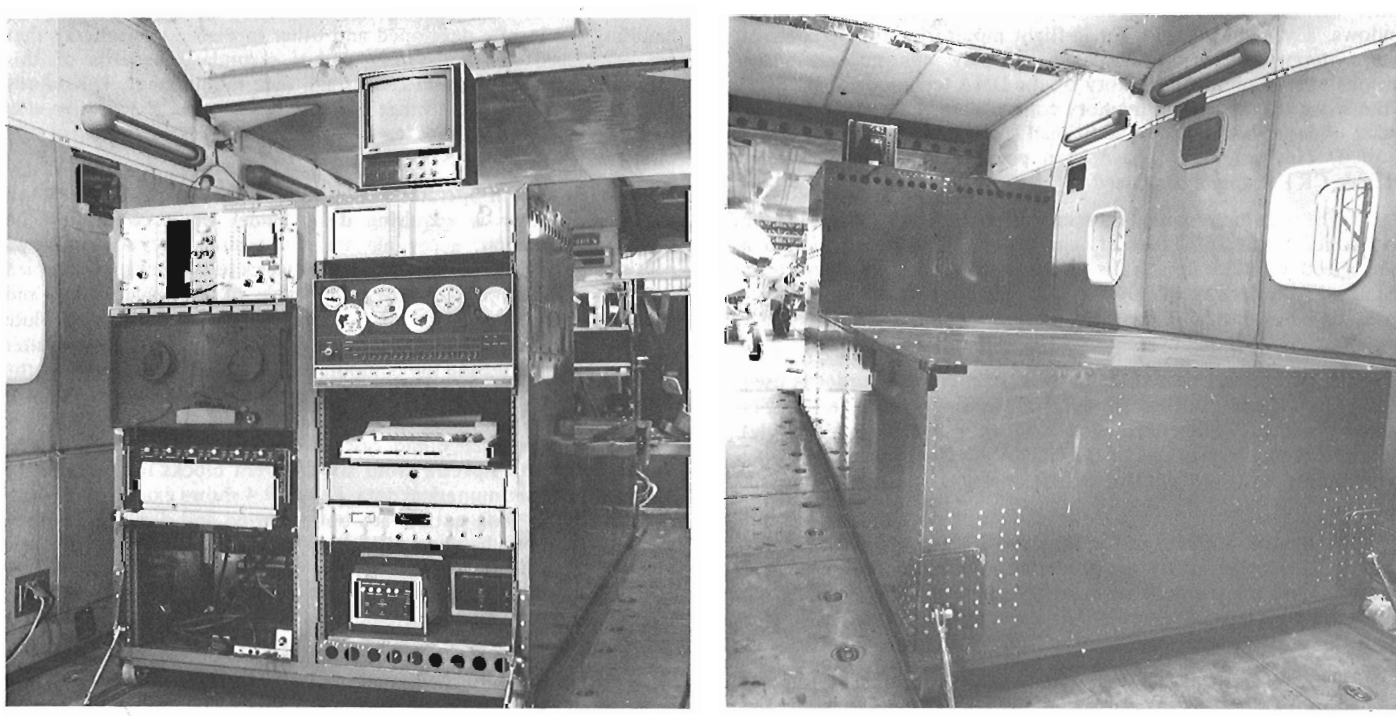

Figure 9-3. Complete gamma ray spectrometer in the Short Skyvan aircraft used for airborne research.

Figure 9-4. Sample display pages; data pages (e.g. top left) are updated internally as memory contents change in the NOVA computer.

function is linear, passes through the origin, and changes in slope only. These assumptions are also implicit in all hardware on-line spectrum stabilization techniques of which the author is aware.

The resolution (F.W.H.M.) of the ^{40}K peak is computed whenever the peak position is updated with all the relevant data being displayed. A keyboard selectable option allows these data to be printed out whenever the update is made which is useful for monitoring peak channel movement and overall detector resolution, either during survey operations or in overnight stability checks.

Automatic Background Subtraction

A technique for background subtraction is incorporated to allow on-line correction of strip chart profiles and to facilitate accurate detector resolution measurements. A keyboard entry will cause the spectra acquired over successive sampling times to be accumulated in a separate block of memory until this mode of operation is ended by another keyboard entry. The accumulated spectrum is then normalized automatically to the mean value for one sample time, after which it can be used to make a background correction to all window count data subsequently acquired.

Detector Resolution Measurement

Detector resolution is an important indicator of performance and is one which most spectrometers of this type are not equipped to measure. With this system a ^{137}Cs resolution check can be run quickly and accurately. A dual gain switch on the summing amplifier allows the gain to be increased so that the 661 keV peak of ^{137}Cs occupies the same position in the spectrum that the ^{40}K normally does. The system computes the peak channel position and also the resolution in per cent. If a background measurement is made first then the background subtract feature described previously can be used to provide a reliable figure for resolutions of individual detectors and overall system resolution.

Programmable Window Capability

The software integrates areas under predetermined regions of the spectrum (windows) by totaling the counts in the channels of the spectrum covered by these windows. These calculations are made at the end of each sampling interval and the results, corrected for deadtime, are displayed and recorded. The energy limits for four of these windows are fixed and cover ranges corresponding to total count and the peak energies 1.46, 1.76 and 2.62 meV, which are those associated with the radioactive nuclides of potassium, uranium and thorium respectively. Provision has been made for keyboard entry of the energy limits for an additional six such windows. These can be defined or changed by the operator at any time and allow complete flexibility for research oriented applications. The channel numbers which set the lower and upper window limits for each one are recomputed each time the ^{40}K peak centroid position is updated, thereby avoiding inaccuracies due to changes in the keV per channel figure with time. The positions of these windows can be seen as intensified regions when the accumulated spectrum used to compute the ^{40}K peak position is displayed.

Programmable Profile Functions

In research oriented measurements it is usually desirable to have as much flexibility as possible in the matter of output presentation. In this instance the only on-line output is via the six channel strip chart recorder and it is very convenient to be able to experiment with various corrections, combinations of window counts etc. Accordingly, a limited capability has been incorporated in the software for entering the required processing functions for each channel as algebraic expressions. Addition, subtraction, multiplication and division of constants and variables can thus be specified to accomplish spectral scattering corrections, height correction, scale changes and ratio plotting. The software adds the equivalent of one chart paper division to all values output to the recorder which allows a true negative excursion of up to one division before the digital/analogue converter overranges. This is a useful feature when background subtraction is being used over a region of near background activity, resulting in a more or less even spread of values above and below the base line.

Operational Experience

The use of a nine-track magnetic tape transport with a comparatively high recording density in routine low-level (130 m) survey operations was a source of some apprehension when the spectrometer was first put into service. In practice no particular problems have been experienced other than one, an occasional loss of tape tension during the 180° turns the aircraft makes as it ends one survey line and prepares for the next one. Attention first turned to the possible effects of lateral acceleration on the tape tension servo-control mechanism. The actual cause proved to be direct sunlight falling on the unit at some point during a turn and interfering with the optical tape sensors.

The technique of using the ^{40}K peak as the basis of a software spectrum stabilizing method has proven successful. A situation has not yet been encountered where the ^{40}K was not sufficiently prominent for lock-on by the system. The update cycle time is set by the operator in terms of the number of counts in the ^{40}K peak channel which must first be reached. A value of 2000 counts for a 256 channel spectrum has been found by experience to require about one minute of accumulation time over average terrain at a ground clearance of 130 m.

Resolution measurements on the system using the standard ^{137}Cs isotope gave the mean of the twelve individually measured detector values at 9.0 per cent and the overall resolution with all detectors operative as 9.3 per cent. This latter figure was obtained at a count rate of approximately 30 000 c/s.

The research-oriented flexibility designed into this system proved valuable when the equipment was pressed into service in the Northwest Territories at a few hours notice to aid in the search for radioactive debris from the Russian satellite Cosmos 954 in January 1978 (Bristow, 1978). The programmable spectral windows and strip chart profile functions were key factors in the detection of the first piece of the debris while the spectrometer was on its second search mission across the frozen surface of Great Slave Lake. The tape replay and analysis capability, together with the relative ease with which the operating software could be modified also proved to be valuable assets during this three month search operation.

Acknowledgments

The author gratefully acknowledges the contributions of J. Parker and Y. Blanchard who assembled and tested much of the hardware and assisted in the software development, and that of T. R. Flint who drew up the specification for and supervised construction of the spectrometer packaging. He was also responsible for design and construction of the multiparameter navigational interface used in the survey aircraft. The author is also grateful to R. L. Grasty and P. B. Holman for a number of suggestions on operational aspects of the equipment.

References

Breiner, S. et al
1976: Gamma-ray measurement and data reduction considerations for airborne radiometric surveys, in Exploration for Uranium Ore Deposits, IAEA, Vienna.

Bristow, Q.
1974: Gamma-ray sensors, *in* Geoscience Instrumentation E. A. Wolff, E. P. Mercanti, ed., John Wiley & Sons, New York.

1978: The application of airborne gamma-ray spectrometry in the search for radioactive debris from the Russian Satellite Cosmos 954 (Operation "Morning Light"), *in* Current Research Part B, Geological Survey of Canada Paper 78-1B, p. 151-162.

Bristow, Q.
"Gamma-ray spectrometric methods in uranium exploration airborne instrumentation", *in* Geophysics and Geochimistry in the search for metallic ores; Geological Survey of Canada Economic Geology Series report No. 31, in press.

Bristow, Q. and Donhoffer, D. K.
1968: An airborne gamma-ray spectrometry system for geological surveying" American Nuclear Society/ Canadian Nuclear Society, Transactions v. 11, no. 1, p. 66.

Chase, R. L.
1961: Nuclear Pulse Spectrometry, McGraw Hill, New York.

Darnley, A. G.
1970: Airborne gamma-ray spectrometry, Canadian Institute of Mining and Metallurgy Transactions, v. LXXIII p. 20-29.

Darnley, A. G. and Grasty, R. L.
1970: Mapping from the air by gamma-ray spectrometry, Canadian Institute of Mining and Metallurgy Special v. 11, Proceeding of 3rd International Geochemical Symposium, Toronto, p. 485-500.

Darnley, A. G., Bristow, Q. and Donhoffer, D. K.
1968: Airborne gamma-ray spectrometer measurements over the Canadian Shield Nuclear Techniques and Mineral Resources (IAEA, Vienna) p. 163-186.

Foote, R. S. and Humphrey, N. B.
1976: Airborne radiometric techniques and applications to uranium exploration, *in* Exploration for Uranium Ore Deposits, IAEA, Vienna, p. 17-34.

Grasty, R. L.
1975: Uranium measurement by airborne gamma-ray spectrometry, Geophysics, v. 40, no. 3, p. 503-519.

1977: A general calibration procedure for airborne gamma-ray spectrometers, *in* Report of Activities Part C, Geological Survey of Canada Paper 77-1C, p. 61-62.

1979: One flight snow-water equivalent measurement by airborne gamma-ray spectrometry presented at World Meteorological Organization Workshop on remote sensing of snow and soil moisture by nuclear techniques, Voss, Norway, 23-27 April.

Grasty, R. L. and Darnley, A. G.
1971: The calibration of gamma-ray spectrometers for ground and airborne use, Geological Survey of Canada, Paper 71-17.

Loijens, H. S. and Grasty, R. L.
1973: Airborne measurements of snow-water equivalent using natural gamma radiation over southern Ontario, 1972-1973; Canada, Department of the Environment, Scientific series no. 34.

Pemberton, R. H.
1969: Airborne radiometric surveying of mineral deposits, in Mining and Groundwater Geophysics, ed., L. W. Morley, Geological Survey Canada Economic Geology Series report no. 26.

10.

OCCURRENCE OF THE UPPER BATHONIAN AMMONITE GENUS INISKINITES IN THE QUEEN CHARLOTTE ISLANDS, BRITISH COLUMBIA

Project 500029

Hans Frebold
Regional and Economic Geology Division

*Frebold, Hans. Occurrence of the Upper Bathonian ammonite genus **Iniskinites** in the Queen Charlotte Islands, British Columbia; in Current Research, Part C, Geological Survey of Canada, Paper 79-1C, p. 63-66, 1979.*

Abstract

*The Jurassic ammonite genus **Iniskinites** Imlay was previously unknown in the Queen Charlotte Islands. Its presence is now established at localities in the Skidegate Inlet area where it occurs in the upper part of the Yakoun Formation slightly below the well known **Kepplerites (Seymourites)** Fauna. Two new species of **Iniskinites** are recognised. Recently described **Iniskinites** faunas from northern Yukon and the Smithers area of British Columbia were assigned to the Late Bathonian. The here described Queen Charlotte Islands specimens are considered to be of the same age.*

Introduction

In a recently published report on the Late Bathonian **Iniskinites** Fauna of central British Columbia (Frebold, 1978), which included description of one specimen collected in northern Yukon, it was suggested that the **Iniskinites** Fauna was probably also present in other parts of Western Canada. At that time two specimens collected by H.W. Tipper at Robber Point on the east shore of Maude Island had already been identified by the author as **Iniskinites** cf. **I. martini** (Imlay) (unpublished GSC report J-19-1976-HF). Recently, three more specimens belonging to the genus were located in the collections of the Geological Survey of Canada. One of these is the holotype of **I. cepoides** (Whiteaves) which had been placed by Whiteaves (1876, 1884, 1900) into various genera. Another specimen was found by F.H. McLearn in 1921 but was not identified or described. A third specimen was collected by A. Sutherland Brown in the type section of MacKenzie's (1916) Yakoun Formation. It had been misidentified by the author as **Chondroceras** (GSC report J-3-1962-HF).

The five specimens are here described and their stratigraphic position and age are discussed. It is hoped that more material from the Queen Charlotte Islands will become available in the near future.

Localities of the Described Specimens (see Fig. 10.1)

GSC no. 4966. **Iniskinites cepoides** (Whiteaves). Holotype. Exact locality unknown. According to H.W. Tipper (personal communication) it seems certain that the specimen came from Maude Island and most probably Robber Point.

GSC nos. 61865 and 61866. **Iniskinites cepoides** (Whiteaves.) Hypotypes. GSC locality 93736. "East shore of Maude Island, at Robber Point. 53°13'00"N, 132°01'40"W. H.W. Tipper coll. 1976."

GSC no. 61867. **Iniskinites** cf. **I. cepoides** (Whiteaves). Hypotype. GSC loc. 48605. "Robber Point, Maude Island. 53°13'N, 132°01'45"W. Sutherland Brown coll."

GSC no. 61868. **Iniskinites mclearni** Frebold n. sp. Holotype. GSC loc. 13633. "Loose. Newcombe Bay, north shore, Maude Island, Skidegate Inlet. F.H. McLearn coll. 1921."

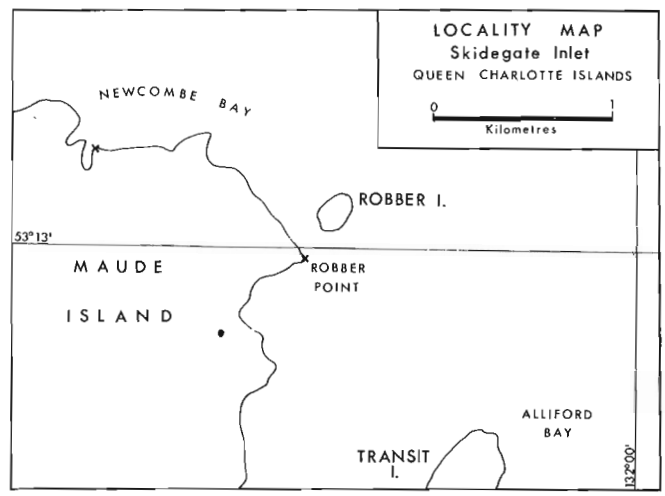

Figure 10.1. *The **Iniskinites** localities in the Skidegate Inlet area.*

The Stratigraphic Position and Age of the Genus Iniskinites in the Queen Charlotte Islands

Of the five specimens of **Iniskinites** described in this report the holotypes of **I. cepoides** (Whiteaves) and **I. mclearni** Frebold n. sp. were collected loose and their stratigraphic position is unknown. It is, however, probable that they came from the same bed as the other three specimens of **Iniskinites** which were found in situ in sections at or near Robber Point. One of them was collected by Sutherland Brown at GSC loc. 48605 in his "E-Member" which is the youngest stratigraphic unit of the type section of the Yakoun Formation (Sutherland Brown, 1968, p. 74). This specimen, which had been misidentified by the author in 1962 as **Chondroceras,** is described in this report as **Iniskinites** cf. **I. cepoides** (Whiteaves). The two other specimens were collected by H.W. Tipper in 1976 on the east shore of Maude Island, at Robber Point (GSC loc. 93736) in beds equivalent to Sutherland Brown's E-Member "a minimum of five feet stratigraphically below **Kepplerites**". They are described in this report as **Iniskinites cepoides** (Whiteaves).

The occurrence of the three specimens of **Iniskinites** in Sutherland Brown's E-Member of the Yakoun Formation and stratigraphically near to **Kepplerites** indicates clearly that they belong to the upper part of the Yakoun Formation. Further detailed stratigraphic studies may

show that **Iniskinites** may form part of McLearn's "Upper Yakoun Fauna" which, according to F.H. McLearn (1929, p. 2; 1949, p. 16, 17), contain various species of **Kepplerites (Seymourites)** and one **Phylloceras** but no other ammonites. The possibility of an association of **Iniskinites** with species of **Kepplerites (Seymourites)** in the Queen Charlotte Islands is supported by the fact that such associations are known from southern Alaska (Imlay, 1975, p. 11, 14) northern Yukon Territory and the Smithers area of British Columbia (Frebold, 1978, p. 1-3).

The age of the **Iniskinites** faunas of southern Alaska, northern Yukon, and the Smithers area of British Columbia was discussed recently by the author (Frebold, 1978, p. 3) and they were assigned to the Late Bathonian. The here described **Iniskinites** specimens from the Queen Charlotte Islands are considered to be of the same age.

Iniskinites cepoides (Whiteaves)

Plate 10.1, figures 4-9

Ammonites loganianus? Form B Whiteaves, 18796, p. 30, pl. 8, Figs. 1, 1a.

Stephanoceras cepoides Whiteaves, 1884, p. 210.

Olcostephanus cepoides (Whiteaves), Whiteaves, 1900, p. 276.

Material. The holotype, GSC no. 4966, exact locality unknown, and two smaller specimens, GSC nos. 61865, 61866, from GSC loc. 93736.

Description. The holotype and the two smaller specimens are somewhat distorted and the upper half of the anterior part of the last whorl of the holotype is missing. In one of the two smaller specimens the inner whorls are badly damaged. The general shape of the specimens is globose, the venter is moderately rounded and grades evenly into the moderately convex flanks. The transition to the very small and deep umbilicus is rounded, the umbilical wall very steep in the anterior part of the whorl, more gentle posteriorly. The slope of the umbilical wall is apparently influenced by the distortion of the specimen. The cross-section is wider than high. Up to a diameter of about 45 to 50 mm the ribs are rather fine and narrowly spaced, anteriorly they become gradually coarser and more widely spaced. The primaries are subdivided into two, occasionally into three secondaries. Some of the secondaries are indistinctly connected with the primaries. The point of division is below the half height of the flanks. Intercalated ribs that reach down to about the line of division of the primaries are quite regularly developed between the pairs of subdivided ribs. The ribs cross the venter almost transversely with a very slight forward bend. A pronounced apertural constriction is preserved in the small fragmentary specimen (GSC no. 61866, Pl. 10.1, fig. 8, 9). In the other small specimen (GSC no. 61865, Pl. 10.1, fig. 6, 7) part of the apertural constriction can still be seen on the left side of the end of the whorl. The aperture of the holotype is not preserved. Suture lines are not visible on any of the specimens.

Due to the deformation of the holotype and the hypotypes no exact measurements can be given. The holotype had an estimated maximum diameter of about 75 mm. At a less damaged part of the holotype the diameter is 53 mm, the whorl height 34 (0.64) mm and the whorl thickness 38 (0.71) mm. The numbers in parentheses are the ratios of the diameter.

Comparisons. In its general shape the holotype of **I. cepoides** (Whiteaves) is somewhat similar to **Iniskinites martini** (Imlay) but is much smaller than the holotype of Imlay's species (Imlay, 1953, p. 80, pl. 32, figs. 1, 4, 6). The small specimen of **I. martini** (Imlay) illustrated by Imlay (1975, pl. 4, figs. 4, 5) compares fairly well with the small specimens GSC nos. 61865, 61866 (pl. 01, figs. 6-9) which has previously been identified as **I. cf. martini** (Imlay) (Frebold, unpublished GSC report J-19-1976-HF).

Iniskinites cf. **I. cepoides** (Whiteaves)

Plate 10.1, figures 10-12

Material. One specimen. GSC no. 61867 from GSC loc. 48605.

Description and Comparisons. The specimen has about the same size as the holotype of the species. As it is fairly strongly distorted, no reliable measurements can be taken. The general shape is globose, the cross-section wider than high, the rounded venter grades into the moderately convex flanks. The transition of the flanks to the deep and narrow umbilicus is rounded, the umbilical wall is moderately steep in the posterior part of the last whorl and vertical in its anterior part. The shape of the umbilicus has been influenced by the distortion of the ammonite. The aperture is marked by a constriction which is deep on the flanks and shallower ventrally. It is followed by a gentle swelling.

The ribs are similar to those of the holotype but they are stronger and the interspaces wider. They are rather strong in the anterior part of the whorl which is not preserved in the holotype. They bifurcate somewhat below the half height of the flanks. Intercalated ribs are present quite regularly between the pairs of subdivided ribs.

PLATE 10.1 (opposite)

Figures 1-3. **Iniskinites mclearni** Frebold n. sp. Holotype. GSC 61868, GSC loc. 13633. (The missing part of the ammonite is replaced by plasticine.)

1. Lateral view, GSC photo 113555-U.
2. Cross-section and part of venter. GSC photo 11355-T.
3. Venter, GSC photo 113555-V.

Figures 4-5. **Iniskinites cepoides** (Whiteaves). Holotype. GSC 4966. Exact locality unknown. Probably from Maude Island, Robber Point or Newcombe Bay.

4. Lateral view, GSC photo 113555-W.
5. Venter, GSC photo 113555-X.

Figures 6-7. **Iniskinites cepoides** (Whiteaves). Hypotype. GSC 61865, GSC loc. 93736.

6. Lateral view, GSC photo 113555-O.
7. Cross-section and venter. GSC photo 113555-M.

Figures 8-9. **Iniskinites cepoides** (Whiteaves). Hypotype. GSC 61866, GSC loc. 93736.

8. Lateral view. GSC photo 113555-P.
9. Venter, GSC photo 113555-N.

Figures 10-12. **Iniskinites** cf. **I. cepoides** (Whiteaves). Figured specimen. GSC 61867, GSC loc. 48605.

10. Lateral view, GSC photo 113555-Q.
11. Venter, GSC photo 113555-S.
12. Venter, cross-section and "depression". GSC photo 113555-R. All photographs are in natural size.

PLATE 10.1

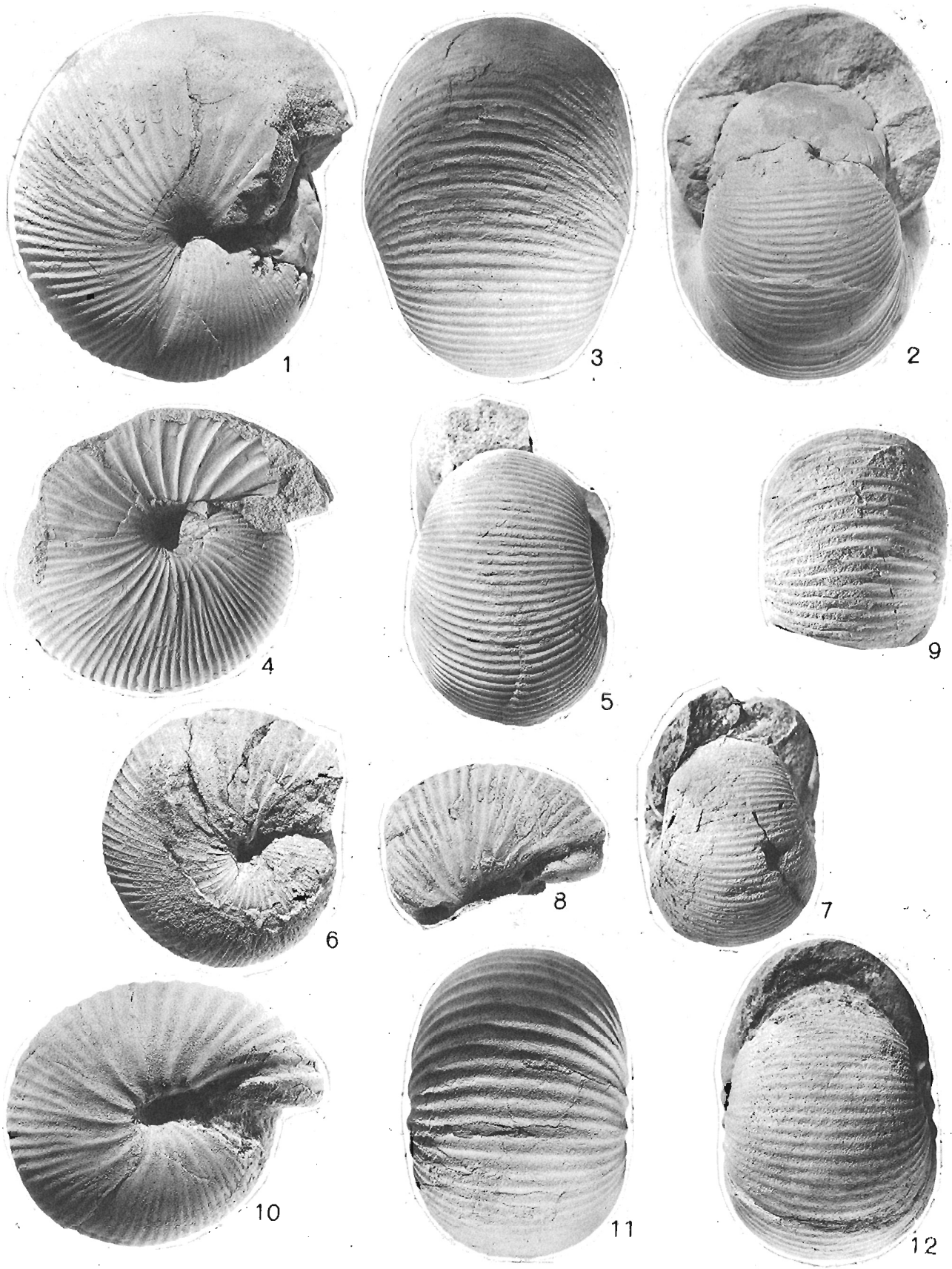

No traceable remnants of the suture line are visible at the beginning of the last whorl.

On the venter a shallow depression is present (see Pl. 10.1, fig. 12) which fades out in the upper part of the flanks. It is caused by the distortion of the ammonite and not a constriction.

Iniskinites mclearni Frebold n. sp.

Plate 10.1, figures 1-3

Material. One fairly well preserved specimen, GSC no. 61868 from GSC loc. 13633.

Description. The general shape of the specimen is globose with rounded venter which grades evenly into the moderately convex flanks. The umbilicus is extremely small, the transition of the umbilical wall into the flanks is rounded. In the anterior part of the whorl the umbilical wall is steeper than in its posterior part.

In the posterior part of the last whorl the ribs are fine. The primaries are subdivided into two or occasionally three secondaries. Some of the secondaries are indistinctly connected with the primaries. The ribs cross the venter almost transversely. Anteriorly the ribs become gradually stronger and more widely spaced. They are gently bent forward on the flanks and on the venter. Most of them are subdivided into two secondaries. Only a few undivided intercalated ribs are present.

In the posterior half of the last whorl a shallow and narrow depression is present which seems to be a constriction. It is, however, possible that this depression may have been caused by a slight distortion of the ammonite as is the case in the above described specimen of I. cf. **I. cepoides** (Whiteaves) (see Pl. 10.1, fig. 12.).

The aperture and the most posterior part of the last whorl are not preserved. Remnants of the suture line showing broad saddles and part of the ventral lobe are present in the posterior part of the whorl.

At the maximum diameter of 73 mm the whorl height is 46 (63) mm and the whorl thickness 50 (68.5) mm. The numbers in parentheses are ratios of the diameter.

Comparisons. In their shape, strength and subdivision the ribs in the posterior part of the last whorl are similar to the ribs in the holotype of **I. cepoides** (Whiteaves) at about the same stages of growth but anteriorly they do not become as coarse and more widely spaced as they do in **I. cepoides** (Whiteaves).

Iniskinites intermedius (Imlay) (Imlay, 1953, p. 81, pl. 31, figs. 1-4; pl. 32, figs. 2, 3, 5, 7, 8; 1975, p. 24, pl. 3, figs. 3, 4) is somewhat similar to **I. mclearni** but is more compressed and has stronger ribs. In its globosity and apparently also in the ribbing **I. mclearni** is similar to **I. martini** Imlay (1953, p. 80, pl. 32, figs. 1, 4, 6) but the holotype of Imlay's species is much larger than the holotype of **I. mclearni** and does not permit detailed comparison. Unfortunately no specimens of **I. martini** equal in size to **I. mclearni** have been described.

References

Frebold, H.
1978: Ammonites from the Late Bathonian "Iniskinites Fauna" of Central British Columbia; Geological Survey of Canada, Bulletin 307.

Imlay, R.W.
1953: Callovian (Jurassic) Ammonites from the United States and Alaska; Pt. 2, Alaska Peninsula and Cook Inlet Regions; U.S. Geological Survey, Professional Paper 249-B.

1975: Stratigraphic Distribution and Zonation of Jurassic (Callovian) Ammonites in Southern Alaska; U.S. Geological Survey, Professional Paper 836.

MacKenzie, J.D.
1916: Geology of Graham Island, British Columbia; Geological Survey of Canada, Memoir 88.

McLearn, F.H.
1929: Contributions to the Stratigraphy and Palaeontology of Skidgate Inlet, Queen Charlotte Islands, B.C.; National Museum of Canada, Bulletin 54.

1949: Jurassic Formations of Maude Island and Alliford Bay, Skidegate Inlet, Queen Charlotte Islands, British Columbia; Geological Survey of Canada, Bulletin 12.

Sutherland Brown, A.
1968: Geology of the Queen Charlotte Islands; British Columbia Department of Mines and Petroleum Resources, Bulletin 54.

Tipper, H.W.
1977: Jurassic studies in Queen Charlotte Islands, Harbledown Island and Taseko Lakes Area, British Columbia; in Report of Activities, Part A, Geological Survey of Canada, Paper 77-1A.

Whiteaves, J.F.
1876: On some Invertebrates from the Coal-Bearing Rocks of the Queen Charlotte Islands; Geological Survey of Canada, Mesozoic Fossils, v. 1, pt. 1.

1884: On the Fossils of the Coal-Bearing Deposits of the Queen Charlotte Islands collected by Dr. G.M. Dawson in 1878; Geological Survey of Canada, Mesozoic Fossils, v. 1, pt. 3.

1900: On some additional or imperfectly understood fossils from the Cretaceous rocks of the Queen Charlotte Islands, with a revised list of the species from these rocks; Geological Survey of Canada, Mesozoic Fossils, v. 1, pt. 4.

11.

EVIDENCE OF CARADOCIAN GLACIATION IN THE DAVIDSVILLE GROUP OF NORTHEASTERN NEWFOUNDLAND[1]

R.K. Pickerill[2], G.E. Pajari[2], and K.L. Currie[3]
Regional and Economic Geology Division

Pickerill, R.K., Pajari, G.E., and Currie, K.L., Evidence of Caradocian glaciation in the Davidsville Group of northeastern Newfoundland; in Current Research, Part C, Geological Survey of Canada, Paper 79-1C, p. 67-72, 1979.

Abstract

The Davidsville Group of northeastern Newfoundland consists essentially of a series of resedimented clastics of Llanvirn/Llandeilo – Late Ordovician age. Within this sequence, immediately underlying graptolitic slates of Caradocian age, are a series of laterally continuous (on outcrop scale) glaciomarine diamictites containing excellently preserved glacially rafted dropstones. These diamictites are associated with thinly, interbedded siltstones and slates probably deposited by turbidity, hemipelagic and normal deep-water bottom marine current activity in a middle-outer submarine fan environment. These rhythmically bedded muds and silts contain isolated dropstones and channelized and lenticular diamictites. We describe here the nature and distribution of these laterally continuous and lenticular diamictites and discuss possible mechanisms of deposition.

Introduction

Undoubted glacial tillites and diamictites have now been documented from many upper Ordovician sequences, particularly those exposed in France, Spain and North Africa (e.g. Tamain, 1971; Beuf et al., 1971; Dangeard and Doré, 1971; Tucker and Reid, 1973; Allen, 1975). Such studies suggest that the Ordovician glaciation was most likely restricted to the Caradocian (Wright and Moseley, 1975) with an ice sheet centred over the present day Sahara and northwest Africa (Harland, 1972).

In the northern Appalachians possible marine rafted 'tillites' and glaciomarine diamictites have already been described from the Caradocian (or younger) White Rock Formation of Nova Scotia by Schenk (1972) and the Late Ordovician – Early Silurian Stoneville Formation of northeastern Newfoundland by McCann and Kennedy (1974). Although Harland and Herod (1975, p. 196) alluded to the possibility of other alleged Late Ordovician tillites on the eastern seaboard of North America, no other occurrences have been adequately documented. We therefore describe here the occurrence of a sequence of Caradocian diamictites recently discovered in the Davidsville Group of northeastern Newfoundland.

General Geology and Localities

The Davidsville Group of Kennedy and McGonigal (1972) outcrops in northeastern Newfoundland on the eastern side of the Dunnage Zone of Williams (1978). In the Carmanville district (Fig. 11.1) the group consists essentially of resedimented clastics (Pickerill et al., 1978) which in part unconformably overlie the allochthonous rocks of the Gander River ultramafic belt. The unconformity has been relatively

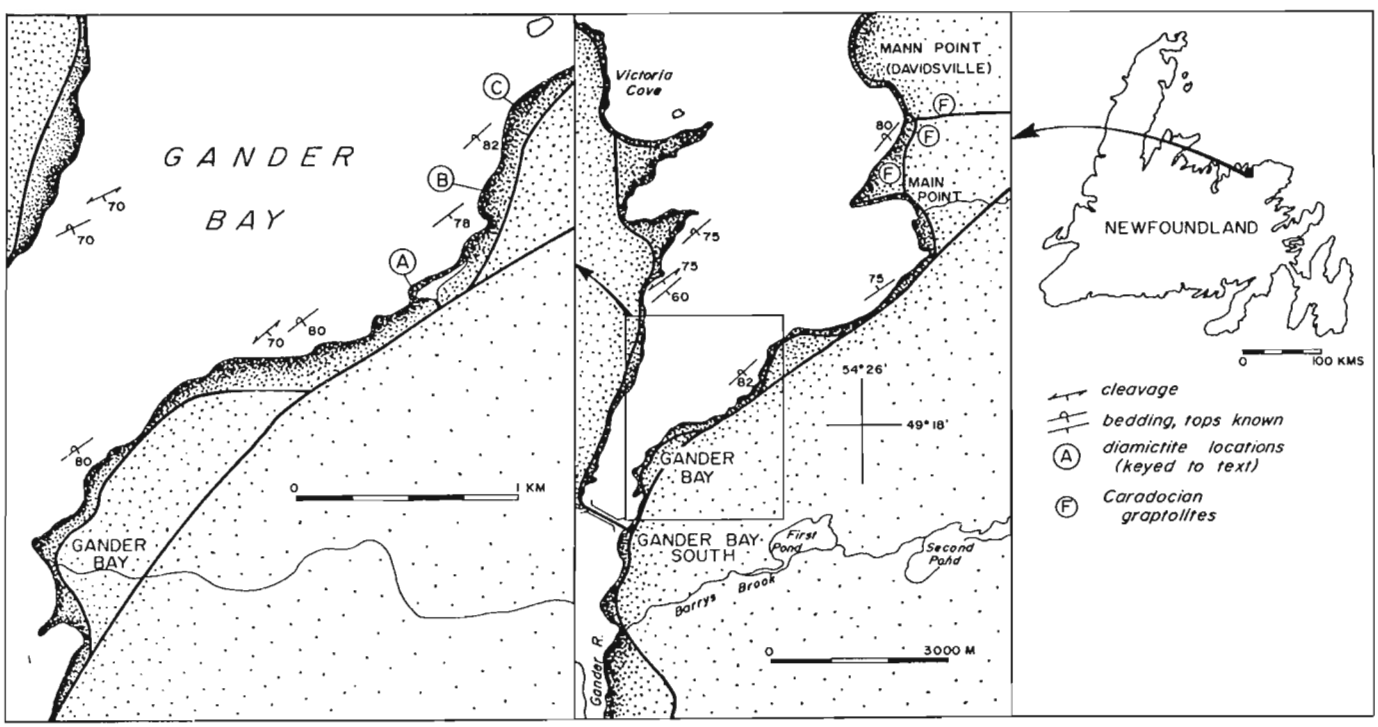

Figure 11.1 *Location map of the three diamictite localities on the eastern side of Gander Bay, northeastern Newfoundland, and within the Davidsville Group.*

[1] Canadian contribution number 13 to the Internation Geological Correlation program, Caledonide Orogen Project 27
[2] Department of Geology University of New Brunswick Fredericton, N.B. E3B 5A3
[3] Geological Survey of Canada

precisely dated as Llanvirn/Llandeilo in age of the basis of reasonably well-preserved conodont elements (Blackwood, 1978; G.S. Nowlan – Personal communication 1978) in lowermost units of the Davidsville Group. The remainder of the succession has failed to yield fossils except at three localities well removed from the base of the succession at Main Point on the eastern side of Gander Bay (Fig. 11.1), which have yielded poorly preserved graptolites of Caradocian age (Bergström et al., 1974) in strongly cleaved pyrite- and pyrrhotite-bearing black slates. Approximately 3 km to the south-southwest of Main Point a series of thinly interbedded siltstones and slates and associated diamictite beds are exposed. These outcrops stratigraphically underlie the fossiliferous black slates and therefore, although themselves not precisely dated, it is reasonable to suggest that the diamictites described here are Caradocian in age.

The diamictites and associated sediments are exposed at three isolated but consecutive shoreline outcrops. In each, bedding is subvertical but stratigraphic relationships between individual outcrops are difficult to assess owing to the presence of small scale (1-3 m 1/2λ) tight to isoclinal tectonic folds, and slumping, rotation and folding of the sediments during or shortly following their deposition (cf. Pajari et al., 1979). The following description incorporates data obtained from each outcrop, though the most complete and detailed exposure is the northeastern one (Locality C of Fig. 11.1), where a continuous 12 m section is well exhibited.

Description of the Diamictites

Diamictite is employed here as nongenetic term (cf. Flint et al., 1969; Harland et. al., 1966) to describe lithified, poorly sorted, matrix-supported, polymictic conglomerates characterized by dispersed clasts of variable size, composition, shape and degree of rounding enclosed within a homogeneous or rhythmically laminated mud/silt matrix (Fig. 11.2a). The term is synonymous with "mixtite" (Schermerhorn, 1966) but has publication priority. The three localities exhibiting the diamictites are located on the southeastern shoreline of Gander Bay (Fig. 11.1). The essential characteristics exhibited at individual exposures are:–

Locality A: 0.75 m channel diamictite immediately overlain by 0.4 m of interbedded muds and silts containing dispersed clasts, some of which are clearly dropstones. Associated underlying sediments (*c.* 8 m) exhibit well developed syndepositional faulting, folding and slump structures.

Locality B: A *c.* 1.8 m diamictite containing dropstones associated with interbedded muds and silts (*c.* 5 m) containing thin, lenticular diamictites, dropstones and syndepositional slumps.

Locality C: Three laterally continuous diamictite horizons, each 1-2 m thick. Associated interbedded muds and silts contain thin lenticular diamictites and dispersed clasts, many of which are dropstones. Soft-rock deformation structures are abundantly developed. Total exposed thickness is *c.* 12 m.

Generally the thicker polymictic diamictites are laterally continuous on outcrop scale, whereas the thinner (commonly 6-8 cm) beds are invariably lenticular, are commonly associated with the intervening mud/silt rhythmites (see below) and have commonly been subjected to syndepositional soft-rock deformation. Lower and upper boundaries of the diamictites are usually gradational with the intervening rhythmites but rarely the lower boundary is erosional and channeled.

The matrix-supported clasts range in size from coarse sand to cobbles and, in places, boulders up to 230 mm in diameter. Clasts constitute between 10-45% of the rock. They are randomly distributed and no concentrations or clusters have been observed (cf. Ovenshine, 1970). On average they are composed of light coloured siltstone (52%), dark coloured siltstone (16%), orthoquartzite (18%), fine sandstone (9%) and granitoid (granite, granodiorite) material (5%). Orthoquartzite and granitoid clasts are invariably coarse sand to pebble size whereas the remainder may all be coarse sand to boulder size. The majority are rounded (70%) or subrounded (24%) and only a small proportion (6%) are angular or subangular. All lithologies exhibit variable degrees of roundness. Surfaces of individual clasts are always smooth and no striations have been observed.

The clasts also exhibit variable shapes. The majority are oblate spheroids with their long axes parallel to stratification. As bedding and cleavage are parallel in these locations this orientation and observed shape could, in part, be deformational. The larger pebbles, cobbles and boulders tend to be equant, while the remainder of the debris is tabular. Occasional pebbles and cobbles are approximately triangular and may represent faceted varieties (cf. Schenk, 1972). Although the majority of the spheroidal clasts are aligned with their long axes parallel to stratification a small percentage are aligned at or near to 90° (Fig. 11.2b).

The clasts are all enclosed within a mud or mud/silt matrix which is characteristically finely (0.5 – 3 mm) and rhythmically laminated or alternatively, but less commonly, appears massive even in thin section. The alternating mud/silt laminae are best observed when the clast/matrix ratio is low. Finer laminae are usually continuous and maintain a constant thickness; coarser laminae may be continuous but are also lenticular. In the upper horizons the diamictites commonly possess thin lenses of more thickly interbedded mud and silt (0.3 – 3 cm), identical in form and composition to the associated sediments described below.

Many of the clasts within the diamictites, both those with their long axes parallel and, in particular, normal to bedding, distort and penetrate the laminae (Fig. 11.2b, 11.2c). These 'dropstones' may be observed within the diamictites themselves, particularly when lamination is well developed, but more commonly at their gradational bases and tops. Distortion of laminae is the more common occurrence. Though clearly in part a result of compaction and tectonic flattening the more pronounced curvature and distortion of laminae below the clasts suggests that they depressed the underlying laminae before those overlying the clasts were deposited (Fig. 11.2b). There is no evidence of penecontemporaneous erosion of the clast-associated laminae, suggesting, therefore, that they are not lag clasts (cf. Crowell and Frakes, 1972; McCann and Kennedy, 1974). Clasts actually penetrating laminae or thin silt horizons are by no means uncommon but are more difficult to readily observe because of the closely spaced bed-parallel cleavage developed in the diamictite matrix but not in the clasts. This tends to mask lamination and results in the apparent truncation of cleavage by the clasts.

Associated Sediments

Interbedded with and/or immediately overlying or underlying the diamictites are a series of rhythmically and thinly interbedded silts and muds, each 0.3-4 cm thick. The silts are generally parallel laminated throughout or alternatively exhibit parallel passing into small scale cross-lamination. Some of the thicker silt beds are graded and/or graded passing into parallel and/or small scale crosslamination. Both the silts and muds are usually laterally continuous on outcrop scale but rarely the silts may be composed of distinctive horizons of isolated pods or lenticles

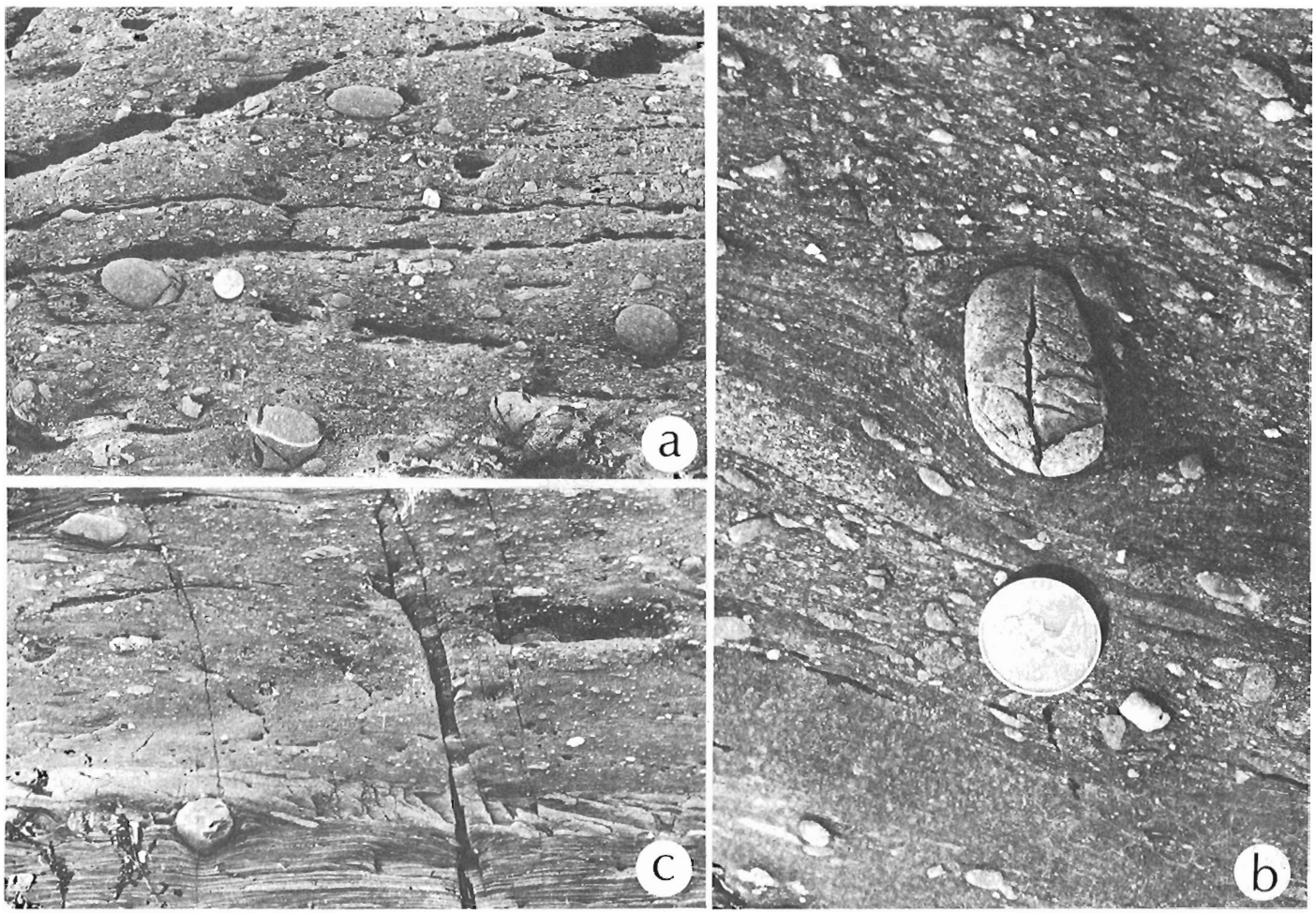

Figure 11.2 *a. Generalized view of diamictite from Locality C. Note the matrix-supported, essentially spherical-shaped clasts orientated parrallel to stratification. Coin diameter 2 cm.*

b. Fine sandstone clast orientated subnormal to stratification within a diamictite from Locality C. The clast both penetrates and distorts the rhythmically interbedded muds and silts. Note the lenticular bedded silts above the coin. Coin diameter 2 cm.

c. Diamictite and associated interbedded mud/silt rhythmites at Locality C. Note the isolated faceted clast penetrating and distorting the rhythmites and the fine lamination within the diamictite. Length of mapping pen (upper left) is 12 cm.

usually <1 cm in thickness and each commonly possessing foreset crosslaminae. Many of the lenticles are flat based and may represent starved ripples. Intervening muds are generally homogeneous but may possess faintly preserved silt laminae. The silt beds are commonly nonerosive but may possess small scours and ? prod marks at their base. Sporadically distributed throughout the sediments are good examples of dropstones which constitute <2% of the rock but, on the other hand, are some of the largest observed. The dropstones both penetrate and/or deform the interbedded silts and muds. As outlined above, these sediments also contain thin lenticular diamictites identical in composition and with the same internal characteristics as those described previously. Many of these diamictites and their associated silts and muds have been involved in penecontemporaneous soft-rock deformation.

Discussion

Throughout the depositional history of the Davidsville Group clastic detritus was derived from at least two contrasting sources. Petrographic studies and field observations suggest that detritus was provided from a continental terrane, from the obducted slabs of the Gander River ultramafic belt and from a further unidentified source. The majority of the group consists of resedimented clastics emplaced by a variety of sediment-support mechanisms, including dominantly turbidity and to a lesser degree fluidized and grain flows (Pickerill et al., 1978). Some of the finer grained sediment may possibly represent material derived from bottom currents and hemi-pelagic settling. The sedimentary pile was all subsequently involved in complex submarine sliding and olistostrome formation (Pajari et al., 1979).

The nature of some of these sedimentation mechanisms can in fact be demonstrated by a more detailed analysis of the sediments associated with the diamictites as described above. These thinly and rhythmically bedded muds and silts are typical of many of the more accessible outcrops of the Davidsville Group in northeastern Newfoundland and have somewhat erroneously prompted previous authors (e.g. Kennedy and McGonigal, 1972; Dean, 1979) to refer to the entire group as a series of black slates and greywackes. Analogous rhythmically bedded sequences exhibiting similar

internal characteristics have been documented by a number of authors (e.g. Mutti, 1977; Shanmugan and Walker, 1978). Comparison with these more detailed studies suggests that the laterally continuous siltstones represent thinly bedded turbidite deposits illustrating Tb, Tb-c and more rarely Ta, Ta-b and Ta-c Bouma sequences. The e interval of the idealized Bouma sequence may be present in association with these sequences but has proved impossible to recognize and differentiate from the normal ?hemipelagic muds. In contrast to the laterally continuous siltstones, the lenticular variety probably represent material deposited and reworked by active ocean-bottom currents (cf. Piper, 1978; Shanmugan and Walker, 1978).

The interbedded muds and muds with silt laminae are more difficult to interpret but possibly represent mud turbidites (in the sense of Piper, 1978) or hemipelagic sediment, both possibly subject to normal bottom current reworking. The fact that a continuum usually exists between dilute turbidity flows, bottom currents and hemipelagic settling (Stow and Lovell, 1978) suggests that all these mechanisms could conceivably have been operative. As with their recent correlatives, however, general criteria for distinguishing between them are difficult to establish.

The paleoenvironmental significance of the facies association is not exactly clear. Historically such an association would perhaps have been referred to as 'distal turbidites' with hemipelagic intercalations. Mutti (1977), however, has demonstrated that similar facies associations need not necessarily be 'distal', but may in fact occur in channel margin, inter-channel, channel mouth and lobe fringe subenvironments of submarine fan complexes. Indeed, identical facies may be observed along strike approximately 1000m to the south-southwest of the diamictite localities where they occur in association with the upper horizons of turbiditic fining- and thinning-upward channel-filled sequences. Thus, although the detailed paleoenvironmental significance of the facies association remains somewhat perplexing, we suggest a middle-outer submarine fan environment as the most likely site for the formation of this particular facies.

It is therefore apparent that the diamictites formed in a deep water submarine fan environment in association with sediments deposited by the interplay of turbidite, hemipelagic and bottom current depositional mechanisms. The association of diamictites (usually interpreted as glacial in origin) and deep water dominantly turbidic sediments has been noted by several authors (Harland et al., 1966; Tucker and Reid, 1973; McCann and Kennedy, 1974). Although the recognition of ancient glacial and glaciomarine deposits has long been a source of controversy, evidence in favour of the Davidsville Group diamictites being glaciomarine in origin is suggested by the criteria:–

1. The presence of large dispersed clasts, some of which are clearly dropstones, both within the diamictites themselves (Fig. 11.2b) and the associated interbedded sediments (Fig. 11.2c). Many authors (e.g. Crowell, 1964; Harland et al., 1966; Frakes and Crowell, 1967, 1970; Tucker and Reid, 1973; McCann and Kennedy, 1974) regard this to be the most convincing single criterion for a glacial origin and usually attribute their occurrence to iceberg rafting.
2. Though shape and surface markings of individual clasts are not definitive of any particular environment (Schenk, 1972) clasts with long axes normal or subnormal to stratification possibly indicate rafting (Crowell, 1964; Harland et al., 1966).
3. The presence of dispersed clasts within thinly laminated (varve-like) and lenticular muds and silts. Such a criterion has been emphasized by Reading and Walker (1966), Lindsay (1971) and Tucker and Reid (1973). Though in itself not definitive of glacial origin it indicates that the diamictites did not result from any massflow phenomenum.
4. The presence of orthoquartzite, granite and granodiorite clasts within the diamictites is clearly indicative of their exotic provenance, as throughout the remainder of the Davidsville Group they are absent. Similarly, the absence of plagiogranite, mafic and ultramafic clasts is further suggestive of an exotic source, as these components, although variably developed, are otherwise present in the coarse clastic units throughout the remainder of the succession. The unique occurrence of certain lithologies and absence of others can only be accounted for by inferring a provenance removed from the source areas characterizing the remainder of the succession. Their unique introduction into their depositional site must represent some anamolous event(s).

Thus we suggest that the diamictites were deposited under glacial conditions. Clasts within the diamictites and associated sediments are most logically attributed to iceberg rafting. The finely and rhythmically laminated diamictite matrix closely resembles that figured by Lindsay (1971) and Tucker and Reid (1973) and considered to be diagnostic of glaciomarine muds and associated sediments. Such rhythmites possibly represent deposition from low-density suspension currents discharged from floating ice (cf. Reading and Walker, 1966) or from bottom current activity (cf. Lindsay, 1971), though the presence of lenticular laminae and thin lenses of interbedded mud and silt in the upper horizons of the diamictites suggests the latter to be more realistic.

If it is accepted that the diamictites are in fact glacial in origin, as we have attempted to demonstrate, then certain observations still remain enigmatic. For example, the channeled and/or lenticular diamictities are somewhat anomalous, as such occurrences have not elsewhere been previously reported in the literature. This variety occurs within the associated mud/silt rhythmites containing isolated dropstones and, as previously outlined, such occurrences are not particularly uncommon. Detailed examination reveals that apart from an homogeneous matrix possessing no internal fabric, these diamictites exhibit essentially the same characteristics as the laterally continuous variety. They are commonly underlain by rhythmically interbedded muds and silts which exhibit soft-rock slumping, folding and disaggregationn. Observations suggest that the channeled and lenticular bedded variety represent diamictites which were resedimented as subaqueous massflow deposits (see Carter, 1975) in the form of partially erosive debris flows or, more likely, slurry flows (mudflows). That the sediments were unstable is indicated not only by the slumping, folding and disaggregation of the associated sediments, but also slumping and folding of the lenticular diamictites themselves following their resedimentation.

Thus, the lenticular diamictites have undergone a complex and varied sedimentation history and recognition of their glacial origin is somewhat dependant on their intimate association and affinities with the laterally continuous and more readily recognizable diamictites. As Harland (1972) pointed out, glaciomarine tillites may be confused with turbidites, mudflows and other massflow deposits, and other after careful and detailed analysis can the origin of diamictites be realistically assessed.

Summary

In summary, we propose that the Caradocian diamictites observed by us in the Davidsville Group of northeastern Newfoundland represent glaciomarine sediments. These sediments accumulated in a middle-outer submarine fan environment which developed on the southeastern margin of the Iapetus Ocean. The laterally continuous diamictites (on outcrop scale) are typical and in many respects identical to previously described glaciomarine sediments formed in association with deep-water, essentially turbiditic, sediments. The occurrence of lenticular and channeled diamictites in association with the laterally continuous variety is somewhat unusual. We interpret this variety to be the result of resedimentation by debris or, more likely, mudflow activity of already deposited unconsolidated and unstable glaciomarine material. Although Caradocian glaciomarine deposits should theoretically be more commonplace in the northern Appalachians than previously reported (cf. Harland, 1972), it is conceivable that their recognition has gone unnoticed because of the possibility of similar resedimentation mechanisms potentially destroying recognizable diagnotic criteria for a glacial origin.

References

Allen, P.
1975: Ordovician glacials of the central Sahara; in Ice Ages: Ancient and Modern (A.E. Wright and F. Moseley, editors). Geological Journal, Special Issue No. 6, p. 275-285.

Bergström, S.M., Riva, J. and Kay, M.
1974: Significance of conodonts, graptolites and shelly faunas from the Ordovician of western and north central Newfoundland; Canadian Journal of Earth Sciences, v. 11, p. 1625-1660.

Beuf, S., Biju-Duval, B., Charpal, O. De, Rognon, P., Gariel, O. and Bennacef, A.
1971: Les grès du Paléozoique inferieur au Sahara; Publications de l'Institut Francais du Pétrole; Collection Science et Technique du Pétrole 18, 464p.

Blackwood, R.F.
1978: Northeastern Gander Zone, Newfoundland; Mineral Development Division; Newfoundland Department of Mines and Energy, Report of Activities for 1977, p. 72-79.

Carter, R.M.
1975: A discussion and classification of subaqueous mass-transport with particular application to grain-flow, slurry-flow and fluxoturbidites; Earth-Science Reviews, v. 11, p. 145-177.

Crowell, J.C.
1964: Climatic significance of sedimentary deposits containing dispersed megaclasts; in Problems in palaeoclimatology (A.E.M. Nairn, editor). Interscience London, p. 86-99.

Crowell, J.C. and Frakes, L.A.
1972: Late Paleozoic glaciation. Part V. Karoo Basin, South Africa; Bulletin of the Geological Society of America, v. 81, p. 2887-2912.

Dangeard, L. and Doré, F.
1971: Facies glaciaires de l'Ordovicien Supérieur en Normandie; in Colloque Ordovicien-Silurien, Memoire Brest Bureau Récherche Géologique et Minéralogique 73, p. 550-565.

Dean, P.L.
1979: The volcanic stratigraphy and metallogeny of Notre Dame Bay, Newfoundland; Geology Report No. 7, Memorial University of Newfoundland, St. John's Newfoundland.

Flint, R.F., Sanders, J.E. and Rodgers, J.
1960: Diamictite: a substitute term for symmictite; Bulletin of the Geological Society of America, v. 71, p. 1809-1810.

Frakes, L.A. and Crowell, J.S.
1967: Facies and paleogeography of Late Paleozoic diamictite, Falkland Islands; Bulletin of the Geological Society of America, v. 48, p. 37-58.

1970: Late Paleozoic glaciation: II, Africa exclusive of the Karoo Basin; Bulletin of the Geological Society of America, v. 81, p. 2261-2286.

Harland, W.B.
1972: The Ordovician Ice Age: Essay Review; Geological Magazine, v. 109, p. 451-456.

Harland, W.B., Herod, K.N. and Krinsley, D.H.
1966: The definition and identification of tills and tillites; Earth-Science Reviews, v. 2, p. 225-256.

Harland, W.B. and Herod, K.N.
1975: Glaciations through time; in Ice Ages: Ancient and Modern (A.E. Wright and F. Moseley, editors); Geological Journal, Special Issue No. 6, p. 189-216.

Kennedy, M.J. and McGonigal, M.H.
1972: The Gander Lake and Davidsville Groups of northeastern Newfoundland, new data and geotectonic implications; Canadian Journal of Earth Sciences, v. 9, p. 453-459.

Lindsay, D.A.
1971: Glacial marine sediments in the Precambrian Gowganda Formation at Whitefish Falls, Ontario (Canada); Palaeogeography, Palaeoclimatology, Palaeoecology, v. 9, p. 7-25.

McCann, A.M. and Kennedy, M.J.
1974: A probable glacio-marine deposit of Late Ordovician – Early Silurian age from the north central Newfoundland Appalachian Belt; Geological Magazine, v. 111, p. 549-564.

Mutti, E.
1977: Distinctive thin-bedded turbidite facies and related depositional environments in the Eocene Hecho Group (South-central Pyrenees, Spain); Sedimentology, v. 24, p. 107-131.

Ovenshine, A.T.
1970: Observations of iceberg rafting in Glacier Bay, Alaska, and the identification of ancient ice-rafted deposits; Bulletin of Geological Society of America, v. 81, p. 891-894.

Pajari, G.E., Pickerill, R.K. and Currie, K.L.
1979: The nature, origin and significance of the Carmanville ophiolitic mélange, northeastern Newfoundland; Canadian Journal of Earth Sciences, v. 16.

Pickerill, R.K., Pajari, G.E., Currie, K.L. and Berger, A.R.
1978; Carmanville Map Area, Newfoundland; the northeastern end of the Appalachians; in Current Research, Part A, Geological Survey of Canada, Paper 78-1A, p. 209-216.

Piper, D.J.W.
1978: Turbidite Muds and Silts on Deepsea Fans and Abyssal Plains; in Sedimentation in Submarine Canyons, Fans, and Trenches (D.J. Stanley and G. Kelling, editors); Dowden, Hutchinson and Ross, Inc., p. 163-176.

Reading, H.G. and Walker, R.G.
1966: Sedimentation of Eocambrian tillites and associated sediments in Finnmark, northern Norway; Palaeogeography, Palaeoclimatology, Palaeoecology, v. 2, p. 177-212.

Schermerhorn, L.J.G.
1966: Terminology of mixed coarse-fine sediments; Journal of Sedimentary Petrology, v. 36, p. 831-835.

Schenk, P.E.
1972: Possible Late Ordovician Glaciation of Nova Scotia; Canadian Journal of Earth Sciences, v. 9, p. 95-107.

Shanmugan, G. and Walker, K.R.
1978: Tectonic significance of distal turbidites in the Middle Ordovician Blockhouse and Lower Siever Formations in east Tennessee; American Journal of Science, v. 278, p. 551-578.

Stow, D.A.V and Lovell, J.P.B.
1978: Contourites: Their recognition in modern and ancient sediments; Earth-Science Reviews, v. 14, p. 251-291.

Tamain, G.
1971: L'Ordovicien Est-Maranique (Espagne) sa place dans la province mediterraneene; in Colloque Ordovicien-Silurien, Memoire Brest Bureau Récherche Géologique et Mineralogique 73, p. 403-416

Tucker, M.E. and Reid, P.C.
1973: The sedimentology and context of Late Ordovician glacial marine sediments from Sierra Leone, West Africa Palaeogeography Palaeoclimatology, Palaeoecology, v. 13, p. 289-307.

Williams, H.
1978: Tectonic lithofacies map of the Appalachian orogen; Memorial University of Newfoundland Map No. 1, St. John's Newfoundland.

Wright, A.E. and Moseley, F.
1975: Ice Ages: Ancient and Modern A Discussion in Ice Ages: Ancient and Modern (A.E. Wright and F. Moseley, editors); Geological Journal, Special Issue No. 6, p. 301-312.

12.

PRELIMINARY RESULTS OF SURFICIAL GEOLOGY AND GEOMORPHOLOGY STUDIES OF THE LOMONOSOV RIDGE, CENTRAL ARCTIC BASIN

Project 780048

S.M. Blasco, B.D. Bornhold[1], and C.F.M. Lewis
Atlantic Geoscience Centre, Dartmouth

Blasco, S.M., Bornhold, B.D., and Lewis, C.F.M., Preliminary results of surficial geology and geomorphology studies of the Lomonosov Ridge, Central Arctic Basin; in Current Research, Part C, Geological Survey of Canada, Paper 79-1C, p. 73-83, 1979.

Abstract

Bathymetric subbottom and shallow seismic reflection profiling, sediment sampling, seabed photography and water column temperature and sound velocity profiling, as well as surface plankton tows, were conducted in April and May 1979 from the ice station ***LOREX*** *as it drifted over the Lomonosov Ridge close to the North Geographic Pole. These seabed geologic studies, in conjunction with other scientific programs, were undertaken to delineate the physical nature and origin of this little-known Arctic submarine feature. The Lomonosov Ridge has a relief of 2800 m and a width of 88 km along the drift path. Asymmetrical in cross-section, the Amerasian flank has slopes as steep as 12 whereas the Eurasian flank slopes are less than 7°. The ridge appears to consist of en echelon fault blocks that give the crest an irregular morphology. A thin veneer of unconsolidated sediments, primarily deposited on the fault block tops, is presently undergoing erosion by current action. These sediments were probably deposited prior to the assumed separation of the ridge from the Barents Continental Shelf. The presence of dinoflagellate* ***Luxadinium propalulum*** *in the surface material recovered from the ridge crest suggests that this separation was initiated no earlier than mid-Cretaceous. Observed thermal alteration of this species could have occurred during the early stages of spreading along the Nansen-Gakkel rift.*

Introduction

The Lomonosov Ridge, linear in form, aseismic in nature, extends across the floor of the Arctic Ocean a distance of 1800 km from the continental shelf adjacent to the New Siberian Islands and to the shelf north of Ellesmere Island and Greenland. This submarine ridge system separates the Amerasian and Eurasian basins as it rises some 3000 m from the abyssal plains to a depth of 1000 m below sea level. Ridge width varies from a maximum of 200 km in proximity to the continental shelves to a minimum of 25 km near the North Geographic Pole.

From March 29 to May 29, 1979, the writers participated in the Lomonosov Ridge Experiment (LOREX) located on a drifting ice floe some 90 km from the pole (Fig. 12.1). The objective of this Earth Physics Branch, multidisciplinary project was not only to define more clearly the geologic nature and origin of the Lomonosov Ridge, but to develop the Canadian expertise for conducting such research from a floating ice platform. The scope of the writers' participation was to conduct comprehensive seabed geological studies of this ridge feature and adjacent areas of the Makarov and Fram basins. This involved seabed photography and sediment sample recovery, acoustic profiling and surface plankton sampling.

With Transit satellite receivers and Omega navigation systems providing positioning control (with an accuracy of ± 100 m for the satellite fixes and ± 1 km for the Omega), the LOREX ice station drifted a net 160 km during the 62 day program. Drift rates varying from 0 to 1200 m per hour were recorded. The closest LOREX was to the pole was 35 km, reached on May 17. During the program the ice floe crossed the Lomonosov Ridge once, approaching approximately

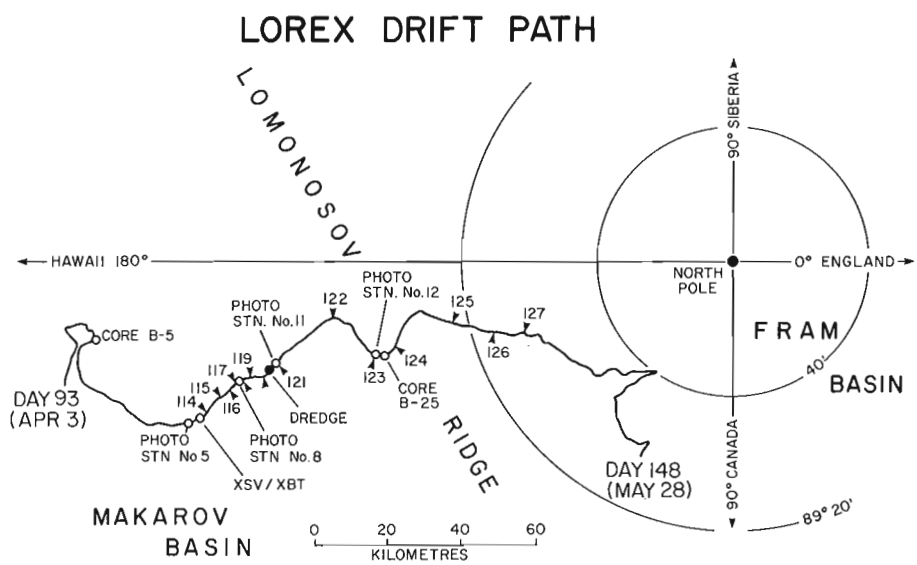

Figure 12.1. *Drift track of* ***LOREX*** *main ice camp from April 3 to May 28, 1979. Time is recorded in Julian days (GMT) and can be related to the bathymetric and seismic profiles (Fig. 12.6, 12.7). Core, dredge, photography and XSV/XBT stations referred to in the text are also located.*

[1]Regional and Economic Geology Division, Pacific Geoscience Centre, 9860 West Saamich Rd., Sidney, British Columbia, V8L 4B2

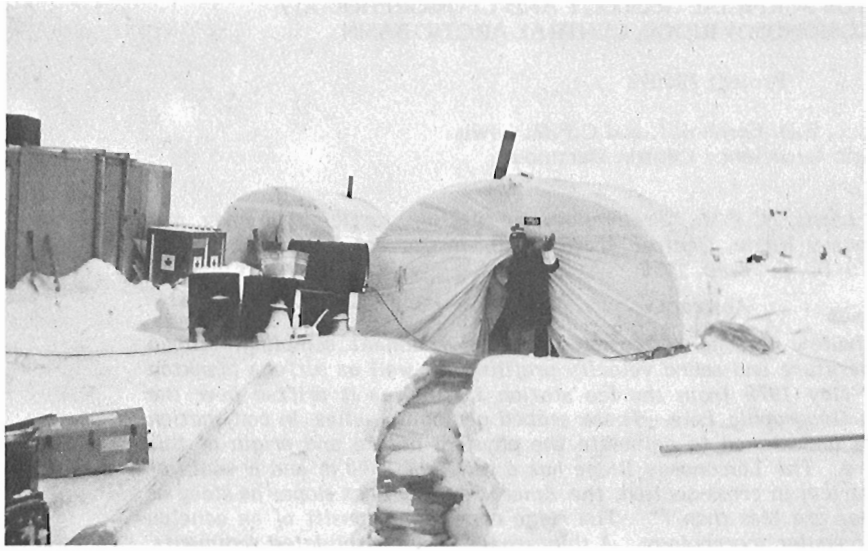

Figure 12.2

Following several hours of high winds in excess of 45 km/h cracks and leads opened up along and across the runways as well as under the marine geology camp. Part of this camp was relocated on more stable ice. (BIO Photo 5415-2).

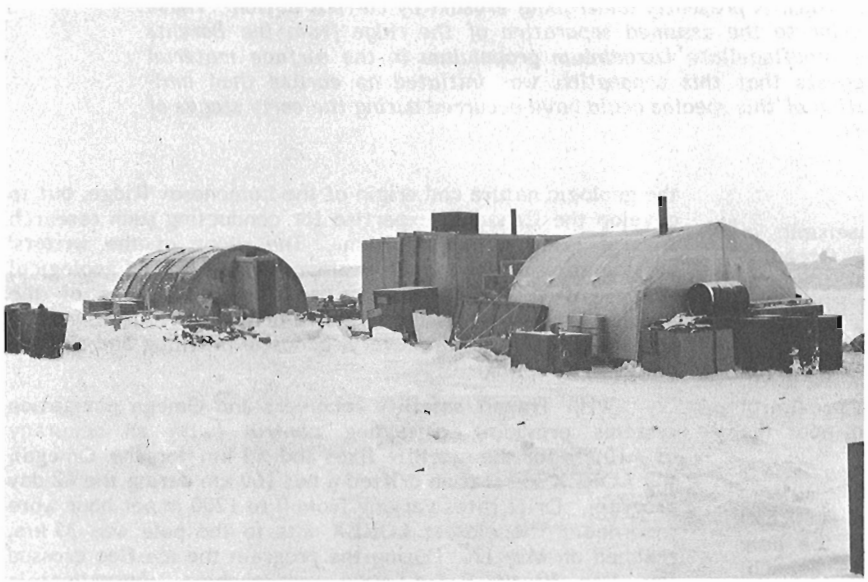

Figure 12.3

The longhouse tent, insulated plywood prefab and parcoll housed the equipment and facilities required for the marine geology program. This program used 1100 L of fuel (250 gal) per week for heat and power (BIO Photo 5300-28)

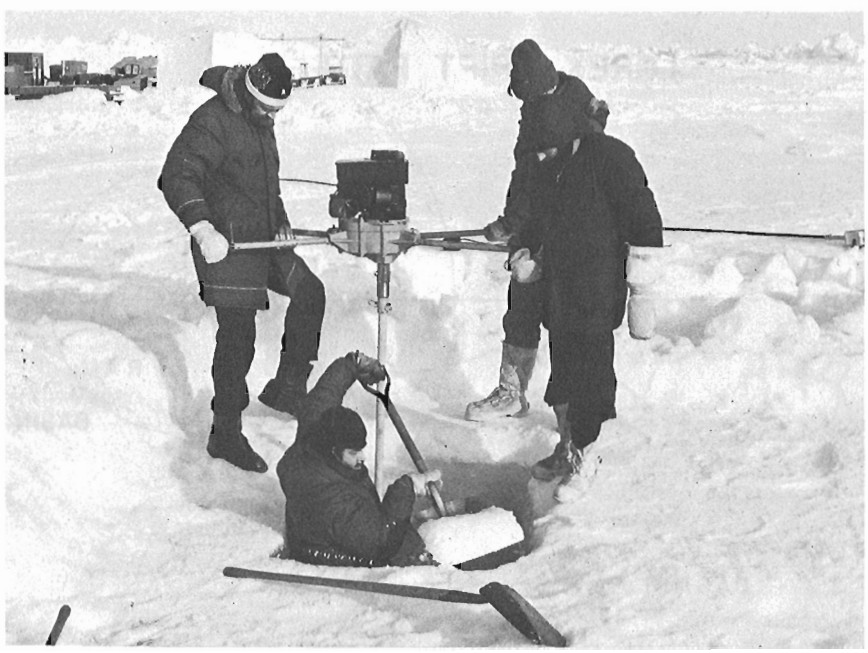

Figure 12.4

Undertaking the arduous task of cutting one of the four hydroholes needed for the operation. Augers (shown here), chain saws and ice chisels were employed. This process had to be repeated when the camp was moved (BIO Photo 5300-297)

normal to its axis from the Makarov basin, but trailing off at an angle to the axis towards the Fram basin (based on remote bathymetric observations from the main camp).

Having taken 9 days to set up and 3 days to break camp, the following data were collected from April 8 through May 26:

- 42 gravity cores (0.2 to 1.7 m long)
- 10 grab samples
- 4 dredge stations
- 14 seabed photography stations
- 1060 hours of continuous 3 kHz bathymetric, subbottom profiling
- 880 hours of continuous, high resolution, shallow seismic, airgun reflection profiling
- 31 expendable sound velocity profiles
- 11 expendable bathythermograph profiles, and
- 14 plankton tows.

Scientific activities were interrupted May 3 to 7 while the acoustic instrumentation and support facilities were transferred to a new location (Fig. 12.2). Unstable ice conditions made the original site unsafe for continued work.

Logistics and Instrumentation

The 'surficial marine geology' program occupied three heated enclosures (Fig. 12.3). A longhouse tent housed generator, compressor, winch hydraulics, workshop and a 1.5 m by 0.5 m hydrohole (Fig. 12.4) to accomodate the subbottom transducer array. An insulated plywood 'prefab' hut contained an array of sampling, photographic, and electronics equipment, and the winch assembly with 6000 m of 5 mm diameter Kevlar cable, sheave frame, and a 1 m diameter hydrohole through which instruments were lowered to the seafloor. A parcoll housed the acoustics instrumentation, a 0.5 m diameter hydrohole for the airgun electronics repair shop, photo lab, drafting table and quarters for two personnel who monitored the acoustics equipment. Bathymetric subbottom profiling instrumentation included an ORE 8 element transducer array and transceiver assembly interfaced with an EPC graphic recorder. The transducer array was mounted in a rigid aluminium frame and suspended in a hydrohole 3 m below ice surface. A central programmer fired the transducer on a one minute interval and triggered the recorder (on a one second sweep rate). This system was tuned to 3 kHz and operated at the 6 kW power rating. Both linear and time varying gain amplification were used.

One 164 cm^3 (10 cubic inch) Bolt airgun and a single active MIT designed hydrophone were the source-receiver equipment used for the high resolution, shallow seismic reflection profiling. Optimum source-receiver separation was determined by monitoring return signals while varying the geometry. This minimized the acoustic interference due to ghosting, camp and ice noise. The airgun was deployed through the hydrohole in the parcoll and tied off 5 m below ice surface. The hydrophone, located 34 m away from the airgun was suspended 6 m below ice surface through a 15 cm hydrohole. Attempts to keep this hole from freezing by filling it with diesel fuel were not very effective, and the hydrophone cable did freeze in. This coupling to the ice unfortunately increased the background noise level. The other hydroholes were kept open with standard lightbulbs suspended close to the base of the hole. A 210 L min^{-1} diesel driven Bauer compressor filled a bank of five, 8.5 m^3 capacity compressed air cylinders to 183 k/cm^2 (2600 psi). An additional 1.5 m^3 tank containing de-icer solution allowed the circulation of vapourized de-icer through the air hoses and airgun to prevent freezing in the intense cold, especially with slow firing rates. With the airgun firing at 113 kg/cm^2 (1600 psi) on a one minute interval, the compressor was needed twice daily for 2.5 hours per run.

Analog signal processing of the reflected pulse included linear pre-amplification followed by passband filtering of 125 Hz to 8 kHz and time varying gain amplification. The processed output was displayed on a second EPC graphic recorder while the 'raw' signal was recorded on a Racal tape transport. The central programmer, previously mentioned, fired the airgun 30 seconds after the subbottom system (to prevent interference) triggered the graphic recorder (on a 2 second sweep rate) and started the tape transport. A variety of source triggering rates was available to accommodate major variations in ice drift speed but the one minute interval was used throughout the survey. In addition, programmable time delay from 0 to 9.9 s was available in 100 ms increments to allow for the elimination of the water column on both acoustic records. The choice and arrangement of acoustics instrumentation for this type of operation was effective and reliable.

To provide for the accurate conversion of travel times to bathymetry, Sippican Corporation's new, 2000 m expendable sound velocimeters (XSV's) were used. These devices employ the 'sing-around' frequency principle and a known fall velocity. The system generates a profile of sound velocity versus depth with a velocity accuracy of ± 0.25 ms^{-1} and a depth accuracy of ± 2 per cent (Balboni and Walsh, 1978). These extended depth probes were released from a handheld launcher and dropped through the sampling hydrohole, taking approximately 6 minutes to fall 2000 m. Returning signals were fed into a processor and this output displayed on a Sippican strip chart recorder. Water column velocities used in this report were determined by analyzing these profiles.

In addition, the Sippican 1830 m expendable bathythermograph (XBT) probes were deployed in the same manner. The results were used to assess the relationship of sound velocity with temperature. Temperature readings had an accuracy of $\pm 0.2°C$ (Sippican Corporation, 1978).

Sediment sampling equipment included a 118 kg, Benthos gravity corer used with 2.4 m lengths of 67 mm (inside diameter) plastic liner sharpened at the end. This configuration, with controlled drop rates (approximately 1 ms^{-1}), provided optimum penetration in cohesive clays. Where less cohesive sediments were anticipated, a cutter and retainer were attached to the liner. In areas of unknown sediment cover, a steel barrel complete with cutter, retainer and liner were used. A 60 kg Shipek grab sampler was effective in retrieving surface sediment samples. A small 35 kg dredge with a 1 m^2 rectangular opening, was also deployed for periods of 4.5 to 6 hours. Plankton were retrieved in vertical tows from 300 m to surface at 30 m min^{-1}, in a 200 mesh net with a triangular 0.5 m^2 opening.

Seabed photography was accomplished by deploying the Bedford Institute's Arctic marine camera system (Fenerty, 1978). The camera and flash units were triggered when a compass-vane assembly, hanging 2.5 m below the camera frame, touched bottom. This contact interrupted signal transmissions from a 12 kHz pinger mounted on the frame. The pinger output was monitored on surface. With the lapse in signal the system operator stopped the winch. Raising and lowering the camera frame one metre or so, on a 10 to 60 second interval (depending on the ice drift rate) allowed for the generation of overlapping photographs of the seafloor. Each frame covered a 3.2 m^2 area of seafloor. Thirty-five millimetre black and white and colour photographs were taken. In a similar manner the National Geographic Society acquired still photographs and colour film footage.

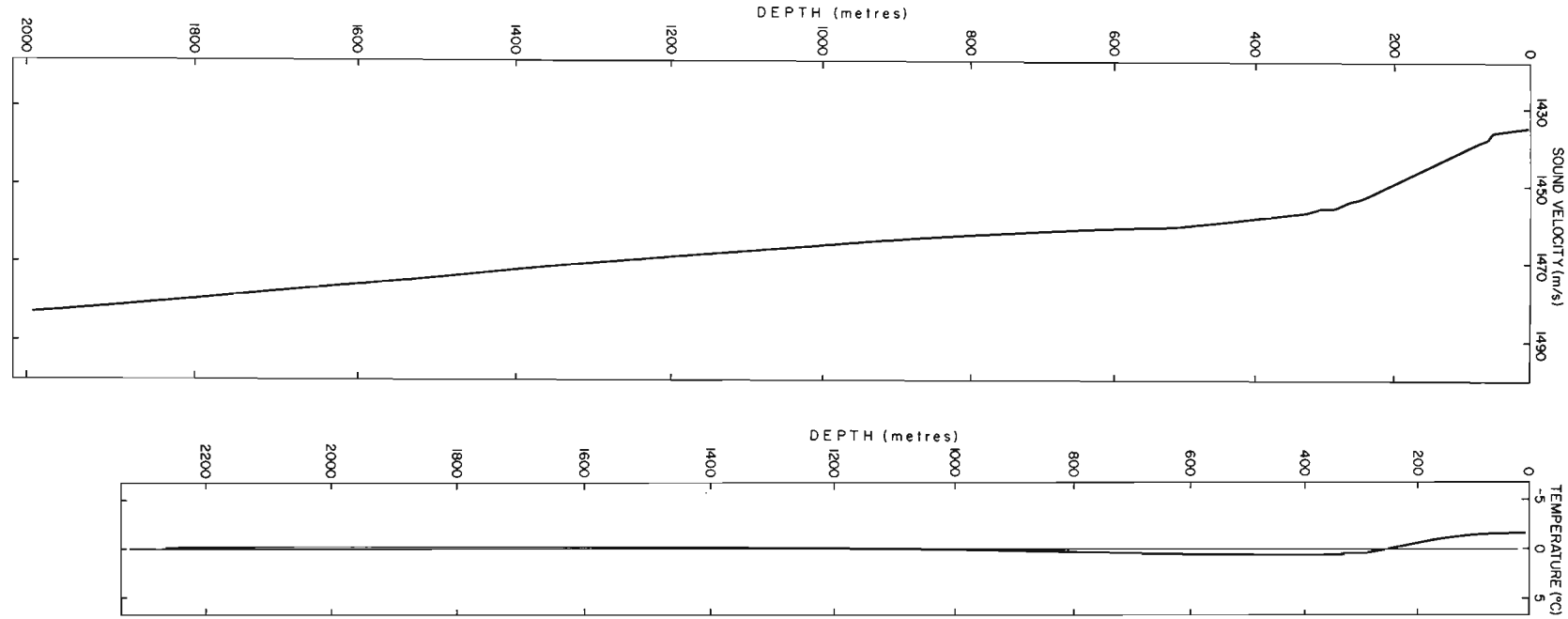

Figure 12.5. *Examples of expendable sound velocity and bathythermograph profiles. Depth scales are not coincident due to differing drop rates of the two probes.*

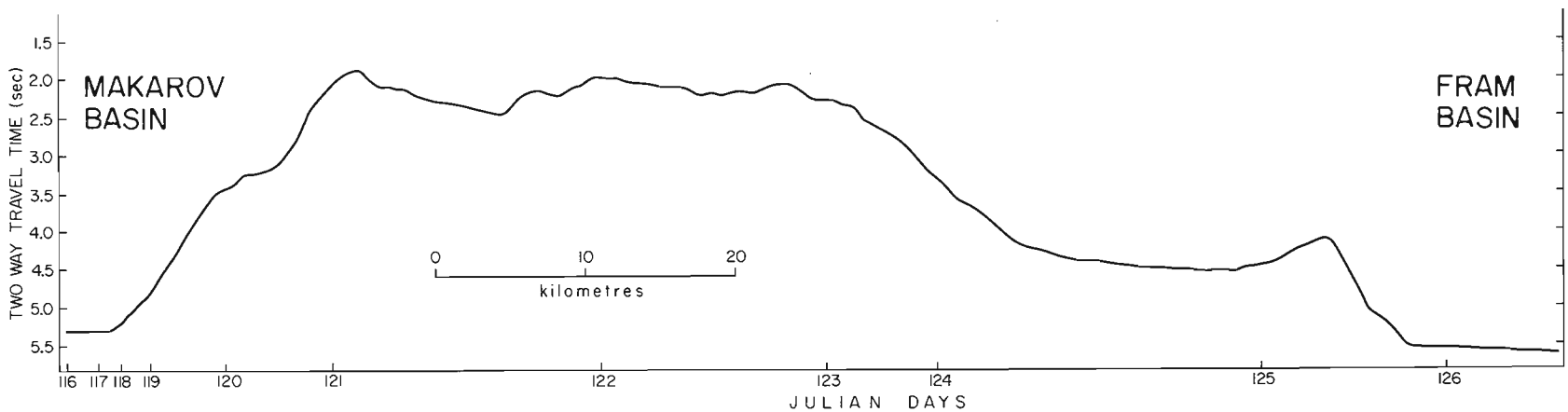

Figure 12.6. *Bathymetric profile of the Lomonosov Ridge along the drift path from the Makarov Basin to the Fram Basin. The profile has been corrected for variations in drift rate only.*

Observations

Bathythermograph and Sound Velocity Profiles

Although not all the XSV/SBT profiles have been analyzed, there appear to be only subtle differences between the Makarov and Fram profiles. Excellent examples of an XBT and XSV profile collected 240 m apart in the Makarov Basin (Fig. 12.1) in 3948 m of water are shown in Figure 12.5. The XBT profile extended to 2270 m before the probe sheared off. The temperature gradient increases evenly from a surface reading of -1.6°C to 0° at a depth of 245 m and to a maximum of 0.6° at 400 to 550 m. The temperature then decreases to 0° again at 1050 m and to a minimum of -0.3° at the base of the profile. The maximum temperature difference along the profile is 2.2°C. Surface temperatures are known to be -1.8°C (A.S. Judge, pers. comm., 1979). The recorded -1.6° is within the ±0.2° error of the XBT's. Also, contact of the XBT wire with the ice at the edge of the hydrohole caused premature termination of some of the profiles.

The XSV probe dropped to 1975 m before shearing off. Probe contact with seawater triggered the recorder but the sound velocity was not printed until 7 m. The reason(s) for this is unknown. Battery activation time and/or initial aeration on the transducer face are possible causes. Three distinct velocity 'zones' can be observed. From 7 to 58 m the velocity appears to increase slightly from 1435 to 1437 ms^{-1}, in response to pressure increase alone. The temperature is constant and probably salinity too in this mixed layer. From 58 m to 280 m the velocity gradient increases rapidly to 1455 ms^{-1}. With a maximum temperature difference of 2.2°C and the temperature and pressure gradients increasing evenly with depth, this increase in velocity is probably due to significant increases in salinity. R. Moore (pers. comm., 1979) confirms this. His **LOREX** salinity studies indicate an increase from approximately 30 to 34 parts per thousand in this zone. From 280 m to 1975 m the sound velocity increases primarily in response to increasing pressure. An integrated average velocity over this and other profiles to 2000 m was 1465 ms^{-1}. Assuming a linear increase in velocity to seabed an integrated average sound velocity from 0 to 4000 m was determined to be 1483 ms^{-1}.

Acoustics

Continuous bathymetric (Fig. 12.6) subbottom and shallow seismic reflection profiles were obtained over the Lomonosov Ridge from Makarov Basin to Fram Basin. The Makarov Basin itself, in close proximity to the ridge is flat with a consistent bathymetry of 5.325 s (3948 m at 1483 ms^{-1}). Local relief of 35 to 75 m on the seafloor reflects the presence of subbottom structures. Some 100 ms (75 m at 1500 ms^{-1} (Demenitskaya and Kiselev, 1968)) of well stratified, conformable, unconsolidated sediments are evident on the subbottom profile. Individual reflectors are 2 to 8 ms (1.5 to 6 m) apart, and some pinch out along the drift track. Variations in record intensity suggest differences in sediment density and/or texture. A minimum of 1.2 seconds (1080 m at 1800 ms^{-1} (Demenitskaya and Kiselev, 1968)) of these undisturbed, stratified sediments infills the Makarov basin adjacent to the ridge (Fig. 12.7). The underlying acoustic unit, bedrock, has an irregular morphology that is responsible for the local relief mentioned earlier. The unconsolidated sediments abut unconformably against these irregularities. The bedrock appears acoustically unstratified. The unit may be massive but more likely the limited output power of the small airgun coupled with the high frequency spectrum recorded prevented much resolution. This lower acoustic unit rises abruptly to form the core of the Lomonosov Ridge, the unconsolidated sediments abutting the flanks (Fig. 12.7).

The 'Makarov' flanks of the ridge rise steeply with 12° slopes to a peak at 1.907 seconds (1392 m at 1460 ms^{-1}) over a drift path of 36 km. Sediment thickness on these flanks is minimal, less than 2 ms on the subbottom profile. The morphology of the ridge crest is somewhat irregular (see Fig. 12.6). Three additional peaks at 2.157, 1.995 and 2.087 seconds were crossed. Unconsolidated sediments lie on the 'Fram'-facing flanks or slopes. These sediments are thin, 20 to 40 ms thick (18 to 36 m at 1800 ms^{-1}), are stratified and appear conformable with the underlying bedrock. The morphology of the 'Fram' flank is more variable, giving the ridge an assymetrical profile along the drift path. Slopes as great as 7° were observed on this flank. A transect normal to the ridge axis would still be assymetrical but less exaggerated.

Like the Makarov Basin, the unconsolidated sediments in the Fram Basin are well stratified, conformable and undisturbed. They also exceed 1.2 s (1080 m) in thickness and abut the ridge structure. However, no local relief due to high amplitude irregularities in the underlying bedrock was intersected, and the seafloor in the Fram Basin was consistently flat with a bathymetry of 5.668 s (4203 m at 1483 ms^{-1}). The maximum relief of the ridge is 2800 m. If the unconsolidated sediments flanking the ridge are ignored this relief is 3500 m. The apparent width of this feature along the drift path is 88 km, its true width at this location being somewhat less.

The acoustic profiles indicate the ridge consists of fault blocks, en echelon. The unconsolidated sediments are primarily associated with the block tops and not the fault faces, suggesting that these sediments were deposited prior to faulting.

Sediments

Sediments from the Makarov Basin include dense brown silts to sandy, clayey silts and firm, thinly layered grey brown clays. Core B-5, 166 cm long, recovered from 3948 m of water (see Fig. 12.1), was examined briefly in the field. Its stratigraphy consisted of 9 cm of soft homogeneous, dark brown silty clay at surface that graded into 87 cm of firm, thinly bedded, dark greyish brown clay. Underlying these units were 57 cm of interlayered dark greyish brown silt and olive brown clay in sharp contact with 13 cm of underlying dark brown, firm homogeneous clay. These distinct sediment types and their stratigraphic relationship are suggestive of interbedded pelagic and turbidite sequences, although grading and other diagnostic physical characteristics were not observed, and detailed sedimentological analyses have yet to be completed.

Sediments from the Fram Basin appear similar in stratigraphy and lithology except for a predominance of firm clays. Layering in these sediments is more obvious and is well defined by marked and abrupt changes in colour from light browns to grey browns. Sediment samples from the ridge itself have a greater proportion of coarse grained material, the sand sized fraction consisting primarily of quartz, with minor feldspar, dark minerals, lithic fragments, worm tubes, foraminifera tests and shell fragments. A 30 cm^3, botryoidal shaped manganese nodule (Fig. 12.8) and a 70 cm^3 subangular, manganese coated, recrystallized, dolomitized piece of chalk were recovered from a single dredge sample in 3190 m of water on the Makarov slopes of the ridge. Neither sample is thought to be 'in situ' and may have been moved into its present position as a result of slumping. The chalk fragment may have been ice rafted, but more probably, and significantly, its origin could be the ridge itself.

The organic-walled microfossils (palynomorphs) from the top 3 cm of core B-25 were briefly examined by J. Bujak of the Atlantic Geoscience Centre. The core was 154 cm

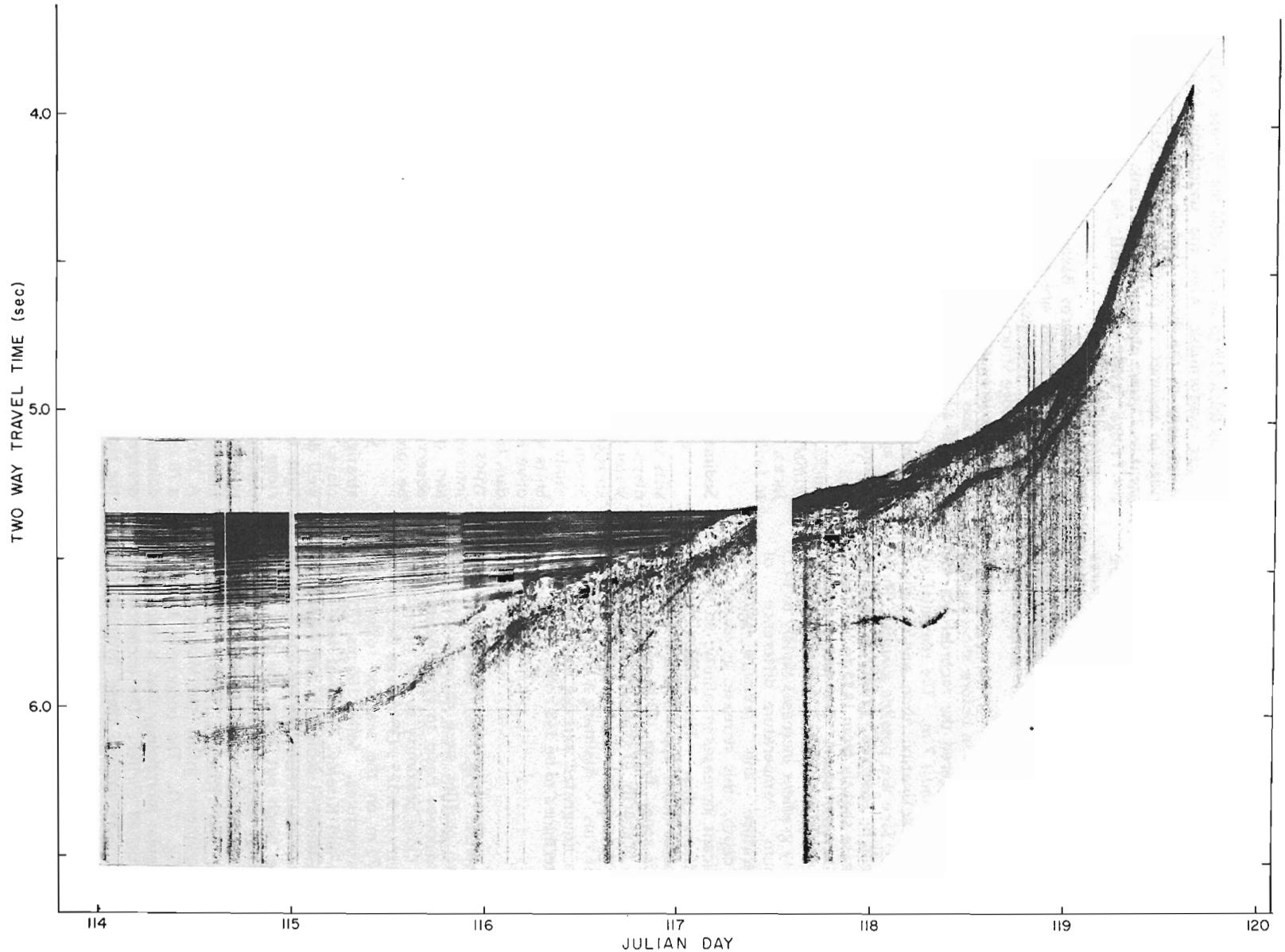

Figure 12.7. *Segment of the high resolution shallow seismic reflection profile adjacent to the Makarov flank of the Lomonosov Ridge. Blank area represents data loss due to equipment failure. The sediments thicken towards the centre of the Makarov Basin. The profile has not been corrected for variations in drift rate.*

long and was taken in 1721 m of water on the Fram flank of the ridge. Preliminary analysis revealed three distinct populations; disaccate pollen of Late Cenozoic age, spores and dinoflagellates (including the high latitude species **Luxadinium propalulum**) of mid-Cretaceous age and poorly preserved spore fragments of **Hystricosporites** or **Ancyrospora** of probable Devonian age. The relative abundance of the Cenozoic, Mesozoic and Paleozoic assemblages is roughly 1 to 7 to 2. The dinoflagellates and spores show significant thermal alteration whereas the Cenozoic pollen is unaltered.

Seabed Photography

Preliminary examination of the 900 black and white and 200 colour photographs of the seafloor provided a wide variety of benthic observations, some similar to those described by Hunkins et al. (1970). In the deepest waters of the Makarov and Fram basins, the soft sediments record several generations and types of winding biogenic tracks and trails some possibly generated by molluscs and bottom feeding fish (Fig. 12.9). In one frame the imprints of fin marks are found on either side of a track. Small mounds, depressions and burrows created by crustacea and other benthic organisms are also common features. In one photograph (Fig. 12.10) three crustacea, approximately 8 cm long, appear to be feeding off organic matter stirred up by previous trigger line impacts. Brittle stars, amphipods, sea anenomes (Coelenterates?), Tunicates, and Crinoids (?) were also observed on the bottom – perhaps indicating a more biologically productive environment than previously suspected. Small shell fragments, including bivalves, litter the seafloor in many places. Several photographs (Fig. 12.10) show ice rafted pebbles and cobbles resting on the soft mud bottom. Lack of accumulated sediments on these rocks indicates recent deposition or the presence of sufficient current action to keep them swept clean. The crest of the ridge appears to be exposed to current action as suggested by ripple marks, scouring and clean, coarse gravel pavements (Fig. 12.11, 12.12). In many cases the ridge floor is covered by gravelly sediments (the coarse fraction far too abundant to be totally ice rafted material). Colour photos reveal many of these pebbles and cobbles to be manganese coated (as were the rock specimens recovered from the dredge). Outcrops (Fig. 12.13) also appear on several ridge crest photographs. First thought to be solution-pitted carbonates or possibly volcanics, the subbottom and seismic records show bedrock to be 100 m below seabed. These outcrops appear to be an older, denser, more consolidated sediment substrate presently undergoing erosion by current action. These outcrops are clear of fine grained material and are more pitted on the upcurrent edge. The down-current periphery of these outcrops is generally less distinct. The observation of embedded cobbles in this substrate suggests that the gravelly sediments overlying it could represent lag deposits derived from the substrate.

Discussion

There is general agreement that the ridge is a linear fragment of the Barents Continental Shelf separated by the inception of spreading along the Nansen-Gakkel rift (Heezen and Ewing, 1961; Harland, 1965; Sweeney et al., 1978 and others). The initial timing of this event is not well defined but is thought to have occurred between 60 and 40 Ma (Osterso and Wold, 1973; Hall, 1973). However, Johnson and Vogt (1973) suggest the Nansen-Gakkel rift may have been active before this. The actual age of the ridge core itself is somewhat controversial and could be Early to Middle Paleozoic (Trettin, 1969; Meyerhoff, 1973 and Harland, 1973). This study has uncovered some evidence bearing on these events.

The reworked nature of the surficial sediments of core B-25 supports the idea that the sediments observed in the seabed photographs taken 1 km from the core site on the ridge crest are lag deposits. But it also appears these lag deposits have been derived from the associated older semiconsolidated substrate also noted in the photographs. The reworked Cretaceous palynomorphs could indicate the presence of mid-Cretaceous outcrops. Unconsolidated sediments of this age have been reported by Clark (1974) to occur elsewhere in the Arctic, in particular on the Alpha Cordillera. In addition, the acoustic evidence suggests that the stratified, unconsolidated sediments overlying the ridge were deposited prior to faulting (and hence ridge separation?). This stratigraphy implies that the sediments certainly are not recent, and in fact, a mid-Cretaceous age is quite acceptable in terms of the known history of the area. The separation of the Lomonosov Ridge could therefore be possibly not much older than mid-Cretaceous. It could however be younger and probably is, for two reasons; an unknown thickness of post mid-Cretaceous sediment may have been eroded after ridge separation, or the Cretaceous palynomorphs in the substrate may have been reworked more than once and hence have been incorporated into sediments of younger, possibly Cenozoic age. More detailed analysis of the **LOREX** sediment cores may or may not resolve these alternatives.

The Devonian spores may have been derived from the substrate or from other rocks. They may also have been reworked several times, but must have been originally derived from rocks of Devonian age. Whether this source was the ridge itself and whether the ridge is at least Devonian in age is difficult to say with such tenuous evidence. One could also speculate that the high degree of thermal alteration observed in these spores could have been the product of orogenesis known to have occurred during this time.

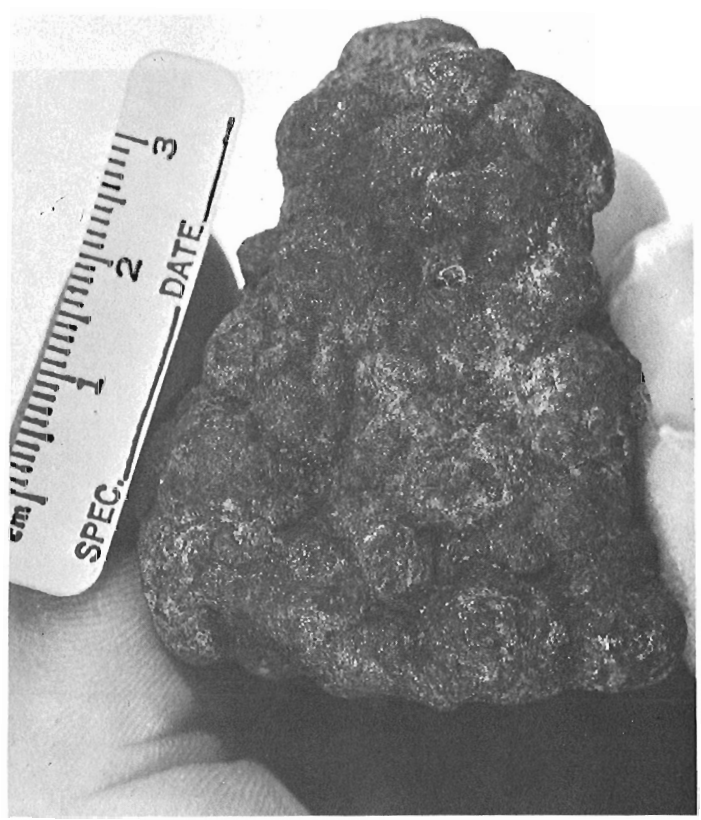

Figure 12.8. *Manganese nodule recovered from 3160 m of water on the Makarov flank of the ridge. Other dredged rock samples were manganese coated as well. (BIO Photo 5413-100)*

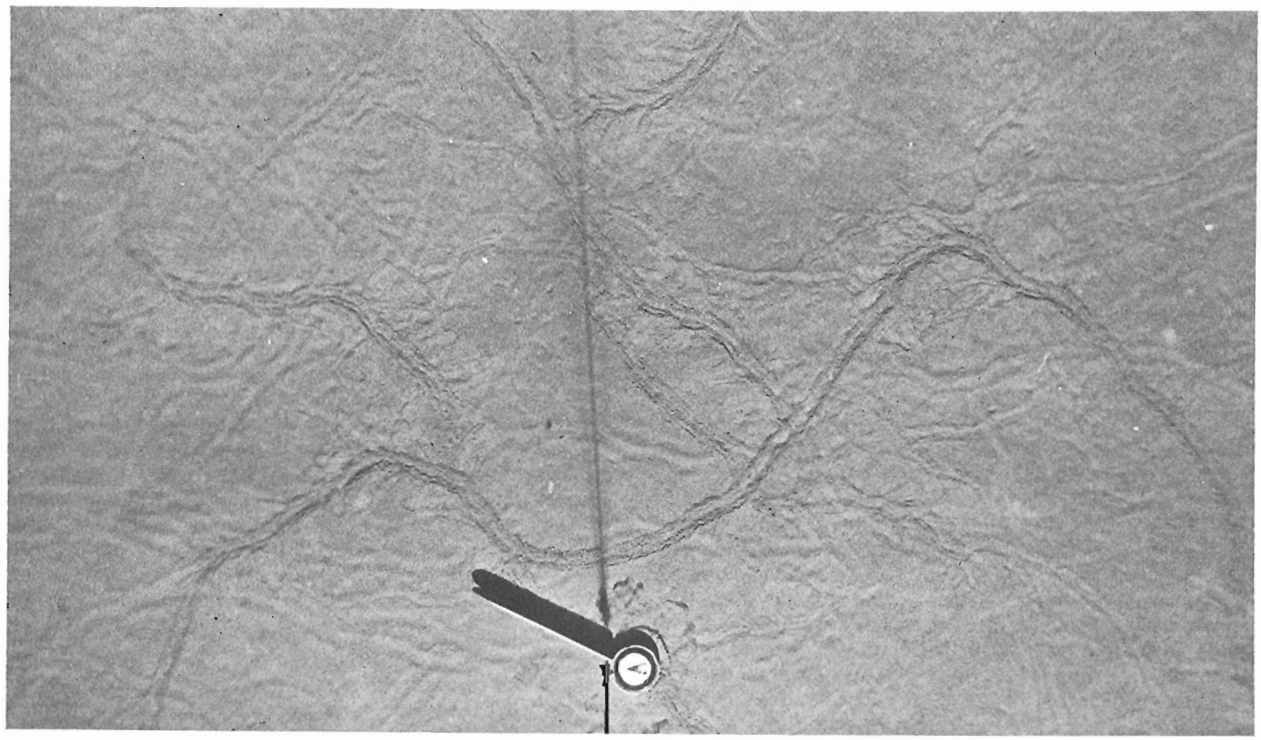

Figure 12.9. *Photo Station 5; 3948 m of water: The soft sediments record several generations of tracks and trails created by benthic fauna. Area covered by this and other photographs is approximately 2.7 m^2. The compass and vane assembly are 33 cm long. (N.E. Fenerty, BIO 5300-STN5)*

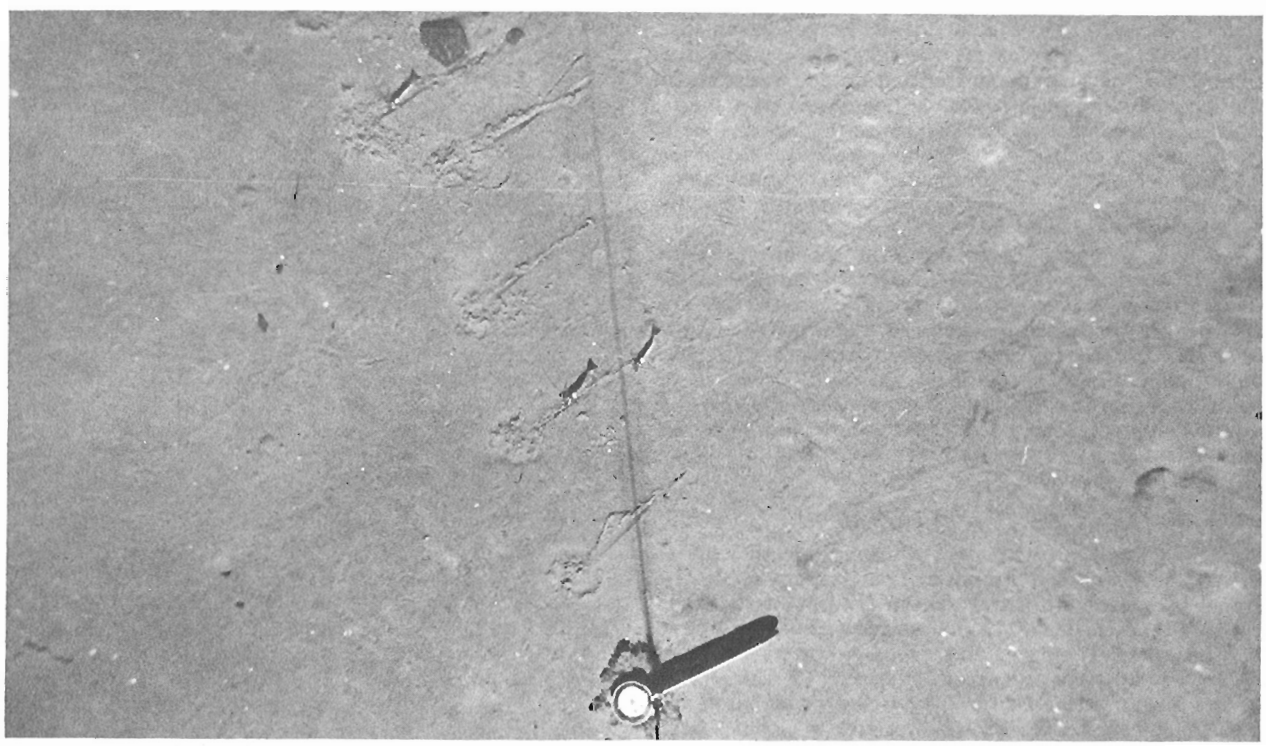

Figure 12.10. *Photo Station 8; 3896 m of water: Three crustacea apparently feeding on organic matter stirred up by previous compass impacts. Note the presence of ice rafted material and shell fragments on the bottom (white spots). (N.E. Fenerty, BIO 5300-STN8)*

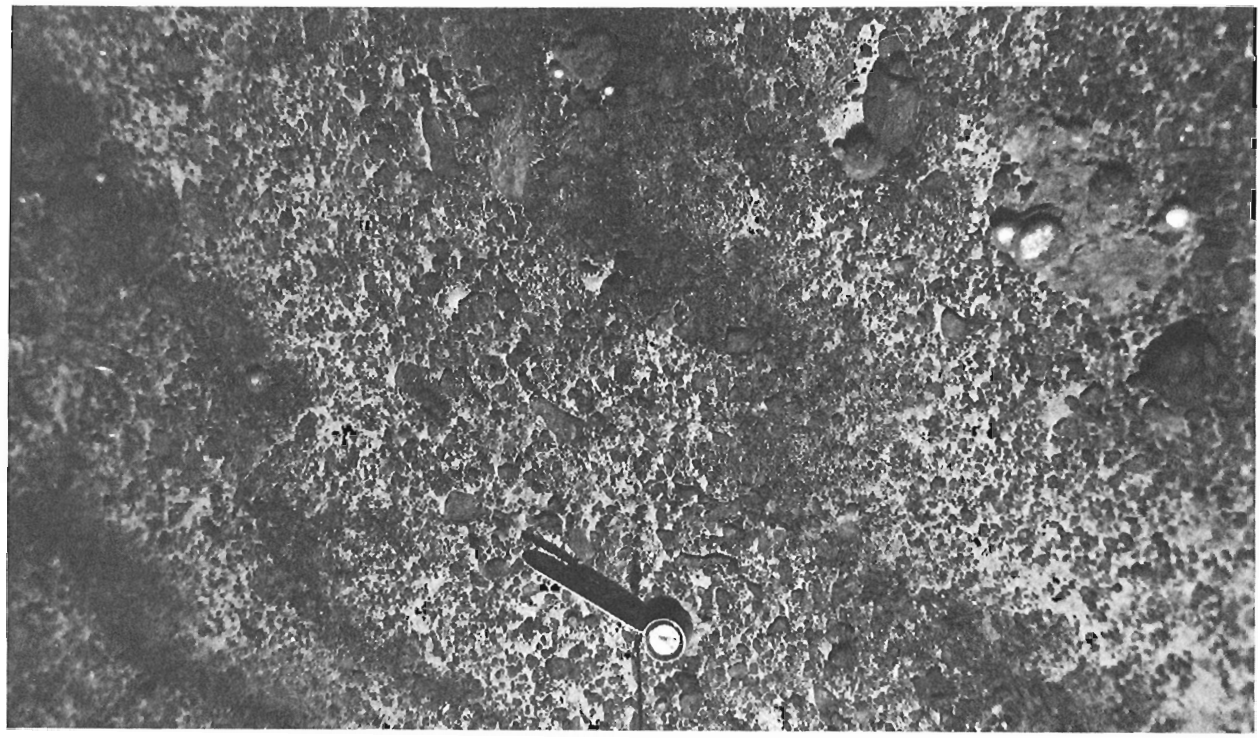

Figure 12.11. *Photo Station 11; 1830 m of water: Current scour and associated coarse gravel pavement. An outcrop of older semiconsolidated sediments is visable in the bottom left. The compass vane is aligned in the direction of current flow towards the bottom right. (N.E. Fenerty, BIO 5300-STN11)*

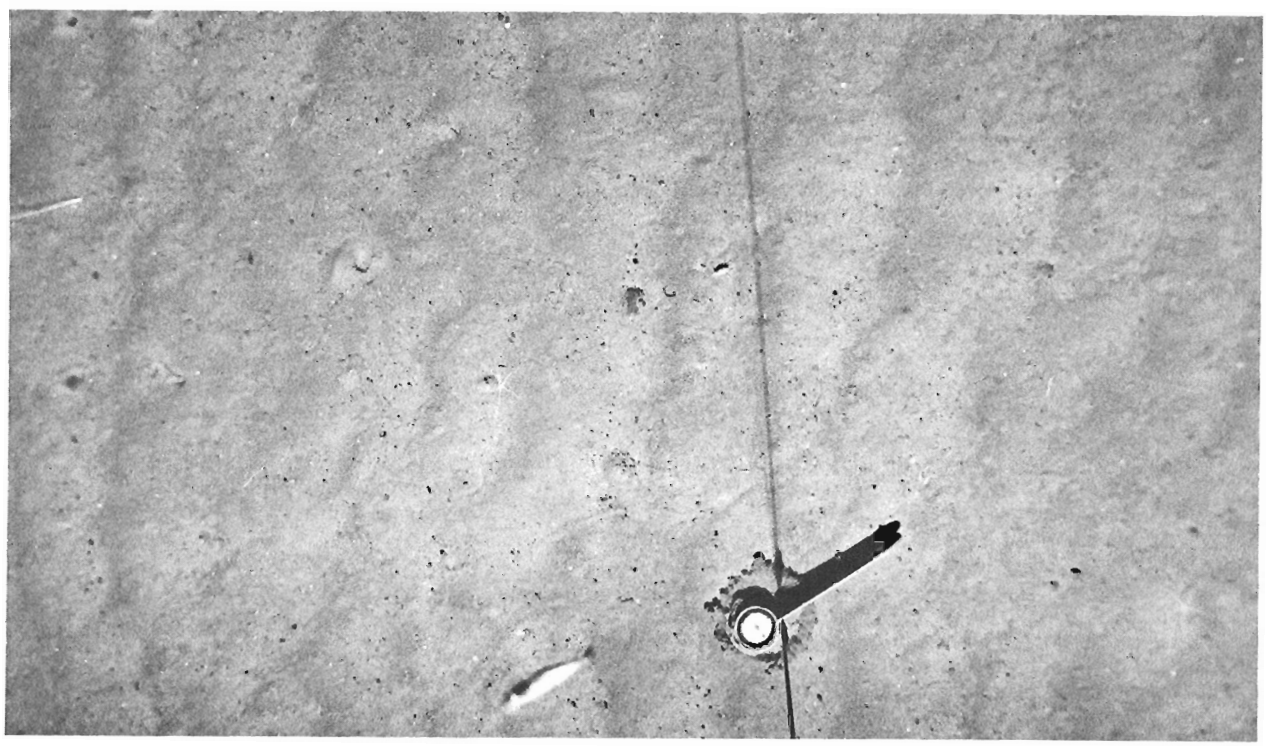

Figure 12.12. *Photo Station 12; 1697 m of water: Ripple marked seafloor with gravelly sediments infilling the troughs. Note the poorly focused crustacean swimming above the bottom; brittle star and burrow close by. (BIO 5300-STN12)*

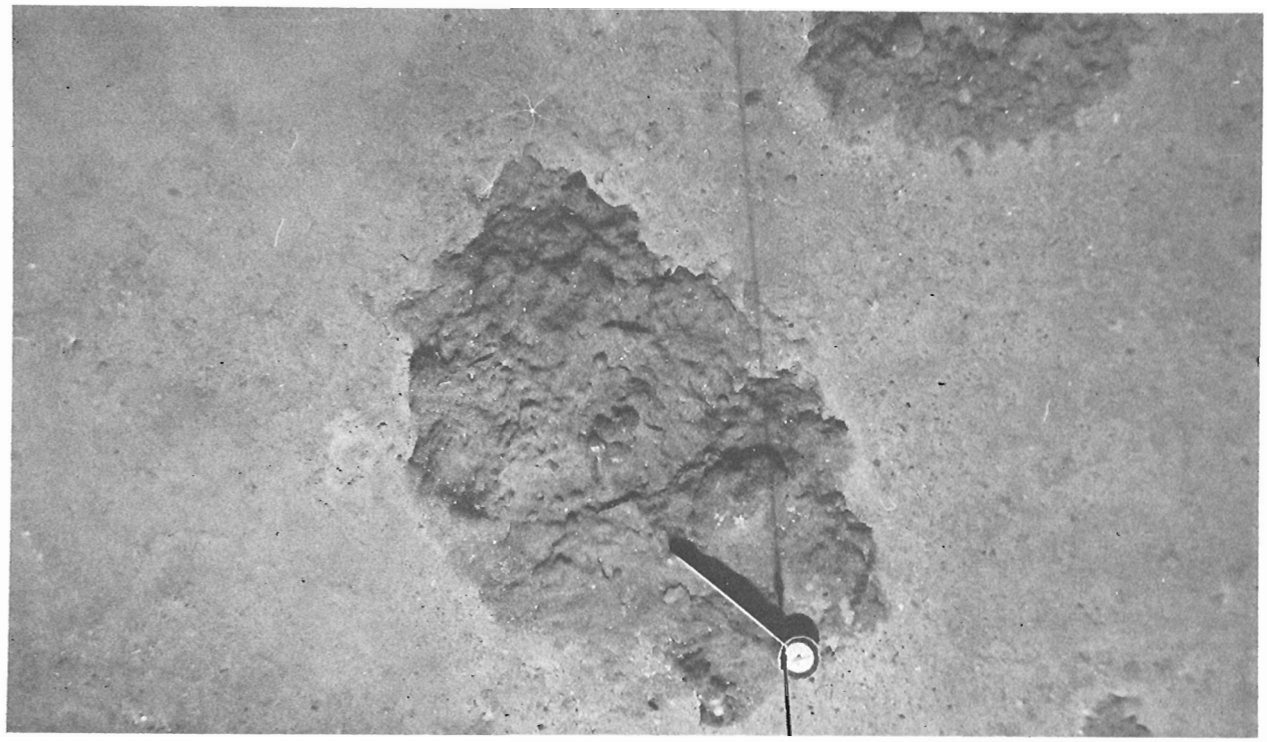

Figure 12.13. *Photo Station 12; 1679 m of water: Three outcrops of older semiconsolidated sediments and the overlying lag deposits possibly derived from this substrate. Three brittle stars and three sea anenomes can also be seen associated with the outcrops. (BIO 5300-STN12)*

The significance of the thermal alteration of the Cretaceous palynomorphs is also speculative. Only slightly anomalous heat flow values have been reported from the ridge (Churkin, 1973). It might be argued that if these sediments were in situ prior to faulting and probable ridge separation, this alteration could have resulted from the proximity of these sediments to the incipient Nansen-Gakkel rift during the early stages of spreading. (This process could also have affected the spore fragments as they have suffered a greater degree of thermal alteration.) Continued analyses of the LOREX data are necessary to reinforce or refute these interpretations.

Acknowledgments

Scientific programs for the **LOREX** expedition were coordinated by J.R. Weber of the Earth Physics Branch of EMR, and logistics support was provided through G.D. Hobson and the Polar Continental Shelf Project of EMR. The writers would like to thank J.R. Weber and G.D. Hobson for their efforts in making this phase of the **LOREX** program a success. N. Fenerty's Arctic seabed camera system was a definite asset to the program, and his participation is gratefully acknowledged. The assistance of F. Alt, F. Hunt, F. Jodrey and R. Jubb was greatly appreciated. F. Benoit's cuisine did much to sustain our enthusiasm during the expedition. G. Vilks kindly reviewed this manuscript, and C.S. Mulkins assisted in its preparation.

References

Balboni, M.J. and Walsh, W.E.
1978: The expendable sound velocimeter (XSV); Sea Technology, November, p. 38-42.

Churkin, M. Jr.
1973: Geologic concepts of Arctic Ocean Basin; in Arctic Geology, ed. M.G. Pitcher; American Association of Petroleum Geologists, Memoir 19, p. 490.

Clark, D.L.
1974: Late Mesozoic and Early Cenozoic sediment cores from the Arctic Ocean; Geology, v. 2, p. 42-44.

Demenitskaya, R.M. and Kiselev, Yu.G.
1968: The characteristic features of the structure, morphology and sedimentary cover of the central part of the Lomonosov Ridge based on seismic data; in Geophysical Methods of Exploration Applied in the Arctic; Arctic Geology Research Institute, Ministry of Geology, USSR, Leningrad, v. 5, p. 33-46.

Fenerty, N.
1978: Innovative photography pays off at World's largest Oceanographic complex; Canadian Photography, v. 9, no. 5, p. 25-33.

Hall, J.K.
1973: Geophysical evidence for ancient sea-floor spreading from Alpha cordillera and Mendelehev Ridge; in Arctic Geology, ed. M.G. Pitcher; American Association of Petroleum Geologists Memoir 19, p. 558-559.

Harland, W.B.
1973: Tectonic evolution of the Barents Shelf and related plates; in Arctic Geology, ed. M.G. Pitcher; American Association of Petroleum Geologists Memoir 19, p. 599-608.

Harland, W.B.
1965: Tectonic evolution of the Arctic-North Atlantic region; Royal Society of London, Philosophical Transactions Series A, v. 258, p. 59-75.

Heezen, B.C. and Ewing, M.
1961: The Mid-oceanic ridge and its extension through the Arctic Basin; in Geology of the Arctic, ed. G.O. Raasch; University of Toronto Press, v. 1, p. 662.

Hunkins, K., Mathieu, G., Teether, S., and Gill, A.
1970: The floor of the Arctic Ocean in Photographs; Arctic, v. 23, p. 175-189.

Johnson, G.L. and Vogt, P.R.
1973: Marine geology of Atlantic Ocean North of the Arctic circle; in Arctic Geology, ed. M.G. Pitcher; American Association of Petroleum Geology, Memoir 19, p. 169.

Meyerhoff, A.A.
1973: Origin of Arctic and North Atlantic Oceans; in Arctic Geology, ed. M.G. Pitcher; American Association of Petroleum Geology, Memoir 19, p. 569.

Ostenso, N.A., and Wold, R.J.
1973: Areomagnetic evidence for origin of Arctic Ocean Basin; in Arctic Geology, ed. M.G. Pitcher; American Association of Petroleum Geology, Memoir 19, p. 506-516.

Sippican Corporation
1978: Specification booklet on XSV/XBT products, Sippican Oceanographic Division, Marion, Mass.

Sweeney, J.F., Irving, E., and Geuer, J.W.
1978: Evolution of the Arctic Basin; in Arctic Geophysical Review, ed. J.F. Sweeney, Publication Earth Physics Branch, v. 45, no. 4, p. 91-100.

Trettin, H.P.
1969: A Paleozoic – Tertiary fold belt in northern most Ellesmere Island, aligned with the Lomonosov Ridge; Geological Society of America Bulletin, v. 80, p. 143-148.

13.

GEOLOGY AND ORGANIC GEOCHEMISTRY OF THE DOME HUNT NEKTORALIK K-59 WELL, BEAUFORT SEA

Projects 790031 and 760063

James Dixon and Lloyd R. Snowdon
Institute of Sedimentary and Petroleum Geology, Calgary

Dixon, James and Snowdon, Lloyd R., Geology and organic geochemistry of the Dome Hunt Nektoralik K-59 well, Beaufort Sea; in Current Research, Part C, Geological Survey of Canada, Paper 79-1C, p. 85-90, 1979.

Abstract

The Hunt Dome Nektoralik K-59 well tested oil, gas and condensate from Paleogene rocks below 2258.6 m (7410 ft). Quaternary and Neogene strata are present to 2258.6 m (7410 ft) and consist of outer shelf to continental slope sand and mud deposits. Below this depth the Paleogene section is mud dominant with local sand units of probable turbidite origin.

Organic geochemical results indicate that the section is terminally immature and partially stained by migrated hydrocarbon. Analysis of the Nektoralik oil suggests that it was derived from stratigraphic equivalents to the source for the oil and gas condensate at Taglu and Niglintgak.

Introduction

The Dome Hunt Nektoralik K-59 was the first of the deep-water offshore wells to test hydrocarbons in the Beaufort Sea. Oil, gas and condensate were recovered on three drill stem tests form zones below 2258.6 m (7410 ft). Drilling began in the summer of 1976 from a drillship anchored in 64 m of water, and was completed the following year to a depth of 2790 m (9154 ft). The well was located at the shelf edge and was drilled into a shale-cored diapir (Oilweek).

Geology[1]

This report outlines the general lithological succession and offers some tentative sedimentological interpretations of a well drilled at the shelf edge into a shale-cored diapir (Oil week, 1979). It is not known, however, whether the lithological divisions are widespread or not. Cuttings sample quality was highly variable due to the unconsolidated nature of the section and consequent caving problems. Large hole diameters were also a problem, especially the effects upon the gamma ray log; opposite sand zones the gamma ray trace tended to be subdued. From sample examination and geophysical log character the following lithological succession was identified:

Depth: m (ft)	Description
0-11.6 (0-38)	KB to sea level
11.6-76.0 (38-249)	Sea level to seabed
76.0-157.3 (249-516)	No samples. 66.2 cm (30 in) casing
157.3-862.6 (516-2830)	Interbedded sand and mud: Approximately 54 per cent of interval consists of sand units. Sand: in units 18-44 m (60-145 ft) thick. Units have thin mud interbeds. Very fine to fine grained, with some granular, medium grained sands. Quartz dominant, grains subangular to rounded and moderately well sorted; sorting is poorer in coarser grained sands. Carbonized wood fragments are very common and clay minerals may be present. Unconsolidated. Gamma log character of the sand units may show a ragged to blocky outline (e.g. 664.5-739.2 m; 2180-2425 ft) or a funnel-shaped outline (e.g. 579.1-609.6 m; 1900-2000 ft). Mud: unit thicknesses similar to sands. Weakly consolidated, silty to sandy, slightly calcareous, brownish grey colour. Woody fragments are common. Slight increase in consolidation with depth.
862.6-1600.2 (2830-5250)	Mud: light to medium grey (note the slight difference in colour from overlying mud), silty to sandy, locally calcareous. Rare claystone concretions. Weakly consolidated. Rare sand beds. Fine to medium grained sand with some coarse to granular grains, argillaceous and unconsolidated.
1600.2-1936.1 (5250-6352)	Interbedded mud and sand (mud predominant). Mud: very similar to overlying mud. More consolidated. Sand: present in the cuttings sample, but poorly defined in the geophysical logs. Fine to medium grained, moderately well sorted, weakly cemented, possibly argillaceous. Well-rounded quartz grains. Carbonized wood fragments are common.
1936.1-225.0 (6352-7300)	Mud: as above. Mud is well compacted but not cemented. Rare sand interbeds.
2225.0-58.6 7300-7410	Interbedded sand and mud: similar to overlying strata; sands tend to be very fine to fine grained.
2258.6-64.7 (7410-7430)	Microcrystalline limestone: grading downwards into a calcareous mud. Limestone is brownish white to light grey. Calcareous mud is light to medium grey.
2264.6-2790.1 (7430-9154 TD)	Mud: with local sand units. Mud: light to medium grey. More consolidated than overlying 2258.6 m (7410 ft), almost mudstone-like. Pyrite and carbonized wood fragments are very common. Sand: fine grained, moderately well sorted, argillaceous, weakly cemented. Thin units (6.1 m; <20 ft). A zone of limestone beds (or concretion horizons) occurs between 2627.4-2641.1 m (8620-65 ft).

[1] by J. Dixon

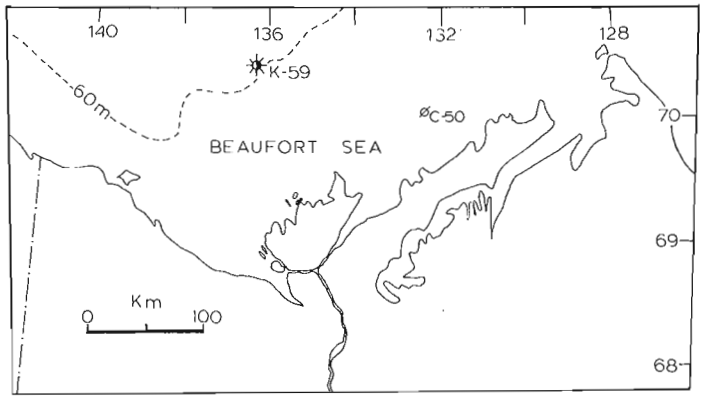

Figure 13.1. *Location of the Hunt Dome Nektoralik K-59 and Dome Gulf et al Ukalerk C-50 wells.*

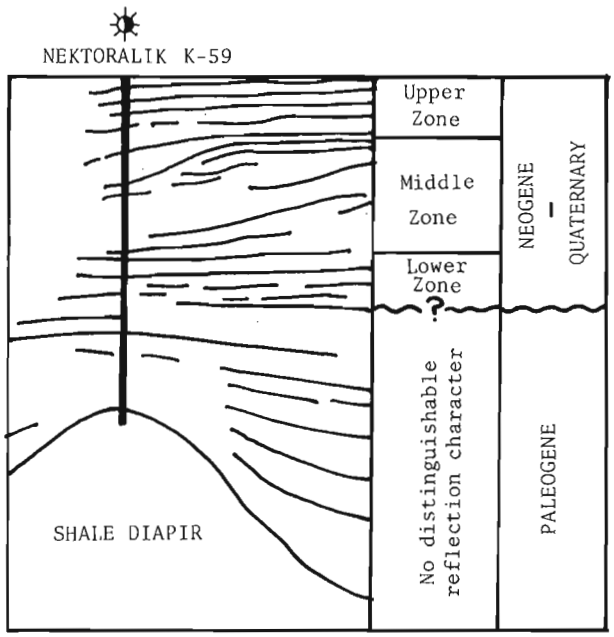

Figure 13.2. *Tracing of prominent reflections from a seismic profile across the K-59 location (seismic profile published in Oilweek, 1979. Note: no reflection times were published with the seismic profile).*

Jones et al. (1979) stated that the section above 2255.5 m (7400 ft) is Neogene and below that depth Oligocene and Eocene strata are present. The limestone at 2258.6 m (7410 ft) forms a prominent marker and a similar horizon occurs in the Ukalerk C-50 well, 140 km to the east-southeast between depths 1572.8-1581.9 m (5160-90 ft), suggesting that this horizon may be immediately below the prominent mid-Tertiary unconformity (see the seismic profile in Hawkings and Hatlelid, in Yorath et al., 1975, Fig. 12). X-ray diffraction analysis of the limestone revealed that aragonite is the sole carbonate mineral. The presence of a pure carbonate in a clay-rich depositional regime suggests a period of extremely slow terrigenous sedimentation.

A seismic profile across the Nektoralik location has been published in Oilweek (1979) and a tracing of prominent reflectors is shown in Figure 13.2. The location of the mid-Tertiary unconformity in Figure 13.2 is approximate, based on a comparison with Hawkings and Hatlelid's Figure 12 (in Yorath et al., 1975) and the change in reflection character at the chosen horizon. A threefold division of the Neogene-Quaternary section is possible, based on seismic reflection

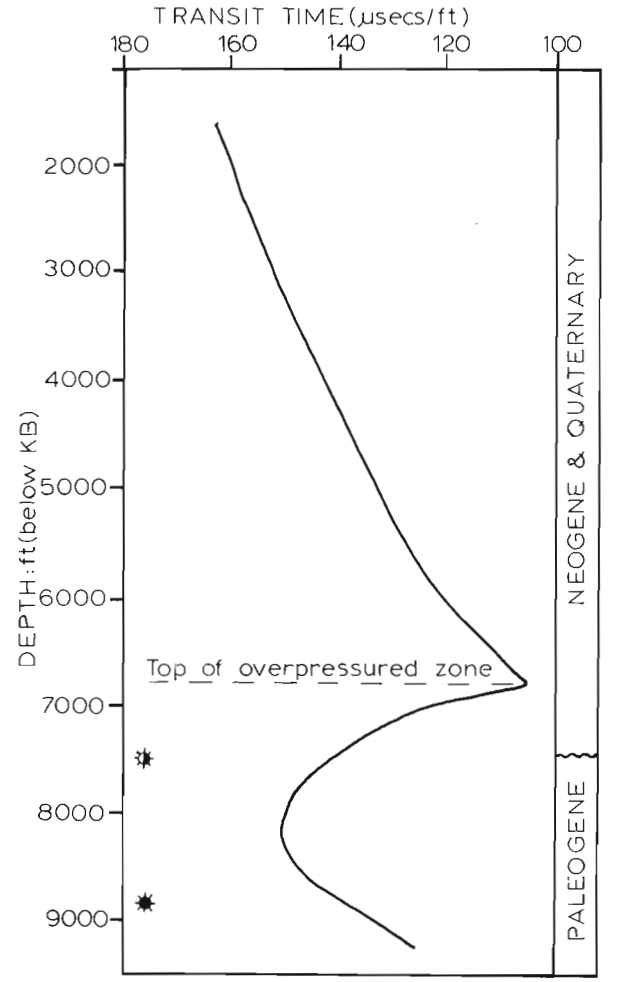

Figure 13.3. *Depth versus Sonic interval transit time (mud units).*

character (Fig. 13.2). The upper zone consists of parallel to slightly divergent reflections, the middle zone has sigmoid and chaotic reflections and the lower zone consists of parallel reflections (terminology of Mitchum et al., in Payton, 1977). The upper and middle zones are part of a prograding outer shelf and continental slope, and the lower zone appears to be the bottomset of continental slope sigmoid reflections. However, in Hawkings and Hatlelid's Figure 12 (Yorath et al. 1975) an additional stratigraphic unit has been identified between the Plio-Pleistocene shelf to continental slope unit and the Paleogene section. The lower zone at the Nektoralik location may be equivalent to Hawkings and Hatlelid's (Yorath et al., 1975) additional unit.

At Nektoralik the upper 862.6 m (2830 ft) has a high percentage of sand, indicating periods of fairly high energy levels during deposition on the outer shelf location. The shapes of the gamma ray log trace are not definitive environmental indicators but one could speculate that knowing the general outer shelf location, the funnel-shaped log trace could be a submarine sand dune and the ragged-outline log trace could be stacked turbidites. Also, being in the upper part of the section, a Pleistocene age seems likely for some, if not all of this sand-rich section. The generally lower sea levels and greater sediment input from glacial meltwaters during the Pleistocene may also have contributed to the sand-rich character of the upper section. The remainder of the Neogene section is mud-dominant and was probably deposited by low velocity, turbid layer density currents down the continental slope. According to

Table 13.1
Extract and Kerogen data for Nektoralik K-59 borehole samples

Depth ft	Depth m	% Corg	Extract Yield*	Hydrocarbon Yield*	% Hydrocarbon	Atomic H/C	Atomic C/N
6200	1889.8	1.19	49.2	5.9	12.1	0.90	36.9
6500	1981.2	1.21	55.0	5.7	10.3	1.01	20.7
6800	2072.6	1.33	55.7	5.5	9.8	0.99	28.9
7100	2164.1	2.07	183.6	136.4	74.3	1.06	47.9
7400	2255.5	1.94	99.9	77.3	77.4	1.08	42.8
7700	2347.0	1.61	74.5	37.7	50.6	0.75	50.4

*mg per gram organic carbon

Sangree et al. (in Bouma et al., 1978) outer shelf and continental slope deposition is characterized by low velocity, turbid layer currents, high velocity turbidity currents, settling from suspension, and downslope mass movement. Downslope mass movement is also possible, resulting in a chaotic reflection characters of parts of the middle zone. Examples of recent slumping on the continental slope can be seen in Figure 12 of Hawkings and Hatlelid (in Young et al., 1976).

The Paleogene section is also mud-dominant and as the Nektoralik location is distal from the main Paleogene deltaic depocentres (Yorath et al., 1975) it seems most probable that the sediments were deposited in outer shelf to abyssal environments. Sand-rich horizons are most likely to be turbidites. The limestone beds between 2627.4-41.1 m (8620-65 ft) may have a similar origin to the limestone at 2258.6 m (7410 ft) and possibly may mark an intra-Paleogene hiatus.

The Nektoralik K-59 well was abandoned before attaining the projected total depth because of excessive overpressure. A plot of depth versus sonic transit time (Fig. 13.3) clearly shows the velocity inversion at the top of the overpressured zone (about 2072.6 m:6800 ft). Also shown in the lack of correlation between overpressuring and stratigraphy.

Organic Geochemistry[1]

Drill cuttings, gas analyses, and total organic carbon determinations have been completed for the Nektoralik K-59 borehole (Fig. 13.4). The total gas yield is low (<20 mL gas per litre of cuttings) but this probably reflects the unconsolidated nature of the samples. Most of the gas would be released into the drilling mud as the cuttings circulated to the top of the hole. The cause of the single, anomalous gas concentration at about 944.9 m (3100 ft) is unknown. The per cent wet gas (ethane, propane, butanes) which is plotted in column 2 of Figure 13.4 begins to increase at about 1585.0 m (5200 ft) and reaches a maximum of about 40 per cent near 2590.8 m (8500 ft) indicating that below about 2133.6 m (7000 ft) the section becomes marginally mature in a thermal metamorphic sense. No wet gas concentration break and hence no thermal maturity discontinuity was noted to correspond with the Neogene/Paleogene(?) unconformity discussed above (Fig. 13.2). It can therefore be concluded that the sub-unconformity sediments have never been buried more deeply than at present.

The total organic carbon log (Fig. 13.4, column 3) indicates a relatively constant concentration of about 1 to 1.5 per cent organic carbon throughout the section. Below about 2377.4 m (7800 ft) the high organic carbon values reported are at least partially due to organic additives in the drilling mud. The lack of character in the organic carbon is

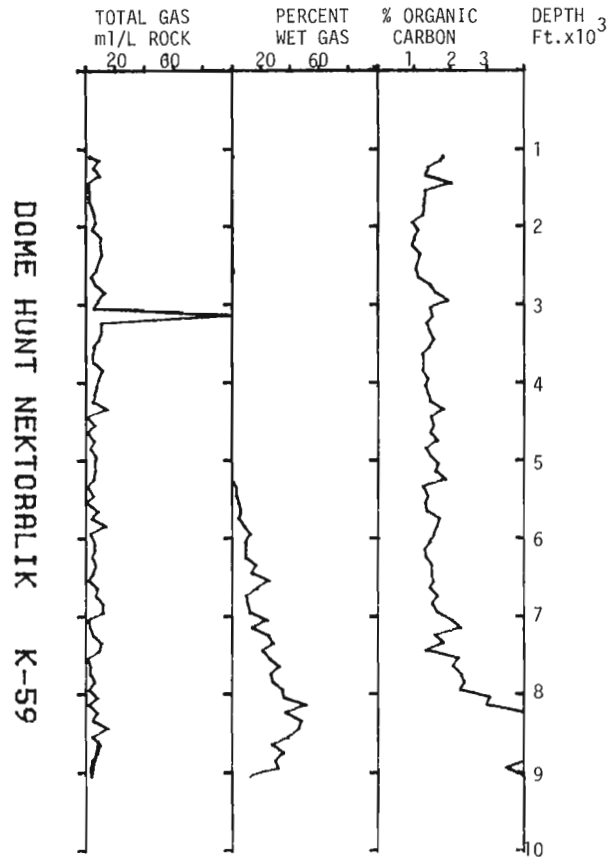

Figure 13.4. Total gas content, per cent wet gas (ethane, propane, butanes), and total organic carbon content versus depth for the Nektoralik K-59 borehole.

possibly due to extensive caving and mixing of the cuttings samples because of less than ideal hole conditions, but could also reflect the more or less homogeneous nature of the organic matter in sediments of the upper part of the section.

Six samples (Table 13.1) have been solvent extracted, chromatographically fractionated, and the saturate fraction analyzed on a gas chromatograph (g.c.) using techniques outlined by Foscolos et al. (1976) and Snowdon (in press). Samples below 2347.0 m (7700 ft) were not extracted because of organic contamination. The three shallowest samples (Table 13.1) have low total extract yields and a very low percentage of hydrocarbons within the extract. The saturate fraction gas chromatograms are all essentially similar and show a large triterpane/sterane hump and a large predominance of odd/even carbon chain length n-alkanes in the C_{21} to C_{31}

[1] by J. Dixon

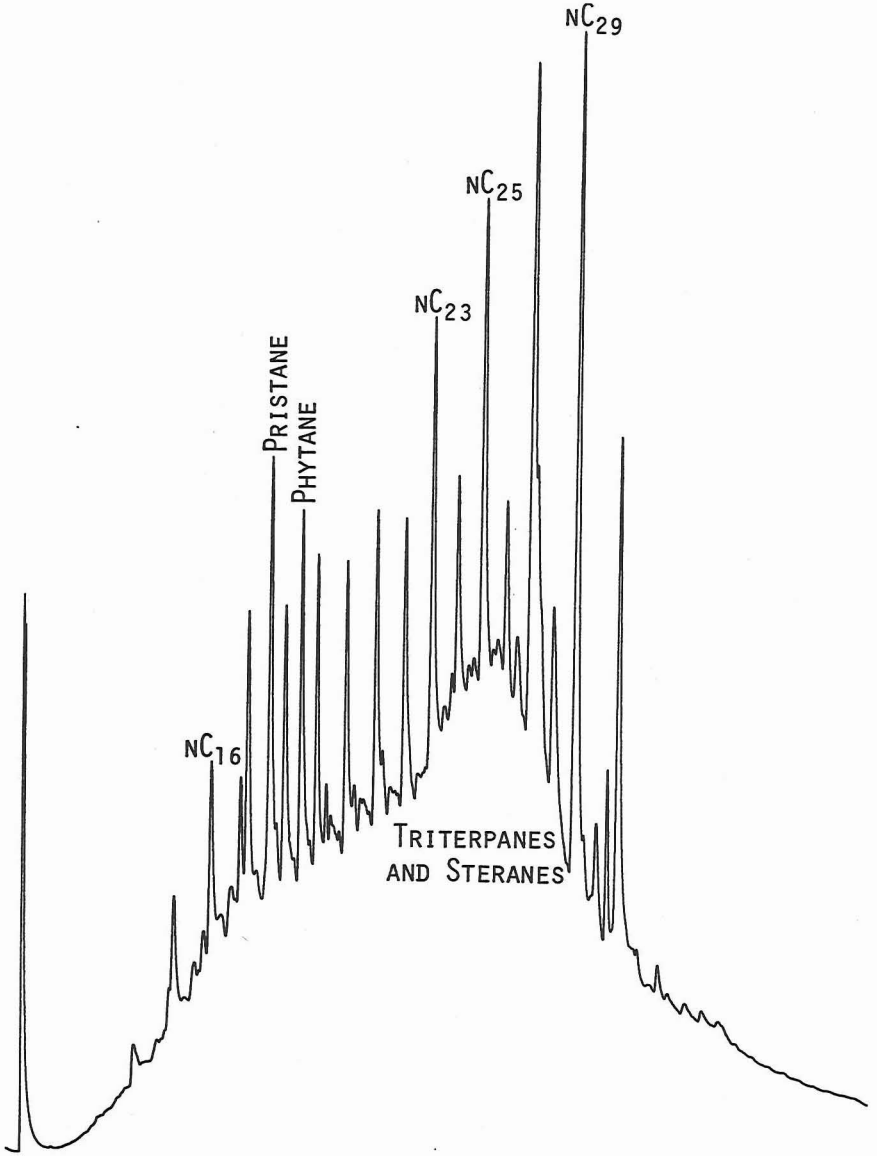

Figure 13.5. *Saturate fraction gas chromatogram of Nektoralik K-59 extract from 2072.6 m (6800 ft) showing large triterpane/sterane hump and strong odd/even n-alkane preference.*

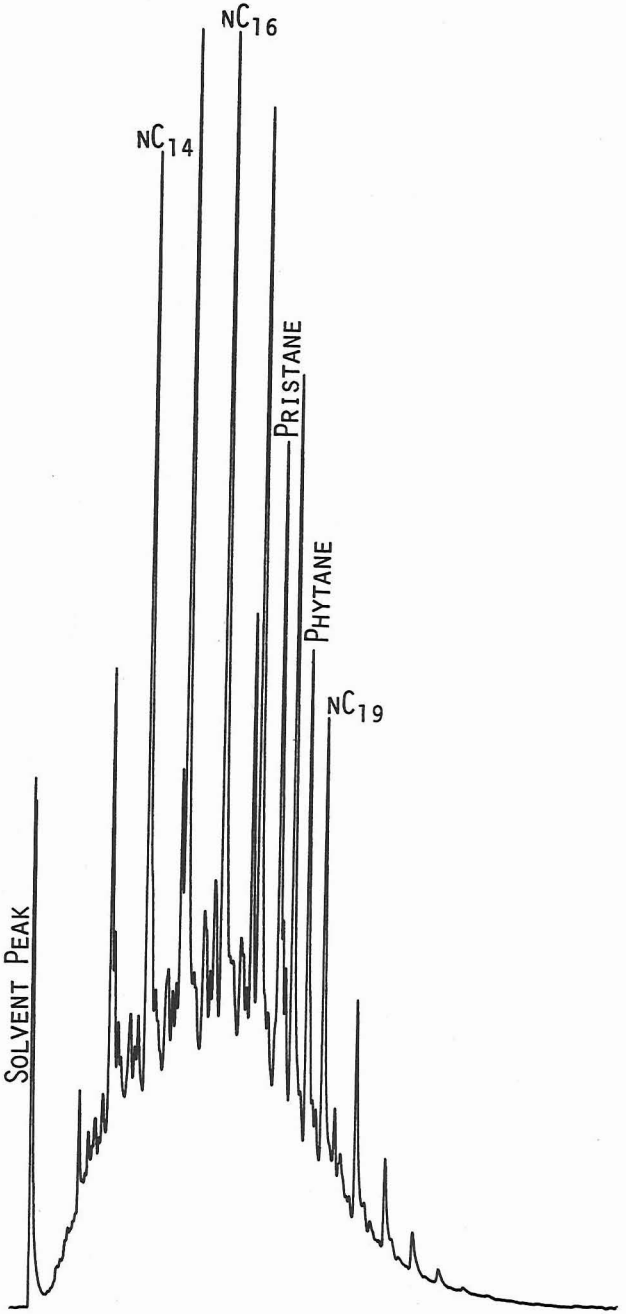

Figure 13.6. *Saturate fraction gas chromatogram of Nektoralik K-59 extract from 2255.5 m (7400 ft) showing napthenic hump and lack of heavy (>C_{22}) hydrocarbons.*

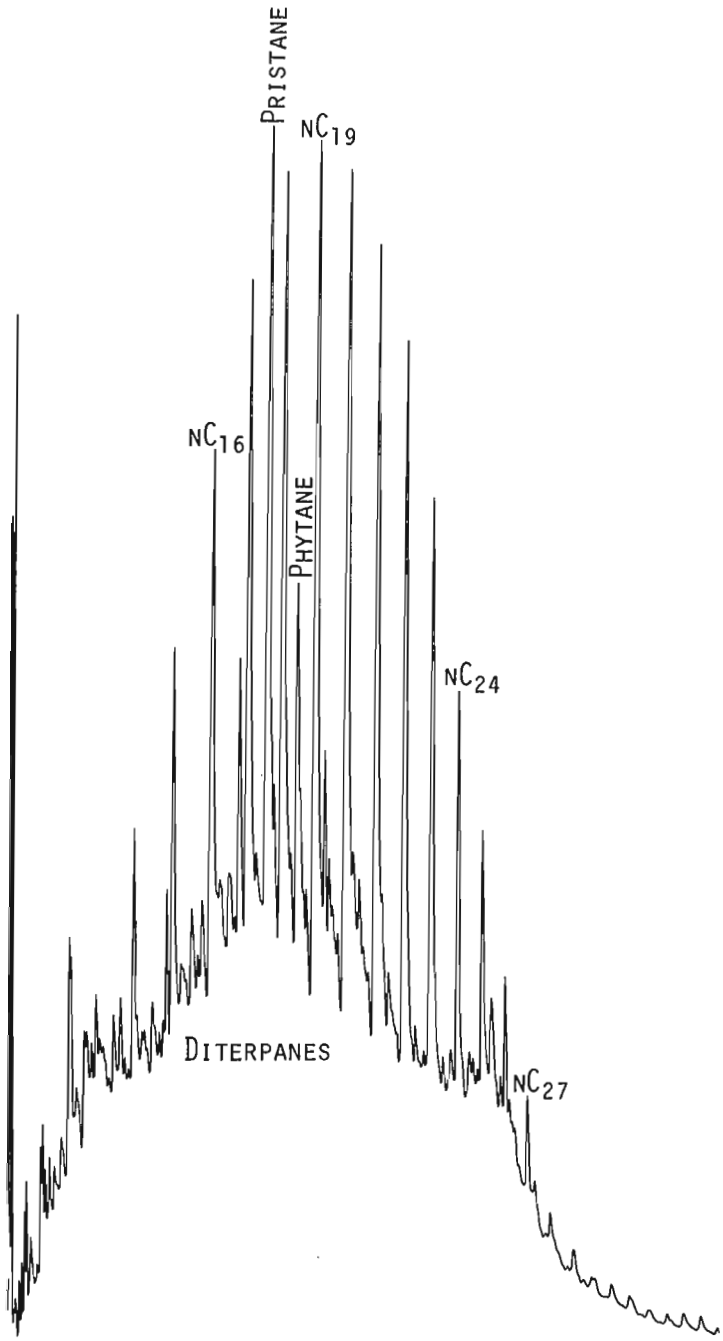

Figure 13.7. *Saturate fraction gas chromatogram of oil recovered on drill stem test from Nektoralik K-59 borehole.*

range (Fig. 13.5). The low extract yield and g.c. character are both consistent with the immature nature of organic matter in the interval.

The three deep extract samples (Table 13.1) are also very similar to each other but markedly different from the samples above 2133.6 m (7000 ft). The extract and hydrocarbon yields and percentage of hydrocarbons in the extract are all quite high. The saturate fraction gas chromatograms (see Fig. 13.6) all show a large naphthenic hump and essentially no hydrocarbons with more than about 22 carbon atoms. The high yields, high percentage of hydrocarbons and mature chromatographic character of these samples indicate that they are stained, that is the hydrocarbons are largely epigenetic rather than syngenetic. If the hydrocarbons were indeed syngenetic, these samples would be classed as marginal to excellent potential petroleum source rocks (Powell, 1978). Because there is no break in the cuttings gas log character which would suggest a rapid rise in the level of thermal maturity, the former interpretation (staining) is preferred. The total quantity of cuttings gas and more or less smooth distribution of the proportion of wet gas suggest that the cuttings gas is syngenetic. Epigenetic gases would be expected to be lost during sample transport up the borehole.

Kerogen (insoluble organic matter) was recovered from the six samples which were extracted and elemental analyses were run. The atomic hydrogen/carbon and carbon/nitrogen ratios are reported in Table 13.1. Except for the deepest sample, all the H/C ratios equal or exceed 0.90. These results are higher than those observed for Tertiary kerogens of the Richards Island area of this same basin (Snowdon, in press). The implication of this data is that the organic matter in the Nektoralik section is enriched in lipids and depleted in higher land plant debris relative to the Richards Island samples, an interpretation which is consistent with the sedimentological interpretation of the depositional environment discussed above. The high H/C ratio also suggests that the level of maturity of these sediments is not high because thermal alteration would cause this ratio to drop markedly.

The increase in the C/N ratio which corresponds to the change in saturate fraction chromatogram character suggests that the lower samples are either significantly more mature than the upper three samples or that the proportion of nitrogen-poor terrestrial organic matter is much higher in the bottom samples. The increased maturity hypothesis is inconsistent with the cuttings gas data and the high H/C ratio; the high terrestrial contribution is also inconsistent with the H/C data and the high extract yields and thus the interpretation of these results is problematical.

A saturate fraction g.c. (Fig. 13.7) and gasoline range (C_5-C_8) analysis were run on a sample of the oil recovered on drill stem test from the Nektoralik K-59 borehole at 2695.0-2701.1 m (8842-8862 ft). The saturate fraction g.c. is essentially similar to that of the oils recovered from the Taglu C-42 and Niglintgak M-19 boreholes. Factor and cluster analysis of the gasoline range data (Snowdon and Powell, in press) indicate that the Nektoralik oil is highly similar to the Taglu and Niglintgak condensates and oils. It is thus probable that the Nektoralik oil and Taglu oil and condensates have a common source. Samples of the condensate recovered from 2258.5-2261.6 m (7410-7420 ft) were not available for analysis and thus no comparison of this material with the high yield extracts was possible.

In summary, all of the data on the post-unconformity section indicate that the organic matter is immature and unrelated to the petroleum deposits associated with this well. The data from the pre-unconformity samples, however, are internally inconsistent in so far as the level of thermal maturity is concerned. While the saturate fraction g.c. data, atomic C/N ratios and occurrence of oil and condensate all suggest that the section is thermally mature, the cuttings gas log and unconsolidated nature of the sediment suggest that the sediments are marginally mature at best. A more definitive hypothesis concerning hydrocarbon generation in this region must await further detailed analyses of the organic fraction and/or additional samples from boreholes drilled with fewer engineering difficulties. The hydrocarbons recovered from the Nektoralik well have probably been derived from a stratigraphically equivalent section to the source for the Taglu and Niglintgak oils and condensates.

References

Bouma, A.M., Moore, G.T., and Coleman, J.M. (ed.)
1978: Framework, facies and oil trapping characteristics of the upper continental margin; American Association of Petroleum Geologists, Studies in Geology, no. 7, 326 p.

Foscolos, A.E., Powell, T.G., and Gunther, P.R.
1976: The use of clay minerals and inorganic and organic geochemical indicators for evaluating the degree of diagenesis and oil generating potential of shales; Geochimica et Cosmochimica Acta, v. 40, p. 953-966.

Jones, P.B., Brache, J., and Lentin, J.K.
1979: Geology of the 1977 offshore hydrocarbon discoveries in the Beaufort Basin, N.W.T. (abs.); Canadian Society of Petroleum Geologists - Canadian Society of Exploration Geophysicists, 1979 Joint Convention, Program and Abstracts, p. 67-68.

Oilweek.
1979: Beaufort: a Canadian North Sea? February 26, p. 16-20.

Payton, C.E.
1977: Seismic stratigraphy - applications to hydrocarbon exploration; American Association of Petroleum Geologists, Memoir 26, 516 p.

Powell, T.G.
1978: An assessment of the hydrocarbon source rock potential of the Canadian Arctic Islands; Geological Survey of Canada, Paper 78-12.

Snowdon, L.R.
Organic geochemistry of the Upper Cretaceous/Tertiary delta complexes of the Beaufort-Mackenzie sedimentary basin, northern Canada; Geological Survey of Canada, Bulletin 291. (in press)

Snowdon, L.R. and Powell, T.G.
1979: Families of crude oils and condensates in the Beaufort-Mackenzie Basin; Bulletin of Canadian Petroleum Geology, v. 27 p. 139-162.

Yorath, C.J., Parker, E.R.,and Glass, D.J. (eds.)
1975: Canada's Continental Margins; Canadian Society of Petroleum Geologists, Memoir 4, 898 p.

Young,F.G., Myhr, D.W.,and Yorath, C.J.
1976: Geology of the Beaufort-Mackenzie Basin; Geological Survey of Canada, Paper 76-11, 65 p.

14. GEOCHEMISTRY OF SNORRI AND GUDRID CONDENSATES, LABRADOR SHELF: IMPLICATIONS FOR FUTURE EXPLORATION

Project 760054

T.G. Powell
Institute of Sedimentary and Petroleum Geology, Calgary

Powell, T.G., Geochemistry of Snorri and Gudrid Condensates, Labrador Shelf: Implications for Future Exploration; in Current Research, Part C, Geological Survey of Canada, Paper 79-1C, p. 91-95, 1979.

Abstract

Geochemical studies on the Gudrid and Snorri condensates have shown that they are sufficiently similar to have had a common or related source. This source was dominated by terrestrial organic matter located at deeper levels of the adjacent sedimentary troughs. Two possible modes of origin are suggested by analogy with Australian examples. At Snorri the gas-condensate may have become separated from oil during migration and at Gudrid the gas-condensate may be an overmature product. In both cases further hydrocarbon accumulations may be located in downdip structures on the flanks of adjacent sedimentary basins. At Snorri these accumulations may include some oil.

Introduction

Several major gas shows with varying amounts of condensates have been recorded on the Labrador Shelf (Purcell et al., in press, McMillan, 1979) (Fig. 14.1). The section comprises an Upper cretaceous-Tertiary clastic sequence resting unconformably on a block faulted basement of varying age (Precambrian, Early and Late Paleozoic). Hydrocarbon traps are formed by drape over the basement blocks. The hydrocarbon reservoirs may be basement (e.g. lower Paleozoic dolomite in Gudrid H-55), lower Cretaceous arkosic sands onlapping the basement blocks (e.g. Bjarni sand in Bjarni H-81) or Tertiary sands with structures developed by draping over the basement blocks (e.g. Snorri J-90).

This note discusses the geochemistry of condensates from the Snorri and Gudrid accumulations and its implication for their source and future exploration on the Labrador Shelf.

Results

The analytical methods used are those described by Snowdon and Powell (in press). The results obtained include gross composition, n-alkane distributions, pristane to phytane ratios, carbon isotope distributions in saturate and aromatic fractions, distribution of twenty four gasoline range components and ring distribution and aromaticity of the aromatic fractions.

The gross compositional data (Table 14.1) indicate that the Gudrid and Snorri condensates are extremely rich in saturated hydrocarbons. The saturates comprise dominantly n-alkanes in the range C_{11} to C_{20} (Fig. 14.2). They differ one from the other in the proportion of isoprenoids (isoC_{16}, isoC_{18}, pristane and phytane) in the saturate fraction and pristane to phytane ratios (Table 14.1). The carbon isotope distributions in the saturate and aromatic fractions of the two condensates are similar.

The Gudrid condensate is richer in alkyl benzenes, acenaphthenes and dibenzofurans and depleted in naphthenebenzenes compared to the Snorri condensate. There is a close similarity in the distribution of the gasoline range hydrocarbons between the two condensates (Fig. 14.3). The main difference in the gasoline range data is the higher content of aromatic hydrocarbons in the Gudrid sample as compared with the Snorri sample. The distribution of compound types with seven carbon atoms is very similar (Fig. 14.3b). The higher content of pentanes in the Snorri sample (Fig. 14.3a) is attributed to evaporative loss of these components from the Gudrid sample during sampling or subsequent handling.

Discussion

Generally the Snorri and Gudrid condensates are similar to one another in overall composition, isotopic distributions and distribution of gasoline range hydrocarbons. They differ in respect of their aromatic composition, isoprenoid content and pristane to phytane ratio. These differences may be due to maturation differences in the original source material. However, they are sufficiently similar in other respects to suggest that they may be derived from a similar or related source despite their wide geographic separation. The paraffinic nature of the condensates and their high pristane

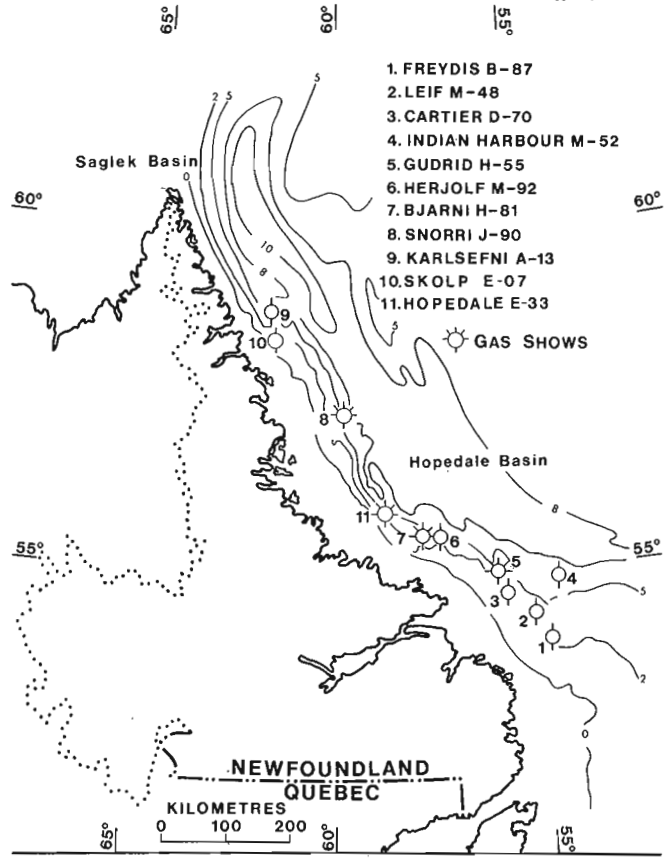

Figure 14.1. *Location of petroleum exploration wells and sedimentary thickness map Labrador Shelf. Contour lines indicate thickness of sediments in kilometres (McMillan, 1979).*

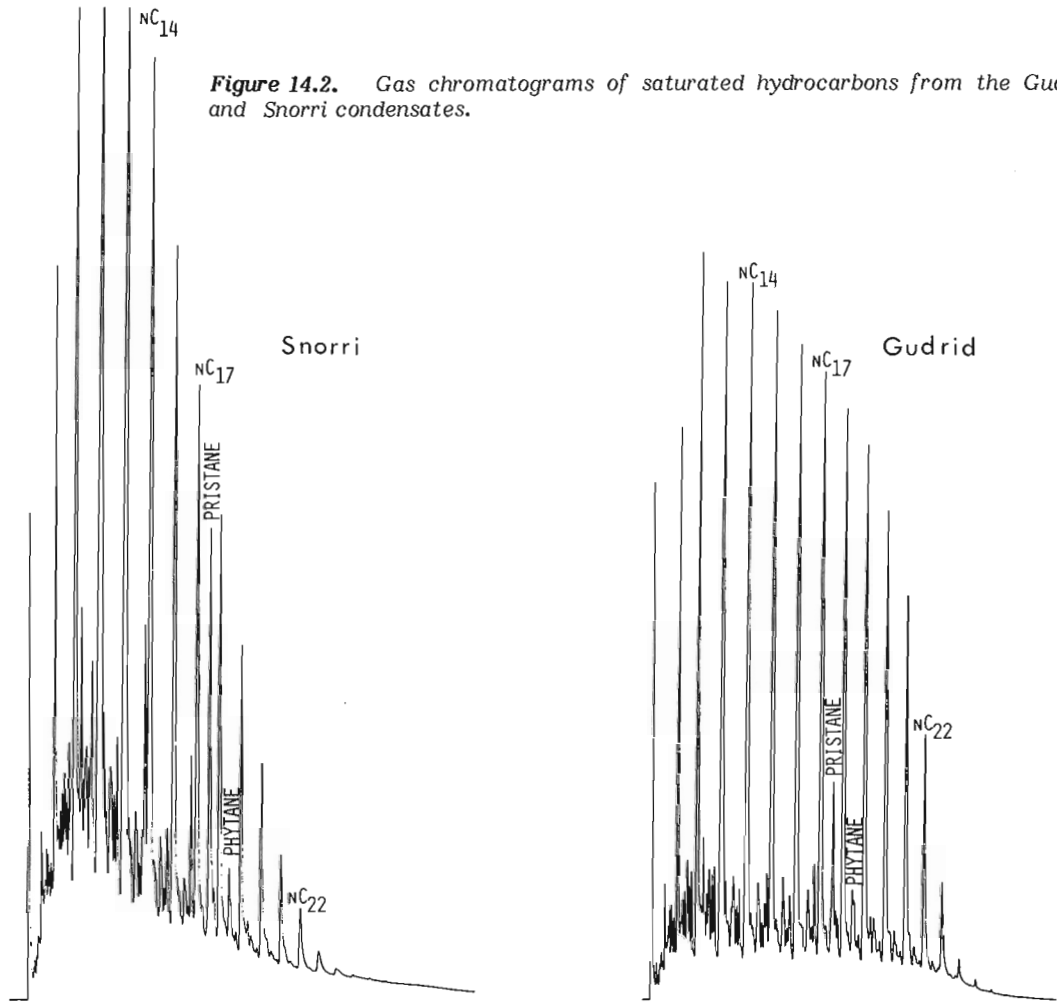

Figure 14.2. *Gas chromatograms of saturated hydrocarbons from the Gudrid and Snorri condensates.*

Table 14.1

Compositional data on Gudrid and Snorri Condensates

Well Test	Gudrid H-55 DST	Snorri J-90 No. 15
Depth (m)	2756.3-2771.9	2496.9
Formation	Gudrid Dolomite	Gudrid Sand Mbr.
Age	Westphalian?	Palaeocene
Weight % <210°C	58	72
Gross Composition Weight % >210°C		
Saturates	84.06	82.09
Aromatics	11.42	13.23
ONS	0.58	0.43
Pristane to Phytane Ratio	4.0	7.1
$\delta^{13}C_{PDB}$		
Saturates	-27.77	-27.25
Aromatics	-25.96	-25.66
Atomatic Composition % Volume of aromatics		
Monoaromatics		
Alkyl Benzenes	45.0	31.9
Naphthenebenzenes	11.7	28.8
Dinaphthenebenzenes	8.7	13.1
Diaromatics		
Naphthalenes	22.0	22.3
Acenaphthenes, Dibenzofurans	9.9	2.2
Fluorenes	0.4	0.2

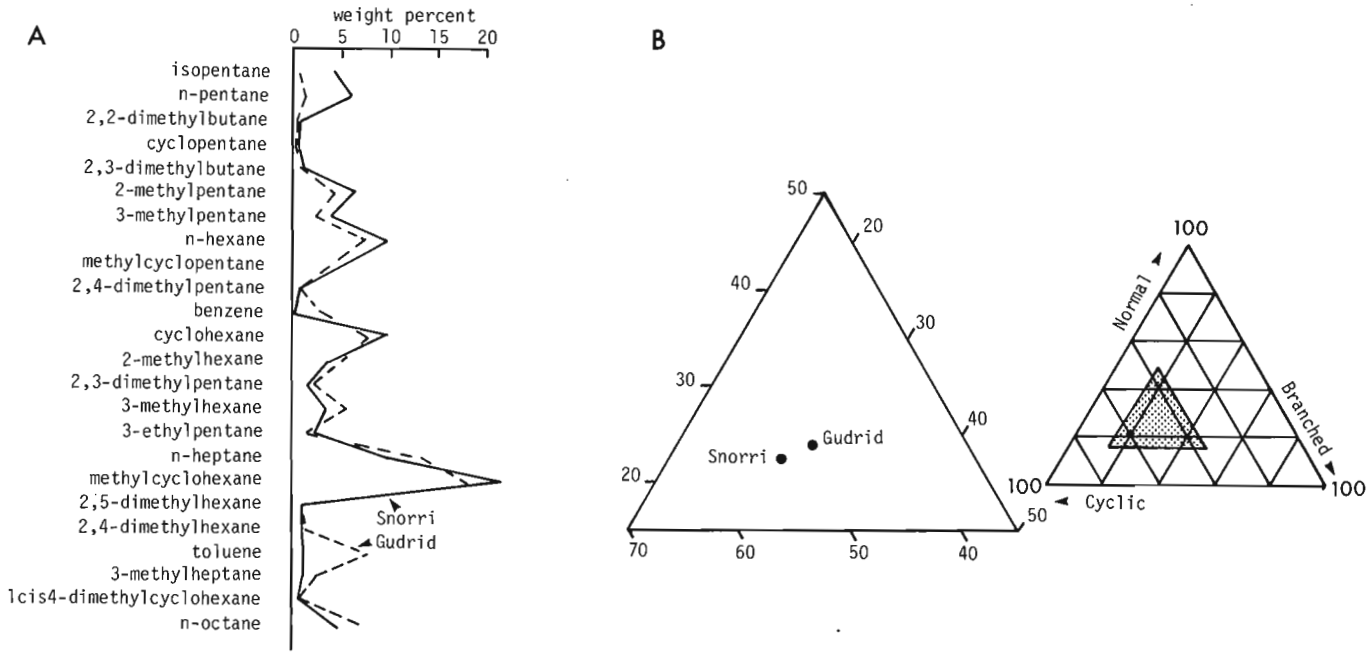

A. Histogram of normalized concentration of gasoline range hydrocarbons
B. Normalized distribution of hydrocarbon types amongst compounds with seven carbon atoms

Figure 14.3 *Distribution of gasoline range hydrocarbons in the Gudrid and Snorri condensates.*

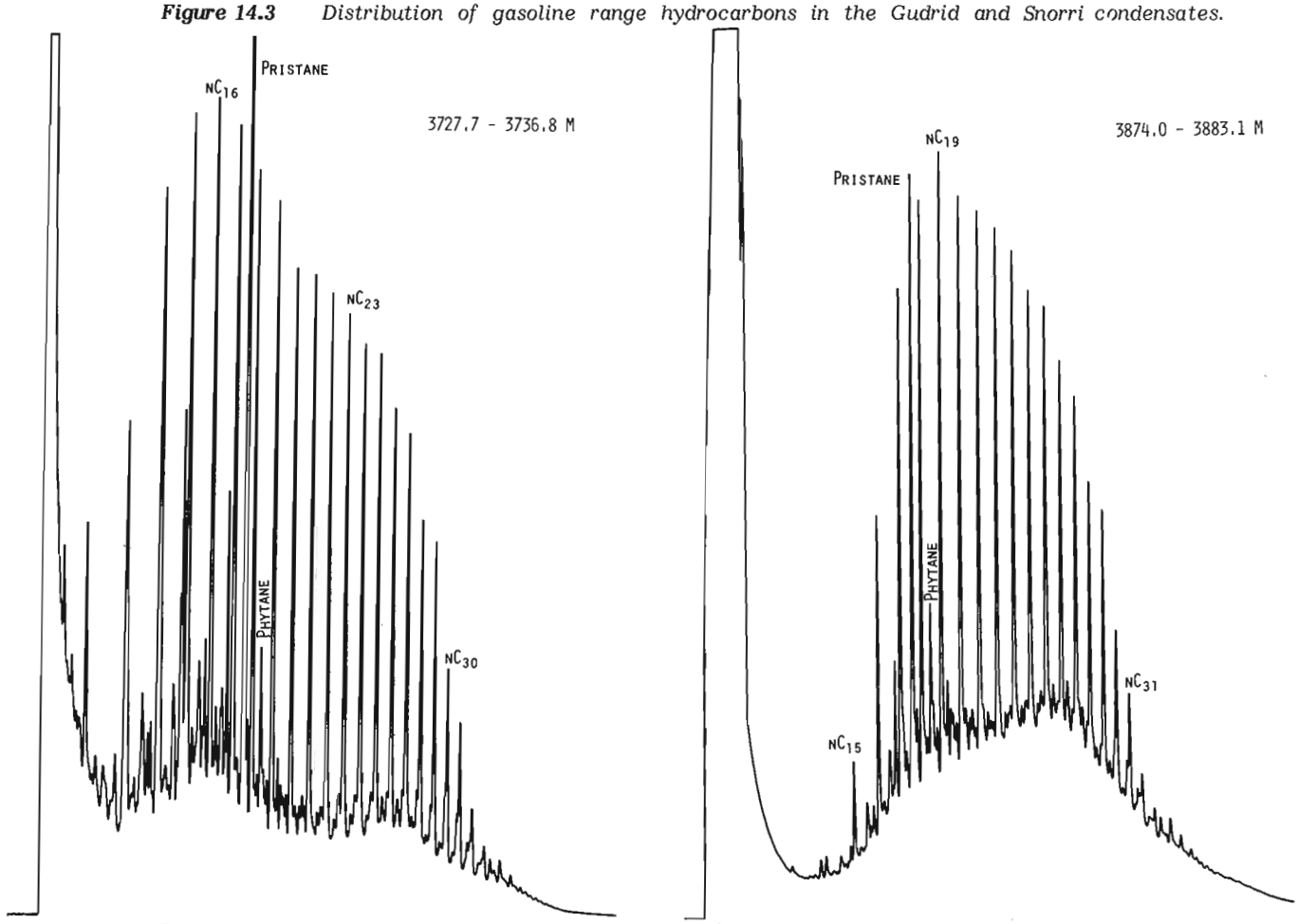

Figure 14.4. *Representative gas chromatograms of saturated hydrocarbons from the Cartwright and Bjarni Formations, Herjolf M-92 well.*

to phytane ratios (particularly Snorri) indicate a source from terrestrial organic matter (Powell and McKirdy, 1975). This conclusion is consistent with the fact that organic matter in the lower part of the Cretaceous-Tertiary section is largely land derived (Rashid et al., in press). Little published information is available on the nature of the source rock for nonmarine paraffinic oils and condensates. Threfall et al. (1976) state that source rock analyses show that nonmarine shales and coals are the source for the waxy oils and gas-condensate in the Gippsland Basin of south-east Australia although no supporting data are given. Smyth (1979) associates the nonmarine paraffinic oils and condensates in the Cooper Basin, Australia with exinite rich coals and associated shales rich in exinitic organic matter. The basal Lower Cretaceous Bjarni Formation on the Labrador Shelf consists of coarse grained continental sandstones with minor shales and coal beds. Gas chromatograms of saturates from this formation and the overlying Cartwright shale are dominated by waxy n-alkanes and high pristane to phytane ratios (Fig. 14.4). Hydrocarbon yields from some samples in these formations in the Herjolf M-92 well approach values at which gas-condensate and minor amounts of oil can be expected to have formed (Powell, 1978) (Table 14.1).

Maturation studies have been undertaken on many of the Labrador Shelf wells by Rashid et al. (in press) and Bujak et al. (1977), respectively. Additional geochemical work has been carried out by the author. These data show that the most southerly wells, Leif M-48 and Freydis B-87 are immature in the Cretaceous-Tertiary section. The sediments in Gudrid H-55 appear to be just mature at the base of the Mesozoic section (2663 m, 8736 ft) and coincide with the occurrence of reservoired hydrocarbons.

In the Herjolf M-92, Snorri J-90 and Karlsefni A-13 wells, the marginally mature zone as defined by the onset of a high proportion of wet gas in the cuttings gas analyses occur at a depth of about 2438 to 2591 m (8000 to 8500 ft). The gas-condensate in the Snorri J-90 well occurs at 2494 to 2516 m. Full maturity is only attained in the Herjolf M-92, Snorri J-90 and Karlsefni A-13 wells in the vicinity of 3658 to 3810 m (12 000 to 12 500 ft). The occurrence of apparently mature gas-condensates at the boundary of the immature to marginally mature zone thus represents an anomaly in respect to the oil and gas generation model unless migration from a deeper part of the basin had occurred. Examination of the distribution of the hydrocarbon discoveries in relation to sedimentary thickness maps of the Labrador Shelf show that they occur at or close to the margins of sedimentary troughs or basins within excess of 8 km of sediment. There is a distinct possibility therefore that the hydrocarbons may have migrated out of these thicker sedimentary sections to the edges where they are now entrapped.

Liquid hydrocarbons derived from terrestrial organic matter usually contain a high proportion of waxes (n-alkanes above nC_{22}) (Powell and McKirdy, 1975). Their absence in this case could be a consequence of either one of two processes. The gas-condensate could be a product of extensive cracking by thermal maturation or of fractionation from an oil during migration. Considering the first case, the maturation levels at the gas-condensate reservoirs is relatively low and the 60°C isotherm is generally coincident with the reservoir horizons (Purcell et al., in press, Rashid et al., in press). Geothermal gradients are generally in the range 2.4°C to 3.2°C per 100 m so that temperatures of 150°C representing the transition from mature to overmature zones, would be expected in the depth range 4700 m to 6200 m. This depth is well within the 8 km sediment thickness of the adjacent Hopedale and Sagalek basins. It is possible therefore that the Snorri and Gudrid condensates are derived from late mature to overmature zones in the adjacent sedimentary troughs. If this is the case the traps located on the downdip flanks of these basins may be full to spill point with gas-condensates.

Condensates and oils derived from mature terrestrial organic matter typically have high pristane contents in their saturate chromatograms with high pristane to phytane ratios (>5), (Powell and McKirdy, 1975). With increasing maturity pristane and phytane became less important components of the saturate fraction and the pristane to phytane ratios diminish (<4) (Brooks et al., 1969; Powell and McKirdy, 1975; Powell, 1978). The Gudrid condensate may be an overmature condensate because of its low pristane content and lower pristane to phytane ratio. A suitable analogy for the Gudrid discovery is the Gidgealpa gas-condensate field in the Cooper Basin of S. Australia (see Beddoes, 1973 for geological details). It is terrestrially derived, and overmature. It is

Table 14.2

Extract data Cartwright Shale and Bjarni Formations
Herjolf H-92 Well

Well - Depth (m)	% Org C	Extract mg per gram Org C	Hydrocarbons mg per gram Org C	Hydrocarbons % in extract
Herjolf M-92				
3572.2-3581.4	4.55	100.3	30.8	30.7
3672.8-3682	2.44	83.7	31.7	37.7
3727.7-3737.0	13.55	72.2	29.8	41.8
3874.0-3883.0	0.29	47.2	12.4	24.8
4029-4038	0.29	31.2	5.6	18.1

Table 14.3

Comparison of gas condensate ratios of Labrador Shelf discoveries and some Australian occurrences

Well/Field	Gas Condensate Ratio (m^3 gas/m^3 condensate)
Labrador Shelf[1]	
Bjarni H-81	21 000
Gudrid H-55	34 000
Snorri J-90	7 900
Hopedale E-33	6 500
Gippsland Basin, Australia[2]	
Barracouta	19 663 to 6292
	avg. 9000
Marlin	7132 to 3012
Dampier Sub-Basin, Australia[2]	
Goodwyn	4025-3725
North Rankin	7279-4641
Cooper Basin, Australia[2]	
Gidgealpa	52 400

[1] Data from McMillan (1979)
[2] Data from Beddoes (1973)

similar to the Gudrid condensate since it has high gas to condensate ratio (Table 14.3) and an intermediate pristane to phytane ration (4.0) and a low proportion of pristane in the saturate fraction. On the other hand the Snorri condensate has a higher content of isoprenoids and a higher pristane to phytane ratio typical of oils derived from terrestrial organic matter. This implies that the Snorri condensate is derived from a thermally mature but not overmature section. A possible explanation for the occurrence of non-associated gas-condensate in this case is that gas-condensate and oil were generated in the adjacent sedimentary basins and became separated during the course of migration such that gas-condensate has become trapped updip from locations where oil might also be trapped. Schowalter (1979) has recently reviewed the mechanisms whereby this might occur. Suitable analogies for this scenario exist in other oil- and gas-condensate-bearing regions in Australia.

In the Gippsland Basin, Australia, terrestrially derived gas-condensate is trapped updip from waxy oil (Threfall et al., 1976). The condensate is a close analogy for the composition of the Snorri condensates. The geological setting, however, is somewhat different. The geographic distribution of oil and gas-condensate in the Gippsland Basin appears to be due to variations in maturation levels (Kantsler et al., 1978). The Dampier sub-basin N.W. Australia represents a closer analogy to the Labrador Shelf. The hydrocarbon bearing Rankin Platform consists of a series of Lower Jurassic/Triassic fault blocks which are covered by relatively thin Upper Cretaceous shales and a thick Tertiary section. The Rankin Platform is separated from the adjacent sedimentary trough by a series of down stepping blocks. Gas-condensate occurs in the upthrown blocks whereas paraffinic oil occurs in the blocks stepping down into the adjacent sedimentary trough. Correlation work has shown that the condensate and oil for example in the Goodywn field have a common source (Powell, 1975). The separation of gas-condensate from the oil presumably occurred during migration. A similar situation may have occurred on the Labrador Shelf. The gas to condensate ratios obtained during testing of the discoveries overlap the range of gas-condensate ratios in the Gippsland and Dampier Sub-Basins (Table 14.3). This perhaps could be taken as indirect evidence for the presence of oil in associated areas.

Conclusions

The Snorri and Gudrid condensates resemble each other sufficiently to have been derived from similar or related sources. Minor variations in composition may be attributed to differences in maturation history. The composition of the condensates is consistent with their having a source from terrestrially derived organic matter. Geochemical evidence suggests that these condensates have formed in and migrated from adjacent sedimentary troughs. The Gudrid sample may represent an overmature condensate in which case gas-condensate can be expected to be trapped downdip on the flanks of the adjacent sedimentary trough. The Snorri condensate is probably mature and may have become separated during migration from oil which also may be trapped downdip from the present discovery.

References

Beddoes, L.R.
1973: Oil and gas fields of Australia, Papua, New Guinea and New Zealand; Tracers., Sydney, 381 p.

Brooks, J.D., Gould, K., and Smith, J.W.
1969: Isoprenoid hydrocarbons in coal and petroleum; Nature, v. 222, p. 257-259.

Bujak, J.P., Barss, M.S., and Williams, G.L.
1977: Off-shore East Canada's organic type and color and hydrocarbon potential; Oil and Gas Journal, v. 75, no. 14, p. 198-202.

Kantsler, A.J., Smith, G.C., and Cook, A.C.
1978: Lateral and vertical rank variation: Implications for hydrocarbon exploration; Australian Petroleum Exploration Association Journal, v. 18, Part 1, p. 143-156.

McMillan, N.J.
1979: Geology of the Labrador Sea and its petroleum potential; 10th World Petroleum Congress. Preprint.

Powell, T.G.
1975: Geochemical studies related to the occurrences of oil and gas in the Dampier Sub-Basin, Western Australia; Journal of Geochemical Exploration, v. 4, p. 441-466.

1978: An assessment of the hydrocarbon source rock potential of the Canadian Arctic Islands; Geological Survey of Canada, Paper 78-12, 82 p.

Powell, T.G. and McKirdy, D.M.
1975: Geologic factors controlling crude oil composition in Australia and Papua New Guinea. American Association of Petroleum Geologists, Bulletin,v. 59, n. 7, p. 1176-1197.

Purcell, L.P., Umpleby, D.C., and Wade, J.A.
Regional geology and hydrocarbon occurrences off the east coast of Canada; in ed., A. Miall, Facts and Principles of World Oil Occurrence, Canadian Society of Petroleum Geologists, Memoir 6. (in press)

Rashid, M.A., Purcell, L.P., and Hardy, I.A.
Geochemical characteristics of the sedimentary rocks in the East Newfoundland and Labrador Shelf areas; in ed., A. Miall, Facts and Principles of World Oil Occurrence, Canadian Society of Petroleum Geologists, Memoir 6. (in press)

Schowalter, T.T.
1979: Mechanics of secondary hydrocarbon migration and entrapment; American Association of Petroleum Geologists, Bulletin, v. 63, no. 5, p. 723-760.

Smyth, M.
1979: Hydrocarbon generation in the Fly Lake - Brolga area of the Cooper Basin; Australian Petroleum exploration Association Journal, v. 19, Part 1, p. 108-114.

Snowdon, L.R. and Powell, T.G.
Families of crude oils and condensates in the Beaufort-Mackenzie Basin; Bulletin of Canadian Petroleum Geology. (in press)

Threfall, W.F., Brown, B.R., and Griffith, B.R.
1976: Gippsland Basin, Off-shore; in ed., R.B. Leslie, H.J. Evans and C.L. Knight, Economic Geology of Australia and Papua New Guinea - 3. Petroleum Australian Institute of Mining and Metallurgy, Melbourne, p. 41-67.

DURANUSITE FROM THE MOUNT WASHINGTON COPPER DEPOSIT, COMOX DISTRICT, VANCOUVER ISLAND, BRITISH COLUMBIA

Projects 680023 and 620308

A.C. Roberts, A.G. Plant, and M. Bonardi
Central Laboratories and Administrative Services Division

Introduction

Duranusite, ideally As_4S, was originally described by Johan et al. (1973) from Duranus, France, where it occurs as "petites plages (0.2mm) au maximum" associated with native arsenic and realgar.

Our interest in duranusite resulted from a routine request by Mr. Stan Leaming of the Geological Survey's Cordilleran Division, for an X-ray powder diffraction identification. Several amateur mineral collectors had approached Mr. Leaming regarding mineral identifications of material collected at the Mount Washington Copper Deposit, Mount Washington, Comox District, Vancouver Island. Two specimens, containing black matted nests on clear quartz crystals, were unrecognizable to Mr. Leaming, who sent them to the Geological Survey's Mineralogy Section in Ottawa, for further work.

The mineral was tentatively identified as duranusite on the basis of its X-ray powder diffraction pattern and this identification was later confirmed by electron microprobe analysis. This short note documents the second reported occurrence of this mineral in the world and the first in Canada.

Mineral Description

Duranusite occurs as black, matted nests on clear euhedral quartz crystals (Fig. 1). The only closely associated mineral is realgar. Scanning electron microscopy (SEM) examination of the matted nests shows that they consist of an aggregate of fibrils which have a maximum size of 200x25 micrometres (Fig. 2). Figure 2 also shows that each fibril is composed of many extremely small (less than one micrometre) individuals, and this accounts for the softness of the material as well as the lack of diffraction spots on precession single crystal films. The fibrils are black with a submetallic lustre and have a black streak.

Chemical Composition

A polished section of duranusite fragments was first analyzed by electron microprobe in 1975. Energy dispersive spectra showed that As, S and Sb were the only elements present. Quantitative analyses (Table 1, analyses 1-3) were obtained using a MAC instrument operated at 20 KV and with a specimen current of 0.03 microamperes measured on a realgar sample that served as a standard for As and S (K α lines). Natural stibnite was used as a standard for Sb (Lα line). A second sample was analyzed in 1979 (Table 1, analyses 4-6) at 25 KV accelerating voltage and using a synthetic iron arsenide as a standard for As and the natural stibnite for S and Sb.

The data in Table 1 show that compared to the average composition of two analyses of duranusite from the type locality (Table 1, analysis 7, Johan et al. (1973)), duranusite from Mount Washington contains a variable amount of Sb. No evidence has been found of any intergrowth of an Sb-mineral such as stibnite with the duranusite, either by X-ray diffraction or SEM examination, and it is concluded that the Sb substitutes for As. Furthermore, calculation of compositions of mixtures of stoichiometric stibnite and duranusite show divergence from the compositions given in Table 1. For example, a mixture of 95.5% duranusite and 4.5% stibnite gives As 86.3, Sb 3.2, S 10.5.

The substitution of antimony for arsenic is accompanied by sulphur, presumably to preserve the integrity of the duranusite structure. Recalculation of the number of atoms in the unit formula based on a total of 5 atoms, yields a consistent value of $(As,Sb,S)_4$ S for the Mount Washington duranusite, in satisfactory agreement with the general formula of As_4S proposed by Johan et al. (1973).

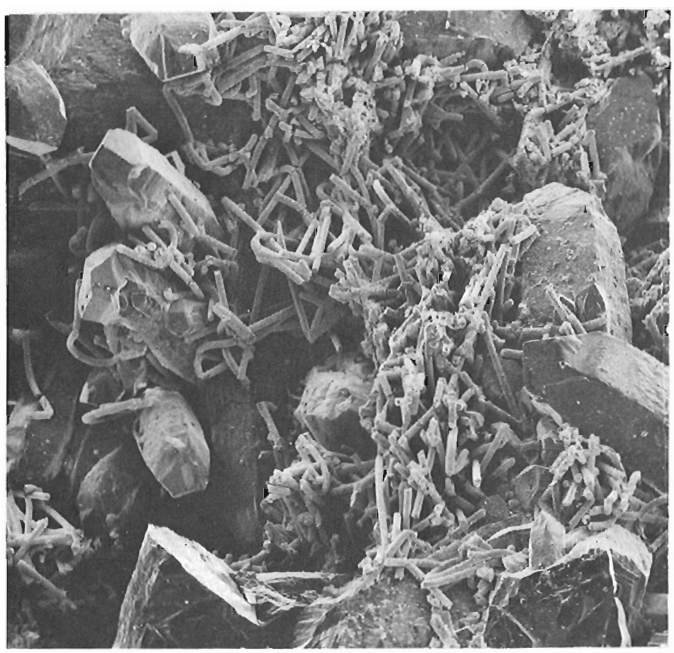

Figure 1. *SEM photomicrograph of nests of duranusite on quartz. Field of view is 2.2 mm.*

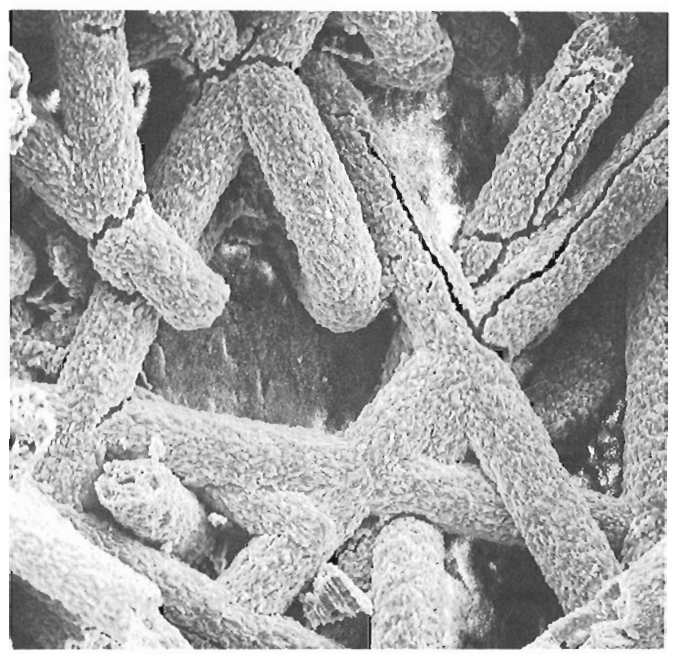

Figure 2. *SEM photomicrograph showing surface texture of individual duranusite fibrils. Field of view is 220 micrometres.*

From: Scientific and Technical Notes in Current Research, Part C; Geol. Surv. Can., Paper 79-1C.

Table 1

Chemical composition of duranusite

		Analysis No.						
		1.	2.	3.	4.	5.	6.	7.
Weight Percent	As	89.8	86.1	80.7	90.8	89.7	86.2	90.4
	Sb	0.6	4.1	8.3	0.1	0.6	4.1	--
	S	9.1	10.2	11.3	9.4	9.9	10.2	10.3
	Total	99.5	100.4	100.3	100.3	100.2	100.5	100.7
Atomic Proportions	As	1.199	1.149	1.077	1.212	1.197	1.151	1.207
	Sb	0.005	0.034	0.068	0.001	0.005	0.034	--
	S	0.284	0.318	0.352	0.293	0.309	0.318	0.321
	Total	1.488	1.501	1.497	1.506	1.511	1.503	1.528
Recalculated to a Total of 5 Atoms	As	4.03	3.83	3.60	4.02	3.96	3.83	3.95
	Sb	0.02	0.11	0.23	0.003	0.02	0.11	--
	S	0.00	0.06	0.18	0.00	0.02	0.06	0.05
		4.05	4.00	4.01	4.023	4.00	4.00	4.00
	S	0.95	1.00	1.00	0.97	1.00	1.00	1.00

Table 2

Unit cell parameters of duranusite

	Duranusite Mount Washington Copper Deposit, Mount Washington, Comox District, Vancouver Island, B.C. (this study)		Duranusite Duranus, France (Johan et. al. 1973)	
Symmetry	C Orthorhombic		Orthorhombic	
a Å	3.555	(1)	3.576	(2)
b Å	6.809	(2)	6.759	(2)
c Å	10.174	(5)	10.074	(5)
V Å^3	246.27		243.5	(3)

Crystallography

The powder pattern of the Mount Washington duranusite was indexed by analogy with the orthorhombic unit cell adopted by Johan et al. (1973) and is presented in Table 2. Unit cell refinement was based on 11 lines between 3.409 Å and 1.777 Å for which unambiguous indexing was possible. The resultant cell parameters, as well as those obtained by Johan et al. (1973), are listed in Table 3. The larger cell volume of the Mount Washington duranusite most likely reflects the partial substitution of antimony for arsenic within the crystal lattice.

Acknowledgments

The writers wish to thank Mr. D.A. Walker for the S.E.M. photomicrographs.

Table 3

Powder Diffraction data for duranusite, Mount Washington Copper Deposit, Mount Washington, Comox District, Vancouver Island**

I est.	dÅ meas.	dÅ calc.	hkl
1	6.81	6.81	010
10	5.68	5.66	011
8	5.10	5.09	002
2	4.09	4.08	012
*6	3.409	3.405	020
*5	3.230	3.229	021
6	3.026	(3.036 (3.010	013 011
*10	2.915	2.914	102
*8	2.830	2.830	022
*7	2.679	2.679	112
*1	2.542	2.544	004
1/2	2.460	2.459	120
*4	2.388	2.390	121
*2	2.270	2.270	030
1/2	2.211	(2.215 (2.214	031 122
*6	1.981	1.979	114
<1/2	1.884	(1.886 (1.880	033 131
*5	1.790	1.791	132
*5	1.777	1.777	200
3b	1.700		
1b	1.639		
1/2b	1.573		
2b	1.518		

** 114.6 mm Debye-Scherrer camera, Cu kα radiation, Ni filter, Si internal standard, film no. 50816

I est. visually

b = broad line

* = lines used in cell refinement

indexed with a = 3.555 Å, b = 6.809 Å, c = 10.174 Å

Reference

Johan, Z., Laforêt, C., Picot, P., and Feraud, J. 1973: La duranusite, As_4S, un nouveau mineral; Bulletin de la Société française de Minéralogie et de Cristallographie, v. 96, p. 131-134.

PARALSTONITE: A NEW MINERAL FROM THE MINERVA NO. 1 MINE, CAVE-IN-ROCK, ILLINOIS

Project 680023

A.C. Roberts
Central Laboratories and Administrative Services Division

Paralstonite, previously referred to as an "unnamed barium calcium carbonate" by Roberts (1976, 1978), has been accepted as a valid mineral species by the Commission on New Minerals and Mineral Names of the International Mineralogical Association. The name, paralstonite, alludes to the mineral's morphological, chemical and crystallographic relationship with alstonite. Holotype specimen (13380), referred to as the "largest specimen" in Roberts (1978), is preserved in the National Mineral Collection at the Geological Survey of Canada.

Pertinent mineral data have been summarized in Tables 1 to 4. Additional information, not previously published, have been incorporated within the tables and marked with an asterisk. The crystal structure of paralstonite is presently being undertaken by Dr. J. Zemann and colleagues at the Institute for Mineralogy and Crystallography, Wien University, Austria.

Table 1

Crystallographic data for paralstonite

Crystal System	Hexagonal (Trigonal)
a (Å)	8.692 (3)
c	6.148 (4)
c/a	0.7073
Space Group	P312 (149), P321 (150), P3m1 (156), P31m (157), $P\bar{3}1m$ (112), $P\bar{3}m1$ (164)†
Volume (Å^3)	402.24
Z	3
*G (meas.)	3.60(2)†† g/cc
G (calc.)	3.62 g/cc

† partial structure determination indicates space group P321 (Dr. J. Zemann, personal communication August 1979)

†† Berman balance on 8.73 mg of hand picked crystal fragments from hototype specimen.

Table 2

Electron microprobe analysis of paralstonite

	wt. %	molecular ratio	
BaO	45.6	0.2985)	
CaO	18.8	0.3365)	0.6854
SrO	5.2	0.0504)	
CO_2 (calc.)	30.0	0.6844	
Total	99.6		
Analytical Formula†	:	$Ba_{0.872}Ca_{0.983}Sr_{0.147}(CO_3)_2$	
Theoretical Formula	:	$BaCa(CO_3)_2$	
Molecular Weight	:	292.14	

†calculated assuming 6 oxygen atoms per formula unit cell.

Table 3

X-ray powder data for paralstonite

I/Io	2θ meas.	dÅ meas.	dÅ calc.	hkl
2	11.79	7.51	7.53	100
18	14.39	6.15	6.15	001
3	18.64	4.76	4.76	101
11	20.41	4.35	4.35	110
100	25.08	3.550	3.549	111
2	27.83	3.206	3.210	201
3	29.03	3.076	3.074	002
11	31.38	2.851	2.846	102
5	34.75	2.581	2.582	211
67	35.71	2.510	2.509	300
1	37.97	2.370	2.381	202
6	38.77	2.323	2.323	301
9	41.52	2.175	2.173	220
8	43.39	2.085	2.088	310
21	44.22	2.048	2.049	221
3	45.96	1.975	1.977	311
18	46.74	1.943	1.944	302
15	49.16	1.853	1.853	113
1	50.76	1.799	1.799	401
3	51.56	1.773	1.774	222
2	53.01	1.727	1.727	320
2	55.23	1.663	1.663	321
2	55.98	1.643	1.643	410
2	57.43	1.605	1.605	402
11	58.13	1.587	1.587	411
1	60.25	1.536	1.537	004
1	61.60	1.506	1.506	104
6	62.30	1.490	1.491	223
2	63.60	1.463	1.463	501
9	64.35	1.448	1.449	330
2	65.65	1.422	1.422	420
2	66.30	1.410	1.410	331
1	67.62	1.385	1.386	403
1	69.55	1.352	1.352	510
2	71.37	1.321	(1.321 (1.320	323 511
8	72.04	1.311	(1.311 (1.310	304 332
1	73.22	1.293	1.291	422
6	73.94	1.282	1.282	413
11	75.77	1.255	1.255	600
3	76.96	1.239	(1.238 (1.238	512 430
2	77.64	1.230	1.230	005
2	78.79	1.215	(1.213 (1.213	503 431

- 114.6 mm Debye-Scherrer camera; Ni filtered Cu Kα radiation;
- line intensities calculated from diffractometer trace;
- indexed with a=8.692 Å, c=6.148 Å;
- film no. 48934 corrected for film shrinkage.

From: Scientific and Technical Notes in Current Research, Part C; Geol. Surv. Can., Paper 79-1C.

Table 4

Physical and optical properties of paralstonite

Colour	:	colourless to smoky white, grading to grey-white in masses
Lustre	:	vitreous
Streak	:	white
Fracture	:	uneven
Opacity	:	transparent to translucent
Tenacity	:	brittle
Fluorescence	:	variable, pale to bright orange under long wave ultraviolet light
Cathodoluminescence	:	negative
Hardness	:	between 4 and 4 1/2
Chemical Tests	:	vigorous effervescence in dilute HCl
Morphological Characteristics	:	euhedral crystals, maximum length 1 mm, length to width ratio approaching 2:1, hexagonal morphology with {221} pyramidal habit, hexagonal dipyramids have been observed but are rare, crystal faces are heavily striated normal to axis of elongation (c-axis) and are divided parallel to c-axis by a medial, irregular, slightly re-enrant "suture"
Optical Characteristics	:	colourless in transmitted light, uniaxial negative, n_ε=1.527(3), n_ω=1.672(3)

*Chemical Refractive Energy (Kc)† = 0.169
*Physical Refractive Energy (Kp) = 0.173 for G(meas.), 0.172 for G(calc.)

† constants taken from Mandarino (1976).

References

Mandarino, J.A.
1976: The Gladstone-Dale relationship. Part 1: Derivation of new constants, Canadian Mineralogist, 14, p. 498-502.

Roberts, A.C.
1976: A mineralogical investigation of alstonite $BaCa(CO_3)_2$; unpublished M.Sc. thesis, Queen's University, Kingston, Ontario, Canada.

1978: Mineralogical study of an unnamed barium calcium carbonate from the Cave-in-Rock district, Illinois; in Current Research Part C, Geological Survey of Canada Paper 78-1C, p. 49-52.

SEABOTTOM SEISMIC REFRACTION ARRAY DESIGNS

Project 730006

J.A. Hunter, R.A. Burns, R.L. Good, and T.E. Harrison
Resource Geophysics and Geochemistry Division

During the last few years we have tested seabottom seismic refraction arrays for shallow marine use on continental shelves. We have established that such arrays can be used for compressional velocity determinations, for conversion from travel time to depth scales on high resolution marine reflection records, and for the identification of high velocity anomalies which may result from the presence of ice-bonded permafrost, gas hydrates, boulder beds or consolidated rock within the shallow seabottom sedimentary column.

The main advantage of a bottom laid refraction array over a similar surface towed array is the removal of the thick water layer from the geometry. The problem of "hidden" layers is largely overcome i.e., thin layers lying immediately below the thick water layer and having velocities only slightly higher than water may not appear as first arrived refractions on a surface-towed array. This problem was encountered by Hunter et al. (1976, p. 65) in the Beaufort Sea where the bottom-laid array was able to provide missing seabottom velocity data.

Since some of the shelf areas in northern Canada are ice-covered for many months of the year, it was decided to design arrays which could be operated from the ice surface, using available leads or by way of small holes drilled through the ice. Two arrays evolved from this project, a 20-m 12-channel array for velocity measurements in the first few metres of the seabottom and a 180-m array for deeper penetration.

The 20-meter array

This array consists of 12 Interocean T-111 hydrophones capable of operating in 1000 m of water attached at equal 1.53 m spacings along a 5 cm diameter nylon tube (Fig. 1). Each hydrophone rests on a 3 cm thick neoprene pad to achieve decoupling from refracted waves along the tube. Metal holders capable of accommodating 6 seismocaps each are attached at a spacing of 1.52 m from the hydrophones at each end. The array is designed in 2.5 m sections for ease of transport and can be quickly assembled at the site and lowered through a 20 cm hole in the ice to the seabottom. Each seismocap can be fired in turn by a shot box on surface to provide 6 reversed refraction profiles. Recording is performed with a Nimbus ES-1200 12 channel seismograph which has the capability of stacking (adding) successive records and providing 0.05 millisecond timing accuracy. Recording is done in analog form on direct-write recording paper.

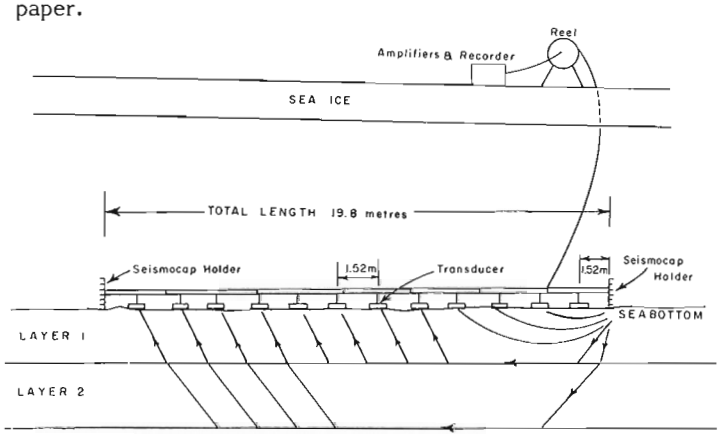

Figure 1. *20 m array configuration for sub-seabottom refraction measurements in water depths up to 300 m.*

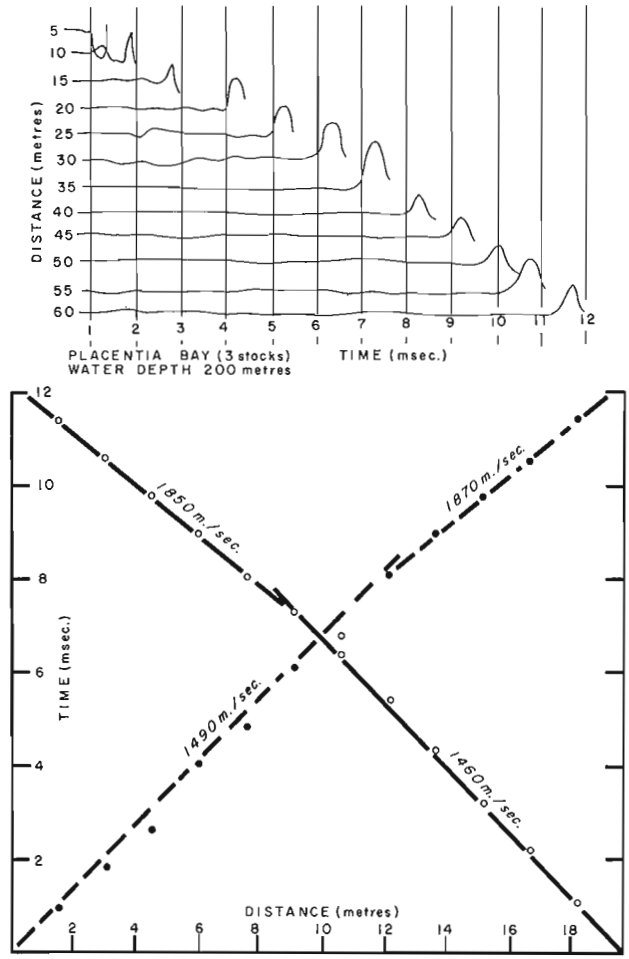

Figure 2. *Seismic record and first arrival travel time plot from the 20 m array for a site in Placentia Bay area, Newfoundland. In this example, the array was deployed from a stationary vessel.*

The system has been tested through the ice in the Beaufort Sea and on board ships for station work in the Beaufort Sea, Lancaster Sound and Placentia Bay area to water depths of 300 m. Figure 2 shows a typical refraction plot for a site in the Placentia Bay area. It was found that in most areas stacking was not necessary since high energies were recorded on all 12 traces using one seismocap. The depth of penetration of this array depends upon the velocity variation with depth below the seabottom. Figure 3 shows a two-layer case with a bottom velocity of 1500 m/s. The variation in the maximum depth of penetration to the lower layer is plotted against the lower layer velocity. For a lower layer velocity of 4000 m/s (consolidated rock or ice-bonded permafrost) the depth of penetration may reach 7 m.

The 180 meter array

This array was designed for deep penetration (up to 60 m) for use through available leads in sea ice or for shipboard station work. The array consists of 12 Mark Products P-38 hydrophones attached by "pig-tail" take-outs to a 28 conductor cable at 15 m spacings (Fig. 4). The hydrophones are capable of operating up to 60 m depth of water; however, good response has been obtained in 80 m water depth. The seismic source consists of 0.2 kg geogel 60% dynamite detonated at measured distances on seabottom off each end of the array. Recording is performed with a 12 channel S.I.E. RS-4 analog seismograph using direct-write paper records.

From: Scientific and Technical Notes in Current Research, Part C; Geol. Surv. Can., Paper 79-1C.

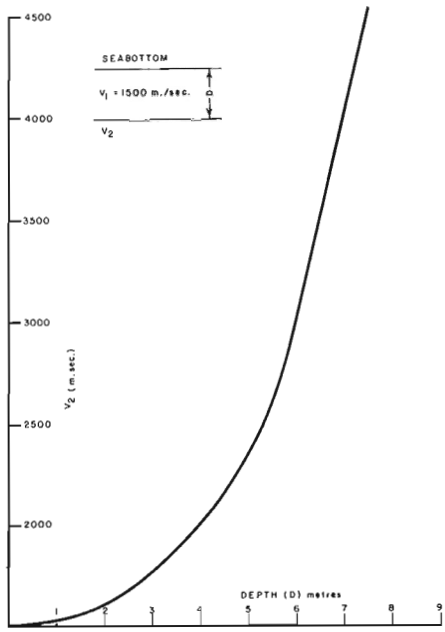

Figure 3. Maximum depth of penetration of refracted waves for a two layer sub-seabottom case with the first layer velocity of 1500 m/sec. The depth of penetration increases with increasing velocity contrast.

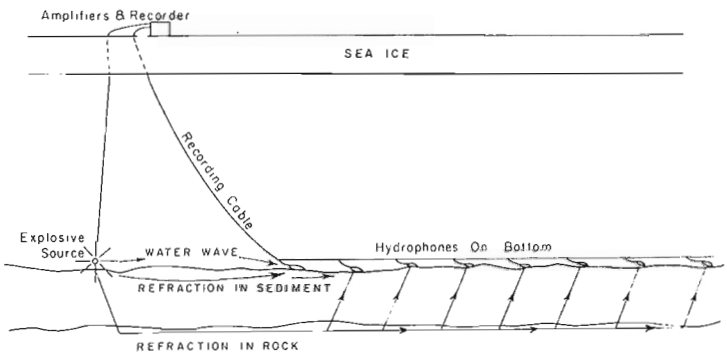

Figure 4. Geometry of 180 m 12 channel array deployed on seabottom.

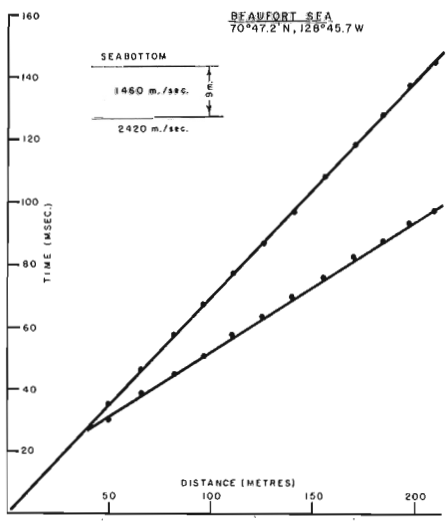

Figure 5. A composite first arrival travel time plot for forward and reverse seabottom refraction shooting at a site in the southern Beaufort Sea. The bottom velocity of 2080 m/s indicates a limited degree of ice-bonding. The lower layer velocity of 4320 m/s at depth of 26 m indicates ice-saturated coarse grained materials.

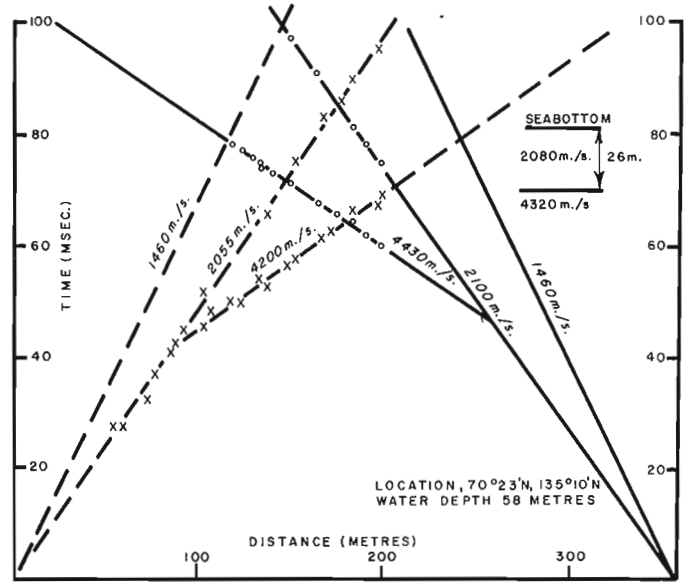

Figure 6. A single-ended first arrival plot for the 180 m array in the eastern Beaufort Sea in 33 m of water indicating ice-bonded permafrost at a depth of 9 m below seabottom.

The array has been tested at 18 sites in the Beaufort Sea for ice-bonded permafrost determinations using available leads in the sea ice. The array is laid out on the ice surface alongside the lead and lowered under tension to the seabottom. Accurate shot-hydrophone distances cannot be established from ice-surface since the ice is often in motion, hence, the first arrival water wave must be identified on each seismic trace; using an average water velocity, the distance may be computed. Successive shots may be detonated at greater distances from each end of the array to obtain deeper penetration. Figures 5 and 6 show plots of first arrival refractions from sites in the Beaufort Sea where ice-bonded permafrost was encountered below seabottom.

From out testing experience we found that the array could be deployed by two men using a small (Bell 206) helicopter for transport and the site survey completed within 1 to 2 hours. Speed of deployment is necessary in rapidly moving ice since the array may develop nonlinear geometry (resulting in difficult interpretations of water wave events); also the leads may close. Velocity-depth structure has been obtained to depths up to 60 m below seabottom with this array; deeper penetration may be possible using larger shot offsets and larger charges of dynamite.

The use of this array is currently limited to available leads in sea-ice and can only be considered for reconnaissance surveys rather than site investigations; however, for ice covered areas where no leads are available, devices may be available in future to enable deployment of the array through holes drilled in the ice. Shipboard use requires the array to be deployed while the ship is under way and subsequently stopping or anchoring during shooting.

Summary

Two seabottom-laid refraction arrays have been developed and shown adequate for use in ice-covered waters capable of providing velocity-depth information to depths of 7 m and 60 m respectively. Such velocity data can be used in the interpretation of high resolution seismic reflection surveying and in the identification of sub-seabottom materials.

Reference

Hunter, J.A., Judge, A.S., MacAulay, H.A., Good, R.L., Gagné R.M., and Burns, R.A.

1976: Permafrost and frozen sub-seabottom materials in the southern Beaufort Sea, Beaufort Sea Project, Technical Report no. 22, Department of Environment, Victoria, British Columbia, 174 p.

A NEW MINERAL OCCURRENCE OF UNKNOWN ECONOMIC POTENTIAL IN NORTHERN YUKON TERRITORY

Project 610007

D.K. Norris
Institute of Sedimentary and Petroleum Geology, Calgary

In the course of field checking geological maps at a scale of 1/250,000 of part of northern Yukon Territory during the summer of 1979 the writer discovered red-weathering goethite (hydrous iron oxide) breccia several feet thick plastering the valley bottom at the headwaters of an unnamed, westward-flowing tributary to Salmon Fork River. Because of limited helicopter fuel, examination of the goethite was restricted to one exposure (Fig. 1), which was subsequently found to contain anomalously high zinc values. The valley warrants further prospecting, because occurrences of similar appearance were observed from the air nearby (Fig. 2).

Figure 1. *Aerial view to the northeast of goethite breccia plastered to valley bottom at the Salmon Fork mineral occurrence, G.S.C. Loc. C-80678. I.S.P.G. Photo No. 1355-1.*

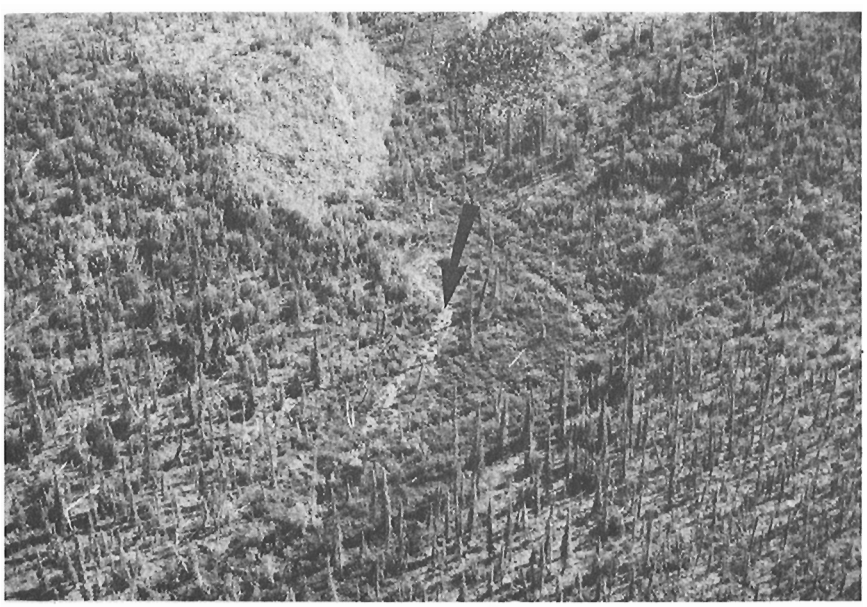

Figure 2. *Aerial view to the southeast of blood red soil in gully one km south of G.S.C. Loc. C-80678. I.S.P.G. Photo No. 1355-2.*

The mineral occurrence, herein termed "Salmon Fork" lies in unglaciated terrain in the Porcupine Ranges (Bostock, 1970) in the Porcupine River map-area [116 J, K(E/2)] (Norris, 1979) at Geological Survey of Canada Locality C–80678. Its longitude is approximately 140°37'28" West and its latitude 66°31'42" North. The precise position of the locality (Norris, 1972) can be identified on National Air Photo Library vertical photograph A 13138-97 at the following Cartesian co-ordinates measured with respect to the centre of the picture, where the positive Y-axis coincides with true north: X=+0.50 cm, Y=+4.32 cm. According to the Supervising Mining Recorder for the Department of Indian and Northern Affairs in Whitehorse, Yukon Territory, the occurrence has not been staked (B.R. Baxter, pers. comm., Oct. 1, 1979). The nearest known mineralization is the Rusty Springs zinc, copper and silver prospect owned by Rio Alto Exploration Ltd. The Salmon Fork occurrence is 11.5 km on a bearing N82°W from Rusty Springs.

The Salmon Fork occurrence is located in a highly deformed fault block bounded by curviplanar, high-angle reverse and/or normal faults. The undifferentiated Upper Paleozoic, sedimentary succession within the block is buckled into acute, north-trending folds cut by longitudinal, steeply dipping reverse faults. Several such blocks lie in a generally north-trending array peripheral to the Mesozoic rocks of the Kandik Basin immediately east of the 141st Meridian (see Norris, 1979). They are flanked on the northwest by the Salmon Fault, a major, northeast-trending discontinuity responsible for Laramide uplift of the Precambrian and Lower and Middle Paleozoic rocks of the Keele Range.

Because of very poor exposure (which led the writer to the occurrence in the first place) the bedrock beneath the Salmon Fork occurrence was not seen. It is presumed, however, to be similar to that exposed on a bare, rounded hill immediately to the southwest and somewhat lower in the stratigraphic succession. There the outcrop (G.S.C. Loc. C-80688) comprises cherty, variably dolomitic, light grey, fine grained limestone containing sparse microfauna and rare, relief weathered, undetermined brachiopods. According to B.L. Mamet, University of Montreal (pers. comm., Oct. 3, 1979) the microfauna is of Pennsylvanian (middle Pennsylvanian or slightly younger) age, and the limestone is accordingly coeval with the Ettrain Formation.

The general lack of good exposures would suggest that there may be significant amounts of shale and other fine clastic rocks associated with these limestones and that the succession is at or near the western edge of the Pennsylvanian carbonate platform outlined by Bamber and Waterhouse (1971, Fig. 13).

Representative samples of the red-weathering breccia and water from the creek flowing over it were collected for chemical analysis. According to A.E. Foscolos (pers. comm., Oct. 9, 1979) the mineral composition of the breccia on the basis of X.R.D. is quartz

From: Scientific and Technical Notes in Current Research, Part C; Geol. Surv. Can., Paper 79-1C.

64 per cent, goethite 32 per cent, and illite 4 per cent. Wet chemistry revealed zinc 2100 ppm, nickel 121 ppm, copper 24 ppm, and hematite 87 per cent. Zinc concentration in the water is 0.1 ppm.

The mineralization at Salmon Fork appears to be derived from undifferentiated Carboniferous and Permian carbonate and clastic rocks (Unit CP of Norris, 1979) and may represent leaching from primary iron and zinc ores hosted in these rocks higher on the valley walls. Should this be so, the Salmon Fork occurrence differs from that at Rusty Springs where the mineralization is reported in Middle Devonian limestones (Rio Alto Exploration Ltd., Annual Report, 1976).

As far as the writer is aware, this is the first reported occurrence of base metal mineralization that may be hosted at this stratigraphic level in the northern Canadian Cordillera. Should the mineralization be stratabound, it could herald renewed and accelerated interest in the mineral potential of Yukon Territory and adjacent Alaska because these rocks at or near the edge of the Upper Paleozoic carbonate shelf are widespread in both the Porcupine Ranges and the Ogilvie Mountains.

The writer deeply appreciates the support provided by E.W. Bamber, B.R. Baxter, A.E. Foscolos and B.L. Mamet in the preparation of this report.

References

Bamber, E.W. and Waterhouse, J.B.
1971: Carboniferous and Permian Stratigraphy and Paleontology, northern Yukon Territory, Canada, Bulletin of Canadian Petroleum Geology, v. 19, p. 29-250.

Bostock, H.S.
1970: Physiographic Regions of Canada; Geological Survey of Canada, Map 1254A.

Norris, D.K.
1972: A method for the determination of geographic position; Geological Survey of Canada, Report of Activities, Part B, Paper 72-1B, p. 124-125.

1979: Geological Maps of northern Yukon Territory; Geological Survey of Canada, Open File 621*.

*Copies of these maps may be obtained at the user's expense from Riley's Data Share International Limited, Box 6730, Station "D", Calgary, Alberta, T2P 2V8; Resident Geologist's Office, Department of Indian and Northern Affairs, 200 Range Road, Whitehorse, Yukon Territory, Y1A 3V1; and the Resident Geologist's Office, Department of Indian and Northern Affairs, Bellanca Building, Box 1500, Yellowknife, Northwest Territories, X1A 2R3.

AGE DETERMINATIONS ON MARINE AND TERRESTRIAL MATERIALS OF HOLOCENE AGE, SOUTHERN ELLESMERE ISLAND, ARCTIC ARCHIPELAGO

W. Blake, Jr.
Terrain Sciences Division

Introduction

Marine mollusc shells frequently have been used for radiocarbon age determinations because they are the most abundant type of material available along many of the world's coasts. Canada is no exception in this regard, and the earliest age determinations on shells from the Canadian Arctic Archipelago and adjacent northwestern Greenland were carried out more than two decades ago by laboratories at Lamont Geological Observatory, New York (Broecker et al., 1956) and by the U.S. Geological Survey, Washington, D.C. (Suess, 1954). At the same time that marine shells were being widely used for dating, doubts were voiced on numerous occasions as to their validity (e.g. see Shotton, 1967). This note re-emphasizes some of the results obtained by comparative dating of terrestrial and marine materials at one locality in southern Ellesmere Island and presents new data from a second locality.

Data from Cape Storm

In an earlier paper radiocarbon age determinations carried out on a variety of materials – driftwood, whale bones, and marine pelecypod shells – from an exceptionally well developed sequence of raised beaches at Cape Storm, southern Ellesmere Island were discussed (Blake, 1975a). For that site an emergence curve for Holocene time was constructed on the basis of 25 age determinations on driftwood logs imbedded in shingle beaches. The wood samples, mainly spruce (**Picea** sp.) and larch (**Larix** sp.), were collected between 1.0 and 71.0 m a.s.l.; their ages range from modern (GSC-1378) to 8300 ± 70 years (GSC-845). Numerous age determinations were also carried out on five whale bones excavated from the same series of beaches; in four of five cases both the collagen and bone apatite fractions were utilized for dating. The uppermost samples in the series, aragonitic **Mya truncata** shells at 100.5 to 101.0 m a.s.l. and whale bones at 118.0 m, gave closely similar ages: 9350 ± 80 years (GSC-1488, outer fraction of shells), 9370 ± 100 years (GSC-1488, inner fraction of shells), and 9340 ± 80 years (GSC-1496-3, a previously unpublished age on whale bone collagen). These values, all of which include a correction for isotopic fractionation, fit well with the lower part of the emergence curve as defined by the age determinations on driftwood. Two conclusions resulting from the studies at Cape Storm follow:

1. Numerous cross-check age determinations between driftwood and whale bones have shown that in this type of arctic environment, utilizing the organic (collagen) fraction of whale bones for radiocarbon dating gives reliable results, whereas in most cases determinations on the bone apatite fraction give ages that are too young.

2. Holocene marine molluscs yield reliable ^{14}C age determinations, even in areas where carbonate rocks are widespread, such as southern Ellesmere Island and northern Bathurst Island.

Despite the availability of examples such as those summarized above, and other data presented by Blake (1975a), doubt persists with regard to the validity of radiocarbon age determinations on marine mollusc shells. In a recent review paper dealing with Arctic coasts, Andrews (1978, p. 383) stated correctly that:

> "There is a strange reluctance on the part of many to recognize that dates on marine shells provide useful and reliable radiometric ages. Why this is so is difficult to understand, especially for workers in arctic areas where probably 90 per cent of our Holocene dates are based on dates reported from assays of marine carbonates."

He then goes on to ask (Andrews, 1978, p. 384):

> "There is also the unanswered question of how does a terrestrial peat or wood sample, dated 8000 BP, compare with a date of 8000 BP on marine shells?"

Data from Swinnerton Peninsula, Makinson Inlet

A series of age determinations, close to 8000 years old, is now available on collections made in 1977 on Swinnerton Peninsula, southeastern Ellesmere Island (Fig. 1). This site, although also in an area where the bedrock is dominated by Paleozoic carbonates, differs from Cape Storm in that the materials whose ages are being compared were extracted from a section of calcareous stony silt exposed at about 42 m a.s.l. along a stream, rather than from shingle beaches. Because shells of identical age to those in the river section were collected close to 82 m a.s.l. on the ground surface 3 km to the west, it is clear that the silt was deposited at a depth of more than 40 m. Details of the collection site are shown in Figures 2 to 4, and pertinent data with regard to the age determinations are presented in Table 1. The dated shells (GSC-2701; ± 100 years, inner fraction), comprising 10 intact pairs of the common arctic pelecypod, **Mya truncata** L., were all collected in the position in which they lived and in which they were buried by subsequent deposition of sediment. The shells varied between 4.1 and 3.3 cm in length and 3.4 and 2.4 cm in height. The sample of **Salix** sp., collected near the base of the same 1.7 m-thick unit, appeared to represent most of a small Arctic willow "tree", including the main

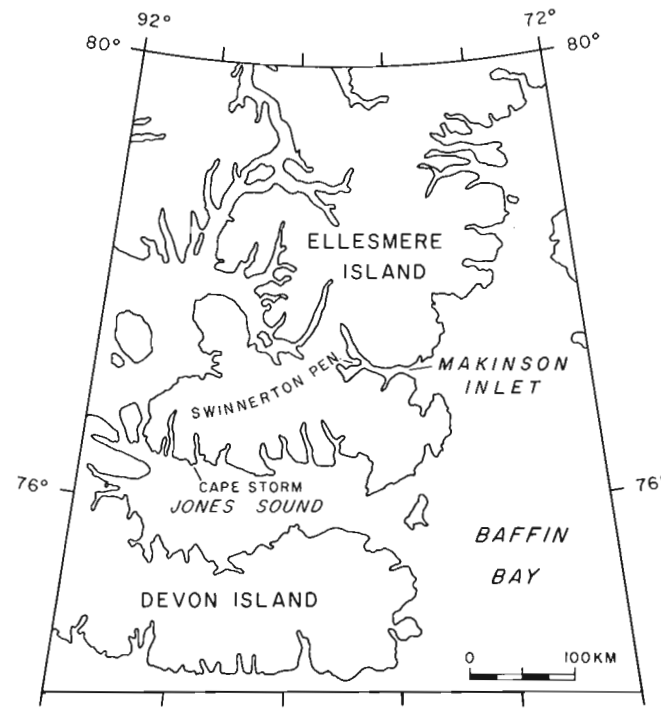

Figure 1. *Location map, southeastern Ellesmere Island.*

From: Scientific and Technical Notes in Current Research, Part C; Geol. Surv. Can., Paper 79-1C.

Table 1

Radiocarbon age determinations, Swinnerton Peninsula

Sample elevation m a.s.l.	Dated material[1]	Field Sample No.	Laboratory dating No.	Uncorrected ^{14}C age	$\delta^{13}C$ ‰	Corrected ^{14}C age[2]	Sample weight (g)	Counter (L)	Pressure (atm)	Counting time (days)	Comments
~82	Marine shells **(Hiatella arctica)**	BS-77-277	GSC-2692	8060 ± 70	+1.4	8090 ± 70	46.4	5	1	3	Highest collection of Holocene shells. Contemporaneous sea level probably several metres higher. Aragonite.
~42	Marine shells **(Mya truncata)**	BS-77-253B	GSC-2701	8010 ± 110	+1.8	8040 ± 110	59.2	2	2	2	Outer fraction (11-55%). Outermost 10% removed by HCl leach. Aragonite.
			GSC-2701	8060 ± 100	+1.7	8090 ± 100		2	2	3	Inner fraction (56-100%).
~42	Wood **(Salix** sp.)	BS-77-249	GSC-2712	7970 ± 110	-28.3	7920 ± 110	7.3	2	2	2	Sample mixed with dead gas for counting.
~40	Marine shells **(Hiatella arctica)**	BS-77-256	GSC-2519	8910 ± 100	+1.4	8930 ± 100	46.0	2	1	5	Lowermost shells in the section exposed along this stream (Blake, 1978). Aragonite.

[1] Determinations of pelecypod species by W. Blake, Jr. The wood sample was identified by L.D. Farley-Gill (unpublished GSC Wood Identification Report 78-28). Determinations of shell mineralogy by X-ray diffraction were carried out by A.C. Roberts, Mineralogy Section.

[2] All age determinations from the Radiocarbon Dating Laboratory, Geological Survey of Canada, are based on a ^{14}C half-life of 5568 ± 30 years and 0.95 of the activity of the NBS oxalic acid standard. Ages are quoted in conventional radiocarbon years before present (B.P.), where "present" is taken to be 1950. All finite age determinations from this laboratory are based on the 2σ criteria, i.e., there is a 95% probability that the correct age in radiocarbon years lies within the stated limits of error. $^{13}C/^{12}C$ ratios were determined at the Department of Earth Sciences, University of Waterloo, under the direction of Professor P. Fritz and R. Drimmie (DSS contracts OSU77-00021 and OST78-00037). Relative to the PDB standard it is GSC practice to normalize $\delta^{13}C$ values on terrestrial organic materials to -25.0 ‰ , whereas marine shells are normalized to 0.0 ‰ (Lowdon and Blake, 1970).

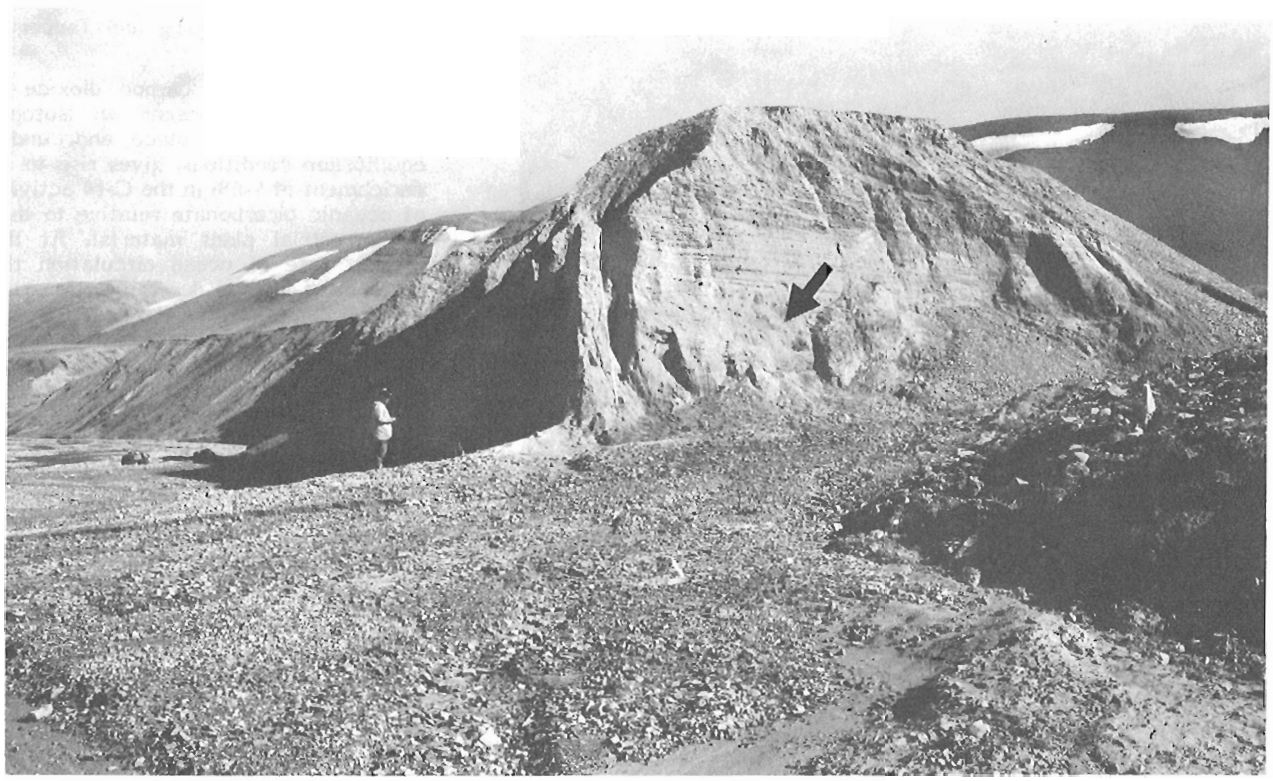

Figure 2. *View northward at the section exposed along a stream near the southern coast of Swinnerton Peninsula. The 1.7 m-thick stony silt unit containing both willow and pelecypod shells is indicated by the black arrow. August 1-2, 1977 (GSC 174612).*

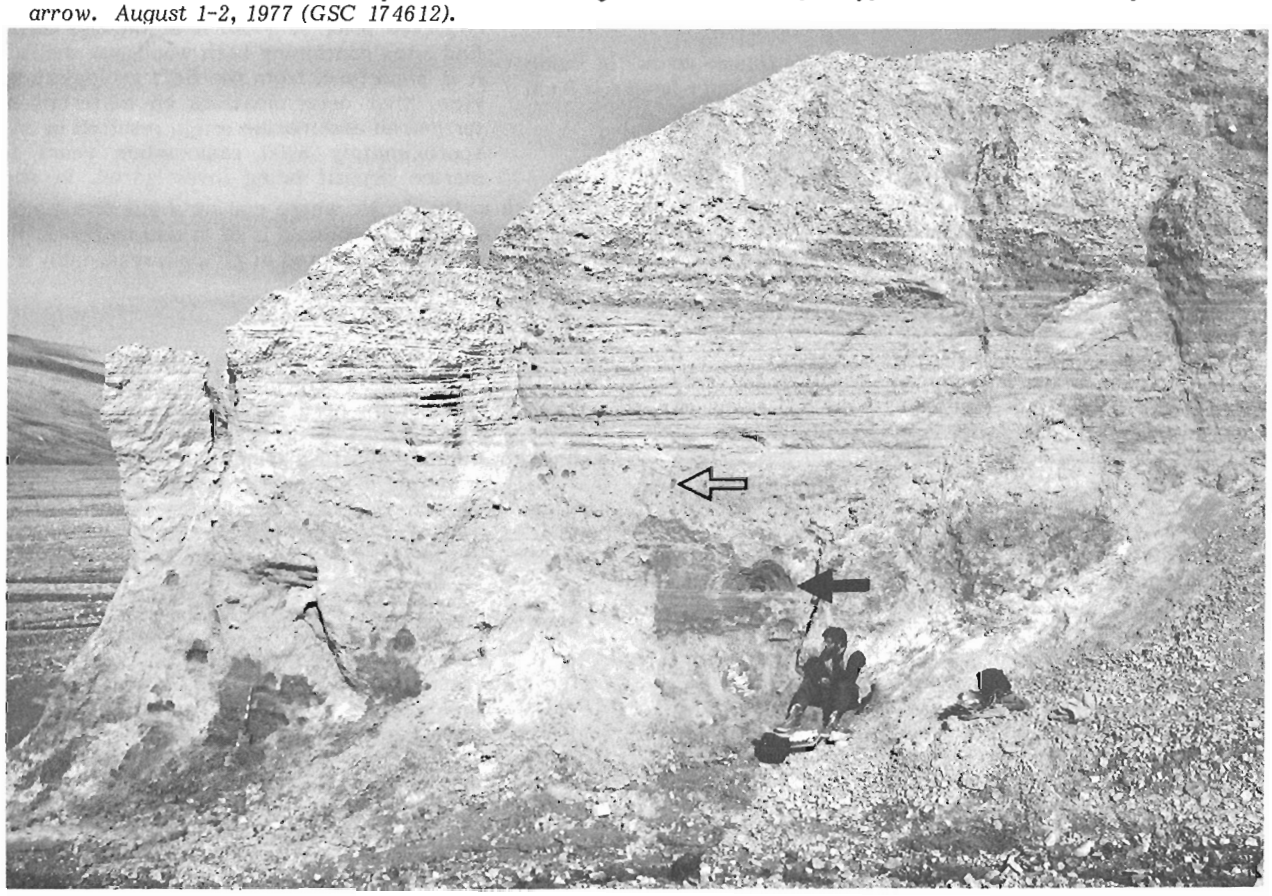

Figure 3. *Detail of the massive stony silt unit at the exposure shown in Figure 2. The willow was excavated at the base of this unit (black arrow); the in situ pelecypods were collected higher in the same unit (the open arrow indicates the position of the paired* ***Mya truncata*** *valve shown in Fig. 4). August 1-2, 1977 (GSC 174605).*

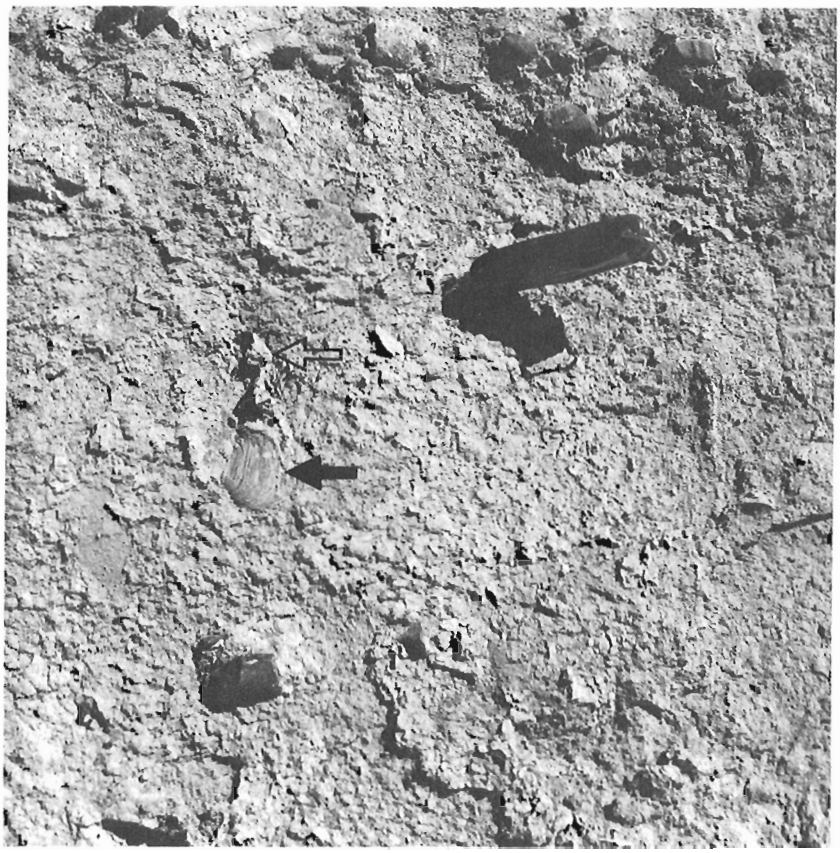

Figure 4. Detail of paired ***Mya truncata*** *valves (black arrow) in living position with attached siphon sheath (open arrow). The knife handle is 9 cm in length. August 1-2, 1977 (GSC-174601).*

stem, plus several branches (with bark still attached in places) and roots. The longest branch was more than 25 cm in length. The age of this piece of wood is 7920 ± 110 years (GSC-2712).

Discussion

When dealing with marine pelecypods, a factor that must be considered is the apparent age of the sea water in which these invertebrates lived, because a certain amount of time is required for atmospheric CO_2 to mix with the surface water of the sea. The correction necessary for Ellesmere Island has been discussed by Mangerud and Gulliksen (1975) and by Blake (1975a,b). Additional age determinations on material collected alive in Ellesmere Island waters by the Second Norwegian Arctic Expedition in the "Fram", 1898-1902, and the Danish Godthaab Expedition, 1928, have been made in recent years in the Radiocarbon Dating Laboratory, Geological Survey of Canada; it appears now that a somewhat smaller correction than the 350 years used earlier might be more appropriate. For the purposes of this paper, however, the amount of the correction is not of great importance. If, as earlier, a correction of -350 years is applied to the age determinations in Table 1, it would have the effect of making the shells above the wood 7740 ± 100 years old (GSC-2701, inner fraction), an age in agreement with the stratigraphic position of the samples. If a correction of -300 years is used, the corresponding value for GSC-2701 would be 7790 ± 100 years, etc. The ages of the other marine samples in this suite would have to be changed by the same amount.

On the other hand, as Krog and Tauber (1974) have pointed out:

> "When atmospheric carbon dioxide is absorbed in the oceans an isotopic fractionation takes place and, under equilibrium conditions, gives rise to an enrichment of 4-6% in the C-14 activity of oceanic bicarbonate relative to that of terrestrial plant material. At the present rate of ocean circulation the enrichment in C-14 due to fractionation and the depletion in C-14 due to ocean circulation almost cancel. In the upper mixed layers of the North Atlantic, and in the adjacent seas with a pronounced marine influence, the C-14 activity of ocean bicarbonate, and of marine shells, therefore broadly equals the C-14 activity of contemporary organic terrestrial material."

Thus a certain rationale exists for not attempting to correct for the "apparent age" (or "reservoir effect") of sea water. Nevertheless, in the case of the site on Swinnerton Peninsula, even better correlation between age and stratigraphic position is achieved when the dates on shell carbonate are corrected to compensate for the mixing time between atmospheric CO_2 and the surface water of the sea.

Unfortunately, for many localities in the Arctic it is difficult, if not impossible, to obtain the necessary control samples, i.e., molluscs collected prior to 1950. It is likewise difficult to find sites containing both wood and shells. Hence it is important, from the field geologist's point of view, that determinations on materials of both terrestrial and marine origin resulted in an age of approximately 8000 radiocarbon years for the marine deposit being investigated. In situations elsewhere in the Arctic where marine shells occur alone, and where the assemblage utilized is of in situ molluscs, the date obtained also can be accepted as giving a reasonably accurate age for the enclosing strata.

Conclusions

The new age determinations (GSC-2692, -2701, and -2712) reported here from Swinnerton Peninsula, Ellesmere Island, confirm earlier results from Cape Storm which showed that in situ marine mollusc shells are reliable materials for dating in the arctic environment. An additional new age determination on the collagen fraction of a whale bone (GSC-1496-3) from Cape Storm shows good agreement with the ages of nearby marine mollusc shells.

Acknowledgments

It is a pleasure to record my appreciation for the base camp facilities provided at Makinson Inlet in 1977 by T. Frisch, Regional and Economic Geology Division, and the logistical support of the Polar Continental Shelf Project (G.D. Hobson, Director). R.J. Richardson assisted in the collection of samples in the field. L.D. Farley-Gill and A.C. Roberts identified the wood sample and determined the mineralogical composition of the shell samples, respectively. The age determinations were carried out in the Radiocarbon Dating Laboratory under the supervision of J.A. Lowdon, who also provided a number of suggestions for the improvement of the manuscript.

References

Andrews, J.T.
1978: Sea level history of arctic coasts during the Upper Quaternary: dating, sedimentary sequences, and history; Progress in Physical Geography, v. 2, p. 375-407.

Blake, W., Jr.
1975a: Radiocarbon age determinations and postglacial emergence at Cape Storm, southern Ellesmere Island, Arctic Canada; Geografiska Annaler, Series A, v. 57, p. 1-71.

1975b: Pattern of postglacial emergence, Cape Storm and South Cape Fiord, southern Ellesmere Island, N.W.T.; in Report of Activities, Part C; Geological Survey of Canada, Paper 75-1C, p. 69-77.

1978: Aspects of glacial history, southeastern Ellesmere Island, District of Franklin; in Current Research, Part A; Geological Survey of Canada, Paper 78-1A, p. 175-182.

Broecker, W.S., Kulp, J.L., and Tucek, C.S.
1956: Lamont natural radiocarbon measurements III; Science, v. 124, p. 154-165.

Krog, H. and Tauber, H.
1974: C-14 chronology of Late- and Post-glacial marine deposits in North Jutland; Danmarks Geologiske Undersøgelse, Årbog 1973, p. 93-105.

Lowdon, J.A. and Blake, W., Jr.
1970: Geological Survey of Canada radiocarbon dates IX; Radiocarbon, v. 12, p. 46-86.

Mangerud, J., and Gulliksen, S.
1975: Apparent radiocarbon ages of recent marine shells from Norway, Spitsbergen, and Arctic Canada; Quaternary Research, v. 5, p. 263-273.

Shotton, F.W.
1967: The problems and contributions of methods of absolute dating within the Pleistocene period; Quarterly Journal of Geological Society of London, v. 122, p. 356-383.

Suess, H.E.
1954: U.S. Geological Survey radiocarbon dates I; Science, v. 120, p. 467-473.

ELECTRON MICROPROBE ANALYSIS OF A SELENIFEROUS BISMUTH SULPHOSALT: CORRECTION FOR MATRIX EFFECTS

Project 620308

G.J. Pringle
Central Laboratories and Administration Services Division

Introduction

Electron microprobe analysis of any material involves firstly the determination of an observed X-ray count ratio of sample to standard for each element being determined and secondly the correction of these ratios to account for the effect of other elements in the matrix. In most laboratories the favoured approach to evaluating the matrix contribution is to calculate correction factors based on a detailed mathematical treatment of X-ray generation. This is often referred to as the ZAF approach. (Sweatman and Long, 1969), (Beaman and Isasi, 1970, 1972). The ZAF program currently in use in this laboratory was developed at CANMET by combining the programs EMPADR VII (Rucklidge and Gasparrini, 1969) and MAGIC IV (Colby). This approach to matrix correction appears to be adequate for most purposes, however when analyses are to be used for the calculation of mineral formulae a particularly high degree of accuracy is required. It has been recognized for some time that the ZAF programs currently in use do a less than adequate job for some minerals with major contents of the heavier elements. Examples include robinsonite ($Pb_4Sb_6S_{13}$ - Jambor and Plant, 1975), stannite ($Cu_2(Fe,Zn)SnS_4$ - Kissen and Owens, 1974), and junoite ($Bi_8Pb_3Cu_2(Se,S)_{16}$ - Large and Mumme, 1975).

A second method of matrix correction involves the use of correction coefficients derived from measurements on known standards, preferably binary alloys. Such a correction scheme has been outlined by Lachance (1970) Lachance and Traill (1966) and Traill and Lachance (1965) and is here used to correct an analysis of junoite from the Kidd Creek mine. The same correction factors have also been applied to the data in Large and Mumme (1975) for material from the Australian location.

General Relationships

Following the Lachance-Traill derivation, the effect of element j on the measured intensity of element i is expressed as

$$\alpha_{ij} = \frac{W_i/R_i - 1}{W_j} \qquad (1)$$

where W is the true concentration and R is the concentration as observed against the pure metal. In a sample with n elements the observed concentration of element i is then converted to a corrected concentration by -

$$W_i = R_i (1 + \alpha_{ij} W_j + \alpha_{ik} W_k + \alpha_{in} W_n) \qquad (2)$$

If each alpha coefficient in this equation has been independently evaluated, then a corrected analyses may be arrived at by solving n linear equations of this form.

A ZAF correction program may be used to generate calculated values of alpha, based on fundamental parameters. The matrix correction provided by these calculated alphas will duplicate the correction provided by the ZAF program. (Fig. 1). Experimentally determined alpha coefficients are best evaluated by measurement of binary standards versus pure metal standards and using equation (1). Commonly, suitable binary standards are not available and more complex standards must be used. If for example, a ternary standard is being used then one coefficient must be available from a previous source. In this case equation (2) becomes

$$W_i = R_i (1 + \alpha_{ij} W_j + \alpha_{ik} W_k) \qquad (3)$$

If α_{ik} is already known then α_{ij} may be derived from the measurement of R_i and the solution of (3).

It is also possible to evaluate alpha coefficients by extrapolating between already determined coefficients. If alpha is plotted versus atomic number it can be shown that the variation is regular over short distances.

In binary materials, alpha varies with the relative concentrations of elements i and j (Fig. 2). The magnitude of the correction is variable (Fig. 1) and often cannot be measured experimentally since suitable suites of standards are not always available. For the purposes of this study the slope of α_{ij}, for changing relative concentrations of i and j in a binary, is presumed to be the same as the slope in calculated values. In ternary and more complex materials this effect on the value of alpha is best evaluated by extrapolating to the concentration level of the element measured (Lachance, 1979). For example, in Figure 2 $\alpha_{SCu} = 0.74$, is a measured value on a binary standard with 66% copper. For a ternary material with 10 wt % sulphur the applicable value of α_{SCu} becomes 0.74-0.04=0.68, that is, the value at the 90% level of elements other than sulphur in the ternary. In this way the experimentally determined alpha coefficients in this study have been adjusted for concentration dependencies using slopes generated by a ZAF program.

The physical properties of some elements preclude their use in the experimental evaluation of alpha in equation (1). In this case compound standards must be substituted and the effect of the additional elements in the standards must be accounted for. Equation (1) may be recast as

$$R_i = \frac{W_i}{1+\alpha_{ij} W_j} \qquad (4)$$

If α_{ij} for a binary standard is known, then evaluation of (4) will give a value R_i^{std} which is the observed concentration of i in the binary standard expressed as a fraction of the pure metal. If I^{samp} and I^{std} are the observed count rates in an analyses of a sample against the binary standard then -

$$R_i \text{ samp} = \frac{I^{samp}}{I^{std}} \times R_i^{std} \qquad (5)$$

where R_i^{samp} is the appropriate value to enter in equation (2).

Experimental Procedure

A MAC instrument was used with operating conditions as follows: 35° take-off angle, 25 KV,0.03 microamperes sample current on chalcopyrite, L_α lines for lead and bismuth, K_α lines for the remaining elements and LiF crystals for all determinations except SK_α on PET. Pure metal standards were used except for sulphur and lead which were determined against pyrite (FeS_2) and galena (PbS).

It has been shown in the previous section that in order to successfully use pyrite as a sulphur standard it is necessary to establish a reliable value for α_{SFe}. The ratio $\frac{I^{FeS}}{I^{FeS_2}} = 1.56$ was experimentally measured on pyrite (FeS_2) versus a synthetic troilite standard(FeS). The ZAF program predicts a

From: Scientific and Technical Notes in Current Research, Part C; Geol. Surv. Can., Paper 79-1C.

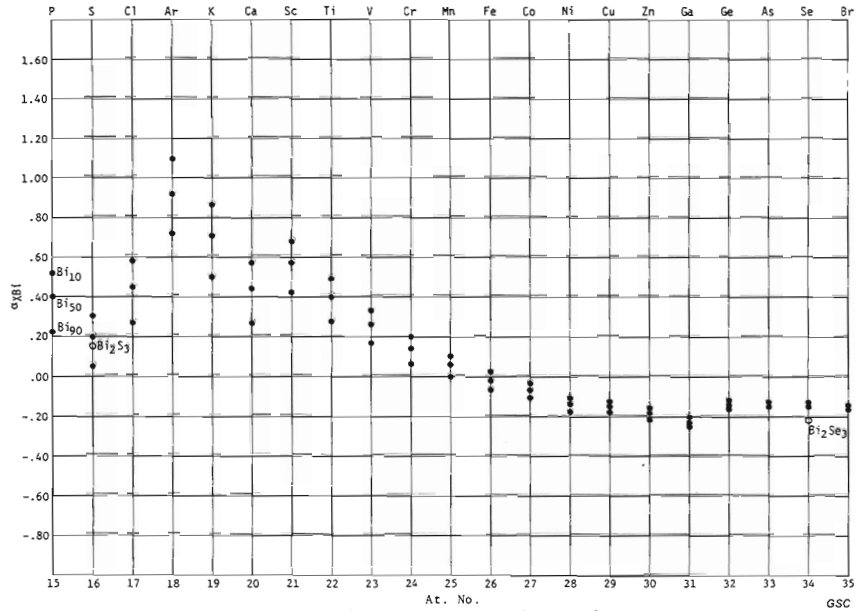

● = calculated o = experimental

Figure 1. *Effect of Bi on element X.*

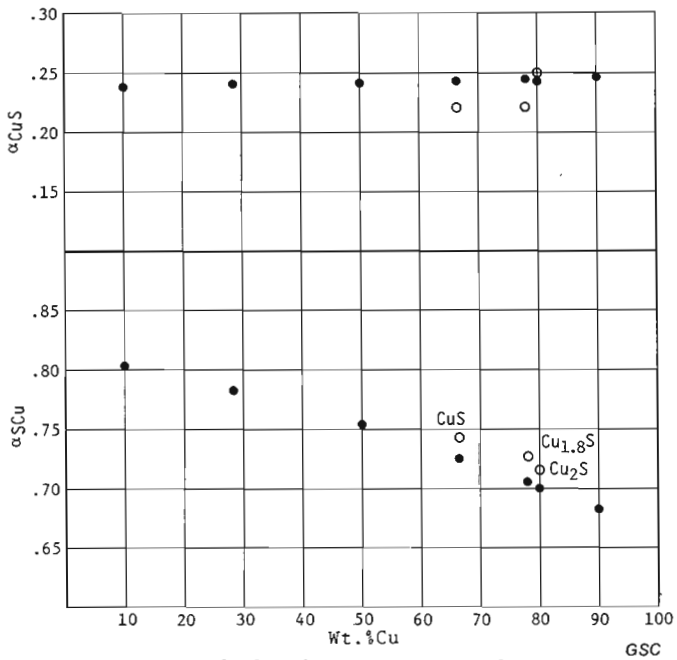

● = calculated o = experimental

Figure 2. *Calculated and experimental alpha factors with varying concentration in the Cu-S binary system.*

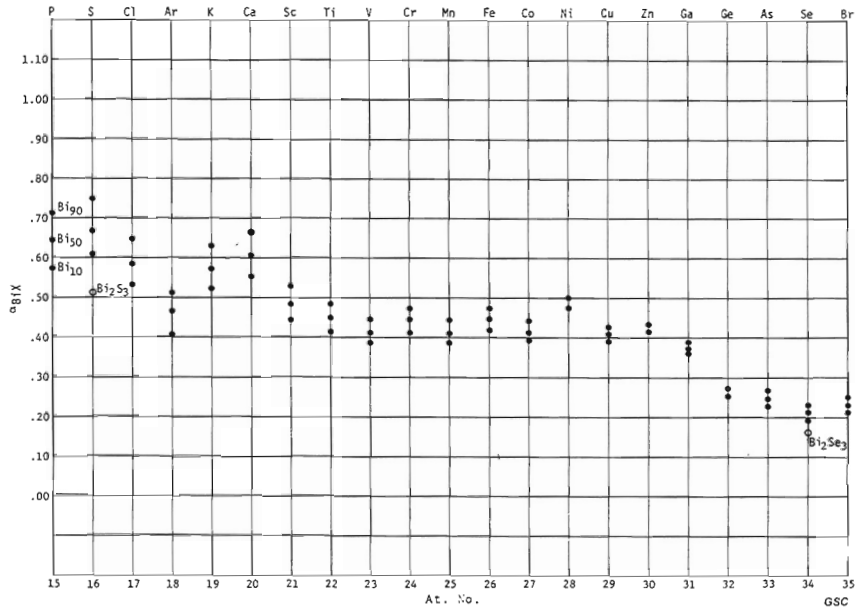

● = calculated o = experimental

Figure 3. *Effect of element X on Bi.*

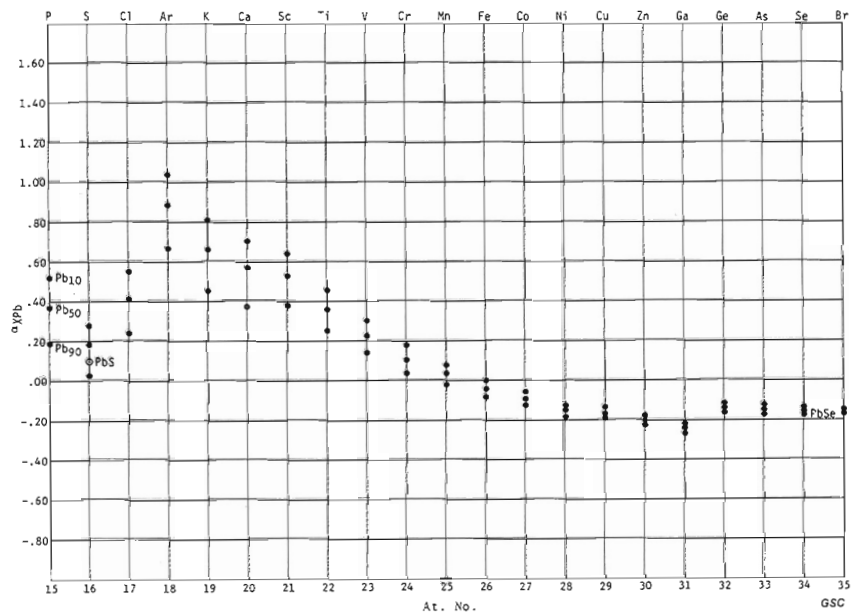

● = calculated o = experimental

Figure 4. *Effect of Pb on element X.*

value of 1.55 for the same ratio, therefore it is assumed that calculated values of α_{SFe} are reliable. Where galena has been used as a standard an assumed value of α_{PbS} has been used. This value was deduced from measurements on a Bi_2S_3 standard.

Evaluation of Alpha

The correction for matrix effects in an analysis of junoite (approx. $Bi_8Pb_3Cu_2(Se,S)_{16}$) requires the solution of five linear equations in the form of equation 2 and the evaluation of twenty individual coefficients. Table 1 gives the experimentally determined alpha coefficients compared with calculated values and also values finally chosen to correct the analyses of junoite.

The calculated values for factors involving lead and bismuth do not show any significant differences (Fig. 1, 4, Table 1), therefore it can be assumed that experimentally determined factors for bismuth may be substituted for lead factors. The values for α_{PbS} and α_{PbSe} were derived in this way from the experimental values of α_{BiS} and α_{BiSe} (Table 1).

In Figures 1, 4 and 6 the discrepancies between experimental and calculated values are within analytical precision. The calculated values of α_{SeBi}, α_{SBi}, α_{SePb} and α_{SPb} have been taken as the most appropriate.

Table 1

			α_{ij} standards		α_{ij} junoite	
i	j	Standard	experimental	calc*	experimental	calc*
Bi	S	Bi_2S_3	.51	.73	.46	
Bi	Se	$Bi_2Se_{2.5}S_{.5}$	.16	.23	.15	
Bi	Cu	Theor $Bi_{50}Cu_{50}$		.41		.41
Bi	Pb					.00
Pb	S				.40**	
Pb	Se				.14**	
Pb	Cu	Theor $Pb_{50}Cu_{50}$		.42		.41
Pb	Bi					.00
Se	S	Extrap. Fig. 5			.31	
Se	Cu	$CuSe_2$	.16	.16	.16	
Se	Bi	$Bi_2Se_{2.5}S_{.5}$	-.21	-.15		-.16
Se	Pb	$PbSe_{.98}S_{.02}$	-.15	-.16		-.16
S	Cu	CuS	.74	.73	.70	
		$Cu_{1.8}S$	.73	.72		
		Cu_2S	.72	.70		
S	Se					1.20 (S = 14%)
						1.17 (S = 10%)
S	Bi	Bi_2S_3	.15	.08		.05
S	Pb	PbS	.11	.04		.03
Cu	S	CuS,$Cu_{1.8}S$	.22	.24	.22	
Cu	Se	CuSe	-.17	-.15	-.20	
		$CuSe_2$	-.19	-.16		
Cu	Bi	Theor $Bi_{50}Cu_{50}$		-.15		-.18
Cu	Pb	Theor $Pb_{50}Cu_{50}$		-.16		-.19

* values derived from ZAF program
** derived from αBiS and αBiSe

Table 2

Junoite, Kidd Creek Mine, Take-off angle = 35°

R_i	From equation 2		ZAF program	
	Total Alpha Correction	wt. % Corrected	Total Correction	wt. % Corrected
Bi .4827	1.083	52.3	1.121	54.1
Pb .1747	1.076	18.8	1.122	19.6
Cu .0421	.916	3.9	.899	3.7
As .0037	1.000	.4	1.000	.4
Fe .0000	1.000	0.0	1.000	0.0
Se .1590	.925	14.7	.937	14.9
S .0817	1.236	10.1	1.212	9.9
		100.2		102.6

Basis 16 (Se,S)

Bi	7.99	Bi	8.33
Pb	2.89	Pb	3.04
Cu	1.96	Cu	1.87
Ag	.12	Ag	.12
Se	5.94	Se	6.07
S	10.06	S	9.93

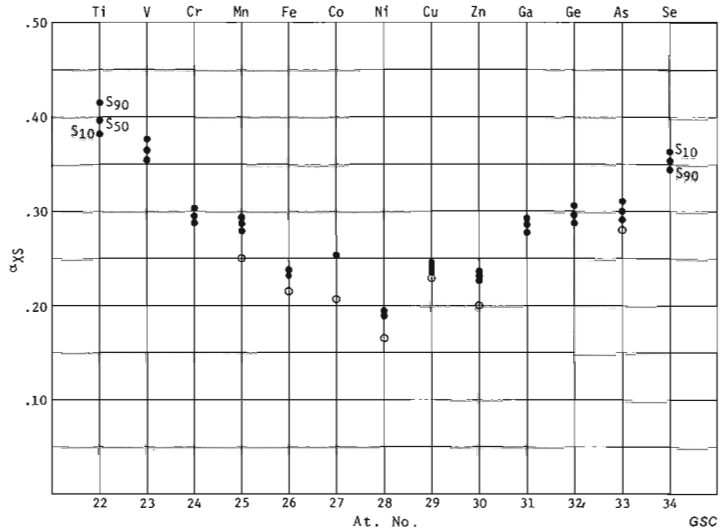

● = *calculated* o = *experimental*

Figure 5. *Effect of S on element X.*

Table 3

Junoite, Juno Mine, Take-off angle = 75°

R_i	From equation 2		ZAF program	
	Total Alpha Correction	wt. % Corrected	Total Correction	wt. % Corrected
Bi .4985	1.097	54.7	1.134	56.5
Pb .1785	1.083	19.3	1.138	20.3
Cu .0484	.846	4.1	.868	4.2
Ag .0010	1.000	.1	1.000	.1
Fe .0010	1.000	.1	1.000	.1
Se .0830	.920	7.6	.940	7.8
S .1322	1.023	3.5	1.021	13.5
		99.4		102.5

Basis 16 (Se,S)

Bi	8.09	Bi	8.32
Pb	2.88	Pb	3.02
Cu	1.99	Cu	2.03
Ag	.03	Ag	.03
Fe	.06	Fe	.06
Se	2.98	Se	3.04
S	13.02	S	12.96

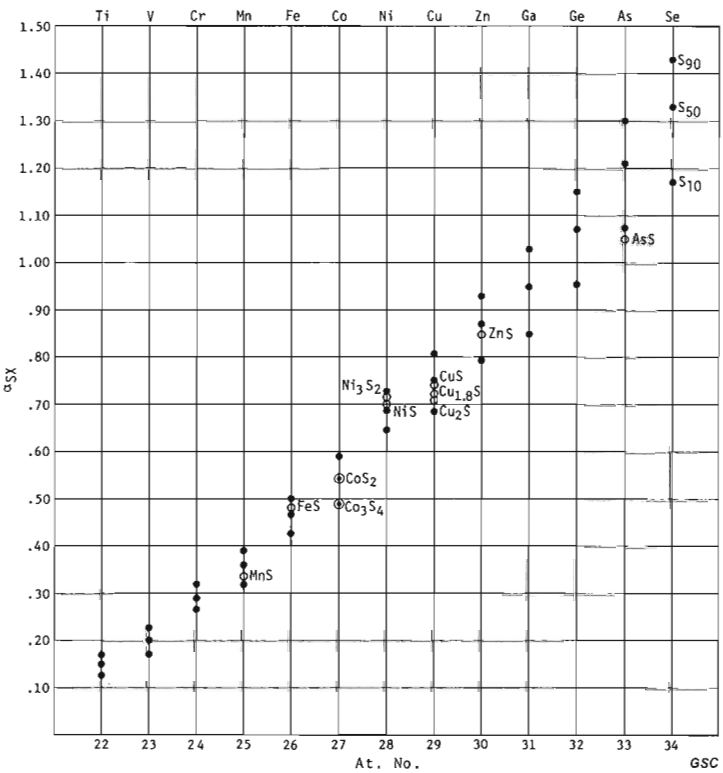

● = *calculated* o = *experimental*

Figure 6. *Effect of element X on S.*

Figure 5 evaluates the effects α_{XS} for elements titanium through selenium. Note that for the experimental results the dependency of alpha on the ratio i/j has not been considered since here the effect is small. In some cases in Figure 5, the experimental results are the averages of determinations on several binary standards, for example the result for α_{CuS} is the average of the determinations shown separately in Figure 2. Figure 5 has been used to obtain the extrapolated value of α_{SeS} used in Table 1.

Experimental values of α_{Scu}, α_{CuS}, α_{SeCu} and α_{CuSe} were chosen over calculated values since these were derived from what are considered to be particularly reliable standards. Standards were not available to evaluate α_{BiPb} and α_{PbBi}.

In summary the principal discrepancies between experimental and calculated values are in the effect on lead and bismuth by selenium and sulphur. There is also a minor but definite discrepancy in the effect of sulphur on selenium and copper.

Junoite Analyses

The factors prepared for Table 1 have been applied to analyses of junoite from the Kidd Creek mine, Timmins, Ont. and the average analyses of junoite from Juno mine, Northern Territory, Australia (Large and Mumme, 1975). The analysis of the Australian material was completed on an instrument with a take-off angle of 75° which is significantly different than the MAC instrument used in this study. The ZAF program was used to reconstruct hypothetical observed intensities (R_i, equation 2) based on the applicable angle for the Australian analysis. Here the assumption is that experimental factors will vary with take-off angle by the same proportion as the variation in calculated values.

It can be seen in Table 2 and 3 that the experimental correction factors have greatly improved the analyses as compared to the stoichiometric formula.

References

Beaman, D.R. and Isasi, J.A.
1970: A critical examination of computer programs used in quantitative electron microprobe analysis; Analytical Chemistry, v. 42, p. 1540-1568.

1972: Electron beam microanalysis: The fundamentals and applications; ASTM STP 506, American Society for Testing and Materials.

Colby, J.W.
MAGIC IV - a computer program for quantitative electron microprobe analysis; Bell Telephone Laboratories, Allentown, Pennsylvania.

Jambor, J.L. and Plant, A.G.
1975: The composition of the lead sulphantimonide, robinsonite; Canadian Mineralogist, v. 13, p. 415-417.

Kissin, S.A. and Owens, D.R.
1979: New data on stannite and related tin sulphide minerals; Canadian Mineralogist, v. 17, p. 125-135.

Lachance, G.R.
1970: Fundamental coefficients for X-ray spectrochemical analysis. Canadian Spectroscopy, v. 15, no. 3, p. 3-11.

1979: Theoretical aspects of alpha coefficients used in X-ray fluorescence analysis. Scientific and Technical Notes in Current Research, Part B; Geological Survey of Canada, Paper 79-1B, p. 416.

Lachance, G.R. and Traill, R.J.
1966: A practical solution to the Matrix Problem in X-ray analysis. Canadian Spectroscopy, v. 11, nos. 3-4.

Large, R.R. and Mumme, W.G.
1975: Junoite, "Wittite", and related seleniferous bismuth sulphosalts from Juno Mine, Northern Territory, Australia; Economic Geology, v. 70, p. 369-383.

Rucklidge, J.C. and Gasparrini, E.L.
1969: Electron microprobe analytical data reduction, EMPADR VII; Department of Geology University of Toronto.

Sweatman, T.R. and Long, J.V.P.
1969: Quantitative electron-probe microanalysis of rock-forming minerals; Journal of Petrology, v. 10, p. 332-379.

Traill, R.J. and Lachance, G.R.
1965: A new approach to X-ray spectrochemical analysis; Geological Survey of Canada, Paper 64-57.

THE PALEOLATITUDE AND PALEOMAGNETIC AGE OF THE ATHABASCA FORMATION, NORTHERN SASKATCHEWAN – DISCUSSION

Paul Ramaekers
Saskatchewan Geological Survey
201 Dewdney Avenue East
Regina, Sask. S4N 4G3

Manuscript received 30 August, 1979

In their paper Fahrig et al. (1978), indicated that the depositional age of the Athabasca Formation is about 1550 Ma and that reversals of polarity of the earth's field during deposition of the Athabasca Formation promise to be of value in the chronostratigraphic correlation of redbed units within the formation. An examination of their data and assumptions strongly suggests that their conclusions are not warranted by the evidence presented.

The Data

Of the 31 samples used by Fahrig et al. (1978), 28 are reported to be of Athabasca Formation. Examination of the original drill logs and of the cores (in the Department of Mineral Resources Subsurface Geological Lab at Regina) shows that of these 28 specimens, 4 (all samples from HL 1, HL 2 and HL 3) are from the basement. If their specimens from these holes are actually sandstone, then the footages given in their report are in error.

Fahrig et al. (1978) reported a Rb/Sr isochron age on "deeply weathered material". An examination of the core at the footages from which their samples were taken shows that these range from deeply altered material to virtually fresh rock. In all but one sample (RL 4878) the original structure of the rock was clearly visible and in three the biotites were virtually unaltered. Of the six samples only RL 4878 did not fall on the isochron and was disregarded (Wanless, pers. comm.); this is by far the most altered sample, and precisely the one that could be most expected to give the age of weathering. Unlike the other samples, which are mafic gneisses, RL 4878 is part of a granitic anatectic melt.

Analysis of the Data by Fahrig et al.

The 29 stably magnetized samples used by Fahrig et al. (1978) include 3 and possibly as many as 7 hematized "regolith" samples from below Athabasca Formation. They used "regolith" samples to derive an age of sedimentation and thus presumed these to have formed at about the same time as the sediments were deposited. Yet Fahrig et al. (1978) also insisted that the Rb/Sr date derived from "regolith" was the age of the weathering– about 80 Ma older than their age of deposition. If such a large gap can exist between the age of weathering and the age of deposition, then clearly the regolith samples should not be used in determining the depositional age. As all but one of the regolith samples give a cluster of steep paleomagnetic inclinations, using them biases the results.

Even if all 29 samples are accepted uncritically a KS test will show that the null hypothesis (that their paleomagnetic inclinations are randomly distributed) cannot be rejected at the usual confidence level ($\alpha = .05$). Without the regolith samples the inclinations do not even come near to forming anything but a random distribution.

Fahrig et al. (1978) divided their stably magnetized samples into two groups, but not at the point where the greatest break falls between sample inclinations (between 66° and 79°). They then disregarded samples with inclinations shallower than 33° without stating reasons, calling these "puzzling". The very fact that they split their samples into groups is a tacit admission that the magnetic inclinations can be reset. If so, their choice of groups and group boundaries must be specified. They do not do so. These decisions have biased their remaining samples (Group 1) towards steeper inclinations, and if their undefended assumption that the magnetic inclinations of the samples were fixed at about the time of deposition is granted, then they have biased their sample towards an older age.

Some samples with reversed and nonreversed magnetizations lie very close together and are irregularly distributed. It is noteworthy that in a similar case, with much more data, Briden and Ward (1966, p. 143), whose statistical methods the authors claim to follow, rejected an explanation in terms of reversals in favour of the supposition that some cores were marked the wrong way up. Briden and Wards' cautions about core orientation apply fully to cores from the friable Athabasca Formation, where the way up can be determined only occasionally from cored sections showing sedimentary structures.

The Central Issue: Hematite Diagenesis

To claim, as Fahrig et al. (1978) do, that the paleomagnetic age is the same as that of deposition implies that the magnetized minerals were emplaced at time of deposition or shortly thereafter in early diagenesis and have not been altered since. However, a short review of papers on redbed paleomagnetism emphatically suggests the contrary, and indicates that hematite is often extensively reworked throughout the postdepositional history of redbed units at low temperatures (e.g. Opdyke, 1964; Piper, 1975; Johnson, 1976 among many others). Of particular interest are papers by Larson and Walker (1975); Walker and Larson (1976); and Larson et al.(1976) because they show that the results obtained by previous authors were not reliable due to postdepositional movement of the magnetic minerals.

Such is the case with the Athabasca Formation. Examination of hand specimens and thin sections makes it evident that the diagenetic history of the Athabasca Formation is long and complex. Many hand specimen and thin sections throughout the basin show specularite filling interstices and covering prominent quartz overgrowths. Thin sections taken at the footages from which the paleomagnetic samples were taken show this complexity clearly. For example, sections at CSP 2-1 385', CSP 2-1 2316', and CSP 8-1 840', indicate that much of the hematite here was precipitated before the quartz overgrowths. The samples used by Fahrig et al. (1978) from two of these footages have shallow magnetic inclinations; the other is very steep. A section at CSP 8-1 1093.5', a few inches from one of their samples with an intermediate magnetic inclination, shows that much of the hematite is still contained in much altered detrital grains, and some is precipitated after the initial quartz overgrowths occurred. Recent literature suggests that apparently initial quartz overgrowths themselves are of various ages. Pagel's (1975) fluid inclusion work indicates a temperature and pressure gradient decreasing up the Rumpel Lake core (Fahrig et al.'s RL core), –i.e. the apparently initial quartz overgrowth now present that Pagel used were formed at more or less the same time throughout the section and after the Athabasca Formation was buried. Pitchblende and quartz overgrowths alternate in the Key Lake deposit (Dahlkamp, 1978) and the age of the pitchblende here is much younger than the age of the Athabasca Formation (Wendt et al., 1978). Postdepositional alteration of the sandstone including hematite precipitation, is also recorded

From: Discussions and Communications in Current Research, Part C; Geol. Surv. Can., Paper 79-1C.

by Ramaekers (1976, 1977), Harper (1978), Hoeve and Sibbald (1978) among others, and it is likely that the basement just below the sandstone was altered at this time as well (Ramaekers and Dunn, 1977), i.e. after deposition of the sandstone. It may be noted that the likelihood of alteration in the cores used by Fahrig et al. (1978) was great, because these cores were drilled by mining companies to find mineralization, not to intersect unaltered sandstone. Cores CSP 2-1, CSP 5-1, CSP 8-1, CSP 10-1 were drilled on prominent magnetic anomalies thought at the time to represent dykes (as can be seen in the Saskatchewan Assessment Files) and since proven to be so (Ramaekers, 1978). At the time of dyke intrusion these areas were in geothermal zones and hydrothermal alteration must have been intense. These dykes are much younger than the age of sandstone deposition (Burwash et al., 1963; Armstrong and Ramaekers, in preparation). Cores RL and DEJ intersect the largest fault and fracture zone in the Athabasca Basin: The Black Lake-Virgin River shear zone, a major Aphebian or Hudsonian structure rejuvenated in post-Athabasca times (Fahrig, 1961; Ramaekers, 1976, 1977, 1978).

Correlation of Redbed "Units"

The first prerequisite for correlating redbed units is the existence of such units. There are mappable areas of leached rock and of intensely hematized rock in the Athabasca Formation, but many of these follow fault zones and cut across stratigraphic boundaries, unconformities, or follow the basement contact. They represent aquifers, not isochronous stratigraphic units. A fluviatile, eolian, lacustrine and/or marine complex such as the Athabasca Formation contains many unconformities. Particularly the fluviatile sectors will have a very incomplete and erratic sedimentary record with gaps of unknown duration separating zones with very rapid deposition. Such gaps represent an unknown number of periods with a reversed magnetic field. In such an environment magnetostratigraphy will be recognizable only after a detailed map of all unconformities and temporal relationships is available, i.e. after the stratigraphy of the basin is known in detail. Under these circumstances we cannot expect magnetostratigraphy to contribute anything to redbed correlation.

Paleomagnetic dating dates the last time of mobilization of the magnetic minerals, in this case largely hematite. Whether or not this is the same as the age of deposition is a point to be proven, not assumed as Fahrig et al. (1978) have done. In view of what is known about the Athabasca Formation and the behavior of iron in redbeds their data are open to other interpretations. The data strongly suggest that the minerals have migrated at various times after deposition. Thus, the magnetic inclination of their samples may be derived from hematite precipitation at a time specified by any intersection of the polar wandering track and the samples' calculated paleolatitude, as long as this age is the same or younger than the age of deposition of the Athabasca Formation.

If it can be shown that the distribution of magnetic inclinations in the data presented by Fahrig et al. (1978) reflects two discrete events rather than many (a hazardous thesis in view of the paucity the scatter of the data points throughout the basin), then each of these clusters gives rise to a series of possible ages for the iron mineralization. If we accept their grouping of the data (which I would not) then two possibilities present themselves. The shallow inclinations (Group 2 of Fahrig et al., unexplained but dismissed by them) which have at least some of the hematization antedating quartz overgrowths, may be due to early diagenetic iron mineralization and be close to the age of deposition. A glance at their Figure 1.5 shows that this would agree very well with Ramaekers and Dunn's (1977) age of 1350 Ma, or with iron mobilization at about 1250 Ma, 1000 Ma or younger dates. Similarily the steeper inclinations could be due to iron remobilization at 1200 Ma, 1050 Ma, or later. These are precisely the ages of intrusion of the dykes, near which most of the samples used by Fahrig et al. (1978) were obtained. Flattering though this interpretation may be to our published date, in view of the widespread evidence of iron and quartz mobility in the Athabasca Formation, I doubt that the original depositional age is recorded anywhere by the iron mineralization. Recording paleolongitudes from outcrop samples offers little hope of settling this problem because of the particular orientation of the polar wandering track in Helikian time relative to the Athabasca Basin. A small change in longitude here corresponds to a large change in age. However, it should serve to distinguish Hadrynian or Phanerozoic mobilizations of the iron minerals.

I suggest that the Rb/Sr date on the "regolith" obtained by Wanless (1969) is the age of a late metamorphic event of the basement gneisses, particularly as the visibly most altered sample, which certainly should have recorded the weathering, is the only sample that does not fall on the isochron. The Rb/Sr isochron method is remarkably capable of dating events of the source rock. For example, fluvial detrital clays within the Athabasca Formation give a Kenoran Rb/Sr isochron age that is compatible with radiometric ages of rocks in the source area (Armstrong and Ramaekers, in preparation). An age of 1633 Ma fits in well with other basement ages from below the Athabasca Formation, e.g. Key Lake, 1700 Ma (Wendt et al., 1978), and late events in major shear zones (1575 Ma, Needle Falls shear zone, Wanless, 1969) such as the Black Lake-Virgin River shear zone which passes through the Rumpel Lake area.

The data presented by Fahrig et al. (1978) are most interesting and further work on the paleomagnetism of the Athabasca Formation may serve to unravel the diagenetic history and paleohydrology of the Athabasca Basin. In view of the long continued movements of uranium through the formation such work has important economic implications and should certainly be continued and expanded. However, two things that such work will not do is (1) give an age of sedimentation of the sandstone or (2) enable correlation of the redbed "units".

References

Armstrong, R.L. and Ramaekers, P.
New radiometric dates from the Athabasca Basin, Northern Saskatchewan. (in prep.)

Briden, J.C. and Ward, M.A.
1966: Analysis of magnetic inclination in boreholes; Pure and Applied Geophysics; v. 63, p. 133-152.

Burwash, R.A., and Baadsgaard, H., and Peterman, Z.E.
1963: Precambrian K-Ar dates from the western Canada Sedimentary Basin; Journal of Geophysical Research, v. 67, p. 1620.

Dahlkamp, F.J.
1978: Geologic appraisal of the Key Lake U-Ni deposits, Northern Saskatchewan; Economic Geology, v. 73, p. 1430-1449.

Fahrig, W.F.
1961: The geology of the Athabasca Formation; Geological Survey Canada, Bulletin 68.

Fahrig, W.F., Christie, K.W., and Freda, G.
1978: The paleolatitude and paleomagnetic age of the Athabasca Formation, northern Saskatchewan; in Current Research, Part C, Geological Survey of Canada, Paper 78-1C, p. 1-6.

Harper, C.T.
1978: Uranium Metallogenic Studies: Cluff Lake; Summary of Investigations, 1978, Saskatchewan Geological Survey, p. 84-89.

Hoeve, J. and Sibbald, T.I.I.
1978: On the genesis of Rabbit Lake and other unconformity-type uranium deposits in northern Saskatchewan, Canada; Economic Geology, v. 73, p. 1450-1473.

Johnson, A.H.
1976: Paleomagnetism of the Jurassic Navajo Sandstone from south-western Utah; Royal Astronomical Society, Geophysical Journal, v. 44, p. 161-175.

Larson, E.E. and Walker, T.R.
1975: Development of chemical remanent magnetization during early stages of red-bed formation in Late Cenozoic sediments, Baja California; Geological Society of America, Bulletin, v. 86, p. 639-650.

Larson, E.E., Hoblitt, R.P. and Walker, T.R.
1976: Evidence of chemical remagnetization long after deposition in red beds of the Moenkopi Formation near Gray Mountain, Arizona; Geological Society of America, Abstracts with Programs, p. 971.

Opdyke, N.D.
1964: The paleomagnetism of the Permian red beds of southwest Tanganyika; Journal of Geophysical Research, v. 69, p. 2477-2487.

Pagel, M.
1975: Détermination des conditions physico-chimiques de la silicification diagénétique des grès Athabasca (Canada) au moyen des inclusions fluides; Academie des Sciences, Compte Rendus, t. 280, sér. D, p. 2301-2304.

Piper, J.D.A.
1975: The paleomagnetism of Precambrian igneous and sedimentary rocks of the Orange River Belt in South Africa and Southwest Africa; Royal Astronomical Society, Geophysical Journal, v. 40, p. 313-344.

Ramaekers, P.
1976: Athabasca Formation, northeast edge (64L, 74I, 74P): Part I Reconnaissance Geology; Summary of Investigations 1976, Saskatchewan Geological Survey, p. 73-77.

1977: Athabasca Formation south-central edge (74G): Part I Reconnaisance Geology; Summary of Investigations 1977, Saskatchewan Geological Survey, p. 157-163.

1978: Athabasca Formation, southwestern edge: Part I Reconnaissance Geology (NTS Areas 74F, 74K); Summary of Investigations 1978, Saskatchewan Geological Survey Miscellaneous Report 78-10, p. 124-128.

Ramaekers, P. and Dunn, C.E.
1977: Geology and geochemistry of the eastern margin of the Athabasca Basin; Saskatchewan Geological Society Special Publication No. 3, p. 297-322.

Walker, T.R. and Larson, E.E.
1976: Hematite authigenesis in the Moenkopi Formation (Triassic Age), Colorado Plateau: a contribution to the origin of magnetism in the red beds; Geological Society of America, Abstracts with Programs, p. 1158.

Wanless, R.K.
1969: Isotopic age map of Canada; Map 1256A, Geological Survey of Canada.

Wendt, I., Hohndorft, A., Lenz, H., and Voultsidis, V.
1978: Short papers of the Fourth Int. Conf. Geochronology, Cosmochronology, Isotope Geology, U.S. Geological Survey Open File Report 78-701, p. 448.

THE PALEOLATITUDE AND PALEOMAGNETIC AGE OF THE ATHABASCA FORMATION, NORTHERN SASKATCHEWAN – REPLY

W.F. Fahrig, K.W. Christie and G. Freda
Geological Survey of Canada
601 Booth Street, Ottawa, Ontario K1A 0E8

Manuscript received 15 October, 1979

The HL samples referred to by P. Ramaekers are all from the Athabasca Formation. The sampling and logging of these cores was the responsibility of the senior author, who was assisted by Paul E. Potter (University of Cincinatti) and A. Kohut. Access to the collection was provided through the courtesy of the Saskatchewan resident geologist at Lac La Ronge. Footages were those given on the core boxes, augmented by figures given on chips of wood which has been placed at various intervals in the core boxes. If the footages no longer indicate the presence of Athabasca at these depths, the most likely probability is that the relationship of cores to boxes was disturbed during transfer of this material from Lac La Ronge to Regina.

The specimens used in the Rb/Sr work were all intensely weathered. For example, they are extremely low in calcium, and correspondingly high in alumina. Inasmuch as the Rb/Sr system in gneissic rocks is very sensitive to weathering, it seems likely that the isochron reflects homogenization at some time after the formation of the gneisses. It would be interesting to attempt an isochron on material from well below the zone of weathering, if such material is available. In any case, the problem in interpreting this isochron was suitably alluded to with the remark . . . . "if this does indeed date the pre-Athabasca weathering". Reference is also made to the large gap, 80 Ma, between the apparent age of basement weathering, as suggested by Rb/Sr age determination, and the age of sedimentation, as suggested by paleomagnetic work on Athabasca redbeds. This gap is covered by the errors inherent in the Rb/Sr and paleomagnetic methods. From the data available one really can't at this stage speculate too intelligently regarding the exact size of gap between weathering and sedimentation.

The possibility that the samples showing reversed magnetization were the result of core orientation, creates a problem in dealing with company drill cores because drillers often put cores the wrong way round in core boxes. In the present case, however, all the sedimentary structures that indicated tops showed that this had not happened. For example, small load casts in silty layers indicated no such error. Furthermore, as emphasized in the note, the magnetization direction of most of the 'reversed' samples changed during step cleaning from a shallow 'up' direction, or even a 'down' direction, to a moderately steep 'up' direction. If those samples with end point 'up' directions were placed wrong way round in the boxes, the step thermal cleaning would indicate an upward-directed viscous component rather than one related to the present earth's field direction. Furthermore, the possibility that they had acquired a component during laboratory storage was discounted because they were stored on their sides and the viscous component in some cases required rather high temperatures to eliminate. The laboratory experiments, therefore, seem to provide strong evidence for the presence of reversals during the magnetization of the Athabasca Formation.

The time of formation of the ferric oxides, as in most redbeds, constitutes a problem. It has been demonstrated in some Phanerozoic sequences that the ferric oxide pigmentation developed during diagenesis and the rocks were progressively reddened during time. In this case the paleomagnetism could be younger than sedimentation. Little is known, however, about this possibility in Proterozoic

From: Discussions and Communications in Current Research, Part C; Geol. Surv. Can., Paper 79-1C.

sequences. Certainly in some cases, for example from the study of interbedded basic volcanics, we know that diagenetic ferric oxide precipitation and magnetization were not much younger than sedimentation. In this regard, it is important to remember the scale of time involved. In considering rocks of Helikian age, diagenesis, a few million years or even a few tens of millions of years after sedimentation, is of far less significance than it would be in rocks only a few hundred million years in age. Furthermore, there is no evidence from the demagnetization experiments of more than one component – i.e. there is no evidence of more than one stage of ferric oxide precipitation whose ages might be significantly different.

The possibility suggested by the reviewer that the iron might have been remobilized by the intrusion of nearby dykes seems remote. Firstly, it is unlikely that the drillholes are close enough to the dykes to have been influenced by them. Secondly, these northwest trending dykes are Mackenzie, and although the products of Mackenzie igneous events (Mackenzie dykes, Sudbury dykes, East Arm sills, Coppermine volcanics, Muskox intrusion) are among the most thoroughly sampled of any Precambrian suite, they have yielded no evidence of polarity reversal.

These preliminary results do suggest the possibility of using reversals for chronostratigraphic correlation of hematite-rich zones in the Athabasca. It is therefore important that efforts be made to obtain material suitable for paleomagnetic study as drilling advances into this great sedimentary basin.

MOUNT GOODSIR, BRITISH COLUMBIA AND ALBERTA Geological Survey of Canada Maps 1476A and 1477A by R.A. Price, E.W. Mountjoy, and D.G. Cook, 1978 – DISCUSSION

William Carruthers Gussow,
188 Dufferin Road,
Ottawa, Canada K1M 2A6

Manuscript Received July 25, 1979.

Introduction

The Geological Survey is to be highly commended for setting up Operation Bow-Athabasca (1965-1969) and the results have long been awaited. The base maps are greatly improved, and the availability of good vertical air photos has made the operation feasible. I have only one complaint in this regard: Why did they copy the inaccurate, sketched trails from the Parks maps, when I gave them a base map of Banff Park area with the trails accurately surveyed? I again point out two errors on base map 1477A: Clawson Peak (8750+ feet) is the higher peak some 600 m to the southeast; and Aquila Mountain is the 9400+ foot peak to the northwest.

We are all exceedingly happy and grateful to see the geological map sheets of the Rocky Mountains appear in print and I have been waiting for the final set to appear before commenting. Accordingly, this discussion is restricted to the Mount Goodsir map sheets. I fully realize that this is intended to be an air reconnaissance with a minimum of ground control, but why did not someone do the geology of the highways and fire roads? I submitted an outcrop map of the Bow River valley which provided accurate ground control for mapping the base of the Cambrian and the Windermere (Miette, or Hector).

My published contributions on the age of the Ice River complex (Gussow, 1977a, b; Gussow and Hunt, 1959) are still being ignored after 20 years. Apparently, the Geological Survey continues to hold firmly to the erroneous belief that the Ice River Complex is intrusive, in spite of the field evidence which proves that it is Precambrian basement, and they still refuse to accept the strong evidence for a second, upper, fault slice of Precambrian basement, unconformably overlain by Ottertail limestone. It is not necessary to go in the field to demonstrate that Clawson Peak ridge is held up by Ottertail limestone – just like Chancellor Peak ridge – yet this is completely ignored by the authors (See Gussow, 1977a, Fig. 1, 4).

Ice River Basement Complex

As pointed out in 1958 (Gussow and Hunt, 1959), and documented in detail by Gussow (1977a, p. 511, and Fig. 1 to 4), the Ice River Complex is a Precambrian basement complex: There is an unconformity. Upper Cambrian dove-grey Ottertail limestone lies directly on coarse plutonic syenite with a basal conglomerate of boulders and pebbles derived from the basement rocks. Furthermore, the Cambrian section thins and onlaps basement topography. No dykes or apophyses of the coarse syenite series intrude the limestone. The overlying Cambrian limestones on Clawson Peak ridge are almost completely unmetamorphosed, whereas the basement rocks immediately adjacent to the Cambrian limestones are a plutonic paragneiss series consisting of gneisses, schists, crystalline limestone, and amphibolite, intruded by nepheline and sodalite syenite. The basement rocks are exposed in two thrust sheets resulting from the Rocky Mountain orogeny. Only one of these (the lower plate) was mapped by Price and Mountjoy (See Gussow, 1977a, Fig. 4). Currie (1975) actually postulates implacement of a liquid magma and liquid immiscibility, but the original sedimentary textures (paragneisses) demonstrate that temperatures were less than half the melting point at the time of metamorphism and remobilization of the crystalline limestone.

Mount Goodsir (West Half), Map 1477A

A comparison of the new map with Currie's (1975) Figure 1, shows roughly the same overall geology and approximately the same shape for the Ice River Complex. However, in detail there are many differences. 1. The most significant difference is the erosional remnant of Ottertail limestone lying on the Ice River Complex on the divide between Sharp Mountain and Helmet Mountain. Currie (1975, Fig. 1) mapped this as syenite. 2. The exposure (window) of Chancellor Formation on Moose Creek shown by Currie (1975, Fig. 1) and Allan (1914, Map 142A) is not shown on Map 1477A. 3. The northwest-southeast trending synclinal axis along the north flank of Mount Goodsir, Sentry Peak, and extending beyond Helmet Mountain (Currie, 1975) is not shown on Map 1477A, although pictured by Allan, who applied the name Syncline Peak to the culmination northwest of the South Tower on Mount Goodsir. 4. Map 1477A shows a large area of Ottertail north of Sodalite Creek. Currie's Figure 1 indicates this as a synclinal area of MacKay, 1.6 km X 800 m in area.

Map 1477A, published three years after a manuscript copy of my last paper (Gussow, 1977a) on the Ice River complex, was sent to the Geological Survey, still relies on the published age dating for the complex, and disregards the field evidence, without even a word of caution that a controversy as to age exist. Actually, the Legend block "Devonian or (?) Mississippian" should be removed and a new block should be shown at the bottom of the column as Precambrian basement complex, pre-Proterozoic in age. The large area of basement complex, capped by Ottertail limestone, below Clawson Peak ridge, is still omitted even though this was brought to the attention of the Geological Survey in 1958 (Gussow and Hunt, 1959), and was observed by Allan and Currie in three separate outcrops over a distance of more than 3 km (See Gussow, 1977a, Fig. 4).

As pointed out by Allan (1914) and Gussow (1977a), a series of minette dykes and sills cuts Precambrian, Cambrian, and Lower Ordovician strata. Allan reported one of these dykes on the peak of the South Tower of Mount Goodsir. Even if they are not shown on the map, they should be indicated on the legend. The legend claims that the Ice River Complex contains inclusions of Ottertail and MacKay. Any sedimentary inclusions must be Precambrian in age.

Mount Goodsir (East Half), Map 1476A

The Precambrian, Windermere Series (Miette Group) outcrops in the northeast corner of the map sheet. Actually, the dip of the unconformity at the base of the Cambrian Gog Formation is much flatter than indicated on the map by contact (80°). It is even flatter than shown on Section 4 (28°). Vermilion Pass is a classic area. This is where Dawson (1885, p. 119B) discovered the first Cambrian fossil in place in the Canadian Rockies. Walcott (1928, p. 300) collected Lower Cambrian fossils (his **Obolella-Wanneria** zone) at the upper (south) end of the Upper lake (Altrude Lakes), and abundant **Scolithos** borings occur in Lower Cambrian quartzites along the highway, just northwest of the Altrude Lakes. An outcrop at the west end of the Lower Lake (middle of three) exposes the unconformity at the base of the Lower Cambrian: White quartzite, with an 8 cm thick basal conglomerate, overlies purple to dark grey Precambrian argillite of the Windermere Series. At the base of Storm Mountain, 3.8 km southeast of Vermilion Pass, **Chuaria** sp. cf. **C. circularis** Walcott was discovered below the basal unconformity, in the Precambrian purple argillites (Gussow, 1973).

From: Discussions and Communications in Current Research, Part C; Geol. Surv. Can., Paper 79-1C.

Section 4

Section 4 will require major revision of the subsurface to show the Precambrian basement complex. In the east, this lies at a depth of about 8000 feet, 2000 feet sub-sea, below the Miette section, and rises to the west to about 1000 feet above sea level in the vicinity of Moose Creek, where it underlies the Ottertail. In this vicinity, the Ottertail has thinned to half its normal thickness by onlap on basement topography, all the Cambrian and Windermere being absent by onlap. The Peace River High in northern Alberta is a similar, well documented example, where Mississippian lies directly on the Precambrian basement (Gussow, 1962, Section KLM).

In conclusion, it will be most interesting to see how Price and Mountjoy (and Currie) will defend their position. It almost looks as if there was another "vote" to ignore the field evidence I presented (Gussow, 1977a). "Fortunately for science, but unfortunately for its students, scientific problems are not settled by majority vote" (Hofmann, 1971).

References

Allan, J.A.
1914: Geology of the Field map-area, British Columbia and Alberta; Geological Survey of Canada, Memoir 55.

Currie, K.L.
1975: The geology and petrology of the Ice River alkaline complex, British Columbia; Geological Survey of Canada, Bulletin 245, 68p.

Dawson, G.M.
1885: Preliminary report on the physical and geological features of that portion of the Rocky Mountains between 49°00' and 51°30'; Geological Survey of Canada, Annual Report, v. 1, pt. B, p. 1, map, cross sections (1886).

Gussow, W.C.
1962: Regional geological cross sections of the western Canada sedimentary cover: Alberta Society of Petroleum Geologists and Geological Association of Canada (one sheet).

1973: **Chuaria** sp. cf. **C. circularis** Walcott from the Precambrian Hector Formation, Banff National Park, Alberta, Canada; Journal of Paleontology, v. 47, no. 6, p. 1108-1112.

1977a: The Ice River complex, British Columbia, is Precambrian basement: Bulletin of Canadian Petroleum Geology, v. 25, no. 3, p. 505-517.

1977b: Review: Geology and petrology of the Ice River alkaline complex, British Columbia, by K.L. Currie, 1975 (1976); Bulletin of Canadian Petroleum Geology, v. 25, no. 3, p. 707-709.

Gussow, W.C., and Hunt, C.W.,
1959: Age of the Ice River complex, Yoho National Park, British Columbia: Alberta Society of Petroleum Geologists Journal, v. 7, no. 3, p. 62.

Hofmann, H.J.,
1971: Precambrian fossils, pseudofossils, and problematica in Canada; Geological Survey of Canada, Bulletin 189, 146p.

Walcott, C.D.,
1928: Cambrian geology and paleontology V, no. 5 – Pre-Devonian Paleozoic formations of the Cordilleran provinces of Canada; Smithsonian Miscellaneous Collections, v. 75, no. 5, p. 171-386.

MOUNT GOODSIR, BRITISH COLUMBIA AND ALBERTA
Geological Survey of Canada Maps 1476A and 1477A
by R.A. Price, E.W. Mountjoy and D.G. Cook, 1978 – REPLY

Raymond A. Price, Department of Geological Sciences
Queen's University, Kingston, Ontario, K7L 3N6; and
Eric W. Mountjoy, Department of Geological Sciences
McGill University, Montreal, Quebec

Manuscript Received October 5, 1979.

William C. Gussow has raised one substantive point in his discussion -- the relationships between the Ice River Complex and the rocks that surround it. Out response is restricted to this one point.

Gussow has taken exception to the fact that we concurred with Allan (1914), Campbell (1961), Rapson (1963) and Currie (1975), as well as others whom he has cited (Gussow, 1977a), but not with him (Gussow and Hunt, 1959; Gussow, 1977a), by concluding that the Ice River Complex consists of igneous rocks that have intruded the enclosing Late Cambrian sedimentary rocks.

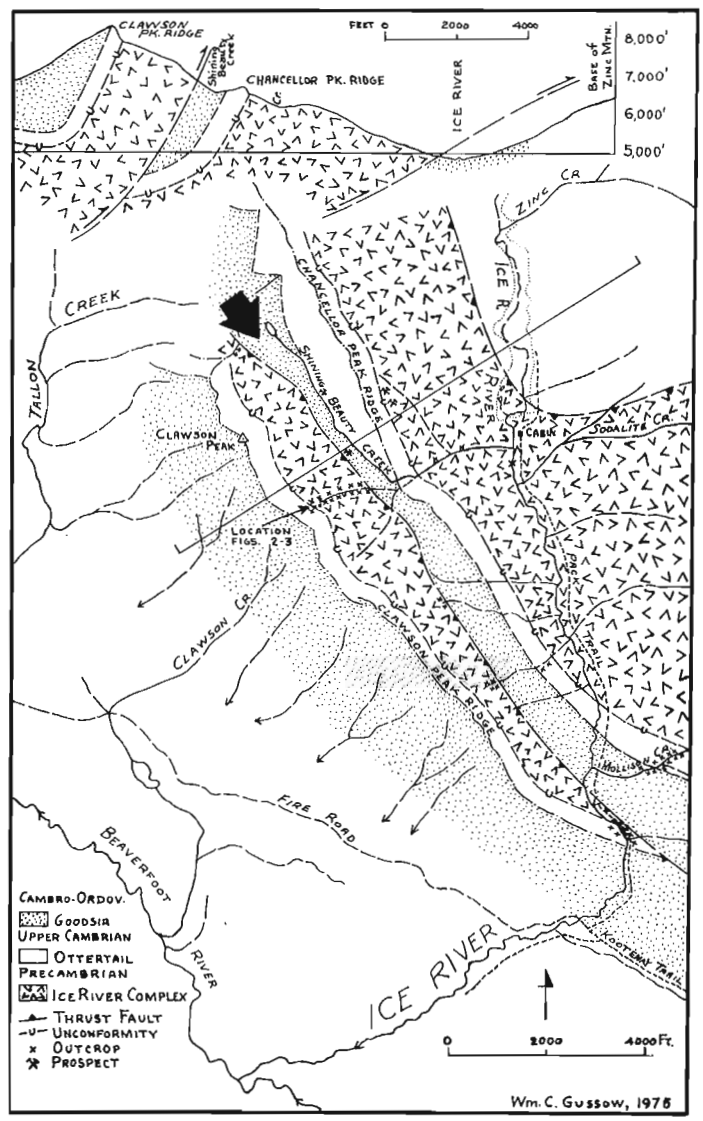

***Figure** 1. Photogeology, Ice River area British Columbia, Wm. C. Gussow, 1976 (after Gussow, 1977a, with permission of the Bulletin of Canadian Petroleum Geology). The arrow which has been added by us shows the location and direction of the view shown in Figure 2.*

From: Discussions and Communications in Current Research, Part C; Geol. Surv. Can., Paper 79-1C.

Figure 2. *View southeast along the upper reach of Shining Beauty Creek, at the northeast slope of Clawson Peak ridge from near the head of Tallon Creek (See Fig. 1 for location and direction of view). ot = Ottertail Formation; mk = McKay Group. Note bedding in dark resistant weathering hornfels of the McKay Group between the Ottertail Formation and the crest of Clawson Peak Ridge (GSC Photo, 175932).*

Our conclusion is based on our observations of cross-cutting relationships between the Ice River Complex and the bedding of the enclosing rocks, and of contact metamorphism in the enclosing rocks. We observed these at the top of the Ice River Complex northwest of Shining Beauty Creek, where the contact-metamorphic aureole extends through the overlying carbonate rocks of the Ottertail Formation into a zone of hornfels in the pelitic rocks of the McKay Group, also between Mount Mollison and Mollison Creek. We observed the same phenomena below the Ice River Complex on the north side of Garnet Mountain, where the contact metamorphism extends down through the carbonate rocks of the Ottertail Formation into a zone of hornfels in the "upper transition unit" of the Chancellor Formation, and also on the southeast side of Sharp Mountain, and on the east and west sides of Zinc Mountain. Nowhere did we observe a fault contact between the base of the Ice River Complex and underlying unmetamorphosed rocks, or an unconformity at the top of the Ice River Complex. The upper contact, where we observed it, is sharp and crosscutting. No basal conglomerate occurs in the overlying rocks, but spheroidal weathering does occur locally within the Ice River Complex, and it bears a superficial resemblance to conglomerate.

Gussow, in advocating his interpretation of the Ice River Complex as Precambrian basement rock that has been thrust over the early paleozoic sedimentary rocks, relies on his repeated assertion (Gussow and Hunt, 1959; Gussow, 1977a, this discussion) that there is an exposure along a principal tributary of Shining Beauty Creek, high on the east slope of Clawson Peak ridge, in which the Ice River Complex is overlain unconformably by unmetamorphosed Ottertail limestone containing clasts of syenite in the lower part. Photographs, which are said (Gussow, 1977a) to document the existence of this unconformity and basal conglomerate, show truncation of layering (bedding?) along a sharp contact between a distinctly layered rock above and a more massive rock below (Fig. 2 of Gussow, 1977a); but no basal conglomerate or boulders of syenite are discernible in the close-up photograph (Fig. 3 of Gussow, 1977a) which is so badly focussed and/or poorly exposed that all significant details are obscured. Accordingly, Gussow's oft repeated assertion has not been documented.

As pointed out by Gussow (1977a, p. 510) we did not visit the locality that has been described. However, while traversing southeastward down Shining Beauty Creek from the divide with Tallon Creek (Fig. 1) we did have an unobstructed view of the northeast slope of Clawson Peak ridge. This is the place where, according to Gussow, there should be an upper thrust sheet of Precambrian basement with unconformable cover of Ottertail limestone, and Figure 2 is a photograph of the view. The contact between the Ottertail and Goodsir formations as mapped by

Allan (1914), Currie (1975) and Price et al. (1978a, b) is identified by annotations on the photograph. None of the rocks overlying this contact show any apparent resemblance to the Ottertail Formation, which should be there, according to Gussow. Moreover, the dark colour, distinct bedding, and resistance to weathering of these overlying rocks make them quite similar to the hornsfelsed McKay Group shales that occur at the locality from which the photograph was taken. Accordingly we have no alternative, on the basis of what we have seen, but to conclude, as did Allan (1914), Cambell (1961) and Currie (1975), that the Ice River Complex was emplaced in these rocks as an igneous intrusion; and that no "upper thrust slice" of the kind described by Gussow (1977a) should be shown in Clawson Peak ridge where our map shows only rocks of the McKay Group.

Although much remains to be learned about the Ice River Complex, it is useful to make interpretations of it on the basis of our present, imperfect state of knowledge, and it is imperative these interpretations provide the most elegantly logical explanation of all the available information. Our interpretations are based on the exercise of our individual scientific judgements. They have not been controlled by any "official" Geological Survey of Canada interpretation, and they may be in profound disagreement with some of our colleagues in the Geological Survey, as well as with William Gussow. We share Gussow's view that the field observations must not be ignored, but we also believe that it is necessary to know what was actually observed in the field, and what was inferred. We do not really know what was observed by Gussow, and what was inferred; but we do know what we saw, and this is the basis for our interpretation of the Ice River Complex.

References

Allan, J.A.,
1914: Geology of the Field map-area, British Columbia and Alberta; Geological Survey of Canada, Memoir 55.

Cambell, F.A..
1961: Differentiation trends in the Ice River complex, British Columbia; American Journal of Science, v. 259, p. 173-180.

Currie, K.L.
1975: The geology and petrology of the Ice River alkaline complex, British Columbia; Geological Survey of Canada, Bulletin 245, 68 p.

Gussow, W.C.,
1977a: The Ice River Complex, British Columbia, is Precambrian basement; Bulletin of Canadian Petroleum Geology, v. 25, p. 505-517.

1977b: Review: Geology and petrology of the Ice River alkaline complex, British Columbia, by K.L. Currie, 1975; Bulletin of Canadian Petroleum Geology, v. 25, p. 707-709.

Gussow, W.C. and Hunt, C.W.
1959: Age of the Ice River Complex, Yoho National Park, British Columbia; Alberta Society of Petroleum Geology, Journal, v. 7, p. 62.

Price, R.A., Mountjoy, E.W., and Cook, D.G.,
1978a: Mount Goodsir, East Half, British Columbia and Alberta; Geological Survey of Canada, Map 1476A.

1978b: Mount Goodsir, West Half, British Columbia; Geological Survey of Canada, Map 1477A.

Rapson, J.E.,
1963: Age and aspects of metamorphism associated with the Ice River Complex, British Columbia; Bulletin of Canadian Petroleum Geology, v. 11, p. 116-124.

METAMORPHIC HISTORY OF THE ARCHEAN ABITIBI BELT – DISCUSSION

Raymond Goldie
9 Palmerston Gardens
Toronto, Ontario. M6G 1V8

The metamorphic geology of the Abitibi Belt is shown on the Geological Survey of Canada Map 1475A, and on Figure 4 of Jolly (1978). Recent work has suggested revisions to this picture. In particular, four granitic plutons, previously mapped as "unmetamorphosed", are now known to contain assemblages of metamorphic minerals similar to those in the rocks which surround them.

Jolly (1978) depicted the Flavrian, Powell, Lake Dufault and Bourlamaque intrusions as postmetamorphic bodies surrounded by aureoles of amphibolites. These aureoles presumably represent "M5" – synorogenic contact metamorphism – superimposed on regional greenschist assemblages. Campiglio and Darling (1976), however, found that the Bourlamaque Batholith has undergone regional greenschist metamorphism. Furthermore, John Allen and I have shown (Allen and Goldie, 1978; Goldie, in press) that:

1. the Flavrian, Powell and Lake Dufault intrusions have also been metamorphosed;
2. albite amphibolites do occur on the margin of the Flavrian Pluton, but they also occur inside the intrusion, and within the Lake Dufault Pluton;
3. greenschists, not amphibolites, surround the Powell Pluton;
4. the core of the Flavrian Pluton and the entire Powell Pluton consist of greenschists.

It is often thought difficult to distinguish hornblende, the key mineral of amphibolite assemblages, from actinolite-tremolite or from relict igneous hornblende. Several criteria can assist identification of metamorphic hornblende:

1. in igneous rocks of the Noranda and Malartic areas, at least, hornblende is markedly different from actinolite-tremolite in thin section: hornblende is green or brown and strongly pleochroic whereas actinolite-tremolite is colourless to very pale green and only weakly pleochroic (Rimsaite, 1974; Allen and Goldie, 1978);
2. irregular "bleached patches" and colourless rims on amphibole crystals (c.f. Figure 8, Rimsaite, 1974) indicate the presence of two coexisting metamorphic amphiboles: either hornblende and actinolite-tremolite, or hornblende and cummingtonite;
3. textural evidence may often be used to infer that an amphibole is metamorphic (e.g. Fig. 2, Goldie, 1978).

Application of these criteria may result in recognition of more amphibolites in the Abitibi Belt. For example, the hornblendes which occur in the Bourlamaque Batholith (Darling and Campiglio, 1976) may prove to be metamorphic.

References

Allen, J.M. and Goldie, R.
1978: Coexisting amphiboles from the Noranda area, Quebec: extension of the actinolite-hornblende miscibility gap to iron-rich bulk compositions, American Mineralogists, v. 63, p. 205-209.

Campiglio, C. and Darling, R.
1976: The geochemistry of the Archaean Bourlamaque batholith, Abitibi, Quebec, Canadian Journal of Earth Sciences, v. 13, p. 972-986.

Goldie, R.
1978: Magma mixing in the Flavrian pluton, Noranda area, Quebec, Canadian Journal of Earth Sciences, v. 15, p. 132-144.

Metamorphism of the Flavrian and Powell Plutons, Noranda area, Quebec, Journal of Petrology. (in press).

Jolly, W.T.
1978: Metamorphic history of the Archean Abitibi Belt in Metamorphism in the Canadian Shield, Geological Survey Canada Paper 78-10, p. 63-78, 1978.

Rimsaite, J.
1979: Mineral assemblages and low-grade metamorphic-metasomatic alterations in an Archean greenstone belt, Malartic, Quebec, Canadian Mineralogist, v. 12, p. 520-526.

METAMORPHIC HISTORY OF THE ARCHEAN ABITIBI BELT – REPLY

In a letter to the Chief Scientific Editor, dated October 4, 1979 Dr. Jolly comments as follows:

> ".....1) The plutons discussed by Goldie were considered by me to have been intruded contemporaneously with the lavas (see class 4a, p. 64 of Jolly, 1978) and thus the aureoles surrounding them formed during M-3, not M-5 as stated in paragraph two of the manuscript; 2) the Powell pluton is not shown on the maps of Jolly, 1978, contrary to implications in point (2) of paragraph two of the manuscript; 3) no mechanism of metamorphism is discussed and seems of critical importance. For example, does Mr. Goldie feel that the alteration of the plutons was facilitated by autometamorphic processes during intrusion or by external factors; if the latter is true, what were the external influences?;....."

From: Discussions and Communications in Current Research, Part C; Geol. Surv. Can., Paper 79-1C.

AUTHOR INDEX